Unveiling Galactic cosmic-ray accelerators with gamma-ray observations: their relation to supernova remnants

Marianne Lemoine-Goumard

université de BORDEAUX

Mémoire présenté par

Marianne LEMOINE-GOUMARD

pour obtenir le diplôme d'

HABILITATION À DIRIGER DES RECHERCHES

en Astrophysique, plasmas, nucléaire

Unveiling Galactic cosmic-ray accelerators with gamma-ray observations: their relation to supernova remnants

---

Habilitation soutenue le 18 Juin 2018 devant le jury composé de :

M. Mathieu de Naurois	Rapporteur
M. Jürgen Knödlseder	Rapporteur & Président
M. Vincent Tatischeff	Rapporteur
M. Giovanni Lamanna	Examinateur
M. Eric Nuss	Examinateur

Centre d'Etudes Nucléaires de Bordeaux Gradignan
19 Chemin du Solarium
CS 10120
F-33175 GRADIGNAN Cedex

CONTENTS

CHAPTER

1

Introduction

When I decided to write this manuscript, I first read a large number of other theses from the domain to see how one should write such a piece of work. And, obviously, as I imagined before hand, there are no strict rules or procedures to follow. Therefore, I decided to devote this time to ask myself the following questions: "What did I learnt since I was hired by CNRS and joined the Astroparticle group in Bordeaux ?", "What have been my main contributions to the domain ?", and more importantly "What are my scientific perspectives for the near future and at more longer term ?". In this sense, the time that I spent to write this manuscript has been extremely fruitful, reading publications and trying to extract the coherence and the link between the works that I carried with different collaborators, on different topics and various experiments. After ten years of observations with *Fermi*-LAT, more than fifteen with H.E.S.S. and just before the start of operation of CTA, it is an ideal time to make a pause and look ahead. Of course, this means that I did not try to write and summarize all the works and publications that I have done in the past eleven years. Several topics of interest, for instance related to pulsars and pulsar wind nebulae, are simply cited or even completely omitted. It is not a lack of interest but rather a personal choice in this manuscript.
To better understand the path that I followed during these eleven years, here is a brief summary of the main achievements:

- I was hired to a permanent research position with the IN2P3-CNRS and joined the Bordeaux group in December 2006. At this time, the group was intensively working on GLAST (then renamed Fermi), devoting their research time to the study of pulsars and active galactic nuclei. To keep a coherence in the group while staying in a domain related to the acceleration by shock waves, I decided to move from supernova remnants (the topic of my PhD thesis) to pulsar wind nebulae. Together with David Smith, I supervised Marie-Helene Grondin's PhD thesis devoted to pulsars and pulsar wind nebulae as seen with the first two years of LAT data. Several publications of great interest have been written during this time: the detection of the Crab pulsar and nebula, the detections of the pulsar wind nebula MSH 15−52, HESS J1825−137 and Vela-X. This experience allowed me to take leadership within the Fermi-LAT collaboration, becoming

co-leader of the "supernova remnants and pulsar wind nebulae" sub-group from 2008 to 2012 and of the whole Galactic group from 2012 to 2014. In this context, I started a collaboration with Professor Roger Romani and Professor Stefan Funk from Stanford University and spent one month at Stanford in July 2008 to work with them. In September 2008, I was awarded a grant of 14 keuros from the France-Stanford center for interdisciplinary studies for a one-year project related to the study of pulsar wind nebulae. The budget covered the travel costs for a two-week visit in Stanford in May 2009 as well as two one-week visits to Bordeaux in March and June 2009. Two methodologies were initiated and tested during this collaborative project: off-pulse analysis of pulsars and analysis of extended sources at GeV energies.

- In parallel to this work, I kept my activities on H.E.S.S. as an affiliate member of the collaboration. My studies were related to supernova remnants and I was heavily involved on the publications related to RX J1713.7−3946 and RCW 86.

- An important achievement was obtained when I received a European Research Starting Grant. To write the scientific project for this grant I thought about my priorities in the domain while keeping a good synergy within the group in Bordeaux. The project entitled "New light on the gamma-ray sky: unveiling cosmic-ray accelerators in the Milky Way and their relation to pulsar wind nebulae" (with its associated acronym P-WIND) was devoted to the analysis of gamma-ray data to look for the cosmic-ray accelerators in the Galaxy. The grant covered the salary of two post-doctoral fellows (Matthew Dalton and Jeremie Mehault) as well as one PhD student (Romain Rousseau). The P-Wind project was extremely fruitful. A very large number of collaborations and publications was developed during this 3-year project. The P-Wind team led 7 papers and contributed to 16 other publications on various topics: pulsar wind nebulae (HESS J1857+026, HESS J1303−631, 3C58 and a systematic search for signal from 58 TeV PWNe with the LAT), unidentified *Fermi*-LAT sources (MSH 11−62, HESS J1356−645), multi-wavelength analysis of supernova remnants (Puppis A, W41). In addition to that, a significant fraction of the time was devoted to the modeling of gamma-ray sources with a special input on pulsar wind nebulae with a one-week stay in Abu Dhabi to work with Joseph Gelfand.

- Thanks to the knowledge and collaboration started during the ERC project, especially the one concerning extended sources, I decided to supervise a third PhD thesis on the spectral and morphological analysis of supernova remnants using the LAT Pass 8 data. Benjamin Condon's PhD thesis was extremely surprising in the sense that, 7 years of LAT data being already analyzed, we were not expecting so many exciting results. The detection of RCW 86, SN 1006 and HESS J1731−347 were unexpected and allowed by the sensitivity of Pass 8 and the possibility to study extended sources with the LAT. The spatially resolved spectral analysis of RCW 86, RX J1713.7−3947 and SN 1006 are even more surprising and seems to show that the only way to understand how cosmic rays are accelerated in our Galaxy is to look at very fine structures and regions within the shock wave.

- After the end of the ERC project, the group in Bordeaux decided to join the CTA collaboration. I am full member since mid-2014 but due to other duties on the H.E.S.S. and *Fermi* collaborations, my contribution has only been marginal until now and mainly related to review scientific publications from the Galactic group.

- In 2016, with the overhead of the ERC Starting Grant, I hired François Brun with a 3-year post-doctoral fellowship to work on Galactic science at TeV energies (H.E.S.S. and CTA). One of

the main achievement from our collaborative work was the Fermi-H.E.S.S. joint publication on the middle-age supernova remnant W49B and the detection of the "pion bump" at low energy, thus indicating that protons are accelerated in this source. This analysis triggered several other contributions on the acceleration of cosmic-rays by middle-age supernova remnants, especially with the japanese teams working at Ibaraki University and Rikkyo University.

Looking at the studies and collaborations carried during these past years (presented in the Diagram 1.1 as well as on my curriculum vitae in Appendix A), my leading interest has always been the acceleration of cosmic rays in the Galaxy. In parallel, and partly because they are the main candidates in our Galaxy, I have been working intensively on supernova remnants. This is why this manuscript focuses on this topic and neglect some important results obtained on pulsars and pulsar wind nebulae. The latter will be cited at the end of the manuscript together with other types of accelerators.

I realize that I have been extremely lucky since my very first steps in this domain. I started my PhD thesis in 2003 at the best time to live the incredible number of detections offered by H.E.S.S. and its Galactic Plane Survey. I joined GLAST in early 2007 and was at SLAC during the Launch and Early Operations just after launch to see the exceptional sensitivity of the LAT and the detections of the Crab, Geminga and Vela pulsar with only one week of data ! Nobody was expecting to perform morphological analyses with the LAT and even less morphologically-resolved spectral analysis: this is what we are starting to do in several cases as you will see in this manuscript. The results are incredible in every domain. I have lived these major breakthroughs in γ-ray astronomy and hope that my enthusiasm will be visible in this manuscript.

I wish you a very pleasant reading.

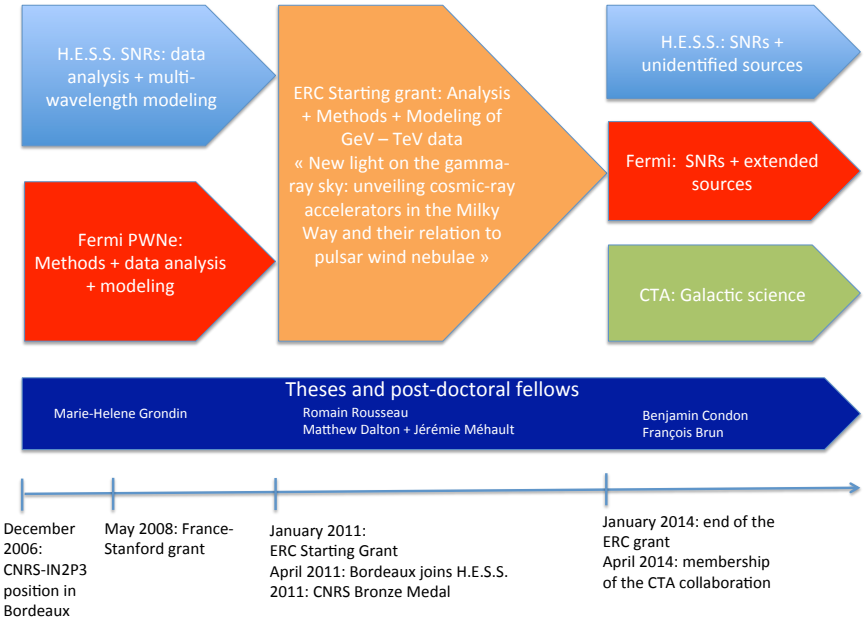

Figure 1.1: *Diagram showing my scientific contributions and evolution since December 2006 when I joined the group in Bordeaux after my PhD thesis defended on May 11th 2006.*

CHAPTER

2

From Galactic cosmic rays to supernova remnants at multi-wavelength frequency

Contents

2.1 Brief introduction to cosmic rays

One century ago, Victor Hess carried out several balloon flights that led him to conclude that the penetrating radiation responsible for the discharge of electroscopes was of extraterrestrial origin. One century from the discovery, thanks to pioneering works and a large amount of measurements, the characteristics of cosmic rays (CRs) are relatively well known. CRs are charged particles that contribute an energy density in the Galaxy of about 1 eV cm^{-3}. This energy density is comparable to the energy density of thermal gas and magnetic field in the Galaxy, which cannot be a simple coincidence and indicate some kind of coupling between thermal and non-thermal constituents of the Galaxy, showing the real importance of cosmic-rays in our Galaxy. These particles are mainly protons (hydrogen nuclei) with about 10% fraction of helium nuclei and smaller abundances of heavier elements and only

1% of electrons. Another important information comes from the all-particle spectrum. It is apparently very regular but shows two main features: the knee at 3×10^{15} eV where the slope of the differential flux changes from -2.7 to -3.1, and a flattening at 5×10^{18} eV called the ankle. Another structure in the spectrum was recently discovered by KASKADE-Grande at $\sim 10^{17}$ eV and called the second knee (Apel et al., 2013).

2.1.1 Galactic or extragalactic origin ?

Since their discovery, there has been a long standing debate concerning the origin of cosmic rays. Electrons have to be galactic since the energy losses by inverse Compton scattering off the microwave background prevent propagation from one galaxy to another. In the case of protons, the situation has improved significantly thanks to the results obtained by EGRET aboard the Compton Observatory. Indeed, the gamma-ray flux obtained by EGRET on the Small Magellanic Cloud was strongly inconsistent with the fact that GeV cosmic-ray protons have uniform density in space (Sreekumar et al., 1993). Therefore, the bulk of the locally observed protons at GeV energies had to be galactic. More recently, the comparison of the Fermi-Large Area Telescope (LAT) all sky maps above a GeV with the distribution of dust and gas revealed by the Planck data shows that they are very similar, implying that the cosmic-ray flux throughout the Galaxy must be uniform except in the neighborhood of the Galactic centre where evidence for a harder spectrum and higher intensity is visible. The Larmor radius of a proton with energy $E_{\rm PeV}$ in PeV gyrating in a magnetic field $B_{\mu\rm G}$ in μG is $\rm r_g$=$E_{\rm PeV}/B_{\mu\rm G}$ parsec. It is mostly assumed with good reason that CRs with energies above the ankle must be extragalactic in origin since their Larmor radius is much larger than the Galaxy. This implies that the transition from a Galactic to an extragalactic origin occurs somewhere between the knee and the ankle. In addition, the extreme regularity suggests that a single class of galactic sources (or a single type of acceleration mechanism such as Diffusive Shock Acceleration, see below) is responsible for the CR spectrum up to this transition energy. Data collected across the knee region by ground based CR experiments show an evolution towards heavier mass groups as expected from acceleration models (see Figure 2.1). A tendency towards lighter elements is then observed starting at energies compatible with the position of the second knee. The energy spectra of individual elements are even more difficult to measure but KASKADE seems to show an average composition at the knee dominated by light elements, in agreement with KASKADE-Grande (Apel et al., 2014). The knee would then be interpreted as the steepening of the proton and He spectra, and the second knee to the steepening of the heavy component, where the Galactic component would cease. In addition, Auger and the Telescope Array experiment agree on the mass composition and spectrum at around 10^{18} eV where CRs are found to be light (Aab et al., 2014; Abbasi et al., 2015). Together with the results from KASKADE-Grande, this implies a change from heavy to light between 10^{17} eV and 10^{18} eV which suggests a possible transition from galactic to extragalactic CRs in this energy domain. And, more recently, the Pierre Auger Observatory detected an anisotropy at more than the 5.2σ level above 8×10^{18} eV that can be described by a dipole with a direction indicating an extragalactic origin for these ultra-high energy particles (The Pierre Auger Collaboration et al., 2017) and confirming that the transition occurs below this energy.

However, it should be noted that a transition between Galactic and extragalactic origin above 10^{17} eV has been questioned by the EAS-TOP and MACRO experiment (Aglietta et al., 2004), CASA-MIA (Glasmacher et al., 1999) and ARGO-YBJ together with a prototype of Cherenkov telescope of LHAASO (Bartoli et al., 2015) that show evidence of a knee-like structure in the spectrum of light nuclei at ~ 700 TeV, well below the knee. Finally, the compilation of measurements of the energy

spectrum of the so-called CNO group (i.e. Carbon-Nitrogen-Oxygen) show a knee at energies not larger than about 7 PeV (see for instance Blümer et al. (2009)). In a scenario with a rigidity dependent knee position, this is not consistent with a position of the proton knee at about 3 PeV.
Even if the energy of the transition between galactic and extragalactic origin is not settled yet, these results suggest that the sources of galactic cosmic rays must be able to accelerate protons up to at least ~ 1 PeV and this is why the community is currently looking for these rare PeVatrons.

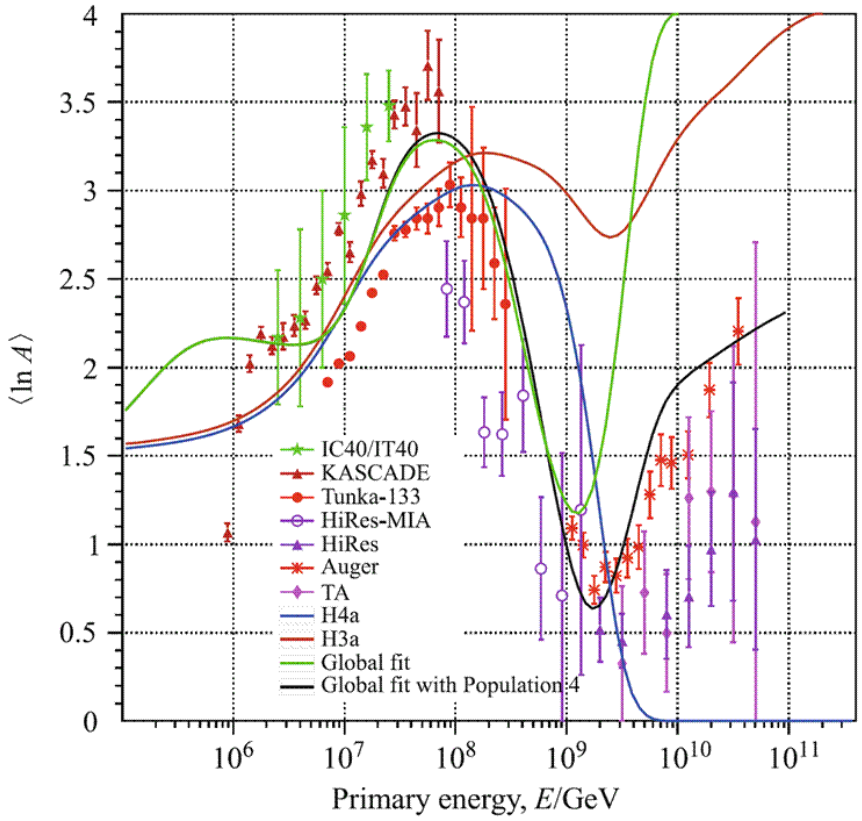

Figure 2.1: *Average value of the estimated CR logarithmic mass, $< lnA >$, from several ground-based experiments. Superimposed are the lines corresponding to mixed composition resulting from multi-population models as given in Gaisser et al. (2013). Plot taken from Gaisser et al. (2013).*

2.1.2 Propagation in the Galaxy

When looking for the sources of galactic CRs, one needs to take into account that protons must escape and diffuse away from their acceleration sites. The transport of CRs in the Galaxy has been subject of active investigation. One of the main quantity that we have to constrain the propagation parameters comes from the measurements of secondary-to-primary ratios, such as the Boron/Carbon, which provide an estimate of the grammage that CRs traverse during propagation. Indeed, under the simplest leaky box model, one expects the path lengths traversed by the cosmic rays to be inversely proportional to the diffusivity D. If $D \propto E^{\delta}$, we expect higher energy particles to diffuse faster out of the Galactic plane, implying that those particles that reach the Solar system, do so earlier at higher energies. As a consequence, higher energy particles should produce less secondaries along the way. Indeed, the ratio between the secondary Boron and primary Carbon nuclei decreases at high energies as expected and the Boron/Carbon ratio is compatible with a diffusion coefficient $\delta = 0.3$ – 0.6

(Strong et al., 2007). The diffusion and escape time from the Galaxy being energy dependent implies that the CR spectrum that we observe on Earth (proportional to $E^{-2.7}$ below the knee) must be steeper than the spectrum that CR sources inject in the interstellar medium. In order to be consistent with observations, CR sources need to inject protons with a spectral index $\Gamma = 2.7 - \delta$ comprised between 2.1 and 2.4. Constraints on the diffusion coefficient are therefore of great interest to constrain as a consequence the type of sources accelerating CRs in our Galaxy. Recently, Blasi and Amato (2012) found that the very weak energy dependence of the anisotropy amplitude below 10^5 GeV and the rise at higher energies as seen by the data from EAS-TOP and the Akeno and Tibet experiments, can best be explained if the diffusion coefficient is $\delta \sim 1/3$. Faster diffusion, for instance with $\delta = 0.6$, leads in general to an exceedingly large anisotropy amplitude. If confirmed, their study would imply that CRs sources inject protons with a steep spectrum $E^{-2.4}$.

2.2 Supernova remnant evolution

The key parameters governing the evolution of a supernova (SN) explosion are the initial energy, progenitor system, and surrounding interstellar medium (ISM), which are all tied together by the late-time evolution of massive stars. The progenitor system can be either a binary system (two objects orbiting one another) composed of a white dwarf and a companion star for Type Ia SNe, or a massive star ($M > 8\ M_\odot$) for type II SNe (also known as core-collapse SNe), or even massive stars that have lost their Hydrogen-envelopes prior to explosion (Wolf-Rayet stars, $> 25\ M_\odot$) for Type Ib/c SNe. The evolution of a SNR is then typically characterized by three phases:

- an ejecta-dominated phase called "free expansion" when the swept-up mass is much less than the ejected mass and does not slow shock expansion,
- a phase called Sedov-Taylor when the swept-up mass is much larger than the ejecta mass and the shock expansion is characterized by adiabatic expansion,
- a radiative phase where recombining gas quickly cools the swept-up gas forming a dense shell (Woltjer, 1970). Toward the end of this radiative phase, the dense shell of the SNR merges with the ISM and becomes indistinguishable from it (Cioffi et al., 1988).

Depending on the density profile of the surrounding gas, SNRs may transition between these phases at very different ages (Dwarkadas and Chevalier, 1998). Some SNe leave behind a rapidly spinning neutron star. These pulsars dissipate their rotational energy via a relativistic wind of electrons and positrons, which is rapidly decelerated at an interaction point with the surrounding dense medium called the termination shock (Gaensler and Slane, 2006; Grenier and Harding, 2015). The pulsar wind nebula (PWN) formed in the interior of the SNR expands outward and may encounter the inward reverse shock of the SNR as illustrated in Figure 2.2. These systems are typified by a radio synchrotron shell for the SNR and a flat-spectrum central PWN, and therefore dubbed composite SNRs. Relativistic electrons produce inverse Compton (IC) gamma rays at GeV and TeV energies. Additional gamma-ray emission from the pulsar magnetosphere and surrounding SNR shock front can also be present, limiting the identification of the primary source of gamma rays. At various points during the evolution of the system, different regions may produce the brightest gamma-ray emission. Models of the evolution of PWNe and SNRs show a diversity of possible observed parameters (Gelfand et al., 2009). While shocks within PWNe are clearly capable of accelerating leptons, it is not clear if protons are also accelerated. This type of source will be discussed in Section 5.2.3.

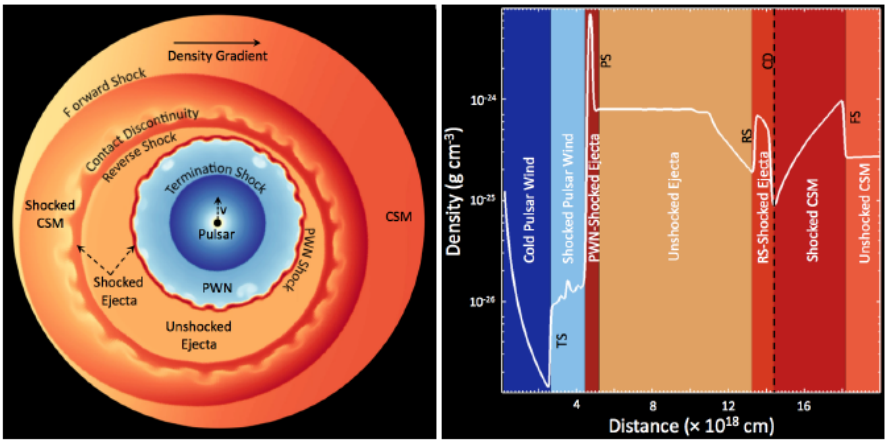

Figure 2.2: *Left: Density image from a hydrodynamical simulation of a PWN expanding into a SNR that is evolving into a medium with a Circumstellar medium (CSM) density gradient increasing to the right. The pulsar itself is moving upward. The reverse shock is propagating inward, approaching the PWN preferentially from the upper right due to the combined effects of the pulsar motion and the CSM density gradient. Right: Density profile for a radial slice through the simulated composite SNR. Colored regions correpond to different physical regions identified in the SNR image. Plot taken from Slane (2017).*

2.3 The link between cosmic-rays and supernova remnants

The association between supernova remnants and Galactic cosmic rays is very popular since 1934, when Baade and Zwicky (1934) argued that this class of astrophysical objects can account for the required CR energetics. Indeed, in order to maintain the cosmic-ray energy density in the Galaxy, about 3 supernovae per century should transform 10% of their kinetic energy in cosmic-ray energy. This argument has also been supported by E. Fermi's proposal of a very general mechanism for particle acceleration (Fermi, 1949), which is very efficient if applied at SNR shocks (Bell, 1978). The extremely interesting point of the diffusive shock acceleration (DSA) mechanism is that it naturally yields power-law spectra for the energy distribution of accelerated particles. Indeed, in DSA, particles with gyroradii larger than the shock thickness can be repeatedly scattered back and forth the shock, gaining energy as if they were squeezed between converging walls (as in the first order Fermi acceleration mechanism). Since both the gain per cycle and the probability of being advected away from the acceleration region are controlled by the shock hydrodynamics only, accelerated particles develop power-law distributions whose spectral index is determined by the downstream/upstream compression ratio[1]. For monoatomic gas with adiabatic index $\gamma = 5/3$, the compression ratio tends to 4 which directly imply that SNR shocks are expected to accelerate CRs with a universal spectrum $N(E) \propto E^{-2}$. This is another criterium that led Bell (1978) suggest that SNRs accelerate Galactic CRs. The other criterium that needs to be fulfilled is that the maximum energy reaches the knee of the cosmic-ray spectrum. The acceleration time for particles undergoing DSA can be written approximately as $t_{acc} \propto D/v_{sh}^2$ where D is the diffusion coefficient, and v_{sh} is the shock velocity. In case of Bohm diffusion, the particle mean free path is of the order of the Larmor radius and we can re-write this equation as $t_{acc} \propto E/(Bv_{sh}^2)$ where E is the energy of the particle, and B the magnetic field. For young SNR, the age of the remnant t_{age} is an obvious limitation on the maximum energy which

[1] A description of the process is provided in https://www.refletsdelaphysique.fr/articles/refdp/pdf/2015/03/refdp201546p14.pdf

can be written as $E_{max} \propto Bv_{sh}^2 t_{age}$ using the above equation. The evolution of a young supernova remnant has been described in many papers (see Truelove and McKee (1999) for more details). In brief, the expansion of SN ejecta into the surrounding medium leads to the formation of a double-shocked structure, consisting of a reverse shock that travels back into the ejecta, and a forward shock that expands into the ambient medium. If the SN ejecta are described by $\rho_{ej} \propto r^{-n}$, and the surrounding medium is described by $\rho_{amb} \propto r^{-s}$, the expansion of the forward shock is $R_f \propto t^m$ where $m = (n-3)/(n-s)$ is referred to as the expansion parameter. We can then express the maximum energy as $E_{max} \propto Bt^{2m-2}t_{age} \propto Bt^{2m-1}$ This means that, as long as $m > 0.5$, and the magnetic field B is constant, the maximum energy is increasing with time. The maximum energy will start to decrease with time once $m < 0.5$, i.e. just before the remnant enters the Sedov-Taylor stage. Current models suggest that, at this epoch, the maximum energy is $\sim$ 100 TeV for Type Ia SNe and $\sim$ 1 PeV for core-collapse SNe (see Section 3.4.4 for more details), which is close to the needed value to reproduce the CR spectrum. However, until recently there were absolutely no observational evidence concerning the acceleration of protons and nuclei in SNRs. Indeed, through their interaction with the interstellar magnetic fields, the charged particles arriving on Earth have lost all directional information and cannot be used to pinpoint the sources. That is why, almost 100 years after their discovery by V. Hess, the origins of the CRs and their cosmic accelerators remain unknown. I will briefly summarize below the evidences that supernova remnants can indeed accelerate particles efficiently.

2.4 First indirect evidences of efficient particle acceleration in supernova remnants with X-ray satellites

Electrons accelerated at SNR shocks radiate through synchrotron emission when spiraling in a magnetic field. This emission extends from the radio to the X-ray domain. While radio synchrotron emission is observed in most SNRs detected in the Galaxy (Green, 2017), X-ray synchrotron emission is observed only in a few remnants up to now. In some of these X-ray detected SNRs, the X-ray synchrotron emission exhibits a filamentary emission just behind the blast wave (for instance in the historical remnant Tycho (Cassam-Chenaï et al., 2007)). One plausible explanation is that the magnetic field is large enough ($\sim 100\,\mu$G) to induce strong radiative losses in the high energy electrons (Vink and Laming, 2003; Parizot et al., 2006), thus creating these very thin structures. If the magnetic field is indeed amplified at the limbs, the maximum energy at which particles can be accelerated is much larger there ($>$ 1 PeV) than outside the limbs (E $\approx$ 25 TeV if B $\approx 10\,\mu$G).
In parallel, a discovery of the brightening and decay of X-ray hot spots in the shell of the SNR RX J1713.7$-$3946 on a one-year timescale has been reported by Uchiyama et al. (2007). This rapid variability implies that electron acceleration needs to take place in a strongly magnetized environment, indicating amplification of the magnetic field by a factor of more than 100.
Another evidence of very efficient particle acceleration in supernova remnants is provided by the postshock plasma temperatures observed in SNRs 1E 0102.2$-$7219 and RCW 86, that are lower than expected for their measured shock velocities (Hughes et al., 2000; Helder et al., 2009). In the second case and for the first time, by comparing the measured post-shock proton temperature with the one determined using the shock velocity, the authors presented the evidence that $> 50\%$ of the post-shock pressure is produced by cosmic rays.
Recently, very unusual structures consisting of ordered sets of bright, non-thermal stripes were discovered by Eriksen et al. (2011) in the historical SNR Tycho with a deep Chandra exposure. In the framework of a non-linear diffusive shock acceleration model (NL-DSA), which includes magnetic

field amplification from a cosmic-ray current driven instability, Bykov et al. (2011) were able to reproduce the stripes assuming that the maximum energy of the CR protons responsible for the stripes is $\sim 10^{15}$ eV. This confirms the claim from Eriksen et al. (2011) that the spacing between the stripes corresponds to the gyroradii of 10^{14}–10^{15} eV protons.

These are strong indirect arguments confirming that electrons and protons are accelerated up to at least TeV energies (maybe even PeV) in supernova remnants. The direct signature of accelerated protons is expected through pion decay emission in the GeV–TeV gamma-ray energy range. Indeed, CRs (ionized nuclei of all species, but mostly protons, plus a small fraction of electrons) can interact with ambient matter and photons producing gamma rays via two different channels. One mechanism invokes the interaction of accelerated protons at SNRs shocks with interstellar material generating neutral pions which in turn decay into gamma rays. We call this mechanism the hadronic scenario. A second competing channel exists in the inverse Compton scattering of the photon fields in the surroundings of the SNR by the same relativistic electrons that generate the synchrotron X-ray emission. This is the leptonic scenario. Being of leptonic or hadronic origin, these gamma rays are not affected while they travel to Earth and can therefore be used to pinpoint the cosmic accelerators in our Galaxy.

2.5 Gamma-ray experiments

Two major breakthroughs in γ-ray astronomy occurred recently thanks to ground-based experiments and to the LAT aboard the *Fermi* satellite.

2.5.1 Ground-based experiments

Firstly, after more than 20 years of development, the first source of very high energy gamma rays, the Crab Nebula, was discovered in 1989 by the Whipple telescope (Weekes et al., 1989). Since this date, the technical progresses in this field have led to important scientific results, especially by the Cherenkov telescopes H.E.S.S. (Namibia), VERITAS (Arizona, United States) and MAGIC (Canary Islands, Spain). Indeed, when I started my PhD thesis in September 2003, 11 sources were detected at TeV energies and only three of them were Galactic: the Crab, TeV J2032+4130 and Cassiopeia A (neglecting the suspicious detections from the CANGAROO experiment). Then, in early 2007 when I joined the Astroparticle group at CENBG, the number of sources was already close to 70 partly thanks to the large number of detections offered by the first H.E.S.S. Galactic Plane Survey (Aharonian et al., 2006a). Figure 2.3 shows the status of the TeV sky reported by Jim Hinton at the ICRC in 2007 in comparison to the one reported by Nahee Park at the last ICRC in 2017. One can see the input coming from two other surveys performed by VERITAS and HAWC: one focusing on the Cygnus region and the other one on the Galactic plane fraction visible from the Northern hemisphere. Today, 198 γ-ray sources have been detected with high significance by the different experiments, $\sim$25 being clearly associated to SNRs or molecular clouds. It is not only the number of sources that is growing but also the diversity (with the detection of a superbubble in the Large Magellanic Cloud for instance), and the quality of the measurement (with the deep observations of the Galactic Centre and RX J1713.7$-$3946 allowing the first detection of a PeVatron and the possible detection of protons escaping the SNR shock). These results will be discussed in more detail in Section 3.3.1 and 5.3.2. We are now in an era of catalogs (thanks to the increased number of sources) and precision (thanks to the increased sensitivity and observing time).

These ground-based experiments for γ-ray astronomy rely on the development of cascades (air-showers) initiated by astrophysical gamma rays. Because of the low flux from Very high energy (VHE) gamma-ray sources, gamma-ray observatories have to overcome a high level of background events from cosmic-ray air showers. Largely there are two main techniques used to study the gamma-ray emission. One is observing the Cherenkov light emitted by secondary particles generated from the air shower thanks to imaging atmospheric Cherenkov telescopes (IACTs). The three currently under operation are H.E.S.S., VERITAS and MAGIC. The other is observing the secondary particles themselves using air shower arrays. The most famous among them is the High Altitude Water Cherenkov (HAWC) Observatory seated at a high-altitude site in Mexico (Abeysekara et al., 2017), successor of the MILAGRO experiment. It is sensitive to gamma rays in the energy range of 100 GeV to 100 TeV which is excellent to study cosmic-ray accelerators in the Galaxy, especially the high energy end. The full HAWC array was completed in March 2015, but science operations already started in August 2013 with a partially-built array. For the near future, another project of importance is being built currently at Daocheng in China: the Large High Altitude Air Shower Observatory (LHAASO, Di Sciascio and LHAASO Collaboration, 2016). It is an ambitious project incorporating HAWC-like water Cherenkov detectors and a very large array of scintillators (KM2A). The installation of the experiment started at very high altitude in China (4410 m a.s.l.). The commissioning of the first quarter of the layout is expected in 2018 with a conclusion in 2021. In a similar way to HAWC, it will present a modest angular resolution together with a high duty cycle and a wide field of view. The current generation of IACT arrays consist of multiple telescopes, and these have the best instantaneous sensitivity to detect VHE gamma rays. A typical IACT detects VHE gamma-ray sources with 1% of the Crab Nebula flux in less than 30 hours. However, IACTs have a small duty cycle of $\sim$15% because the observation requires a clear, dark night. Also, their field of view (FoV) is relatively small ($< 5^{\circ}$). Compared to the IACTs, the duty cycle of air shower arrays is $\sim$90% and their FoVs represent a much larger area on the sky ($\sim$2 sr). With this large FoV, the air shower array can survey a large portion of the sky ($> 50\%$) without pointing bias and is very well suited to the study of extended sources or diffuse emissions in the plane. However, the sensitivity and angular resolution of the air shower arrays are worse than IACTs, especially for energies lower than 1 TeV. This shows the complementarity between these different instruments.

Personally, I have worked only on the H.E.S.S. data. H.E.S.S. was originally an array of 4 12m diameter telescopes. Since 2012, a fifth telescope of 28m located at the center of the array is operational. This allows to lower the energy threshold down to 30 GeV at zenith. In 2016, H.E.S.S. completed an upgrade of the cameras for the four 12 m telescopes to reduce the dead time, the failure rate, and to operate smoothly with the 28 m telescope which has higher trigger rates. I have been full member of the H.E.S.S. collaboration until the end of 2006, then associate member of the collaboration until April 2011 and again full member when Bordeaux officially joined the H.E.S.S. collaboration, taking the lead on the copy of the data on site and their copy on the computer cluster in Lyon. This was made possible thanks to the ERC Starting Grant that allowed two post-doctoral fellows and one PhD student to work partly on H.E.S.S..

Looking ahead, the Cherenkov Telescope Array (CTA) is currently the biggest project of very high energy astrophysics, gathering at this time more than 1500 members spread in 32 countries. CTA represents the new generation of gamma-ray imaging Atmospheric Cherenkov telescope, that will succeed to the current arrays H.E.S.S., VERITAS, and MAGIC. CTA will be composed of two distinct arrays, one for each hemisphere for a full-sky coverage. The northern array will take place on the MAGIC site, while the southern one will be located in Chile (Paranal). Thanks to CTA, the far end of the electromagnetic spectra from 20 GeV up to 300 TeV will be observed with an unprecedented sensitivity and angular resolution (Cherenkov Telescope Array Consortium et al., 2017). The first

telescope is being built at La Palma (Canary Islands, Spain) and will start taking data in 2018.

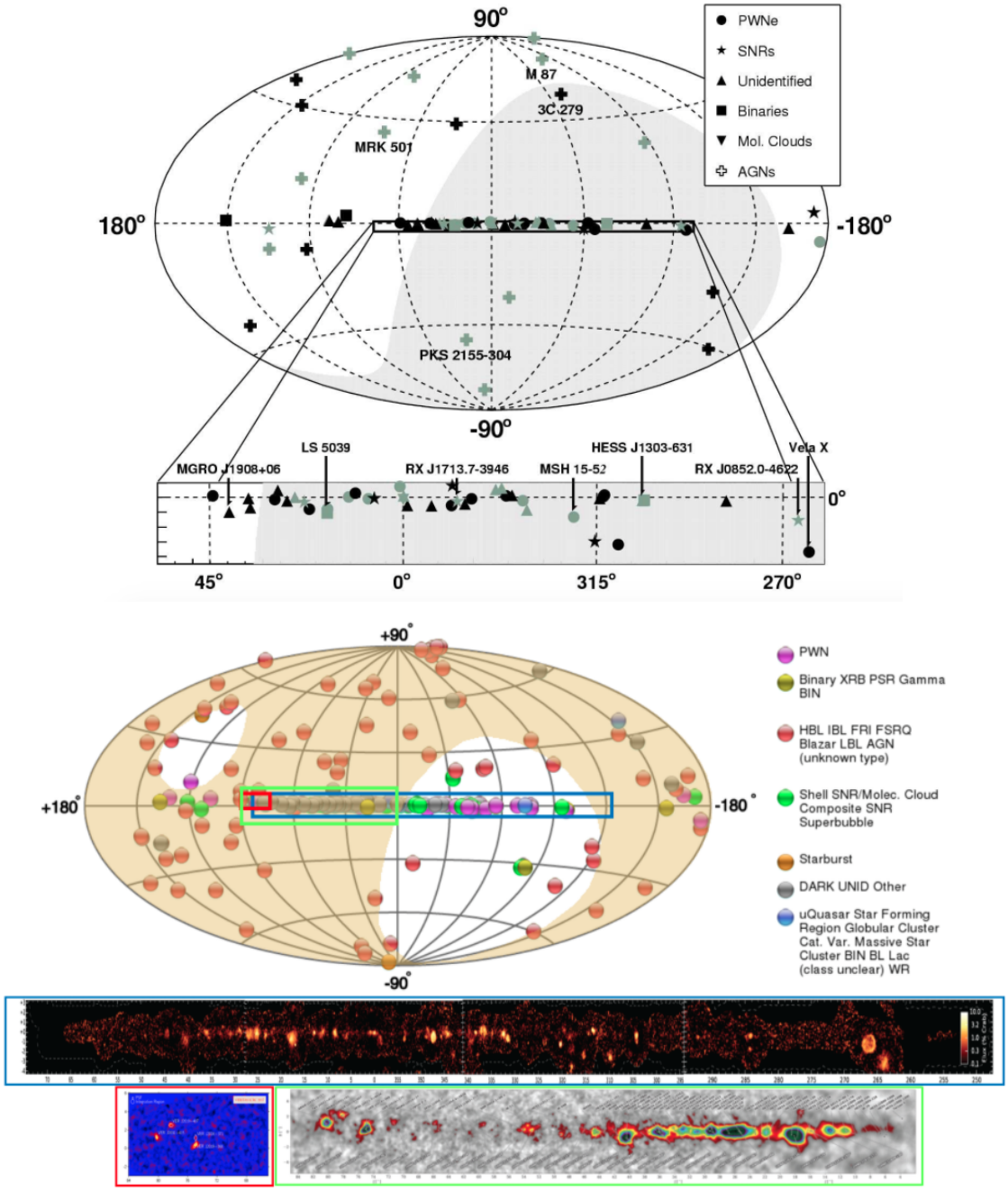

Figure 2.3: *The catalogue of known TeV sources as of the 30^{th} ICRC in 2007 (Top) and 35^{th} ICRC in 2017 (Bottom). Top: The positions of the known TeV emitters are shown in Galactic coordinates. Darker symbols indicate discoveries since the 29^{th} ICRC. The shaded region indicates the part of the sky more readily accessible from the southern hemisphere (Declination $> 0°$). Plot taken from Hinton (2007). Bottom: The blue rectangular area indicates the region of the H.E.S.S. Galactic plane survey (H. E. S. S. Collaboration et al., 2017b). The red rectangular area indicates the region of VERITAS's Cygnus sky survey (Bird and for the VERITAS Collaboration, 2017). The green rectangular area indicates the Galactic plane shown by the HAWC collaboration (Abeysekara et al., 2017). The yellow shaded area indicates the sky coverage of the HAWC observatory. The skymaps of each survey indicated with rectangular boxes are shown under the source map. Plot taken from Park (2017).*

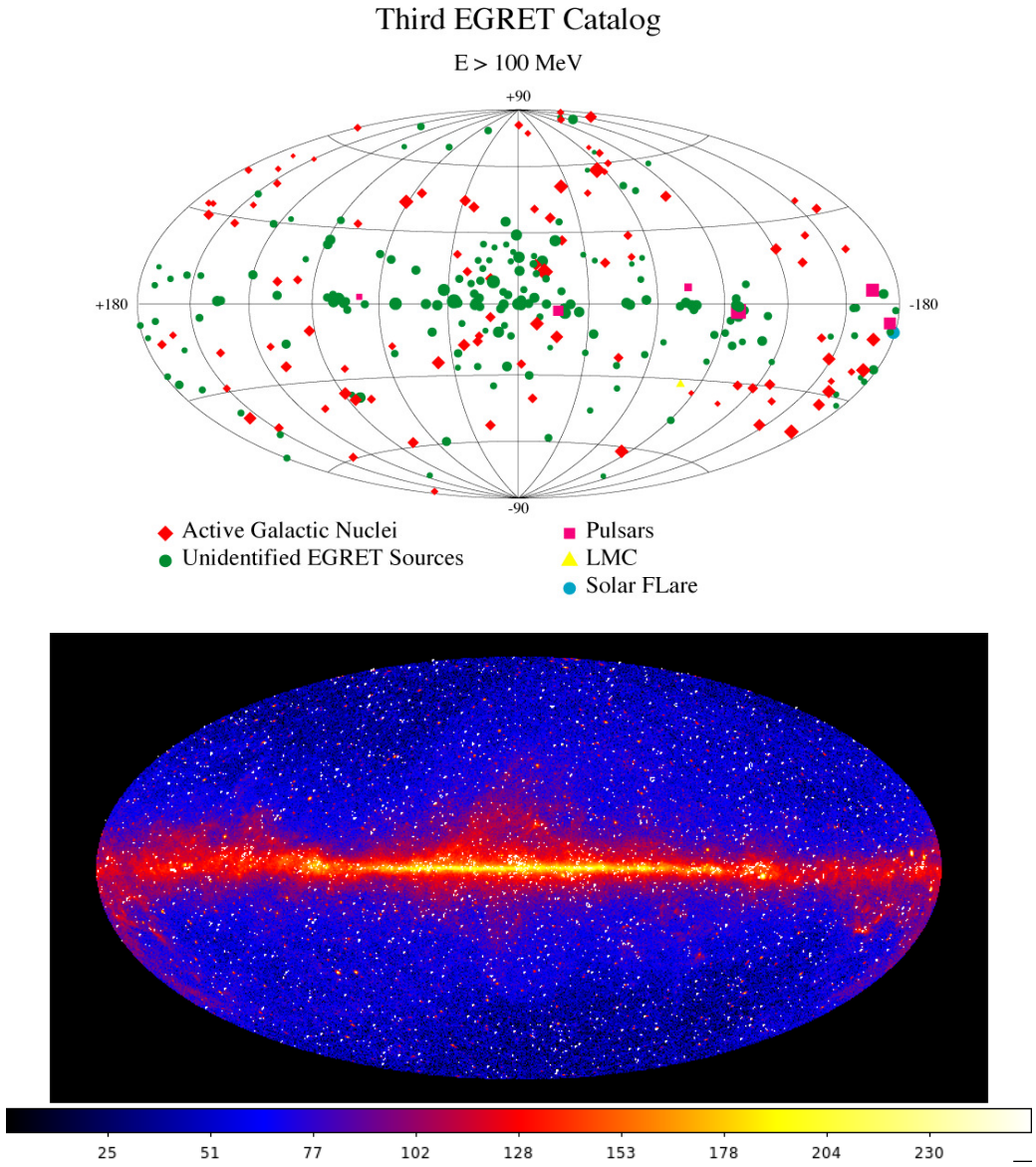

Figure 2.4: *The catalogue of known GeV sources from EGRET (Top, Hartman et al. (1999)) and the LAT FL8Y (Bottom) in Galactic coordinates. The LAT image is based on 9-year (August 4, 2008 - August 4, 2017) Pass 8 Source class, PSF3 event type above 1 GeV. The image is smoothed with a 0.25 deg FWHM Gaussian. The map is in intensity units with a logarithmic scaling. The white dots indicate the position of sources in the FL8Y source list.*

2.5.2 The Large Area Telescope

In early 2007, when I joined the group in Bordeaux working on the GLAST satellite (now renamed *Fermi* for the physicist Enrico Fermi), we were still relying on the EGRET catalog in the GeV energy domain. This was our best guide to estimate what would be our science and our results with the LAT. The third catalog of high-energy gamma-ray sources detected by the EGRET telescope on the Compton Gamma Ray Observatory contains 271 sources above 100 MeV. It includes a solar flare, the Large Magellanic Cloud, five pulsars, one probable radio galaxy detection (Cen A), 66 high-confidence

identifications of blazars, 27 lower confidence potential blazar identifications and 170 sources not yet identified firmly with known objects, although potential identifications were suggested for a number of those (Hartman et al., 1999). This means that EGRET was unable to identify (or even detect) clearly any SNR in our Galaxy ! This was largely due to the poor angular resolution of EGRET and the large confusion of sources in the Galactic plane where SNRs are located.
The *Fermi*-LAT is a γ-ray telescope which detects photons by conversion into electron-positron pairs in the energy range between 20 MeV to higher than 500 GeV, as described in Atwood et al. (2009). The LAT is composed of three primary detector subsystems: a high-resolution converter/tracker (for direction measurement of the incident γ-rays), a CsI(Tl) crystal calorimeter (for energy measurement), and an anti-coincidence detector to identify the background of charged particles. Since the launch of the spacecraft in June 2008, the LAT event-level analysis has been periodically upgraded to take advantage of the increasing knowledge of how the *Fermi*-LAT functions as well as the environment in which it operates. Following the Pass 7 data set, released in August 2011, Pass 8 is the latest version of the *Fermi*-LAT data. Its development is the result of a long-term effort aimed at a comprehensive revision of the entire event-level analysis and comes closer to realizing the full scientific potential of the LAT (Atwood et al., 2013). The LAT has considerably improved our knowledge of the 100 MeV – 100 GeV γ-ray sky: it has moved the field from the detection of a small number of sources to the detailed study of several classes of Galactic and extragalactic objects as can be seen in Figure 2.4 (Bottom). Based on the first eight years of science data from the Fermi Gamma-ray Space Telescope mission and the 100 MeV – 1 TeV range, the preliminary LAT 8-year point source list (FL8Y) is the deepest view of the sky in this energy range [2]. Relative to the 3FGL catalog, the FL8Y source list has twice as much exposure as well as a number of analysis improvements, but is lacking an updated model for Galactic diffuse gamma-ray emission. The FL8Y source list includes 5524 sources above 4σ significance, with source location regions and spectral properties. Fifty-eight sources are modeled explicitly as spatially extended, and overall 303 sources are considered as identified based on angular extent or correlated variability (periodic or otherwise) observed at other wavelengths. For 2130 sources we have not found plausible counterparts at other wavelengths. More than 2900 of the identified or associated sources are active galaxies of the blazar class, 217 are pulsars. This incredible number of sources, large variety of classes and precision of measurement (with morphological studies as we will see in Section 5.1) is remarkable and was not suspected before launch. For what concern SNRs more specifically, a catalog of SNRs was released by the collaboration (Acero et al., 2016), reporting 30 sources as likely GeV SNRs as well as 14 marginal associations and 245 flux upper limits. A comparison of the sensitivity of all instruments at gamma-ray energies above 10 GeV is provided in Figure 2.5.

These observations at GeV and TeV energies show a diversity in the observed luminosities and spectra of SNRs that indicate a wide range of physical conditions that give rise to gamma rays. Today, there is no doubt that SNRs can accelerate efficiently particles up to 10^{14} eV. The question in early 2007 was whether these particles are protons or electrons and if they can be accelerated up to the knee of the cosmic-ray spectrum (10^{15} eV) with a reasonable efficiency. In this thesis, I will mostly focus on supernova remnants as the most famous candidate for the acceleration of Galactic cosmic rays. I will report my main contributions in this domain and I will review several other results of particular interest for this field. The growing number of sources detected at these energies also allow the study and comparison of other types of accelerators which will be reviewed in Chapter 5. Finally, a discussion on the perspectives for this field will be provided at the end of this manuscript.

[2]The public release of the source list is available at: https://fermi.gsfc.nasa.gov/ssc/data/access/lat/fl8y/

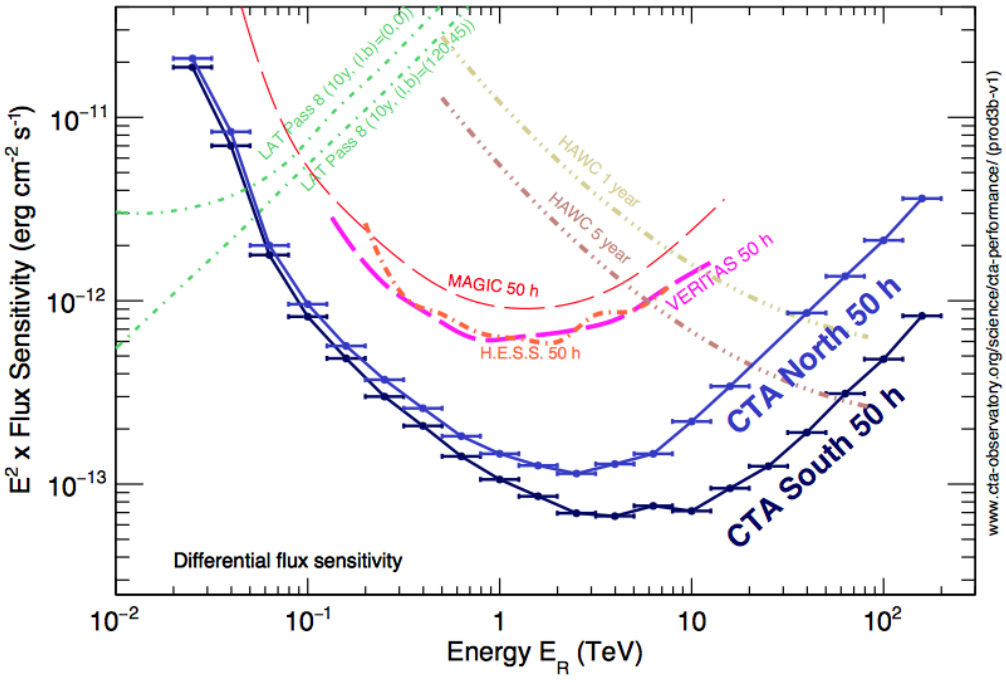

Figure 2.5: *Differential energy flux sensitivities for CTA (south and north) for five standard deviation detections in five independent logarithmic bins per decade in energy. For the CTA sensitivities, additional criteria are applied to require at least ten detected gamma rays per energy bin and a signal/background ratio of at least 1/20. The curves shown give only an indicative comparison of the sensitivity of the different instruments, as the method of calculation and the criteria applied are different. In particular, the definition of the differential sensitivity for HAWC is rather different due to the lack of energy reconstruction for individual photons in the HAWC analysis. This Figure is taken from Cherenkov Telescope Array Consortium et al. (2017).*

Summary

- The transition energy between galactic and extragalactic origin of the CRs is not settled yet, but all results suggest that the sources of galactic cosmic rays must be able to accelerate protons up to at least ~ 1 PeV.
- In order to be consistent with observations, CR sources need to inject protons with a spectral index $\Gamma = 2.7 - \delta$ comprised between 2.1 and 2.4. Recent studies conclude that CR sources inject protons with a rather steep spectrum $\mathrm{E}^{-2.4}$.
- Through Diffusive Shock Acceleration (DSA), SNRs, the main candidate for the acceleration of CRs, inject protons with a E^{-2} power-law spectrum and the energy involved is high enough to maintain the cosmic-ray energy density in the Galaxy.
- Several indirect evidences at radio and X-ray frequencies show that particles are indeed accelerated at SNR shock with high efficiency through amplified magnetic field.
- At gamma-ray energies, thanks to the LAT and the ground-based experiments, we have entered an era of catalogs, revealing different classes of astrophysical sources. Among them, SNRs is a key component in the Galaxy with ~ 30 candidates detected at GeV and TeV energies.

The results presented in this chapter have been published in (bold faces indicate those for which I am corresponding author):

- **Lemoine-Goumard M., 2015, Rapporteur talk of the 34th International Cosmic Ray Conference (ICRC2015), The Hague, The Netherlands: "Ground-based gamma-ray astronomy"**
- **Hewitt J. W., Lemoine-Goumard M., 2015, Comptes rendus de l'Academie des Sciences - Physique, Volume 16, Issue 6-7, p. 674-685: "Observations of supernova remnants and pulsar wind nebulae at gamma-ray energies"**
- **Lemoine-Goumard M., 2014, Proceedings of the International Astronomical Union, IAU Symposium, Volume 296, pp. 287-294: "Gamma-ray observations of supernova remnants"**
- **Lemoine-Goumard M., 2012, Proceedings of the 13th ICATPP Conference, pp. 266-274: "Acceleration of cosmic rays at supernova remnant shocks:. constraints from gamma-ray observations"**

CHAPTER

3

Young SNRs: efficient accelerators ?

Contents

A number of young supernova remnants are now known to have non-thermal X-ray spectra. The steepness of the X-ray emission suggests that it is synchrotron from TeV electrons, and that efficient shock acceleration is likely occurring in these objects. Gamma-ray observations made by H.E.S.S. on RX J1713.7−3946 confirmed that, indeed, particles (protons and/or electrons) are accelerated up to ~ 100 TeV to be able to produce the observed gamma-ray emission. This class of SNRs is therefore likely to be the most efficient to accelerate CRs. In this chapter, I will review the latest results obtained in the domain, focusing on the ones for which I contributed most.

3.1 The very young SN 1987A

Located in the Large Magellanic Cloud at only 50 kpc from Earth, SN 1987A is the closest observed with modern telescopes. After evolving for nearly three decades, the radio flux has been steadily

increasing, suggesting increasing acceleration, albeit with a steep spectrum ($F_\nu \propto \nu^\alpha$ where $\alpha = 0.8 \pm 0.1$, where F_ν is the energy received per unit area, unit time and unit frequency) with no evidence of a spectral break (Indebetouw et al., 2014). This is inconsistent with expectations from diffusive shock acceleration which predicts $\alpha = 0.5$, and perhaps indicative that the shock is modified by pressure from accelerated particles (Ellison et al., 2000) or by an amplified magnetic field (Reville and Bell, 2013). A flat-spectrum radio excess appears at the center of the remnant, and may be attributed to a newly formed PWN (Zanardo et al., 2014). Multi-wavelength studies of SN 1987A suggest that the shock at the current epoch has reached the dense equatorial ring made by the progenitor system for which densities of 10^3 to 10^4 cm^{-3} have been found (Mattila et al., 2010). Even with a deep exposure of 210 hours, significant emission from SN 1987A is not detected by H.E.S.S. (H.E.S.S. Collaboration et al., 2015). The 99% flux limit above 1 TeV is 5.6×10^{-14} cm^{-2} s^{-1}, assuming a photon index of 2, which translates into an upper limit for the γ-ray luminosity of 2.2×10^{34} erg s^{-1}. This would imply that less than 1% of the explosion energy of 10^{51} erg is carried by accelerated CR nuclei. Since it is not clear when, during the transition from SN to SNR, shock acceleration becomes efficient, these γ-ray observations of the youngest nearby SN are a strong help to constrain theories in the future.

3.2 Historical SNRs: the case of Cas A and Tycho

Two historical SNRs have been detected both at GeV and TeV energies: Cassiopeia A (Cas A, Abdo et al., 2010a; Albert et al., 2007a) and Tycho (Giordano et al., 2012; Acciari et al., 2011). Although I haven't contributed to the publications on these two SNRs, I will briefly summarize below the results obtained since they are of great interest in the context of cosmic-ray acceleration.
Cas A is the remnant of SN 1680. It is the brightest radio source in our Galaxy and its overall brightness across the electromagnetic spectrum makes it a unique laboratory for studying high-energy phenomena in SNRs. Although the TeV γ-ray observations can be interpreted by interactions of both accelerated electrons and protons/ions, the measurements by *Fermi*-LAT of a low-energy break in the spectrum at $1.72^{+1.35}_{-0.89}$ GeV give a preference to the hadronic origin of gamma rays (Yuan et al., 2013). Modeling the multi-wavelength data in the framework of a hadronic scenario, these authors concluded that the total proton content amounts to 4×10^{49} erg, which is less than 4% of the estimated explosion kinetic energy of a supernova. However, Zirakashvili et al. (2014) state that this claim is based on the high gas density derived from X-ray observations which was strongly overestimated because the non-thermal X-ray component was not properly taken into account. In the opposite, they find that the acceleration efficiency in Cas A should be very high and that, at present, 25% of the energy of supernova explosion is transferred into accelerated particles. Both models find anyway that the maximum energy of accelerated particles in Cas A is relatively low and cannot exceed 100 TeV. This was confirmed very recently by the MAGIC collaboration with the detection of a clear turn off (4.6σ) at the highest energies in the TeV spectrum, which can be described with an exponential cut-off at ~ 3.5 TeV (Ahnen et al., 2017). The authors concluded that the γ-ray emission from 60 MeV to 10 TeV can be attributed to a population of high-energy protons with spectral index ~ 2.2 and energy cut-off at ~ 12 TeV which directly indicates that Cas A is not contributing to the knee of the cosmic-ray sea in a significant manner at the present moment.

Tycho is certainly the best SNR to test the shock acceleration theory thanks to the large amount of data collected. It corresponds to the historical SN 1572 (so that its age is known), it is the remnant of a type-Ia explosion setting the SN energy to $\approx 10^{51}$ erg and the ejecta mass at about one solar mass. A distance of 2 – 4 kpc has been derived using both kinematic and echo-light measurements, implying

a circumstellar density of $\sim 0.3\,\mathrm{cm}^{-3}$. Using the precise radio and X-ray observations of this SNR, Morlino and Caprioli (2012) have shown that the magnetic field at the shock has to be > 200 μG to reproduce the data. Then, using multi-wavelength data, especially the GeV and TeV detections, they could infer that the γ-ray emission detected from Tycho cannot be of leptonic origin, but has to be due to accelerated protons (this result is consistent with another modeling proposed by Giordano et al., 2012). These protons are accelerated up to energies as large as ~ 500 TeV, with a total energy converted into CRs estimated to be about 12% of the forward shock bulk kinetic energy. However, the new and softer spectrum, down to 400 GeV thanks to the improved low energy sensitivity of VERITAS and deeper exposure, reported by Archambault et al. (2017), is now in clear tension with previous models, showing that this source needs to be investigated further at the light of these new data. Recently, Morlino and Blasi (2016) presented a multi-wavelength modeling of Tycho taking into account the presence of neutral atomic hydrogen in the acceleration region. They showed that the steep spectrum observed in Tycho can be well reproduced if the fraction of neutral hydrogen is $\sim 70\%$. According to this theory, the environment of the SNR would significantly influence the γ-ray spectrum below 1 TeV.

Two other Galactic SNRs are known to have similarly young ages but have not yet been detected in gamma rays. Kepler's SNR (SN 1604) is a type Ia or II-L SN (Chiotellis et al., 2012) with detected synchrotron X-rays. Detailed modeling predicts detectable gamma rays for existing observatories in both GeV and TeV regimes. However, the non-detection by H.E.S.S. may be explained if the distance is at least 6.4 kpc as suggested by hydrodynamical models (Patnaude et al., 2012), or the magnetic field behind the shock is greater than 52 μG (Aharonian et al., 2008a). SNR G1.9+0.3 has an age of 181$\pm$25 years estimated from proper motions, making it the youngest known Galactic SNR (De Horta et al., 2014). Interestingly, the parent SN was not visible since it has been obscured by the dense gas and dust of the Galactic Center. Synchrotron emission from G1.9+0.3 from radio and X-rays shows electrons with a power-law index of 2.27 and a roll-off frequency of $(3.07 \pm 0.18) \times 10^{17}$ Hz (Zoglauer et al., 2015). This implies that the maximum energy of accelerated particles is about 80 TeV for a magnetic field of about 10 μG. If the roll-off in the spectrum results from cooling and is not age limited, higher energies may be reached by nuclei. H.E.S.S. observations set an upper limit on the photon flux from this remnant of 5.6×10^{-13} cm^{-2} s^{-1} above 0.26 TeV, which in a one-zone leptonic scenario places a lower limit on the interior magnetic field of 12 μG (H.E.S.S. Collaboration et al., 2014b). Future γ-ray detection of either remnant will help to diversify the sample of young, active accelerators that can be studied.

3.3 Individual analysis of shell-type SNRs

Five young SNRs with clear shell-type morphology resolved in VHE gamma rays have been detected by H.E.S.S.: RX J1713.7$-$3946 (Aharonian et al., 2004), RX J0852.0$-$4622 - also known as Vela Junior - (Aharonian et al., 2007), RCW 86 (Aharonian et al., 2009), SN 1006 (Acero et al., 2010) and HESS J1731$-$347 (H.E.S.S. Collaboration et al., 2011a). Two of them, RX J1713.7$-$3946 (Abdo et al., 2011), Vela Junior (Tanaka et al., 2011) were detected early in the LAT mission. The three others were then detected during Benjamin Condon's thesis, allowing direct investigation of young shell-type SNRs as sources of CRs. The shell-type morphology of the γ-ray emission, which is associated with the SN blast wave, provides convincing evidence that DSA is the mechanism producing the high energy particles radiating at γ-ray energies. A critical issue for DSA, and for the origin of CRs, however, concerns the radiation mechanism responsible for the GeV$-$TeV emission: is it dominated

by π^0-decay emission from nuclei or IC emission from leptons ? Here again, I will focus on the results for which I contributed most, neglecting Vela Junior that was intensively studied during my PhD thesis. The GeV and TeV characteristics of this remnant is very similar to the four other shell-type SNRs. A general view of this type of source is provided at the end of this section.

3.3.1 Evidence of protons accelerated in RX J1713.7−3946 ?

RX J1713.7−3946 (also known as G347.3−0.5) is a young 'historical' remnant suggested by Wang et al. (1997) to be associated with the appearance of a guest star in the constellation of Scorpius in AD393. RX J1713.7−3946 is located in the Galactic plane (at a distance of 1 kpc) and was discovered in soft X-rays in 1996 in the ROSAT all-sky survey (Pfeffermann and Aschenbach, 1996b). In X-rays, RX J1713.7−3946 has a diameter of 1°, twice the size of the full moon. It is the first SNR for which TeV γ-ray emission was clearly detected emerging from the shell (Aharonian et al., 2004). The γ-ray emission as detected by H.E.S.S. and *Fermi*-LAT closely matches the non-thermal X-ray emission. Recently, the H.E.S.S. angular resolution, better than 0.05°, and the increased dataset of 150 hours of observation enabled for the first time a detailed investigation of morphological differences between TeV gamma-rays and X-rays. The broader radial profile seen in gamma rays in comparison to X-rays may be the first evidence of escape of protons that would emit gamma rays through proton-proton interactions when interacting with surrounding matter. Alternatively, regions of low magnetic field values could also be bright in gamma-rays while being rather faint in X-rays, explaining as well the differences between the γ-ray and X-ray detected signals (H. E. S. S. Collaboration et al., 2016a). The TeV spectrum of RX J1713.7−3946 is certainly the most precisely measured among the SNR shell class and shows significant emission up to ∼100 TeV, clearly demonstrating particle acceleration to beyond these energies in the shell of the SNR. However, the hard GeV spectrum measured by the early observations of the LAT (Abdo et al., 2011) is in contradiction with most hadronic models published so far and requires an unrealistically large density of the medium. Alternative and more complex hadronic scenarios have been recently introduced to fit the GeV-scale emission from RX J1713.7−3946, for instance the possibility of a shell of dense gas located a short distance upstream of the forward shock that would be illuminated by the runaway CRs that have escaped from the shock and by the CR precursor to the forward shock (for more details see Federici et al., 2015). In leptonic scenarios, the agreement with the expected IC spectrum is better but requires a very low magnetic field of ~ 10 μG in comparison to the value of ~ 100 μG measured in the thin filaments with X-ray observations (Parizot et al., 2006). It is possible to reconcile a high magnetic field with the leptonic model if GeV gamma rays are radiated not only from the filamentary structures seen by Chandra, but also from other regions in the SNR where the magnetic field may be weaker. All these characteristics clearly show that most constraints on the acceleration mechanisms come from the GeV energy domain covered by the LAT. This is why we started a new analysis of this remnant using the latest LAT Pass 8 data with my PhD student Benjamin Condon.

Fermi-LAT analysis of the entire remnant

In this work, we analyzed 7.5 years of Pass 8 data collected between August 4^{th} 2008 and February 19^{th} 2016, in the energy range 200 MeV – 2 TeV. To allow a very precise measurement, we took advantage of the possibility to split all γ-ray events into four types (PSF0, PSF1, PSF2, PSF3) according to the quality of their reconstruction (PSF0 is formed by the 25% lowest quality events while PSF3 corresponds to the 25% best quality events). We optimized the event selection along the energy

range: between 200 MeV and 1 GeV, PSF0 events were rejected to improve the global angular resolution. Moreover the cut on the maximum zenith angle was more drastic at low energy ($z_{max} = 90°$) than above 1 GeV ($z_{max} = 105°$) to avoid any contamination from the Earth Limb without rejecting good events. Finally the time intervals when the *Fermi* spacecraft was within the South Atlantic Anomaly were excluded to assure good quality events. The spectral analysis is then done using the Summed Likelihood function from $gtlike$ which can perform a joint likelihood fit where each PSF type is loaded separately with its corresponding Instrument response function (IRF) and thus avoiding to mix well-reconstructed events with low quality events. The best fit is obtained for a log-parabola or a smoothly broken power-law (SBPL). Since the latter is in better agreement with the TeV data (see Figure 3.1), we based our discussion on this model. The second index of the SBPL function was fixed at 2.0 to reduce the number of degrees of freedom without degrading the likelihood of the fit. This value was motivated by the shape of the γ-ray spectrum between 100 GeV and 1 TeV. When fitting Γ_2, we obtained $\Gamma_2 = 1.97 \pm 0.11_{\rm stat} \pm 0.05_{\rm syst}$, confirming our educated guess.

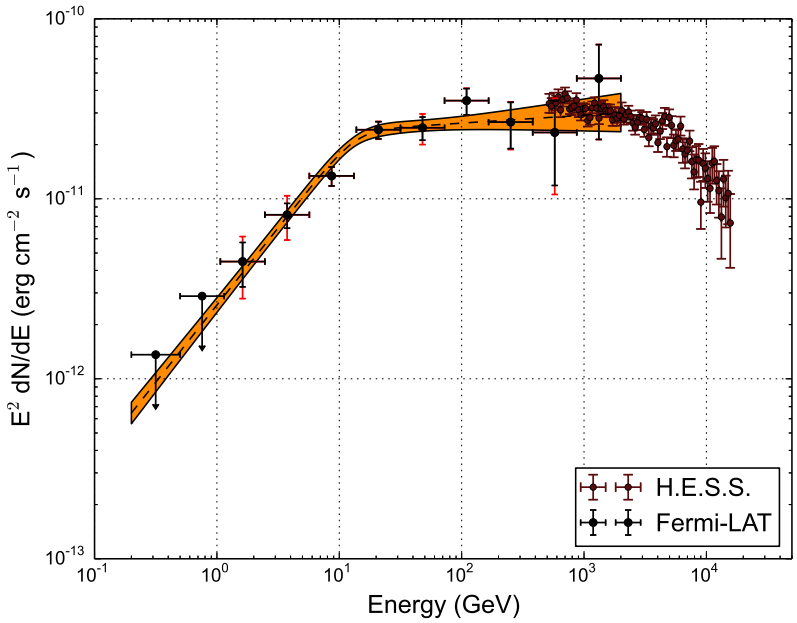

Figure 3.1: *Spectral Energy Distribution of the γ-ray emission of RX J1713.7−3946 measured between 200 MeV and 2 TeV with Fermi-LAT spectral points in black. TeV spectral points (red) are from H. E. S. S. Collaboration et al. (2016a). The orange shaded area represent statistical uncertainties of the smoothly broken power-law fit.*

Looking at the SED, we can clearly see the evolution of the γ-ray emission in the GeV band: a hard spectrum at low energy with an index of $1.13 \pm 0.23_{\rm stat} \pm 0.20_{\rm syst}$, then a break at $14 \pm 7_{\rm stat} \pm 4_{\rm syst}$ GeV followed by a flat spectrum ($\Gamma = 2.0$) which goes up to 2 TeV, towards the H.E.S.S. data. Thanks to the improved acceptance at high energy gained with Pass 8, *Fermi*-LAT detects significant γ-ray emission up to 2 TeV (TS[1] ~ 15 for the bin 1.5 - 2 TeV) and allows a complete overlap with TeV data. The break seen in the γ-ray spectrum directly implies that a break also exists in the particle population responsible for this emission (namely electrons or protons) at ~ 500 GeV. In the leptonic

[1]The test statistic is defined as $\mathrm{TS} = 2(\ln \mathcal{L}_1 - \ln \mathcal{L}_0)$, where $\mathcal{L}_0$ and $\mathcal{L}_1$ are the likelihoods of the background (null hypothesis) and the hypothesis being tested (source plus background).

scenario, a break in the electron spectrum could be due to synchrotron losses: electrons at higher energies suffer faster synchrotron cooling and therefore a break is introduced at the energy for which the synchrotron loss timescale and SNR age are equal. Considering an SNR age of the order of 2000 yr, a magnetic field of $\sim$ 100 μG is needed to create a break at 500 GeV, following the relation $E_b \simeq 1.25 \left(\frac{B}{100\ \mu\mathrm{G}}\right)^{-2} \left(\frac{t}{10^3\ \mathrm{yr}}\right)^{-1}$ TeV. However, the simultaneous fitting of X-ray and γ-ray data of the whole SNR in such leptonic scenario indicate a present-age average magnetic field strength of $B = 14.3 \pm 0.2$ μG for the SNR, which is much less than the 100 μG required to explain the energy break. More sophisticated modeling, taking into account the evolution of the magnetic field (which is higher at early time of the SNR evolution), is thus needed. In a hadronic scenario, a break could result from the diffusion of protons in high-density cold clumps within the SNR: higher energy protons diffuse faster and interact with the highest density regions within the clumps, whereas lower energy protons only probe the outer, lower density regions and therefore have a lower emissivity. This scenario would arise from a massive star exploding in a molecular cloud that itself has been swept away by a wind of the progenitor star, resulting in a rarefied cavity with dense clumps. The break energy depends on the age of the SNR and the density profile of the clouds (Gabici and Aharonian, 2014). However, such models concentrate on the spectral aspects of the result and the correlation between X-ray and γ-ray emission, as well as the significant signal in regions of very low density, are not modeled yet. It is clear now that one-zone models are much too simple to model this remnant and that mixed models (hadronic + leptonic) are needed to reproduce the multi-wavelength data. Another argument in favor of such complex models was brought by the detection of a significant improvement of the likelihood (at more than 3σ level) when dividing RX J1713.7−3946 into two halves for the fit.

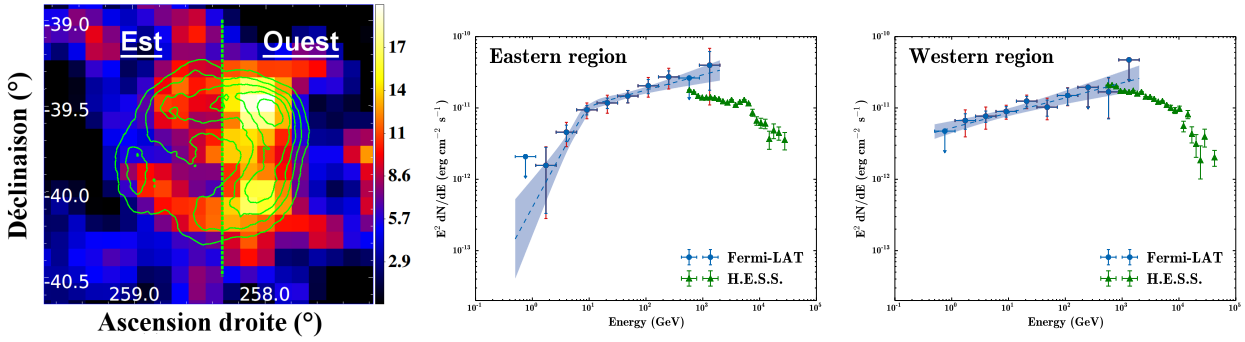

Figure 3.2: *Left:* Fermi-*LAT counts map of RX J1713.7−3946 with the H.E.S.S. contours superimposed together with the division axis. Spectral Energy-Dependent Distribution of the Eastern (Middle) and Western (Right) regions of RX J1713.7−3946. LAT spectral points are in blue while red points correspond to H.E.S.S. (H. E. S. S. Collaboration et al., 2016a).*

Fermi-LAT analysis of the Western and Eastern regions of the remnant

For this analysis, we divided the H.E.S.S. template from North to South, such that the Western side is located in a dense region close to the Galactic plane, and the Eastern region is located in a tenuous medium as presented in Figure 3.2 a). To improve the angular resolution of our dataset and minimize the contamination due to photons leaking from one region to another, we decided to use only photons above 500 MeV. In addition, since the spectrum of the entire remnant is described by a smoothly broken power-law (SBPL), we tried both the power-law (PL) and the SBPL for each region. The best fit is obtained for a SBPL for region East and a simple PL for region West. The significance

of the break in region East is detected at 4.3σ level. The best parameters are ($\Gamma_1 = 0.32 \pm 0.08$, $\Gamma_2 = 1.80 \pm 0.07$ and $E_\mathrm{b} = 9 \pm 2$ GeV) for the Eastern region and ($\Gamma = 1.82 \pm 0.04$) for region West. As can be seen in Figure 3.2 b) and c), the spectrum of the Eastern is similar to the spectrum of the entire SNR, while the difference between the Eastern and Western spectra mainly comes from the low energy domain. This points towards an additional particle population in the Western side at low energy to explain the spectral difference. Proton-proton interaction occurring in the dense Western region could play a significant role.

To confirm such hypothesis, we tried to model the multi-wavelength data of the Eastern and Western regions of the SNR within two different scenarios: a leptonic-dominated scenario (power-law or smoothly broken power-law for the Western region) and a hadronic-dominated scenario. The model used was first developed during my PhD thesis at LLR and was then improved during the three PhD theses that I supervised: Marie-Helene Grondin, Romain Rousseau (both focusing on a modification to fit PWNe) and Benjamin Condon. The values of the parameters are reported in Table 3.1 while our results are presented in Figures 3.3 and 3.4. It is not a suprise that the parameters for the Eastern region are very close to those obtained for the whole SNR since the γ-ray spectra are very similar: for a hadronic scenario, one needs a dense medium (in contradiction with the lack of thermal X-rays) while the leptonic scenario requires a low density (~ 0.1 cm^{-3}) and a low magnetic field value (14 μG in contradiction with the spectral break detected by the LAT). For the Western region, again a dense medium is required in a hadronic scenario but it is the only one able to reproduce the radio data simultaneously with the high flux detected at low energy by the LAT. However, no firm conclusion can be reached for the moment since these models are far too simple. In addition, RX J1713.7$-$3946 is a faint radio emitter and the flux estimate in the radio band suffers large systematics. Future observations, especially with CTA, should be able to confirm such scenario. These results are being written in a Category II *Fermi* paper under preparation and were presented at the last *Fermi* symposium.

Model	Γ_e	$E_\mathrm{b,e}$ (TeV)	$E_\mathrm{max,e}$ (TeV)	W_e (erg)	Γ_p	$E_\mathrm{b,p}$ (TeV)	$E_\mathrm{max,p}$ (TeV)	W_p (erg)	B (μG)	n (cm^{-3})
East $-$ 1	1.5 / 2.7	0.5	150	1.8×10^{47}	2.0	–	150	1.8×10^{49}	14.0	0.1
East $-$ 2	2.0	–	50	1.0×10^{47}	1.5 / 2.3	1.0	100	1.0×10^{49}	16.0	4.0
West $-$ 1	2.2	–	60	1.6×10^{47}	2.2	–	60	1.6×10^{49}	15.0	0.1
West $-$ 2	1.8 / 2.5	0.5	150	2.6×10^{47}	2.0	–	150	2.6×10^{49}	12.0	0.1
West $-$ 3	1.9	–	50	5.0×10^{46}	1.9	–	100	1.0×10^{49}	25.0	5.0

Table 3.1: *Values of the parameters for the models of regions East and West of RX J1713.7$-$3946. $\Gamma_\mathrm{e,p}$ is the spectral index for the injection of electrons and protons, $E_\mathrm{b,e,p}$ is the spectral break energy in the electron or proton spectrum, $E_\mathrm{max,e,p}$ is the maximum energy of the electron and proton distribution, $W_\mathrm{e,p}$ is the total energy injected in electrons or protons, B is the magnetic field in the source and n is the density of the medium.*

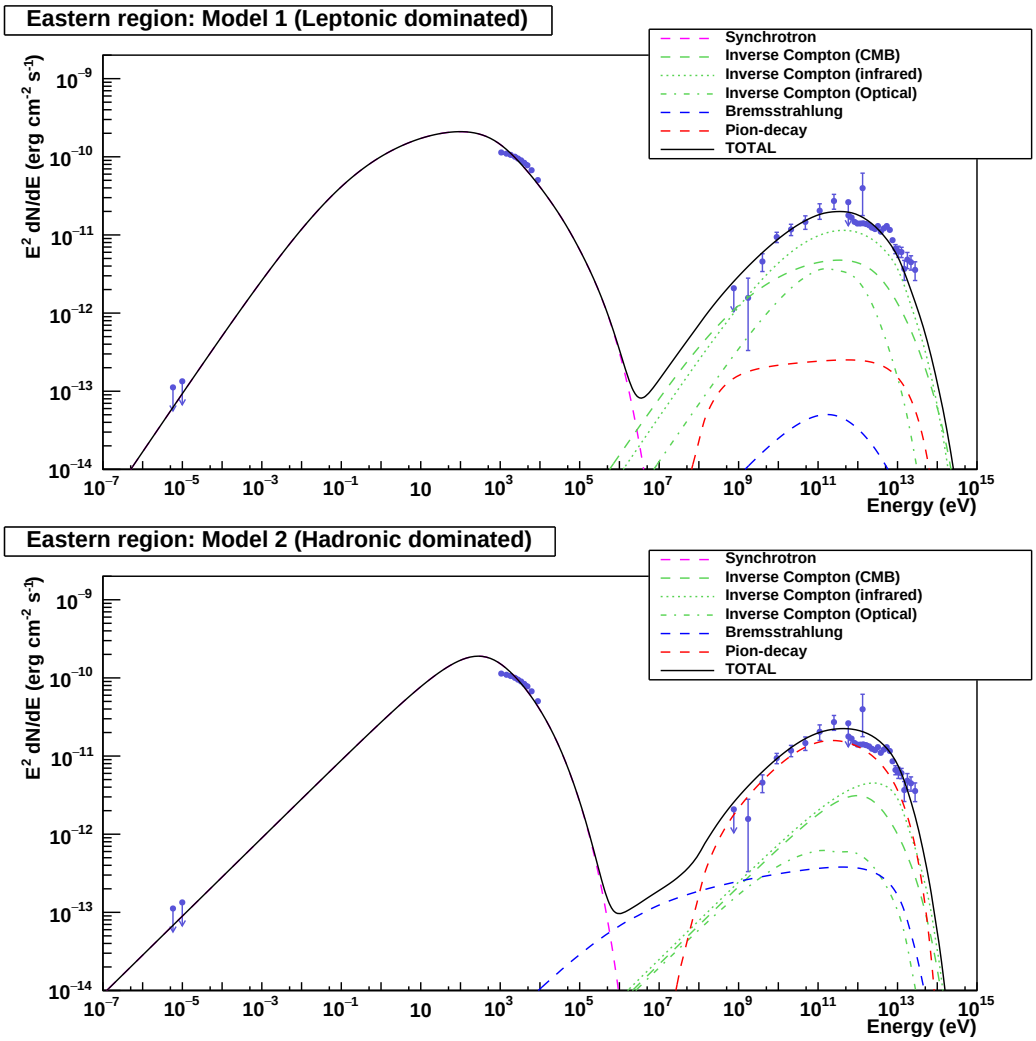

Figure 3.3: *Modeling of the multi-wavelength data from the Eastern region of RX J1713.7−3946. Values of the parameters are reported in Table 3.1.*

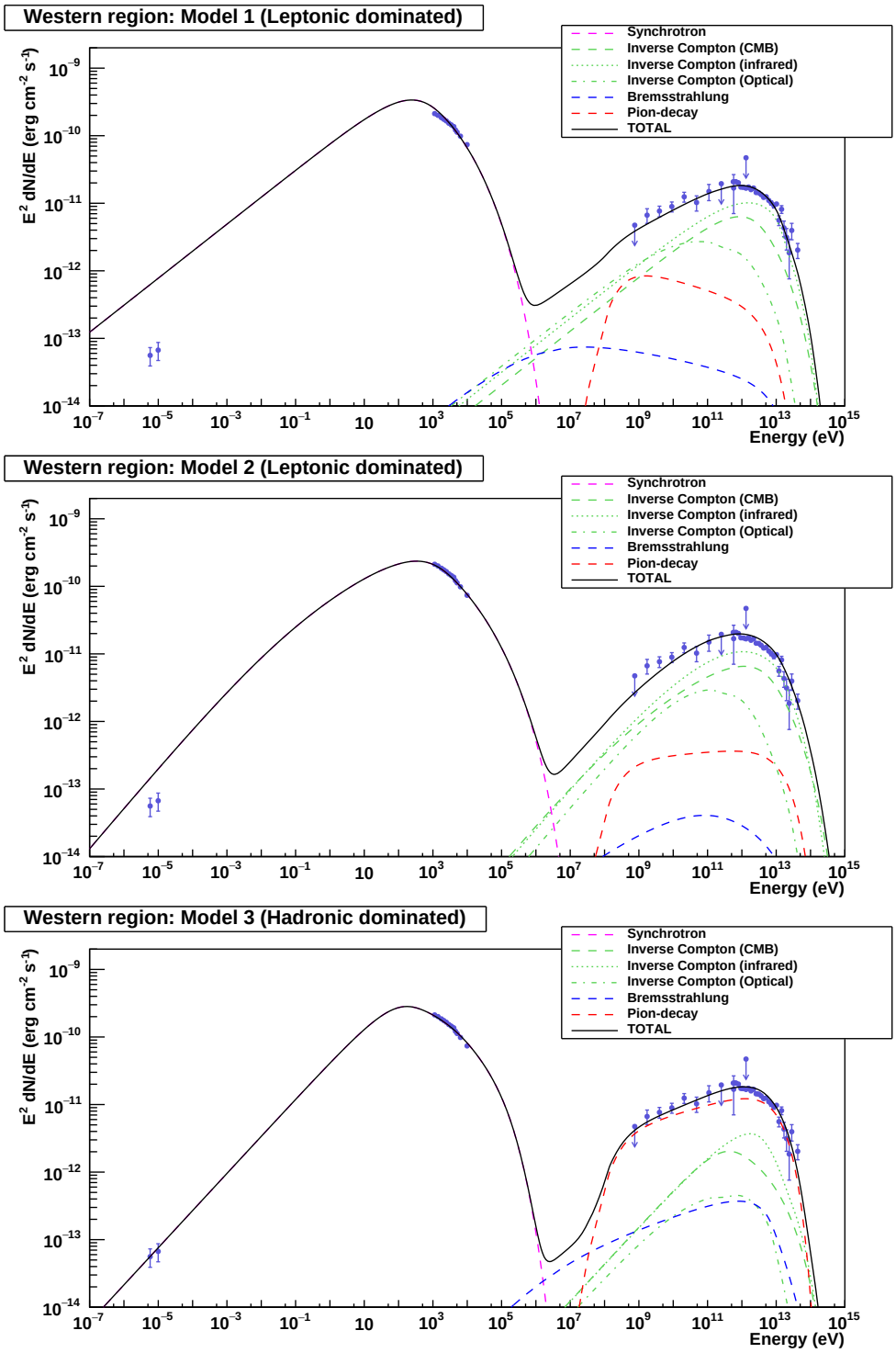

Figure 3.4: *Modeling of the multi-wavelength data from the Western region of RX J1713.7−3946. Values of the parameters are reported in Table 3.1.*

3.3.2 Two-particle populations in RCW 86

Early observations of RCW 86

Before the launch of GLAST, I worked intensively on the H.E.S.S. data of the shell-type SNR RCW 86 and was corresponding author of the H.E.S.S. paper reporting the discovery of γ-ray emission from this remnant using 31 hours of observation time (Aharonian et al., 2009). At this time, the morphological study did not allow to show that the emission was coming from the shell but additional observation time made this possible recently (H. E. S. S. Collaboration et al., 2016d). This new study also revealed that the TeV emission and the high-energy X-ray emission (2 – 5 keV) are correlated throughout the remnant, whereas radio and low-energy X-ray emission regions are further away from the center and show lower levels of emission in the central region of the remnant. This could point towards two-particle populations emitting the radio and low-energy X-ray with respect to the high-energy X-ray and γ-ray signals. For instance, some of the VHE γ-ray emission could come from the region shocked by the reverse shock. A possible hint for this is provided by the more centrally filled morphology of the VHE γ-ray emission with respect to the radio emission. In addition, the high-energy X-ray emission is spatially near to a Fe-K line. Rho et al. (2002) argued that the hard X-ray continuum is synchrotron radiation produced by electrons, which are accelerated in the reverse shock.
To constrain the emission mechanisms taking place in this remnant, I conducted a first analysis of 40 months of Pass 7 LAT data above 100 MeV (Lemoine-Goumard et al., 2012). No significant γ-ray emission in the direction of RCW 86 was detected in any of the 0.1–1, 1–10 and 10–100 GeV *Fermi*-LAT maps. This work was completed by Matthieu Renaud's re-analysis of archival X-ray data from the ASCA/Gas Imaging Spectrometer (GIS), the XMM-Newton/EPIC-MOS, and the RXTE/Proportional Counter Array (PCA) in order to gather all multi-wavelength data needed for the modeling. Our modeling used the same model developed during my PhD thesis in a one-zone hypothesis and two-zone hypothesis (justified by the absence of correlation between the radio and γ-ray data). The derived High energy (HE) upper limits, together with the H.E.S.S. measurements in the VHE domain, were incompatible with a standard E_p^{-2} hadronic emission arising from proton-proton interactions, and could only be accommodated by a spectral index $\Gamma \leq 1.8$, i.e. a value in-between the standard (test-particle) index and the asymptotic limit of theoretical particle spectra in the case of strongly modified shocks. In such a hadronic scenario, the total energy in accelerated particles is at the level of $\eta_{CR} = E_{CR}/E_{SN} \sim 7\%$ (assuming a distance of 2.5 kpc and an effective density of 1 cm^{-3}), and the average magnetic field must be stronger than 50 μG in order to significantly suppress any leptonic contribution. On the other hand, the interpretation of the γ-ray emission by inverse Compton scattering of high energy electrons reproduced the multi-wavelength data using a reasonable value for the average magnetic field of 15–25 μG. In this leptonic scenario, we derived a conservative upper limit to η_{CR} of 4%.

Pass 8 analysis of the whole remnant

The increased performance allowed by Pass 8 is very well highlighted by the case of RCW 86. Indeed, during Benjamin Condon's thesis, 6.5 years of Pass 8 LAT data were analyzed allowing both the detection of RCW 86 and a significant extension measure from this remnant at γ-ray energies (Ajello et al., 2016). The morphological study performed in our *Fermi* paper shows the same trend reported at TeV energies, namely that the LAT data correlate well with the high-energy X-ray emission (and with the TeV data) but poorly with the radio and low-energy X-ray data as can be seen

in Figure 3.5. The spectrum is described by a power-law function with a very hard photon index ($\Gamma = 1.42 \pm 0.1_{\rm stat} \pm 0.06_{\rm syst}$) in the 0.1–500 GeV range and an energy flux above 100 MeV of $(2.91 \pm 0.8_{\rm stat} \pm 0.12_{\rm syst}) \times 10^{-11}$ erg cm^{-2} s^{-1}. We also performed several fits while fixing the index of the power law at different values: 1.5, 1.6, 1.7 and 1.8. In each case, we measured the deterioration of the log-likelihood by computing the difference between the TS of the best-fit and the TS obtained with the fixed index. As a result, we excluded $\Gamma > 1.7$ at more than 3σ.

To investigate the characteristics of the surrounding gas, we have worked with Gloria Dubner (University of Buenos Aires, Argentina) who analyzed the cold neutral gas in the environs of RCW 86. To carry out this search she used data at $\lambda = 21$ cm acquired with the Australia Telescope Compact Array (ATCA) on 2002 March 24. To recover the missing short spatial frequencies, the ATCA data were combined in the u–v plane with single dish observations performed with the Parkes radio telescope. These data revealed the presence of an elongated cavity, about 1.5° in size, that runs almost parallel to the Galactic plane, in the velocity interval between ~ -38 km s^{-1} and ~ -32 km s^{-1} (all velocities are referred to the Local Standard of Rest, LSR). Within this velocity range, more precisely between ~ -35 km s^{-1} and ~ -33 km s^{-1} the SNR appears surrounded by a tenuous, approximately circular HI shell with variable brightness distribution. These morphological findings are in very good agreement with the predictions made on the basis of radio continuum, X-rays, infrared observations and hydrodynamic simulations (Williams et al., 2011; Broersen et al., 2014). After applying a circular rotation model for our Galaxy for $l = 315.4^\circ$, $b = -2.3^\circ$, the LSR radial velocity interval of the observed features translates into a distance of $\sim 2.5 \pm 0.3$ kpc. This distance is in very good agreement with that previously obtained for RCW 86 on the basis of optical measurements of proper motions of the filaments (Rosado et al., 1996), suggesting that this gas is placed at the same distance as RCW 86. The HI observations can be used to carry out independent estimates of the volume density of the SNR environs. We considered four regions corresponding to the four quadrants of two concentric circles traced with inner and outer radii coincident with the radio shell. For region 1 (NW quadrant) $n_{\rm H} \sim 1.5$ cm^{-3}; for region 2 (NE quadrant) $n_{\rm H} \sim 1$ cm^{-3}; for region 3 (SE quadrant) $n_{\rm H} \sim 1$ cm^{-3} and for region 4 (SW quadrant) $n_{\rm H} \sim 1.2$ cm^{-3}. In all cases the intrinsic error of the quoted numbers is of about 30% taking into account the uncertainty in the distance and the approximate background subtraction. For the interior of the SNR we estimated $n_{\rm H} \sim 0.5$ cm^{-3}. These results show that the assumed density of 1 cm^{-3} is a good average estimate for the entire remnant. However, one should note that the ambient density around RCW 86 is known to be rather inhomogeneous and the shock speed value, as well as the magnetic field, change along the shell-like structure. In particular, in the southwest and northwest regions shocks are slow, around ∼600–800 km s^{-1} (Long and Blair, 1990), and post-shock densities are relatively high ($\sim$ 2 cm^{-3}; Williams et al. (2011)). Whereas, faster shocks (∼2700 km $^{-1}$ and 6000 $\pm$ 2800 km $^{-1}$; Vink et al. (2006); Helder et al. (2009)) and lower densities (~ 0.3 cm^{-3}; Yamaguchi et al. (2008)) have been measured in the north-east (NE) region. It was even proposed by Williams et al. (2011) that RCW 86 would be a Type Ia supernova in a wind-blown bubble. The fast shocks observed in the NE are propagating in the low-density bubble, where the shock is just beginning to encounter the shell, while the slower shocks elsewhere have already encountered the bubble wall. The large systematic error on our measurement and the large size of the regions analyzed did not allow us to reach such precision and see a significant density gradient as it has been done in infra-red.

Then, we used all the multi-wavelength data gathered for our previous publication and performed a broadband modeling of the non-thermal emission of RCW 86. For the whole SNR, a pure hadronic scenario requires unlikely parameter values such as a very hard spectral index for protons (spectral index harder than 1.7) and a very high value of the magnetic field. Therefore, we did not consider this case. In the framework of a leptonic scenario, the radio points in the one-zone model imply a soft

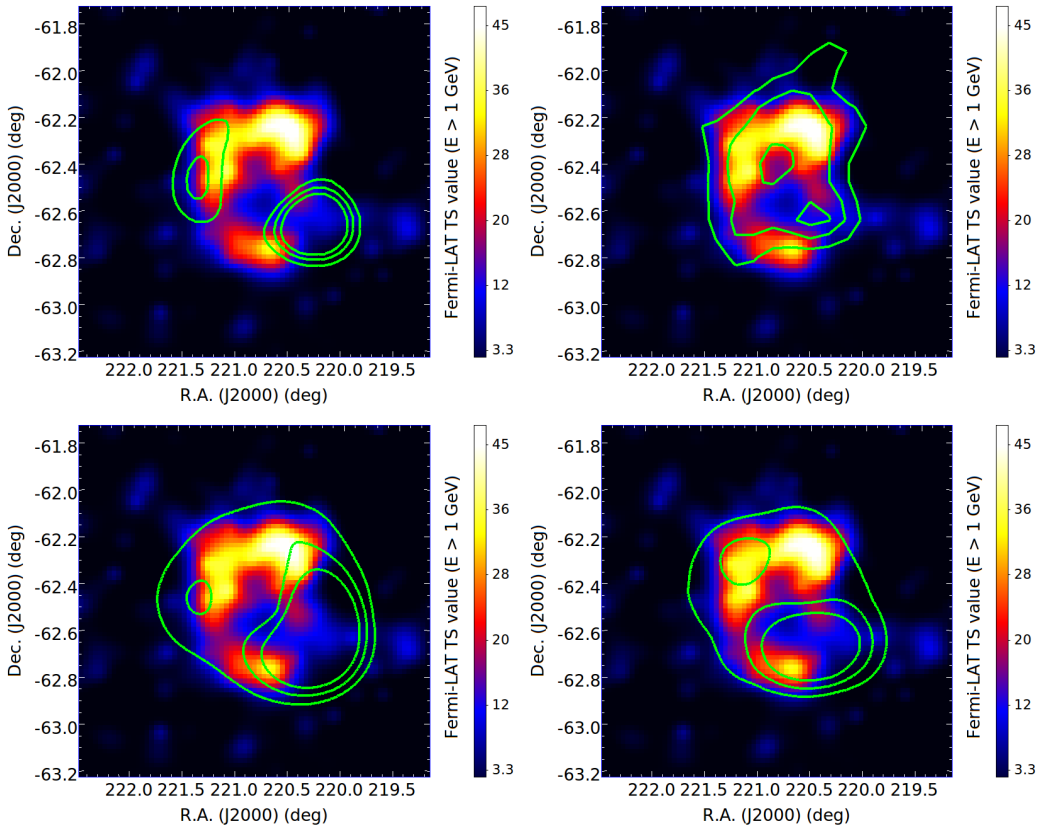

Figure 3.5: *Test Statistic (TS) map above 1 GeV centered on RCW 86 with MWL contours. All data sets have been smoothed such that their angular resolution is similar to the Fermi-LAT PSF (0.27° at 68% C.L.). The radio (top-left), TeV (top-right), thermal (bottom-left) and non-thermal (bottom-right) X-ray data are from Murphy et al. (2007), H. E. S. S. Collaboration et al. (2016d) and Broersen et al. (2014) respectively.*

spectral index (~ 2.4) which would lead to a very strong bremsstrahlung component below 1 GeV. To reconcile this low energy component with the new *Fermi*-LAT upper limit at 1 GeV, a maximum density of 0.1 cm^{-3} needs to be assumed which is in contradiction with our study of the ISM with the ATCA data. Therefore, the modeling favors a leptonic scenario in the framework of a two-zone model with an average magnetic field of 10.2 ± 0.7 μG and a limit on the maximum energy injected into protons of 2×10^{49} erg for a density of 1 cm^{-3} (the parameters are summarized in Table 3.2).

Pass 8 analysis of individual regions

The absence of correlation between the radio/low-energy X-ray data and the γ-ray data (both at GeV and TeV) and the preference of a two-zone model to reproduce the multi-wavelength data points towards a more complex modeling and possible spectral variations throughout the remnant. Therefore, we decided to study the spectrum of the two specific areas that were defined in H. E. S. S. Collaboration et al. (2016d). The NE and SW quadrants were fitted in two different fits. For each quadrant we subtracted it from the rest of the disk and fitted both the quadrant and the complementary region simultaneously. The analysis of the *Fermi*-LAT data revealed significant γ-ray emission at $\sim 4.7\sigma$ ($TS = 22$) in the NE region but no signal was detected in the SW region ($TS < 3$). The spectrum of the NE signal is well-fitted by a power law function with a hard index of 1.33 ± 0.20 and an energy flux of $(1.2 \pm 0.5_{\rm stat}) \times 10^{-11}$ erg cm^{-2} s^{-1} and we derived a 95% C.L. upper limit for the SW region

(1.09×10^{-12} erg cm^{-2} s^{-1}). Then, we worked together with Dave Green from Cambridge University to estimate the radio flux from these two quadrants using the Parkes survey observations at 2.4 GHz from Duncan et al. (1995), which gives 4.3 Jy in the NE quadrant and 10.4 Jy in the SW quadrant. Finally, to estimate the non-thermal X-ray emission from the NE and SW regions of RCW 86, we worked with Jacco Vink from the Anton Pannekoek Institute at the University of Amsterdam who analyzed the spectra of these two regions using data of the EPIC-MOS2 instrument of XMM-Newton. From the best fit models we obtained the non-thermal fluxes in the 3–5 keV band, which for RCW 86 is totally dominated by synchrotron emission. The fluxes are estimated to be 10.0×10^{-12} erg cm^{-2} s^{-1} and 4.3×10^{-12} erg cm^{-2} s^{-1} for the SW and NE regions, respectively. The flux measurements have errors of the order of 5%–10%, mostly dominated by systematic errors, as absolute flux calibration of X-ray instruments is accurate at the 5% level. For both regions, the power law index is measured to be 3.0 ± 0.2. For our modeling, to limit the number of fitted parameters, the density was assumed to be of 1.0 cm^{-3} for both regions (which is in agreement with the values derived in our study of the ISM). We also decided to use the best index previously obtained for the whole remnant, in the case of a two-zone model, ($\Gamma = 2.21$) and fixed it for both electron and proton distributions for the two regions, since there is no evidence in favor of different injection slopes in the remnant. Results are shown in Figure 3.6 and Table 3.2 summarizes the parameters for the two models, obtained with a χ^2 fit. We note that, in our modeling, the magnetic field is slightly higher in the SW than in the NE, implying a magnetic field gradient in a direction away from the Galactic plane possibly due to the shock interaction with a denser medium. Moreover, $E_{\rm max}$ is also higher in the SW than in the NE which is in agreement with the values of the magnetic field: at early times, when the maximum energy is not limited by synchrotron losses, a higher magnetic field implies a higher $E_{\rm max}$. Overall, our model suggests that variations of the magnetic field exist within the SNR. The radio emission corresponds to regions with high magnetic fields whereas the GeV emission detected by *Fermi*-LAT corresponds to regions with mixed magnetic fields. And since the H.E.S.S. map shows brighter emission coming from the inside of the remnant than in radio and X-rays, the reverse shock could also be responsible for the CR acceleration but with a lower magnetic field. However, this model uses a strong assumption: the same index is used for the electron distribution in both regions. Recently, new studies have shown that the presence of neutral hydrogen in the shock proximity changes the structure of the shock and affects the spectra of particles accelerated through the first-order Fermi mechanism (Morlino and Blasi, 2016). For Tycho, these authors concluded that spectra of accelerated protons steeper than E^{-2} may be a natural consequence of charge exchange reactions (see Section 3.2). It could well be the case for RCW 86, especially in the South-West region where the shock is starting to encounter a denser medium of ~ 2 cm^{-3}. The absence of detection by *Fermi*-LAT does not allow us to constrain the injection spectrum in this region and future observations with CTA (Cherenkov Telescope Array Consortium et al., 2017) would be very useful. Observations with *Athena+* (Barcons et al., 2017) could also help constrain the magnetic field and provide a precise map of its fluctuation at smaller scales.

Table 3.2: *Values of the parameters for the different modelings of the broadband spectrum of RCW 86. Convention for the names are the same as in Table 3.1.* K_{ep} *is the electron-to-proton ratio.*

Parameters	Whole remnant			Regions	
	One-zone	Two-zone		NE	SW
		Radio	X-ray		
Density (cm^{-3})	0.1	1.0	1.0	1.0	1.0
B (μG)	10.2 ± 0.5	24	10.5 ± 0.7	11.6 ± 0.7	16.8 ± 2.1
$\Gamma_{e,p}$	2.37 ± 0.03	2.2	2.21 ± 0.1	2.21	2.21
E_{max} (TeV)	75 ± 5	2	67 ± 4	40 ± 5	61 ± 5
W_e (10^{49} erg)	3.84 ± 0.5	0.03	0.37 ± 0.02	0.14 ± 0.04	0.16 ± 0.04
W_p (10^{49} erg)	2	-	2	0.5	0.5
K_{ep} ($\times 10^{-2}$)	11.1 ± 1.5	-	13.6 ± 0.5	5.2 ± 1.5	5.9 ± 1.5

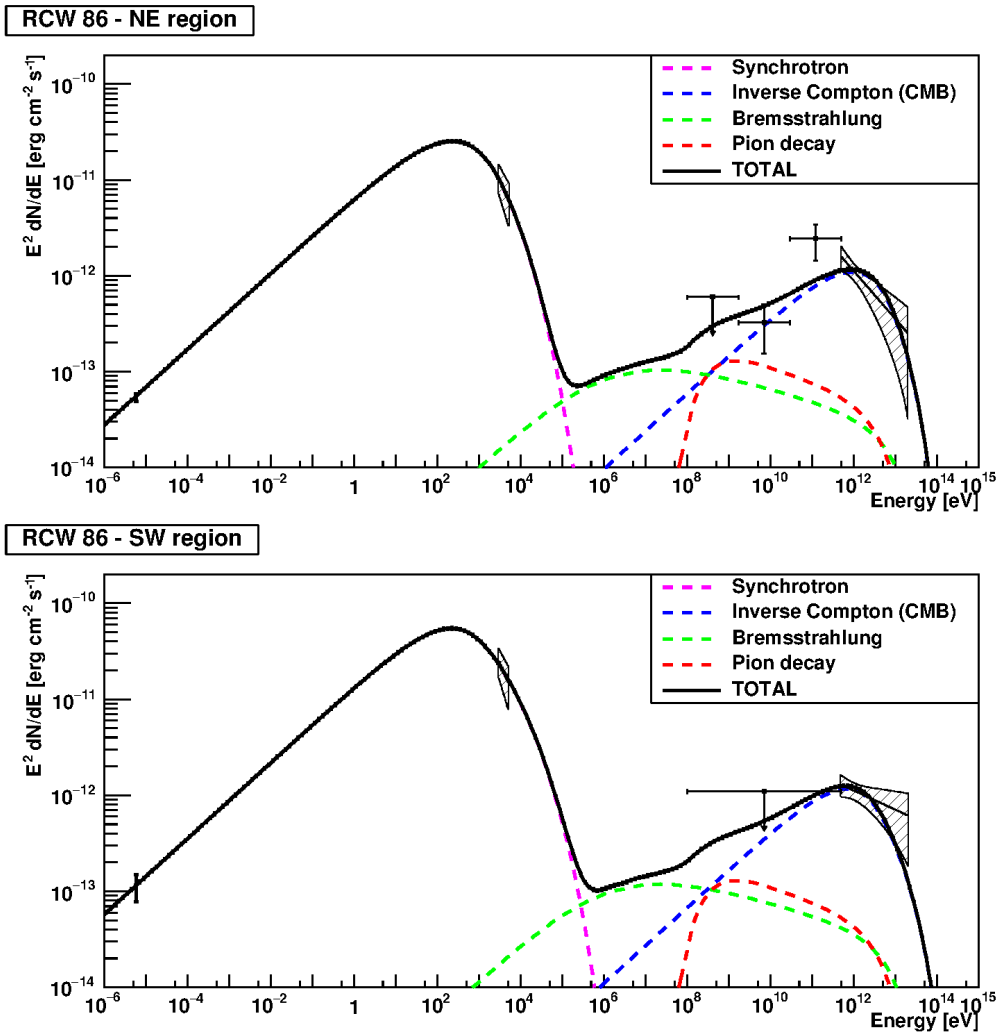

Figure 3.6: *SED modeling for the NE (top) and SW (bottom) regions of RCW 86. The radio fluxes were derived from Parkes observations at 2.4 GHz, the X-ray fluxes are estimated using XMM-Newton/MOS data and the TeV points are from H. E. S. S. Collaboration et al. (2016d).*

3.3.3 Detection of SN 1006 and HESS J1731−347 at GeV energies

The exciting results obtained on RCW 86 were largely due to the performance of Pass 8 since no significant signal was seen previously with Pass 7. I realized that the same could be occurring as well for the two TeV shell-type SNRs still undetected at GeV energies: SN 1006 and HESS J1731−347. Indeed, using 6 years of Fermi P7 reprocessed data, Fabio Acero and I studied the HE counterpart of the SNRs HESS J1731-347 and SN 1006 in 2014. In our analysis, the two SNRs remained not detected and we derived upper limits that significantly constrain the γ-ray emission mechanism, ruling out a standard hadronic scenario (E^{-2}) with a confidence level > 5σ (Acero et al., 2015). Then, two years later, a quick analysis of SN 1006 as a point-like source reported first evidence of γ-ray emission with $\sim 4\sigma$ significance using the public release of Pass 8 (Xing et al., 2016). Therefore, we started a re-analysis of this region trying to take advantage of the analysis methods adapted for extended sources that we use in Bordeaux. Both sources were studied in the same conditions (identical data selection and analysis methods). For this work, we analyzed 8 years (August $4^{\rm th}$ 2008 − August $28^{\rm th}$ 2016) of LAT Pass 8 data (Atwood et al., 2013), selecting photons with a reconstructed energy between 1 GeV and 2 TeV in order to lower the contamination from the Galactic diffuse background, which is crucial for HESS J1731−347. We also rejected events with zenith angle greater than 100° to reduce the contamination from the Earth limb.

The TeV detected remnant HESS J1731−347

HESS J1731−347 is located in a complex region, close to the Galactic plane and the Galactic center. In the $10^\circ \times 10^\circ$ region, seventeen sources were detected with a TS higher than 25 and thus added to the model in addition to the sources from the *Fermi* Third Source Catalog ! To avoid any contamination, we also took into account an excess (called 'S0') with a TS of only 22 because of its position, very close to the SNR. Figure 3.7 (left) shows the $2^\circ \times 2^\circ$ TS map centered on the position of HESS J1731−347. In this case, S0 was not included in the model in order to show its corresponding γ-ray emission. The analysis and discussion concerning S0 is done in Section 4.2.3. The γ-ray excess detected by *Fermi* was first fitted as a point source and then as a uniform disk. Their positions are represented in Figure 3.7 (left) by the black cross and the green circle, respectively, and the precise value of each parameter can be found in Table 3.3. In the case of a uniform disk, we obtained a radius of $0.15^\circ \pm 0.04^\circ$ and a $\mathrm{TS_{ext}}$ value of 6.3, indicating that the source is not detected as extended. If the search for an extension of the source is performed above 10 GeV, the analysis yields a $\mathrm{TS_{ext}}$ of 7.2 and a larger radius ($0.21^\circ \pm 0.03^\circ$, see left panel of Figure 3.7). Although it is still not significant, it indicates that the source is probably extended and that we are only limited by low statistics. After having determined the best spatial parameters of the geometrical models, we performed an unbinned likelihood analysis with `gtlike` for various morphologies. The fit between 1 GeV and 2 TeV yields a TS value of 25.2, 31.5 and 25.1 for the point source, the disk and the H.E.S.S. template, respectively. The γ-ray excess found by *Fermi* at the position of HESS J1731−347 is therefore significant, whatever the assumed shape. Using alternative diffuse emission models also resulted in TS > 25. Regarding the spectral index, the fit yields $\Gamma = 1.87$, $\Gamma = 1.71$ and $\Gamma = 1.66$ respectively, with an error of $\pm 0.16_{\rm stat} \pm 0.12_{\rm syst}$. Although consistent within errors, the spectral index seems to harden when the spatial model gets larger. This is likely due to the presence of high-energy photons located in the shell region that are taken into account by the TeV template but not in the hypothesis of a point source. Spectral results are summarized in Table 3.3. Assuming a connection between the GeV emission and HESS J1731−347, the SED was derived using the H.E.S.S. template. By doing so, we are also able to compare directly the GeV spectral points with the TeV data. The hypothesis that the GeV

emission is correctly described by the H.E.S.S. template can be considered since the likelihood was not significantly degraded when using the H.E.S.S. template in comparison to the point source or disk hypothesis. As shown in the right panel of Figure 3.7, the LAT data (blue points) match very well the TeV data (green triangles), supporting our assumption that the γ-ray excess detected by the LAT is the GeV counterpart of HESS J1731$-$347. The hard index obtained in the GeV band ($\Gamma \sim 1.66$) is very similar to the results obtained above for RX J1713.7$-$3946 and RCW 86 for which a leptonic scenario was suggested. Our results (together with SN 1006 discussed below) are published in Condon et al. (2017).

In 2013, I have been invited to give a review talk on "Gamma-ray observations of supernova remnants" at the IAU Symposium held at Kolkata in India. There, I met Professor Alak Ray and Poonam Chandra, both working in India and experts of radio observations with the Giant Metrewave Radio Telescope (GMRT) located near Puna in India. This meeting allowed us to start a collaboration on supernova remnants with a few other colleagues, and more specifically, on HESS J1731$-$347. We submitted proposals of observation and obtained 5.4 hours in October 2013 at 325 MHz, 2.5 hours in December 2013 at 610 MHz and 3.5 hours in August 2015 at 1390 MHz. These data permit the detection of a radio counterpart of the SNR HESS J1731$-$347 at 325 and 610 MHz. The SNR is not detected in the 1390 MHz GMRT map. The radio maps at 325 and 610 MHz clearly show a shell-like structure with filaments. The extent of shell structure is $\sim$30 arcminute, in agreement with the TeV data, but the finer structure do not seem to be correlated. Indeed, the bright filaments in radio (south-east filament and eastern filament) are faint in the H.E.S.S. map. The peak in VHE emission is from the north-east region, where the radio emission is faint. Assuming that the medium surrounding the SNR is reasonably uniform as suggested by the flat structure of the γ-ray azimuthal profile, the variation in radio brightness can be most likely due to the variation of magnetic field if the injection is isotropic (the efficiency of injection does not depend on the angle between shock normal and magnetic field). Radio brightness increases in the region of high magnetic field since synchrotron emissivity is proportional to $B^{3/2}$ for a particle distribution N(E) scaling as E^{-2}. In a leptonic scenario, these electrons produce the γ-ray signal by inverse Compton (IC) scattering and experience ample radiative losses in this region with an energy loss rate proportional to E^2B^2. Thus in the region of high magnetic field, the number of electrons emitting IC γ-rays deplete faster. This results in a low brightness of VHE emission where the radio brightness is still high (Petruk et al., 2009), thus potentially explain the anti-correlation between the radio and γ-ray emission. This explanation is valid only in the case of synchrotron-loss limited acceleration scenario where $E_{max} \propto B^{-1/2}$ (Reynolds, 2008). In the case of age-limited accelaration scenario, $E_{max} \propto B$ (Reynolds, 2008) and the anti-correlation cannot be explained. This directly means that in a leptonic scenario with synchrotron-loss limited acceleration, one can explain the anti-correlation between the radio and γ-ray data as follows: the magnetic field strength is relatively high in the region of the south-east and eastern filaments, and hence it is bright in radio. Due to high synchrotron cooling, there are fewer IC electrons, and hence the VHE emission is faint here. The magnetic field strength is low towards the northern region of the SNR, and this results in less energy loss of electrons and bright IC emission. Our radio data thus further supports the fact that the γ-ray emission is dominated by IC scattering. The results were published in Nayana et al. (2017).

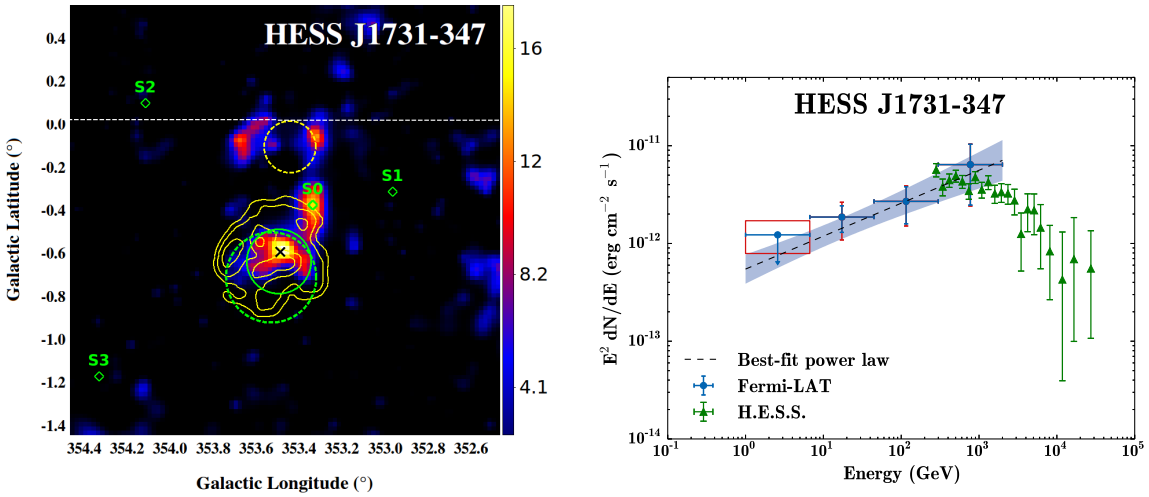

Figure 3.7: *(Left) TS map (1 GeV − 2 TeV) in Galactic coordinates showing a 2° × 2° region centered on the position of HESS J1731−347. Green diamonds correspond to additional background sources while the black cross and green circle correspond to the best-fit position (for $E > 1$ GeV) of HESS J1731−347 as a point source and a uniform disk respectively. The best uniform disk above 10 GeV is represented by the green dashed circle. The TeV morphology of the shell is represented by the yellow contours and the yellow dashed circle shows the position of HESS J1729−345. (Right) Spectral Energy Distribution for HESS J1731−347. Blue points correspond to the* Fermi *data and blue shaded areas represent the 68% confidence band of the* Fermi *spectral fit (statistical errors). Red error bars are the quadratic sum of statistical and systematic errors. The variation of the upper limit with alternative IEMs is represented by the red rectangle that surrounds it and the green triangles represent the H.E.S.S. data points.*

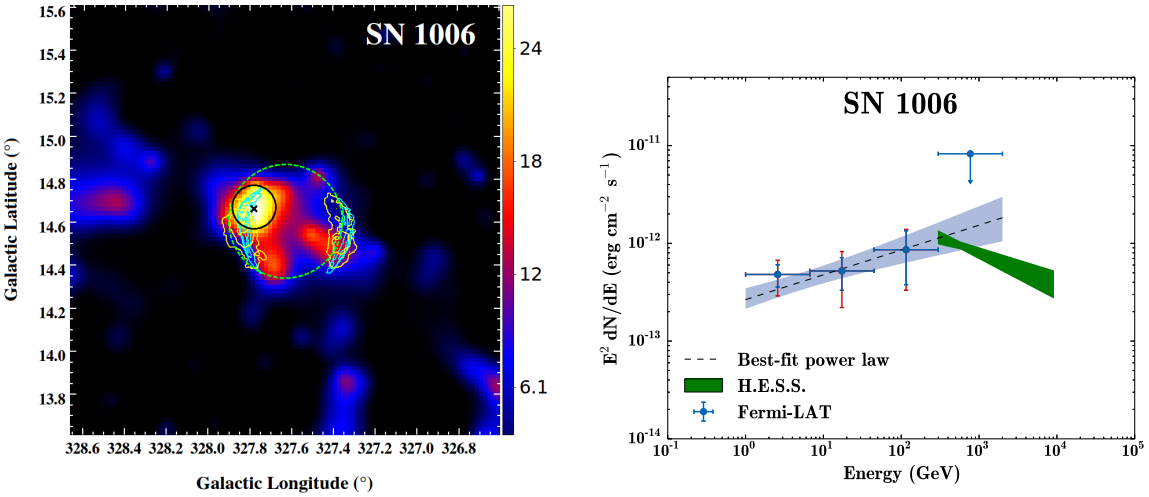

Figure 3.8: *(Left) TS maps (1 GeV − 2 TeV) in Galactic coordinates showing a 2° × 2° region centered on the position of SN 1006. The best-fit position assuming a point source and a uniform disk are represented by the black cross and circle, respectively. The green dashed circle shows the result obtained with an initial disk matching the TeV shape. Yellow and cyan contours correspond to H.E.S.S.and XMM-Newton, respectively. No background sources were found in the close vicinity of SN 1006. (Right) Spectral Energy Distribution of SN 1006 using the same conventions as Figure 3.7 (right).*

Table 3.3: *Summary of the results obtained between 1 GeV and 2 TeV for HESS J1731−347 and SN 1006. Parameters of the geometrical models were adjusted with* `pointlike` *while TS values and spectral indices were obtained using* `gtlike`*. Only statistical errors are given here.*

Source	Spatial Model	R.A. (°)	Dec. (°)	Radius (°)	Spectral Index	Energy Flux (erg cm^{-2} s^{-1})	TS	$N_{\rm dof}$
HESS J1731−347	Point Source	262.92 ± 0.02	-34.77 ± 0.02	–	1.87 ± 0.12	$(0.78 \pm 0.31) \times 10^{-11}$	25.2	4
	Disk	262.97 ± 0.03	-34.79 ± 0.02	0.15 ± 0.04	1.71 ± 0.17	$(1.61 \pm 0.50) \times 10^{-11}$	31.5	5
	H.E.S.S.	–	–	–	1.66 ± 0.16	$(1.91 \pm 0.63) \times 10^{-11}$	25.1	2
SN 1006	Point Source	225.88 ± 0.04	-41.75 ± 0.02	–	1.55 ± 0.10	$(5.56 \pm 2.57) \times 10^{-12}$	28.6	4
	Disk	225.90 ± 0.04	-41.74 ± 0.03	0.10 ± 0.04	1.57 ± 0.11	$(5.82 \pm 2.60) \times 10^{-12}$	31.0	5
	H.E.S.S.	–	–	–	1.79 ± 0.17	$(6.99 \pm 2.03) \times 10^{-12}$	34.4	2
	H.E.S.S.(NE)	–	–	–	1.47 ± 0.26	$(6.14 \pm 2.53) \times 10^{-12}$	28.3	2
	H.E.S.S.(SW)	–	–	–	2.60 ± 0.80	$(0.88 \pm 0.24) \times 10^{-12}$	12.9	2

The historical remnant SN 1006 and its asymmetric γ-ray emission

SN 1006 is located far off-plane and its analysis with *Fermi* is therefore easier. We followed the same procedure used for HESS J1731−347 but each step was achieved with less troubles. First, we looked for new background sources in a 10° square region and found only three significant excesses in addition to 3FGL sources. The number of free parameters in this region is therefore limited. The TS map in Figure 3.8 (left) reveals a bright spot of γ-ray emission at the top of the northeast (NE) limb of SN 1006, along with some diffuse emission. Using `pointlike` for the spatial analysis, we tested the point source and the uniform disk hypotheses and determined the best parameter values (see Table 3.3). Assuming a uniform disk initially centered on the pixel of highest TS value with $R_{\rm init} = 0.01°$, we measured an extension of $0.10° \pm 0.04°$ with $\mathrm{TS}_{\rm ext} = 1.8$: SN 1006 is therefore not detected by the LAT as an extended source. The positions of the point source and the disk are represented in Figure 3.8 (left) by the black cross and black circle respectively. Since we know that SN 1006 is a large source at TeV energies, we also measured the extension for an initial disk matching the TeV shape ($R_{\rm init} = 0.25°$). In this case, we obtained $\mathrm{TS}_{\rm ext} = 7.7$ and $R = 0.26° \pm 0.03_{\rm stat}$ (the green dashed circle in the left panel of Figure 3.8). Although the extension is still not significantly detected, this result indicates that we are only limited by the statistics and that the extension should be revealed with a few years of additional data. Then we used `gtlike` to perform a spectral analysis between 1 GeV and 2 TeV to evaluate the spectral index. For the point source, the uniform disk and the H.E.S.S. template, we obtained $\Gamma = 1.55$, $\Gamma = 1.57$ and $\Gamma = 1.79$ respectively, with errors of $\pm 0.17_{\rm stat} \pm 0.27_{\rm syst}$. When taking into account uncertainties, these results are consistent with 1.9 ± 0.3, published in Xing et al. (2016), but with a smaller statistical error bar due to the enlarged dataset. Spectral results are summarized in Table 3.3. Again for this source, the hard spectrum is very similar to the one obtained for the other shell-type remnants detected at TeV energies, even if it tends to be slightly softer. We will see a potential reason in the following, looking at the Eastern and Western spectra separately. But before that, since there are very few modelings of SN 1006 taking into account the latest *Fermi* points, I decided to gather the multi-wavelength data published in the literature and try to reproduce them using the simple model used for RCW 86 and other shell-type SNRs. To allow a comparison with previously published models, I decided to neglect radiative losses. For this reason, a low energy cut-off for the electrons is expected. In a hadronic scenario, one needs a fine tuning of the parameters to reproduce the data: the very low ambient density (< 0.05 cm^{-3}) implies a large energy injected in protons ($> 2.7 \times 10^{50}$ erg), a hard injection spectrum for the protons (< 1.9) with a maximum energy of 50 TeV, a very low electron to proton ratio ($< 10^{-3}$) to suppress the IC scattering on the Cosmic microwave background (CMB) photons and a very high magnetic field (~ 120 μG) to produce the strong synchrotron emission observed in the X-ray and radio bands. The injection spectral index for the electrons is well constrained by the radio data at 2.2,

very different than the proton's index. In the leptonic scenario, the magnetic field value is 22 μG, the maximum energy reached by electrons is 15 TeV with an injection index of 2.2 and a total energy injected above 1 GeV of 1.6×10^{47} erg. In this case, due to the low density, the proton-proton interaction does not contribute if the electron to proton ratio is above 0.01. Figures 3.9 present these two different scenarios. These values are very similar to the one that we derived for the case of RCW 86 and are in perfect agreement with those derived by Xing et al. (2016) using their *Fermi* spectral points.

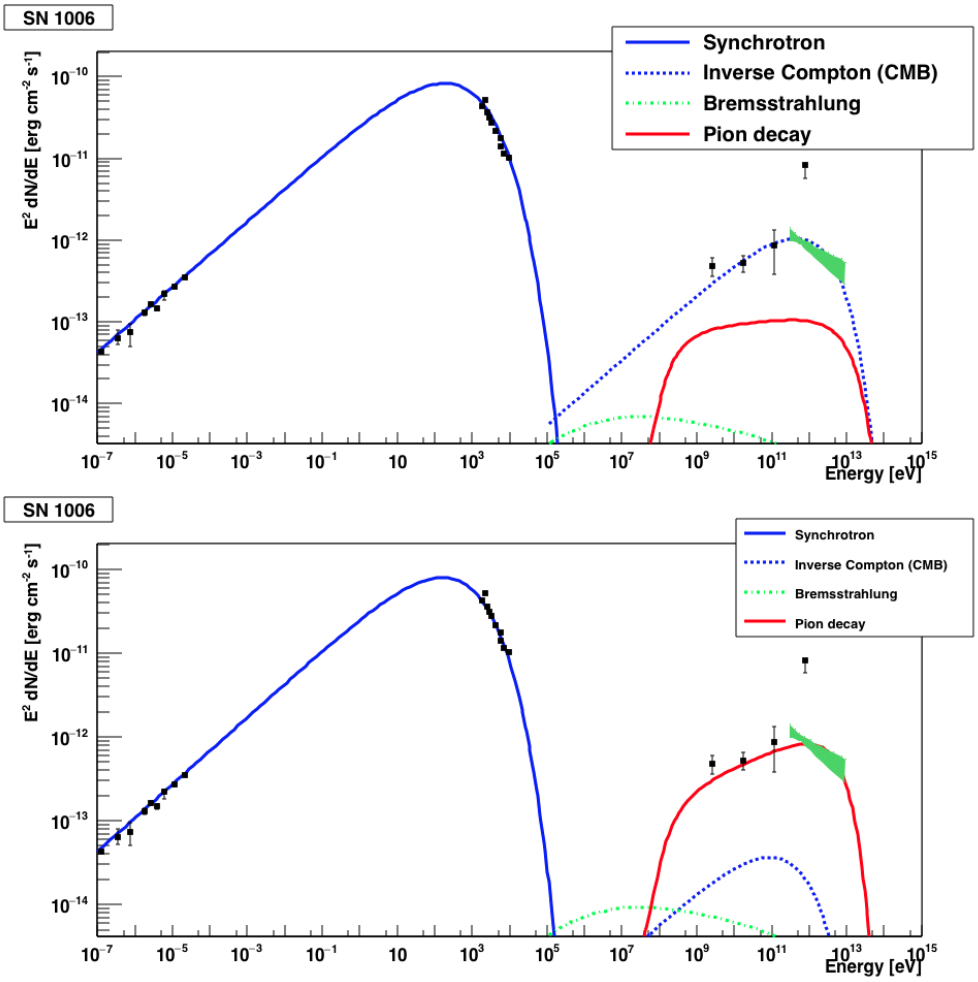

Figure 3.9: *Broadband SED models of SN 1006 for a leptonic scenario (top) and a hadronic one (bottom). Top: Modeling was done by using an electron spectrum in the form of a power law with an index of 2.2, an exponential cut-off at 15 TeV and a total energy of* 1.6×10^{47} *erg above 1 GeV. The magnetic field amounts to* 22 μ*G. Bottom: Modeling using a proton spectrum in the form of a power law with an index of 1.85, an exponential cutoff at 50 TeV and a total proton energy of* 0.13×10^{50} $(n_{\rm H}/1\ cm^{-3})^{-1}$ *erg above 1 GeV. The electron/proton ratio above 1 GeV was* 3×10^{-4} *with an electron spectral index of 2.2 and cut-off energy at 6 TeV. The magnetic field amounts to* 120 μ*G and the average medium density is 0.05* cm^{-3}.

Since SN 1006 is known to be a very symmetric shell-type remnant, the apparent asymmetry in the γ-ray emission detected by *Fermi* as seen in Figure 3.8 (left) is quite intriguing. Therefore, we studied the NE and the SW limbs of the remnant separately. To do so, the H.E.S.S. template was divided into two parts and their spectral parameters fitted independently. The division axis was defined as the symmetry axis of the X-ray emission as seen by XMM-Newton (see Figure 1 in Miceli

et al., 2012). The NE region was significantly detected (TS = 28.3, $\Gamma = 1.47 \pm 0.26_{\rm stat}$) but the SW region was not (TS = 12.9, $\Gamma = 2.60 \pm 0.80_{\rm stat}$). Comparing the log-likelihood obtained, we found an improvement of 10.5 when dividing the H.E.S.S. template, corresponding to a TS value of 21.0 with two additional degrees of freedom (3.6σ). This is a first indication of an asymmetry of the high-energy γ-ray emission: the likelihood favors separate fits for the two limbs by 3.6σ whereas the X-ray and TeV morphologies are rather symmetrical. The insignificant detection of the SW region suggests a fainter IC emission in this part of the remnant than in the NE part, although it is hard to explain since the ambient photon fields are identical and the shock velocity is ~ 5000 km^{-1} in both regions (Winkler et al., 2014). A clue could come from the latest results obtained recently: Dubner et al. (2002) revealed the presence of a dense HI cloud matching the morphology of the southwestern rim of SN 1006 and Miceli et al. (2014) found evidence of interaction between this HI cloud and the shock of SN 1006. Neutrals could play a significant role: at the interaction region, the shock is slowed down because of the larger inertia of swept up material, but also the magnetic field is suppressed because of a more efficient ion-neutral damping. This is indeed what is observed at X-ray energies with XMM-Newton with a cutoff energy of the synchrotron emission decreasing in SW limb of the remnant where the interaction with the HI cloud is occurring (Miceli et al., 2014). These authors also proposed recently a model with two hadronic components, one from the shocked cloud and one from the shocked interstellar medium, the latter being too faint to be detectable (Miceli et al., 2016). The hadronic component related to the cloud is characterized by a low cutoff (~ 3 TeV) and drops drastically above 100 GeV. It dominates over the IC peak below 10 GeV as can be seen in Figure 3.10. Interestingly, the LAT flux that we derived in the SW region agrees relatively well with their model for an energy injected of 5×10^{49} erg in the SW. This model also seems to show that the IC emission should be detectable by the LAT with additional observation time and is just below our current sensitivity. Neutrals could also affect the injection spectrum of the particles in this region (as already suggested for RCW 86 in Section 3.3.2), making it steeper. This could also be a reason why it is not yet detected by our LAT analysis.

3.3.4 Similarities between γ-ray shell-type SNRs

Interestingly, as can be seen in Figure 3.11 and in Table 3.4, the five shell-type SNRs detected at γ-ray energies show hard HE spectral indices ($1.4 < \Gamma < 1.9$) that exclude the standard hadronic test particle scenario[2]. All photon indices (except for RX J0852.0$-$4622 and SN 1006) are compatible with a test particle leptonic dominated scenario where the electron slope of 2.0 translates into a photon spectral index of 1.5. In the case of RX J0852.0$-$4622, the slightly softer HE photon index ($1.85 \pm 0.06_{stat} \pm 0.19_{syst}$, Tanaka et al. (2011)) could be due to a deviation from the test particle case, a mix of hadronic and leptonic contributions or a possible contamination from the PWN seen around PSR J0855$-$4644 (Acero et al., 2013b) that is located right on the south-eastern part of the SNR shell. For SN 1006, we have seen above that a potential hadronic contribution is not excluded in the SW region of the remnant. In the NE region of SN 1006, where no contribution of hadrons is expected, the spectral index derived in our analysis is hard (1.47 ± 0.26) and translates in an electron slope of 2.0. The similarity of hard photon spectral indices in this SNR sample tends to point towards a common leptonic dominated scenario for the HE and VHE γ-ray emission. Still, there could be some smaller subregions (e.g. dense clumps) where the hadronic mechanism significantly contribute to the local γ-ray emission as we have seen for SN 1006 in the SW or RX J1713.7$-$3936 near the

[2]The test particle scenario neglects the retro-action of the CRs on the shock structure and produces a proton energy distribution which converts into a photon spectral index $\Gamma = 2$.

Galactic plane.

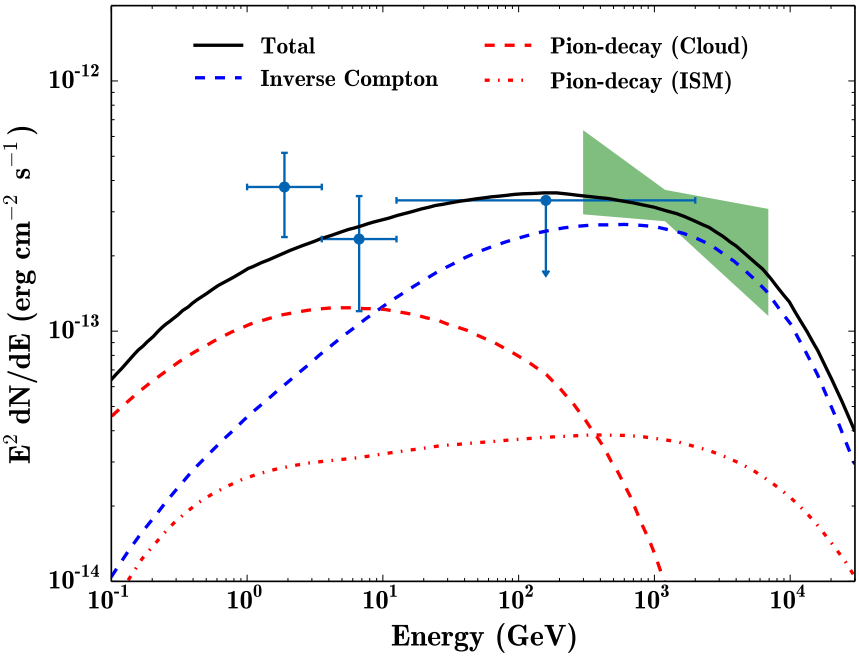

Figure 3.10: *Modeling of the SW region of SN 1006 proposed by Miceli et al. (2016) for an energy injected of* 5×10^{49} *erg (black solid line). The inverse Compton contribution (dashed blue line) and the hadronic contribution of the shocked cloud (dotted red line) and of the shocked ISM (dash-dotted red line) are highlighted. The* γ*-ray spectrum observed with H.E.S.S. in the SW is shown with the green butterfly, and the* Fermi*-LAT points derived for the SW limb in our analysis are indicated by the blue points*

In addition to a similar HE spectral index, these five shell-type SNRs present a striking similarity in terms of peak luminosity and spectral shape. This contrast is highlighted when compared with the SNR W44 where the evidence for hadronic emission is the most secure (Ackermann et al., 2013a). One can note that the γ-ray luminosity of SN 1006, as presented in Figure 3.11, is lower than for other SNRs. However, this is mainly related to its bipolar morphology, which is a clear difference with the other TeV detected shell-type SNRs. This bipolar morphology caused by the orientation of the magnetic field in the NE-SW direction produces a reduced effective area for particle acceleration since the acceleration is more efficient when the magnetic field is parallel to the shock normal. If we correct for this effect by a renormalization factor of 0.2 (Berezhko et al., 2009), the peak luminosity is comparable to other SNRs. This similar luminosity also points towards leptonic emission as the dominant mechanism in play for these remnants. Indeed, in such scenario, the spectral shape and flux level of the γ-ray emission is produced via the IC mechanism and only depends on the electron spectral distribution (which is similar for the five SNRs as discussed just above) and on the photon field density. Due to the omnipresence of the CMB and the limited effect of the infra-red photon field, one could explain why we observe such a small scatter in the γ-ray luminosity of young shell-type SNRs.

3.4 General properties of young SNRs

To finalize this chapter, I decided to gathCassiopeia Aer the main properties of the young SNRs detected at GeV and TeV energies in Table 3.4 for completeness. This allows a comparison between these seven sources. It is very similar to the one that we published in Acero et al. (2015), but here I added the results concerning Cassiopeia A and Tycho and updated the results concerning RX J1713.7−3946, RCW 86, SN 1006 and HESS J1731−347. We can see from this table that all types of SNe are detected. The SN type does not seem to affect the HE and VHE spectral parameters. Since we are discussing here the acceleration of cosmic rays, I made a choice to cite the model parameters in the case of a hadronic scenario with direct interaction, meaning that the γ-ray emission is dominated by neutral pion decay due to proton-proton interaction. This is obviously an ideal case, and we have seen above, that for shell-type SNRs, the IC scenario seems to be dominant. The objective of this table is to see, at maximum, what could be the cosmic-ray efficiency of young SNRs and the maximum energy reached by protons. Indeed, if SNRs are the main accelerators of CRs, they need to fulfill four important criteria: 1) they accelerate protons, 2) the cosmic-ray efficiency ξ_{CR} is high enough and close to the standard value of $\sim 10\%$, 3) the injected CR spectrum follows a power-law which translates into an index of 2.7 after diffusion in the Galaxy to reproduce the CR spectrum below the knee, 4) the maximum proton energy is at the knee of the CR spectrum.

3.4.1 Hadronic or leptonic ?

As stated regularly during this chapter, the overall spectral slope from GeV to TeV energies is an indicator of the nature of the emission: SNRs exhibiting hard spectra are more naturally explained in leptonic scenario (even though some hadronic models assuming cosmic-ray escape in very dense clumps are able to reproduce the multi-wavelength data). However, a caveat comes from the finite (or even poor) resolution of the gamma-ray instruments which cannot resolve exactly the region in which the gamma-ray emission is taking place. This is crucial when density gradient or variation exists within the remnant, which is the case in most cases. In RX J1713.7−3946, the variation is extreme: from the lack of thermal X-ray observations, an upper limit on the density was derived at $<$0.02 cm^{-3} (similarly to the case of the other young shell-type SNRs). However, CO and HI observations of the medium surrounding the SNR (Fukuda et al., 2014), especially near the Galactic plane, shows an average density in this region of 100 cm^{-3}, with clumps as dense as 1000 cm^{-3}. This is why we naturally expect to see variations of the dominant mechanism throughout the remnant, the hadronic mechanism being dominant in dense regions. The case of Tycho and SN 1006 is paradigmatic: they both have Type Ia progenitor and are just at the beginning of the Sedov phase, but SN 1006 seems to be leptonic-dominated because it is expanding in a much more rarefied medium on average (0.05 cm^{-3} vs 0.3 cm^{-3}). In the South-Western region where the density in SN 1006 is ten times higher, the hadronic scenario might dominate. It seems that for most young SNRs, due to the low-density ambient medium on average, the hadrons do not encounter sufficiently high target densities to produce a level of hadronic flux that can compete with the leptonic emission for the whole SNR, except for Cassiopeia A and Tycho in which the average density is more than ten times higher than inside shell-type SNRs. As stated in Acero et al. (2015), the correct question is not anymore "Is the γ-ray emission leptonic or hadronic dominated ?" but rather "In which region of the SNR is the emission leptonic/hadronic dominated ?".

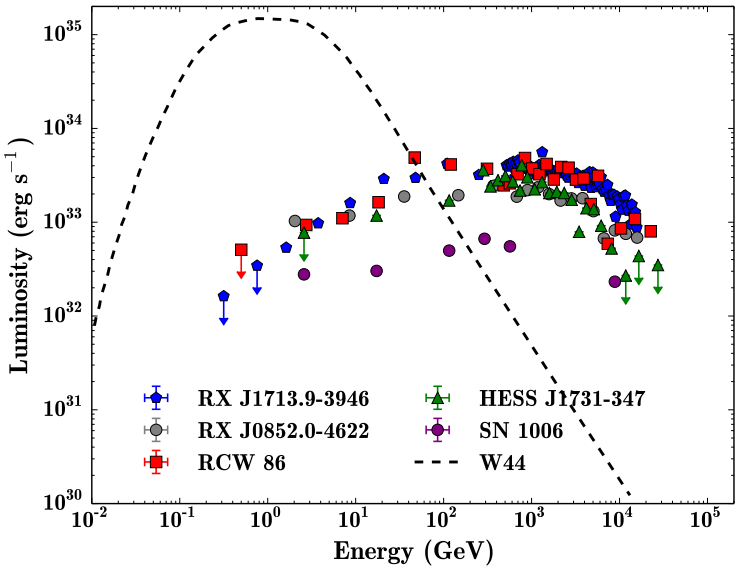

Figure 3.11: *Gamma-ray luminosity of the five shell-type SNRs detected by* Fermi*-LAT and H.E.S.S.. For the sake of comparison the SED from the SNR W44 is shown by the dashed line. This Figure was taken from Benjamin Condon's thesis.*

3.4.2 Cosmic-ray efficiency in young SNRs

Due to this density variation and gradient and the poor angular resolution of the current instrument, the energy injected in protons in the hadronic scenario suffers large systematics. In the hadronic models of Tycho and Cassiopeia A, which are the youngest SNRs detected at gamma-ray energies, 16% (for an average density of 0.3 cm^{-3}) and 9.9% (for an average density of 10 cm^{-3}) of the kinetic energy of a supernova (10^{51} erg) is injected in protons which is not far from the standard value of 10% used regularly to maintain the CR energy flux in the Galaxy. Using a lower density for Cassiopeia A, Zirakashvili et al. (2014) even found that the acceleration efficiency in Cas A should be very high and that, at present, 25% of the energy of the supernova explosion is transferred into accelerated particles. Even if these values vary from one model to another, it seems that SNRs are able to inject a significant fraction of their energy, at least during the first few hundred years after the explosion.

3.4.3 Universal power-law spectra reproducing the CR spectrum

The standard SNR paradigm predicts that the spectrum of CRs accelerated at strong shocks through DSA is very close to E^{-2}. Surprisingly, in the two cases in which the gamma-ray emission is attributed to hadronic interactions (Cas A and Tycho), the inferred proton spectrum appears to be steeper than E^{-2}, with an average index of 2.25. As explained in Section 2.1.2, for a given injection rate $Q(E) \propto E^{-\gamma}$, after propagation in the Galaxy, the spectrum observed at Earth is $E^{-\gamma-\delta}$, where δ is the diffusion coefficient in the Galaxy. Since the spectrum observed at Earth is $\sim E^{-2.7}$, the SNR paradigm would imply a diffusion coefficient proportional to $E^{0.7}$. This coefficient is in contradiction with the latest estimate of $\delta \sim 1/3$ using the primary to secondary ratios and the anisotropy in the CR fluxes at Earth (Blasi and Amato, 2012; Vladimirov et al., 2012). A natural conclusion is that protons need to be accelerated at their sources with steep spectra $\sim E^{-2.3}$ which is in perfect

agreement with the models proposed for Cas A and Tycho. The distribution of the target material for proton-proton interaction and/or the presence of neutral atomic hydrogen in the acceleration region can explain these modifications in the spectrum of accelerated particles, highlighting again the importance of the environment in which a SNR evolves. Therefore, this criterium seems to be fulfilled.

	RX J1713	Vela Jr	HESS J1731	RCW 86	SN 1006	Cas A	Tycho
SN nature	CC	CC	CC	Type Ia	Type Ia	CC	Type Ia
Distance (kpc)	0.9 – 1.3	0.6 – 0.9	≥ 3.2	2.3 – 2.8	2.0 – 2.4	3.3 – 3.7	2 – 4
Radius (pc)	10	12	14	15	10	$\sim$2.4	$\sim$3.5
Age (kyrs)	1.6	2 – 4	2 – 6	1.8	1	0.316 – 0.352	0.446
Density (cm^{-3})	<0.02 – 100	<0.03 – 40	<0.01 – 60	0.5 – 2	<0.05 – 1.5	4 – 10	0.1 – 3
References	12, 17, 11, 38	13, 9, 38	21, 3, 22, 5, 38	19, 10, 25	23, 2, 14, 16	31, 32, 33	30, 34, 35
$\Gamma_{\rm HE}$	$1.13 \pm 0.26 - 2.0$	1.85 ± 0.06	1.66 ± 0.16	1.42 ± 0.1	1.7 ± 0.17	$0.89 \pm 0.29 - 2.17 \pm 0.09$	2.14 ± 0.09
$\Gamma_{\rm VHE}$	2.06 ± 0.02	1.81 ± 0.08	2.32 ± 0.06	1.6 ± 0.2	2.30 ± 0.15	2.4 ± 0.1	2.92 ± 0.42
$\rm Ecut_{VHE}$ (TeV)	12.9 ± 1.1	6.7 ± 1.2		3.5 ± 1.2		$3.5\ (^{+1.6}_{-1.0})$	
References	6, 24	7, 18, 20	22, 5	15, 8, 25, 26	4, 22	27, 29	28
Pref. Model	L	L	L	L	L	H	H
$s_{\rm p}$	1.53 – 1.94	1.83	1.7	1.7	1.85	2.21	2.3
$\rm Emax_p$ (TeV)	93	55	38	50	50	12	37
$\rm W_p$ (10^{49} ($\rm n_H$/1 cm^{-3})$^{-1}$ ergs)	5.8	7.1	15	13	1.4	99	4.8
Reference	6	7	39	40	Section 3.3.3	27	37

Table 3.4: *Summary of the physical properties of the detected young SNRs at gamma-ray energies. The corresponding nature of the SN explosion is noted as core collapse (CC) or thermonuclear (Type Ia). The ambient medium densities shown in this table have been derived from the presence/lack of X-ray thermal emission and on the HI and CO observations of the environment, creating large variations in values. The errors reported on the HE and VHE parameters are statistical. When a break is detected at HE, the indices below and above the break are listed. In the third part of the table, the best-fit hadronic model for each SNR is reported. The proton energy budget ($W_{\rm p}$) is given for $E_{\rm e} > 1$ GeV for a density of 1 cm^{-3}. The model preferred (following the above discussion on each source) is indicated as H (hadronic) or L (leptonic). For each of them, the index of the proton spectrum $s_{\rm p}$ is provided as well as its maximum energy $Emax_{\rm p}$ and the total energy injected in protons $W_{\rm p}$. References: 1) Acero et al. (2015), 2) Acero et al. (2007), 3) Doroshenko et al. (2017), 4) Acero et al. (2010), 5) H.E.S.S. Collaboration et al. (2011a), 6) H. E. S. S. Collaboration et al. (2016a), 7) H. E. S. S. Collaboration et al. (2016b), 8) H. E. S. S. Collaboration et al. (2016d), 9) Allen et al. (2015), 10) Bocchino et al. (2000), 11) Cassam-Chenaï et al. (2004), 12) Fesen et al. (2012), 13) Katsuda et al. (2008), 14) Katsuda et al. (2009), 15) Lemoine-Goumard et al. (2012), 16) Miceli et al. (2014), 17) Moriguchi et al. (2005), 18) Paz Arribas et al. (2012), 19) Sollerman et al. (2003), 20) Tanaka et al. (2011), 21) Tian et al. (2008), 22) Condon et al. (2017), 23) Winkler et al. (2014), 24) Condon (2017), 25) Ajello et al. (2016), 26) Dubner et al. (2002), 27) Ahnen et al. (2017), 28) Archambault et al. (2017), 29) Yuan et al. (2013), 30) Sato and Hughes (2017), 31) Hwang and Laming (2012), 32) Zirakashvili et al. (2014), 33) Reed et al. (1995), 34) Krause et al. (2008), 35) Badenes et al. (2007), 36) Zhang et al. (2013), 37) Slane et al. (2014), 38) Fukuda et al. (2014), 39) Guo et al. (2018), 40) Yuan et al. (2014).*

3.4.4 Maximum proton energy

Interestingly, in all cases listed in Table 3.4, the GeV-TeV γ-ray detections of these seven SNRs imply a low maximal energy for the accelerated particles below 100 TeV, i.e. well below the knee of the CR spectrum. A recent review by Aloisio et al. (2017) reported the latest estimates calculated by several

authors concerning the maximum energy that can be reached at a SNR shock (Schure and Bell, 2013; Bell et al., 2013; Cardillo et al., 2015). For a type Ia SN with ejecta mass M_{ej} and total kinetic energy E_{SN}, exploding in the ISM with density n_{ISM}, the maximum energy can be written as

$$E_M \cong 130 \left(\frac{\xi_{CR}}{0.1}\right) \left(\frac{M_{ej}}{M_\odot}\right)^{-\frac{2}{3}} \left(\frac{E_{SN}}{10^{51}\mathrm{erg}}\right) \left(\frac{n_{ISM}}{\mathrm{cm}^{-3}}\right)^{\frac{1}{6}} TeV. \tag{3.1}$$

Despite the efficient magnetic field amplification due to CR streaming, the maximum energy falls short of the knee by about one order of magnitude if the fraction of the energy injected into proton ξ_{CR} is $\sim 10\%$ as assumed for SNRs, thereby leading to the conclusion that type Ia SNe are unlikely to act as PeVatrons. If we look at the case of the young SNR Tycho, the best hadronic model proposed by Slane et al. (2014) using a CR-hydro-NEI code[3] uses a density of 0.3 cm^{-3}, an ejected mass of $1.4 M_\odot$ and a total kinetic energy of 10^{51}erg. This would mean that the maximum energy, reached at the beginning of the Sedov-Taylor phase, is $\sim$ 100 TeV. Currently, the maximum proton energy reproducing the multi-wavelength data is $\sim$ 40 TeV, not far from this estimate. This confirms that, even if Tycho is at the transition between the ejecta-dominated and the adiabatic stages, it is not a PeVatron.

Most core collapse SNe on the other hand explode in the wind produced by their pre-supernova red giant progenitor. For a reference value of the mass loss rate $\dot{M} \sim 10^{-5} M_\odot \mathrm{yr}^{-1}$ and wind speed $V_w \sim 10$ km/s, the maximum energy can be estimated as

$$E_M \approx 1 \left(\frac{\xi_{CR}}{0.1}\right) \left(\frac{M_{ej}}{M_\odot}\right)^{-1} \left(\frac{E_{SN}}{10^{51}\mathrm{erg}}\right) \left(\frac{\dot{M}}{10^{-5} M_\odot \mathrm{yr}^{-1}}\right)^{\frac{1}{2}} \left(\frac{V_w}{10\,\mathrm{km\,s}^{-1}}\right)^{-\frac{1}{2}} PeV\,. \tag{3.2}$$

In the case of Cassiopeia A, X-ray observations indicate that the ejecta mass was only $\sim 3 M_\odot$ and the total kinetic energy was 2.3×10^{51} erg (Hwang and Laming, 2012). Two-dimensional multi-species hydrodynamical simulations have shown that the observed shock wave positions and expansion can be interpreted in a model of supernova interaction with a freely expanding red supergiant stellar wind with a mass loss rate of $1.54 \times 10^{-5} M_\odot \mathrm{yr}^{-1}$ and a wind velocity of $4.7\,\mathrm{km\,s}^{-1}$ (van Veelen et al., 2009). This would imply that the maximum energy reached at the beginning of the Sedov-Taylor phase was ~ 1.4 PeV, if 10% of the energy of the SN was injected in protons. The very low value of $\mathrm{Emax_p}$ reproducing the MAGIC spectrum, reported in Table 3.4, is 100 times lower than this estimate which is a tough result for the "SNR paradigm". It should be noted that a type II SN enters its adiabatic phase only a few tens of years after the explosion and Cassiopeia A is clearly not anymore in the free-expansion phase which could explain part of the discrepancy. Alternatively, Cassiopeia A may also be located in a very diffusive region of the Galaxy, resulting in a very fast escape of protons of TeV and higher energies. If this is the case, escaped protons would be interacting with the medium surrounding the SNR and observations of a halo around Cassiopeia A by LHAASO could be a proof of the acceleration of protons at PeV energies (Di Sciascio and LHAASO Collaboration, 2016). A last possibility would be that core collapse SNe do not accelerate protons up to 1 PeV, which would imply that another type of source significantly contributes at least in the "knee" region of the CR spectrum. We will develop such possibility in Section 5.3.2.

[3] A CR-hydro-NEI code models the SNR hydrodynamics including the effects of non-linear diffusive shock acceleration using a semi-analytic solution. The resulting non-thermal proton and electron spectra, coupled with the calculated magnetic field, are used to calculate the synchrotron, bremsstrahlung, inverse-Compton, and pion-decay emission. The thermal X-ray emission is calculated by following the ionization of the shocked gas through the hydro simulation and coupling this to a non-equilibrium ionization emission code.

Summary

- Two historical SNRs are detected both at GeV and TeV energies: Cassiopeia A and Tycho. Multi-wavelength modeling and the spectral break at low energy for Cassiopeia A favor a scenario in which the gamma-ray emission is produced via proton-proton interaction: protons are accelerated in historical SNRs.
- The five shell-type SNRs observed at TeV energies are now detected by the LAT. These five shell-type SNRs present striking similarities in terms of peak luminosity and spectral shape. The hard spectral shape at GeV energies points towards leptonic emission as the dominant mechanism in play for these remnants.
- The environment (dense HI cloud, CO clouds or tenuous ISM) in which the SNR is evolving is a key ingredient. There could be some smaller subregions (e.g. dense clumps) where the hadronic mechanism significantly contribute to the local γ-ray emission. This could be the case for SN 1006 in the SW or RX J1713.7$-$3936 near the Galactic plane.
- Young SNRs seem to fulfill three important criteria to be the prime CR accelerators: 1) they accelerate protons, 2) the cosmic-ray efficiency ξ_{CR} is high enough and close to the standard value of $\sim 10\%$, 3) the injected CR spectrum follows a power-law which translates into an index of 2.7 after diffusion in the Galaxy, well reproducing the CR spectrum.
- However, the maximum energy reached in young SNRs is well below the knee of the CR spectrum ($E_{max} < 100$ TeV). SN Ia are not expected to act as PeVatron but core collapse SNe could. The case of Cassiopeia A is intriguing.

The results presented in this chapter have been published in (bold faces indicate those for which I am corresponding author; I am co-author of all others):

- **Condon B. et al., 2017, The Astrophysical Journal, 851, 100: "Detection of Two TeV Shell-type Remnants at GeV Energies with Fermi-LAT: HESS J1731-347 and SN 1006"**
- Nayana A.-J. et al., 2017, MNRAS, 467, 155: "325 and 610 MHz radio counterparts of SNR G353.6-0.7 also known as HESS J1731-347"
- **Ajello M. et al., 2016, The Astrophysical Journal, 819, 98: "Deep Morphological and Spectral Study of the SNR RCW 86 with Fermi-LAT"**
- Abdalla H. et al., 2016, to be published in Astronomy & Astrophysics, arXiv:1609.08671: "H.E.S.S. observations of RX J1713.7-3946 with improved angular and spectral resolution; evidence for gamma-ray emission extending beyond the X-ray emitting shell"
- Abramowski A. et al., 2016, to be published in Astronomy & Astrophysics, arXiv:1601.04461: "Detailed spectral and morphological analysis of the shell type SNR RCW 86"
- **Acero F. et al., 2015, Astronomy & Astrophysics, 580, A74: "Study of TeV shell supernova remnants at gamma-ray energies"**
- Abramowski A. et al., 2015, Science, 347, 406: "The exceptionally powerful TeV γ-ray emitters in the Large Magellanic Cloud"

- Abramowski A. et al., 2014, Monthly Notices of the Royal Astronomical Society, 441, 790: "TeV γ-ray observations of the young synchrotron-dominated SNRs G1.9+0.3 and G330.2+1.0 with H.E.S.S."
- **Lemoine-Goumard M. et al., 2012, Astronomy & Astrophysics, 545, A28: "Constraints on cosmic-ray efficiency in the supernova remnant RCW 86 using multi-wavelength observations"**
- Tanaka T. et al., 2011, The Astrophysical Journal Letters, 740, L51: "Gamma-Ray Observations of the Supernova Remnant RX J0852.0-4622 with the Fermi Large Area Telescope"
- Abdo A. et al., 2010, The Astrophysical Journal, 710, L92: "Fermi-Lat Discovery of GeV Gamma-Ray Emission from the Young Supernova Remnant Cassiopeia A"
- **Aharonian F. et al., 2009, The Astrophysical Journal, 692, 1500: "Discovery of Gamma-Ray Emission From the Shell-Type Supernova Remnant RCW 86 with H.E.S.S."**
- Aharonian F. et al., 2008, Astronomy & Astrophysics, 488, 219: "HESS upper limits for Kepler's supernova remnant"

CHAPTER

4

Middle-aged SNRs: ideal proton targets ?

Contents

4.1 Middle-aged SNRs interacting with molecular clouds

Excellent γ-ray targets are provided by dense regions of the interstellar medium or in some cases dense molecular clouds interacting with middle-aged SNRs (3000–30000 yr). They are the most numerous subclass of GeV SNRs due to enhanced target densities for accelerated particles, which in cases of interaction with a molecular cloud can increase γ-ray luminosities by factors of $10^2 - 10^3$. The shape of the gamma-ray spectra among all SNRs interacting with Molecular clouds (MCs) is very similar[1], with a flux increasing quickly below 1 GeV and a steepening above a few GeV which implies an internal break around 10 GeV in the parent particle spectrum, as can be seen in Figure 4.1. For more information on the γ-ray characteristics of this sample of SNRs, see the review by Slane et al. (2015). For all of them, the observed large luminosity of the GeV γ-ray emission precludes the

[1]Two outliers, W41 and W30, have been studied individually during the ERC Starting Grant, showing a potential contamination at very high energy from a PWN.

inverse-Compton scattering off the CMB and interstellar radiation fields as the main emission mechanism since it would require an extremely low density (to suppress the bremsstrahlung and proton-proton interaction), a low magnetic field to enhance the gamma/X-ray flux ratio and an unrealistically large energy injected into electrons (or very high electron-to-proton ratio in comparison to Galactic standards). In addition, the break in the electron spectrum corresponding to the γ-ray spectrum directly appears in the radio data leading to a bad modeling of the radio data and therefore disfavors the bremsstrahlung process. A model in which gamma rays are produced via proton-proton interaction gives the most satisfactory explanation for the GeV gamma rays observed in SNRs interacting with molecular gas. Two different types of scenarios are put forward to explain the bright gamma-ray emission from these SNRs. The first scenario is called the "Escaping scenario" (Aharonian and Atoyan, 1996). It explains the gamma-rays as the pion-decay emission due to interactions between nearby molecular clouds and relativistic protons escaping from the SNR system. The second scenario is a direct interaction scenario and is called the "Crushed Cloud model" (Uchiyama et al., 2010). In this model, when a SNR collides with nearby MCs, the shock front is slowed down by dense clouds in the interaction region. Consequently, the postshock temperature drops, which then triggers efficient radiative cooling and the formation of a thin shell with high density and magnetic field behind the shock front. The thin radiative shell then becomes an ideal site for both pion-decay emission in γ-ray and synchrotron emission in radio. An excellent review discussing these two scenarios was recently published by Tang (2017). He shows that the escaping scenario can reproduce the observed γ-ray emission of all middle-aged SNRs detected, if the SNRs and MCs satisfy a special configuration in space. Hence, the similarity in γ-ray spectra is inconsistent with the escaping scenario in a statistical way and cannot explain all of them. In the direct interaction scenario, involving either pure adiabatic compression or re-acceleration of pre-existing cosmic-rays plus adiabatic compression, the similarity in γ-ray spectra can be interpreted as a reflection of almost homogeneous CR background in our Galaxy. In this case, a transition in seed particles must occur from thermal injected particles in young SNRs to pre-existing ambient CRs in middle aged SNRs. For instance, Tang (2017) suggests that in W44 thermal injected particle still dominates the seed particles, while in the other middle aged SNRs ambient CRs already become the dominant component in seed particles. Whatever the scenario, the acceleration process is not expected to reach very high energies for such old systems in comparison to shell-like SNRs and very few interacting SNRs are thus detected at TeV energies.

4.1.1 *Fermi*-LAT and HESS observations of the distant SNR G349.7+0.2

G349.7+0.2 is one of the rare clearly identified middle-aged SNRs detected by H.E.S.S. It is a bright radio Galactic SNR with a small angular size of $\sim$ 2.5' $\times$2' (Green 2009). The coincidence of G349.7+0.2 with a dense MC (Dubner et al. 2004), the detection of five OH (1720 MHz) masers towards the centre of the SNR (Frail et al. 1996) and of line emissions from several molecular transitions (Reynoso and Mangum, 2000; Lazendic et al., 2010) provide evidence in support of an interaction between the SNR and the MC. At a distance of 11.5 kpc (Tian and Leahy, 2014), the SNR radius and age are $\sim$3.8 pc and $\sim$1800 yr, respectively.
The total dataset comprises 113 hours of observations with the four-telescope H.E.S.S. array. The energy spectrum of the VHE emission coincident with G349.7+0.2 was extracted above 220 GeV and is well described by a power-law with a photon index of $\Gamma_{\rm VHE} = 2.8 \pm 0.27_{\rm stat} \pm 0.20_{\rm syst}$. The integrated photon flux above 400 GeV is $F(E > 400\,{\rm GeV}) = (6.5 \pm 1.1_{\rm stat} \pm 1.3_{\rm syst}) \times 10^{-13}$ ph cm^{-2} s^{-1} which corresponds to 0.7% of the Crab Nebula flux (Aharonian et al., 2006b) and to a luminosity of $\sim 10^{34}$ erg s^{-1} above the same energy threshold. Spectral models of a curved power-law and a power-law with exponential cutoff did not improve the fit of the spectrum significantly.

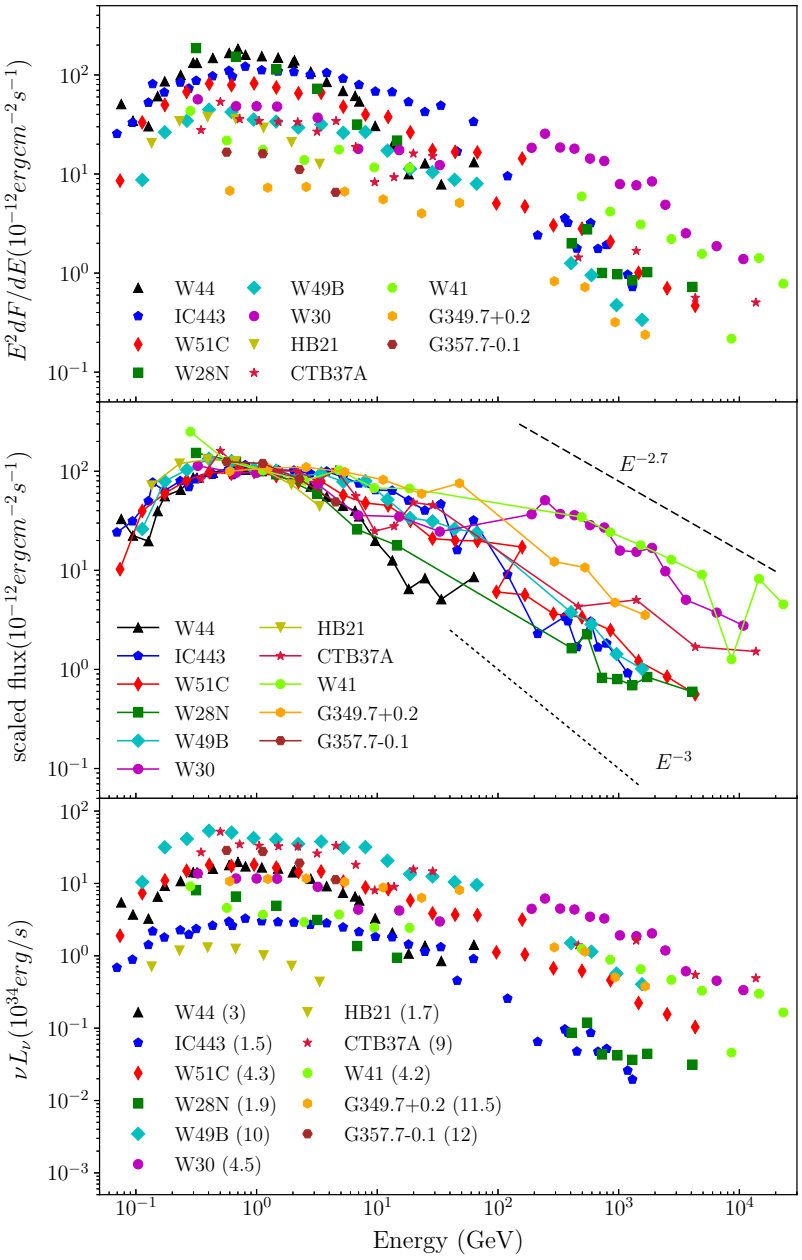

Figure 4.1: *Upper panel: Gamma-ray flux (E^2dF/dE) as a function of photon energy. Middle panel: scaled gamma-ray flux as a function of photon energy, where the flux around 1 GeV is normalized to $\approx 10^{-10}$ erg $cm^{-2}s^{-1}$. Solid lines connecting the data points are used to show the overall shape of the spectrum. Dashed line and dotted line indicate the slope for $E^{-2.7}$ and E^{-3} respectively. Lower panel: gamma-ray luminosity as a function of photon energy. Numbers in brackets are distance in kpc adopted for the luminosity calculation. This Figure was taken from Tang (2017).*

For what concern the *Fermi* analysis, due to the high level of Galactic gamma-ray diffuse emission in this region, the spectral analysis was performed in the 0.2–300 GeV energy range. The TS of the source at the position of the SNR is 201 and the best fit photon index $\Gamma_{\rm HE} = 2.2 \pm 0.04_{\rm stat}\,^{+0.13}_{-0.31{\rm sys}}$. The energy flux at the decorrelation energy E_0 = 3.8 GeV is $F_{E_0} = (6.1 \pm 0.43_{\rm stat}\,^{+3.1}_{-2.7{\rm sys}}) \times 10^{-12}\,{\rm erg\,cm^{-2}\,s^{-1}}$. The flux in the full energy range is $F_{0.2-300\,{\rm GeV}} = (2.8 \pm 0.32_{\rm stat}\,^{+1.4}_{-1.2{\rm sys}}) \times 10^{-8}\,{\rm ph\,cm^{-2}\,s^{-1}}$. The γ-ray source detected with *Fermi* and H.E.S.S. towards the SNR shows that the object is a luminous Galactic SNR, with luminosities in the $0.2-300$ GeV energy range and above 400 GeV of $L_{\rm HE} \sim 3 \times 10^{35}\,{\rm erg\,s^{-1}}$ and $L_{\rm VHE} \sim 10^{34}\,{\rm erg\,s^{-1}}$, respectively. The steepening of the spectrum from HE (*Fermi*) to VHE (H.E.S.S.) of $\Delta\Gamma = 0.60 \pm 0.27_{\rm stat}\,^{+0.23}_{-0.37{\rm sys}}$ is visible in Figure 4.2. The position of the spectral break was estimated through a likelihood ratio test statistic (Rolke et al., 2005) applied to both H.E.S.S. and *Fermi* data, and reached at the photon energy $E_{{\rm br},\gamma}$= 55 GeV (with a 68% confidence interval of $[25; 125]$ GeV). Following the same procedure, the spectral turnover is found to be at $E_{{\rm cut},\gamma} = 1.4^{+1.6}_{-0.55}$ TeV assuming a power-law spectrum with an exponential cutoff.
Multi-wavelength published data were assembled to constrain the origin of the gamma-ray emission. As for others SNRs interacting with a molecular cloud, a large electron to proton ratio and a low magnetic field is required in the Bremsstrahlung and IC-dominated scenarios. This disfavors a leptonic origin for the signal seen by H.E.S.S. and *Fermi*. For the hadronic scenario, the density of the medium is a key quantity. A post-shock Hydrogen density of $\sim \mathbf{7}\,{\rm cm^{-3}}$, leading to an ISM density of $\sim \mathbf{1.7}\,{\rm cm^{-3}}$ under the assumption of a strong shock was derived from the soft component of the SNR thermal X-ray spectrum (Lazendic et al., 2005). From $^{12}{\rm CO}$ observations, Dubner et al. (2004) reported that G349.7+0.2 is associated with a MC, whose total mass and average density are estimated to be of $M_{\rm MC} \sim 5 \times 10^3\,{\rm M_\odot}$ and $n_{\rm MC} \sim 2 \times 10^4\,{\rm cm^{-3}}$, respectively. Another density estimate comes from the presence of 5 OH (1720 MHz) masers and strong $\rm H_2$ lines (Hewitt et al., 2009) towards the centre of the remnant, both tracers originating from shocked molecular region of very high density (10^4 – $10^6\,{\rm cm^{-3}}$). As discussed by Lazendic et al. (2005) and Castro and Slane (2010), these differences in density estimates indicate that the SNR is expanding in an inhomogeneous, likely clumpy, medium. With an ISM density of $\sim \mathbf{1.7}\,{\rm cm^{-3}}$, the hadronic scenario would require an energy injected in the protons of 3.3×10^{51} erg at a distance of 11.5 kpc which is larger than the kinetic energy of an average SNR. Thus the gamma-ray emission coincident with G349.7+0.2 clearly can not arise from the whole SNR shell assumed to evolve in an homogeneous $\sim \mathbf{1.7}\,{\rm cm^{-3}}$ ISM, but rather from the region of the SNR-MC interaction. The π^0-decay emission spectrum obtained with the best fit proton distribution is shown on Figure 4.2.
This led us to investigate a scenario in which the interaction region between the blast wave and the cloud is at the origin of the HE/VHE emission. The spectral turnover found at $E_{{\rm br},\gamma}$= 55 GeV resembles the case of other SNRs interacting with a molecular cloud. This spectral feature is not predicted by the DSA theory and several scenarios have been proposed to explain it. This spectral break can be due to ion-neutral collisions occurring when a shock wave interacts with a partially ionized material, leading to the reduction of the confinement of the highest energy particles which escape the system. This effect was investigated by Malkov et al. (2012) who concluded that a spectral break occurs at a few GeV, above which the particle spectrum steepens by one power Δp = 1. Then, Ohira et al. (2011) re-investigated the distribution of CRs escaping from a SNR of finite size (escaping scenario) when the observed SNR and MCs are very close or even in physical contact. In this special configuration, they argue that CR particles with all energy can escape the remnant and diffuse into the adjacent MCs once the forward shock approaches the MC modeled as a shell surrounding the SNR. Besides the breaks arising from the finiteness of the source and emission regions, another break, interpreted as the maximum particle energy in the SNR when it encounters the MC, is found. Both scenarios could reproduce the gamma-ray spectrum from G349.7+0.2, though at the expense of several free parameters

related to the diffusion and the MC properties. However, when SNR and MCs are directly interacting with each other, the validity of the escaping scenario proposed by Ohira et al. (2011) becomes an open question. In the unshocked part of the MCs, the γ-ray emission can possibly be interpreted by the illuminated cloud model. But in the interaction region between SNR and MCs the γ-ray emission is instead most likely described by the direct interaction scenario. In fact, a hybrid model with both CR particles that escaped the remnant and those confined at the SNR/MC might be a more reasonable solution for the observed γ-ray emission. Such model does not exist yet in the domain.
Following the Memorandum of Understanding signed between *Fermi* and H.E.S.S., I was appointed as "expert" to validate the *Fermi* analysis and internal referee of the H.E.S.S. publication reporting the results on this source (H. E. S. S. Collaboration et al., 2015a).

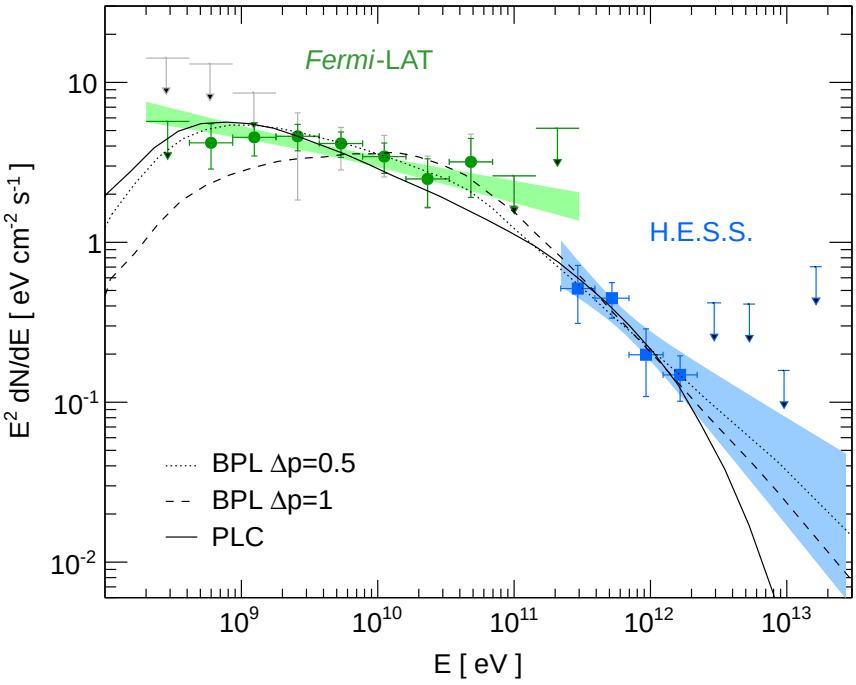

Figure 4.2: *Gamma-ray spectrum of SNR G349.7+0.2 reported in H. E. S. S. Collaboration et al. (2015a). The H.E.S.S. (blue) and* Fermi*-LAT (green) spectra are shown with their 68% CL bowtie. For the* Fermi*-LAT spectral points the statistical errors are green while the systematic errors are grey. The H.E.S.S. points are given with their statistical errors only. The π^0-decay emission models obtained with the best fit proton distributions are shown as dotted and dashed lines for the broken power-law (BPL) distributions with steepening Δp=0.5 and 1, respectively, and as a solid line for the power-law with exponential cutoff (PLC) distribution.*

4.1.2 The "pion bump" and the interesting case of W49B

Ackermann et al. (2013b) detected the characteristic pion-decay feature in the γ-ray spectra of W44 and IC 443, providing the first direct evidence that cosmic-ray protons are accelerated (or simply re-accelerated) in these shells as shown in Figure 3.11. Similar spectral characteristics were then detected for the case of W51C (Jogler and Funk, 2016) and W49B, showing that the first two are not isolated cases. I have personnally worked intensively on the case of W49B, which is one of the few papers signed by both the *Fermi* and H.E.S.S. collaborations (H. E. S. S. Collaboration et al., 2016c), by providing the *Fermi* analysis of this source.

W49B represents one of the most interesting regions in the Galaxy to study cosmic-ray acceleration. This region contains two remarkable objects: a young SNR (W49B) and a star-forming region (W49A). The SNR W49B (G43.3−0.2) is another example of a SNR/MC association. With a flux density of 38 Jy at 1 GHz, this source is one of the brightest SNRs of the Galaxy at radio wavelengths. Extensive infrared and X-ray studies revealed that W49B's progenitor was a supermassive star that created a wind-blown bubble in a dense molecular cloud in which the explosion occurred (Keohane et al., 2007). Observations of mid-infrared lines from shocked molecular hydrogen show that W49B is interacting with molecular clouds, but, contrarily to the 20000 year-old SNR W44, W49B is estimated to be relatively young with an age between 1000 and 4000 years (Zhou et al., 2011). The *Fermi* analysis of W49B is relatively complex since it lies in a diffuse region of the Galactic plane and needs to start at 60 MeV to be able to detect the "pion bump" feature. Due to the large Point spread function (PSF) of the LAT at low energy, a region of 20° radius needs to be analyzed while the model describing the region contained sources up to 25° from the source to account for photons leaking at the edges of our region of interest. Due to the very large number of parameters to fit in such crowded regions, I left free only the spectral parameters of sources closer than 5° to W49B or with a TS larger than 400, while the parameters of all other sources were fixed at the values from the 3FGL catalog. The spectral analysis was then performed with gtlike including all events between 0.06 and 300 GeV. To derive the spectral points, this energy range was divided into 20 logarithmically-spaced energy bins and a maximum likelihood spectral analysis was performed in each interval, assuming a power-law shape with a fixed spectral index of $\Gamma = 2$ for W49B. The spectrum below 300 MeV is steeply rising, clearly exhibiting a break at around 300 MeV as seen in Figure 4.3. To quantify the significance of this spectral break, a log-likelihood fit of W49B between 60 MeV and 4 GeV was performed. The improvement in log-likelihood when comparing the broken power-law to a single power-law corresponds to a formal statistical significance of 8σ for the low-energy break (TS of 84 for 2 additional degrees of freedom). The break is located at $304 \pm 20_{\rm stat} \pm 10_{\rm syst}$ MeV while the spectral indices below and above the break are $0.10 \pm 0.30_{\rm stat} \pm 0.28_{\rm syst}$ and $2.21 \pm 0.05_{\rm stat} \pm 0.06_{\rm syst}$. Taking advantage of the smooth connection between the HE and VHE spectra visible in Figure 4.3, the presence of another break at high energy was evaluated through a likelihood ratio test statistic applied to both the H.E.S.S. and *Fermi*-LAT data. For this test, a single power-law and a smoothly broken power-law between 500 MeV and 10 TeV – above the low energy break found above – were used and the statistical and systematic uncertainties have been taken into account. The minimum of the likelihood ratio is reached at 8.4 GeV with a 6.5σ improvement of the smoothly broken power-law model with respect to the power-law one. The 68% confidence interval is [5.9; 10.6] GeV and the spectral indices below and above the break are respectively 2.17 ± 0.06 and 2.80 ± 0.04. This result has been checked by fitting the *Fermi*-LAT fluxes of W49B between 500 MeV and 300 GeV with both a single power-law and a smoothly broken power-law. A 3.3σ (TS of 14 for 2 additional degrees of freedom) improvement is obtained for an energy break at $9.4 \pm 2.9_{\rm stat} \pm 3.8_{\rm syst}$ GeV. This energy, as well as the spectral indices above and below the break, are compatible with the values obtained from the *Fermi*-LAT and H.E.S.S. joint fit. Interestingly, while W49B is estimated to be 1000 – 4000 years old, it exhibits spectral features similar to the other detected SNR/MC systems which are believed to be ~ 10 times older. Likewise, G349.7+0.2 which has roughly the same age as W49B, shows an energy break which is ~ 5 times higher. This emphasises the importance of the environment in the evolution of the γ-ray luminosity of these objects. The broad band spectrum of W49B was fit by Junichiro Katsuta. It can be explained either by leptonic or hadronic models. However, the sharp break detected with the *Fermi*-LAT data at 304 MeV ("pion bump") favours a hadronic origin of the gamma-ray emission since the leptonic models require a very hard spectrum for the electron population as well as a very high electron-to-proton ratio. All results are reported in the H.E.S.S.-Fermi

paper (H. E. S. S. Collaboration et al., 2016c).

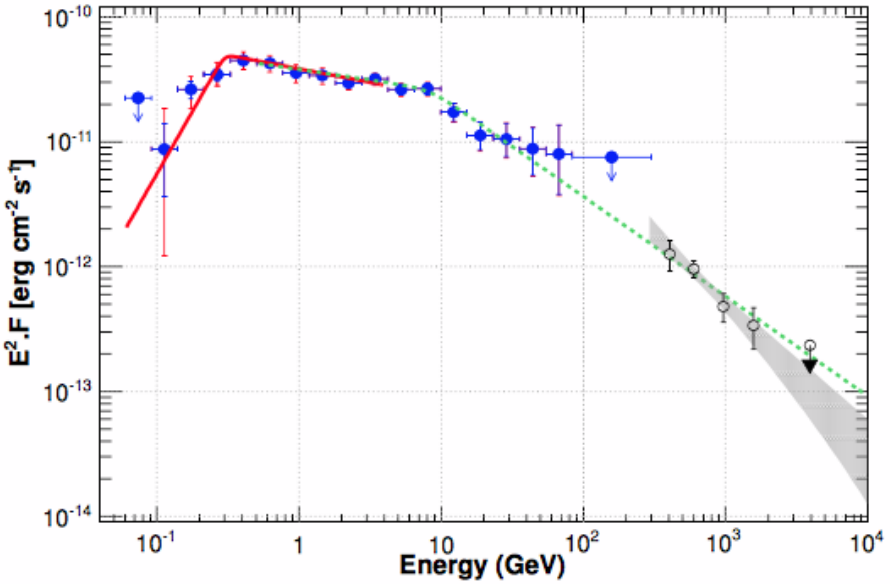

Figure 4.3: Fermi-*LAT and H.E.S.S. spectrum of W49B from H. E. S. S. Collaboration et al. (2016c). The red line shows the best fit of a smoothly broken power-law derived between 60 MeV and 4 GeV and the blue data points indicate the fluxes measured in each energy bin with the* Fermi-*LAT. The statistical errors are shown in blue, while the red lines take into account both the statistical and systematic errors. The gray band shows the 68% confidence level (CL) uncertainty of the best-fit power-law model with H.E.S.S. The open black circles are the spectral points computed from the forward-folding fit with their statistical errors shown in black. For both instruments, a 95% CL upper limit is computed when the statistical significance is lower than* 2σ*. The dotted green line shows the best smoothly broken power-law model obtained from the joint fit of the* Fermi-*LAT and H.E.S.S. data between 500 MeV and 10 TeV.*

4.2 Particle escape from SNRs interacting with MCs

Though the details of the escape of CRs from SNR shocks are still debated, it is generally believed that the highest energy protons are released first and that particles of lower energy are released gradually as the shock speed decreases. Once released, relativistic protons produce gamma-rays due to proton-proton interactions in the surrounding interstellar medium (see Gabici (2011) for more details). This means that insights on the mechanism of escape can be obtained from gamma-ray observations because runaway CRs can interact with massive MCs located in the vicinity of the parent SNR and make the former bright gamma-ray sources. To date, a clear detection of gamma rays from the vicinity of SNRs has been reported for the SNRs W44 and W28. In addition to these two sources, the detection of gamma-ray emission beyond the X-ray shell of the SNR RX J1713.7-3946 as discussed in Section 3.3.1 can be interpreted either as a signature of particle escape, or as the first detection of a shock CR precursor. Finally, it has been suggested by Cui et al. (2016) that HESS J1729−345 is due to emission from runaway cosmic rays accelerated by the SNR HESS J1731−347 and that are now interacting with MCs coincident with the unidentified TeV source. I will review briefly the cases of W44 and W28 for which I acted as internal referee and analysis cross-check of the Category II *Fermi* publications and the case of HESS J1729−345 that was analyzed during Benjamin Condon's thesis.

4.2.1 Illuminated clouds in the W28 region

The W28 SNR has an age greater than 10^4 years, and is likely in the Sedov or radiative phase (Westerhout, 1958; Lozinskaya, 1974). In our *Fermi* paper, we adopted the same age of 4×10^4 years. The SNR is located within a molecular cloud complex with a mass of $1.4 \times 10^6 M_\odot$ (Reach et al., 2005) and interacts with some parts of the cloud, traced by the detection of OH (1720 MHz) masers (Frail et al., 1994; Claussen et al., 1997). Observations of molecular lines placed W28 at a distance of ~ 1.9 kpc (Velázquez et al., 2002). H.E.S.S. observations of W28 have revealed four TeV γ-ray sources (Aharonian et al., 2008b): HESS J1801−233, located along the northeastern boundary of W28, and a complex of three sources, HESS J1800−240A, B, and C, located to the south, outside the radio boundary. The southern H.E.S.S. sources spatially correspond with molecular clouds whose masses and distances from the centre of the SNR can be estimated from CO measurements and result in ∼5, 6, and 4 $\times 10^4 M_\odot$, respectively, and ∼12, 20, and 20 pc, respectively (Aharonian et al., 2008b). This led several authors to suggest that the gamma-ray emission from the W28 region could be the result of hadronic interactions of CRs that have been accelerated in the past at the SNR shock and then escaped in the surrounding medium (Gabici et al., 2010). Complementary information can be obtained using CO, HCO+, and DCO+ millimetre line observations. Towards positions located close to the supernova remnant W28, Vaupré et al. (2014) find cosmic ray ionisation rates much larger (> 100) than those in standard Galactic clouds, supporting the hypothesis made in the *Fermi* paper that the gamma-rays observed in this region have a hadronic origin. Conversely, towards one position situated at a larger distance coincident with a southern hotspot, they derive a standard cosmic ray ionisation rate, suggesting that the ionising lower energy CRs remain confined closer to the SNR. The picture that emerges is that of a stratified structure with CRs of larger and larger energies occupying larger and larger volumes ahead of the shock, in agreement with the current theory. This region is therefore an excellent site to study CR diffusion and *Fermi*-LAT data are crucial to constrain the associated parameters.

Using the first year of *Fermi*-LAT observation, Abdo et al. (2010b) detected a source coincident with HESS J1801−233 and only one source to the South associated with HESS J1800−240B. Then, the second *Fermi*-LAT catalog reported the detection of two LAT sources in the southern region: 2FGL J1800.8−2400 and 2FGL J1758.8−2402c (Nolan et al., 2012). Our new analysis was based on 4 years of data above 2 GeV (Hanabata et al., 2014), focusing on the high energy band of the LAT to allow a comparison with the TeV observations made by H.E.S.S.. Figure 4.4 (left and right) shows a close-up view of the LAT counts map above 10 GeV, superimposed on the H.E.S.S. significance map (Aharonian et al., 2008b) and the radio image by the Very Large Array (Brogan et al., 2006). In addition to HESS J1801−233 and the two hotspots associated to HESS J1800−240B and HESS J1800−240C, the region coinciding with HESS J1800−240A is now bright at GeV energies, as well as an additional GeV source to the west (called Source W) beyond the observed TeV emission. We performed a series of maximum likelihood fits to investigate the GeV morphology around W28, adopting a power-law spectral form for all sources of interest. The best-fit model for the GeV emission is provided by including the H.E.S.S. template and a separate point-source for Source W, thus highlighting the very good correspondence of the LAT signal with the TeV emission. We found no other obvious multi-wavelength counterparts to Source W, such as pulsars and blazars, within the positional error radius of 0.054° at the 95% confidence region. Then, using the best spatial model, we performed a spectral analysis of the sources in this region. W28 (HESS J1801−233) is well fit with a simple power-law with an index of 2.77 ± 0.06, in agreement with the previous result reported by Abdo et al. (2010b) which also reported the detection of a significant break at ~ 1 GeV (thanks to a larger energy range from 200 MeV to 100 GeV). The LAT spectra of HESS J1800−240B and

HESS J1800−240C smoothly connect to the H.E.S.S. measurements, while HESS J1800−240A has a slightly harder spectral index than the value of 2.55 ± 0.18 found by H.E.S.S.. Thus, we expect a spectral break in the GeV to TeV range. The absence of detection of Source W by H.E.S.S. also hints for a spectral break between the energy domains covered by the two experiments. The main part of the paper, led by the Japanese group at Ibaraki University, explore the possibility that the three H.E.S.S. sources are attributed to the pion-decay gamma rays from molecular clouds illuminated by the escaping particles accelerated in W28. The conclusion of this work is that the GeV–TeV spectra of the four sources surrounding W28 can naturally be explained by a single model in which the diffusion constant D_{27} at 10 GeV c^{-1} is 0.5–5 in units of 10^{27} cm^2 s^{-1} and the power-law index of the energy dependence δ is 0.1–0.35. These values are smaller than those based on the Galactic CR propagation model: $D_{27} \sim 10$ and $\delta \sim 0.6$ (Ptuskin et al., 2006). D_{27} is also smaller than that of W44 derived by Uchiyama et al. (2012) (see Section 4.2.2). However, for an SNR in a dense environment, D_{27} is expected to be as low as ~ 0.1 (Ormes et al., 1988) and to depend on the magnetic field strength in the molecular cloud into which the runaway CRs propagate (Gabici et al., 2007). D_{27} and δ would also be affected by the amplification of Alfvén waves generated by the escaping CRs (Fujita et al., 2011). Interestingly, considering the masses of the molecular clouds responsible for the emission, the lower limit on the total energy of the escaped CRs is constrained to be $\sim 2 \times 10^{49}$ erg, in agreement with the conjecture that SNRs are the main sources of the Galactic CRs.

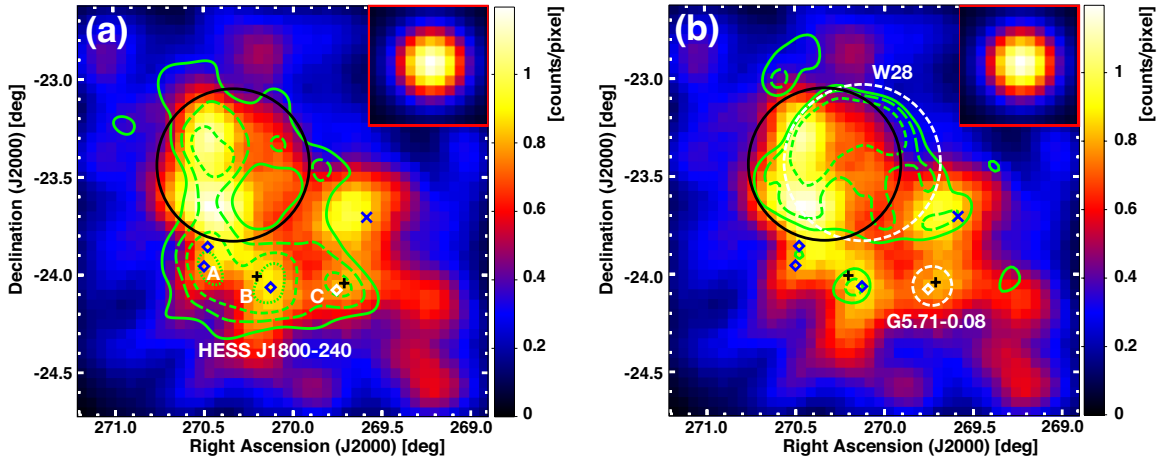

Figure 4.4: *The LAT count map between 10 and 100 GeV around W28 superimposed on (a) H.E.S.S. and (b) VLA contours. The maps have a pixel size of* 0.05° *and are smoothed by a Gaussian kernel of* $\sigma = 0.20^\circ$*. The inset of each figure shows the simulated LAT PSF with a photon index of 2.5 in the same energy range, adopting the same smoothing. Locations of 2FGL catalog sources included in the emission model are indicated with black marks; circle for W28, left-hand cross for 2FGL J1800.8−2400, and right-hand one for 2FGL J1758.8−2402c, respectively. A blue* $\times$ *indicates the best-fit position of W28. Blue diamonds on the left indicate HII regions: G6.1−0.6 and G6.225−0.569. The blue diamond on the right is W28A2 (see the text). The white diamond indicates the OH maser spot associated with G5.71−0.08. Green contours in panel (a) show the H.E.S.S. significance map for TeV* γ *rays at 20, 40, 60, and 80% levels (Aharonian et al., 2008b). Bright TeV spots in the south are A, B, and C as indicated in the figure. Green contours in panel (b) indicate the VLA 90 cm image at 5, 10, and 20% of the peak intensity (Brogan et al., 2006). Outer boundaries of SNR W28 and G5.71−0.08, as determined from the radio images, are drawn as white dashed circles. Plot taken from (Hanabata et al., 2014).*

4.2.2 Cosmic-ray escape at high energy from W44

The SNR W44 is a middle-aged ($\sim 2 \times 10^4$ years old) SNR located in the Galactic Plane (l,b) = ($34.7°$,$-0.4°$) at a distance of ~ 3.1 kpc (Clark and Caswell, 1976). In the southeast side of the SNR, a molecular cloud complex embedded in the SNR shell interacts with the source (Wootten, 1977; Rho et al., 1994). The OH maser (1720 MHz) emission detected in correspondence with the SNR/MC region, confirms their interaction (Claussen et al., 1997). At gamma-ray energies, this source was first detected by *Fermi*-LAT observations above 200 MeV that showed a GeV emission morphology with an apparent good correlation with the radio shell (Abdo et al., 2010c). Its associated spectrum showed a prominent peak near 1 GeV and a clear decrease at higher energies with a steep spectrum for the photon index near 3, explaining why it is not detected at TeV energies. A few years later, it attracted much attention because of its relevance regarding the origin of Galactic cosmic-rays with the identification of a spectral decrease below 200 MeV (known as the "pion bump") by the missions AGILE and *Fermi* (Giuliani et al., 2011; Ackermann et al., 2013a). This feature can naturally be attributed to a neutral pion emission. It is a clear evidence that protons are being accelerated (or re-accelerated, depending on the mechanism of acceleration invoked) by the SNR shock. The gamma-ray analysis of the neighborhood of this SNR is clearly tempting to look for interaction of escaping protons with the surrounding MCs. The analysis and modeling was led by Yasunobu Uchiyama at Stanford Linear Accelerator and the paper published in The Astrophysical Journal Letters (Uchiyama et al., 2012).

For this analysis, we used the LAT data above 2 GeV acquired from 2008 August 4 to 2011 September 6. We employed a synchrotron radio map of SNR W44 taken from Handa et al. (1987) to model the spatial distribution of the gamma-ray emission from W44 given that the synchrotron and gamma-ray emission from W44 are expected to be co-spatial (as seen in the first *Fermi* analysis of this source in 2010). Figure 4.5 b) shows a residual count map, where the observed count map in 2–100 GeV is subtracted to the best-fit sky model. Significant excess γ-rays are seen in the vicinity of W44; the features are referred to as SRC-1 and SRC-2 in the paper. The statistical significance is found to be $\sim 9\sigma$ for SRC-1 and $\sim 10\sigma$ for SRC-2. The residual count map depends weakly on the choice of the spatial template that describes γ-rays from W44. Our simulations using the $gtobssim$ tool from the *Fermi* Science Tools verified that SRC-1 and SRC-2 are not caused by photons leaking from W44 due to the PSF of the LAT. We also checked the robustness of the results by selecting only the front-converted events. A spectral analysis was then performed showing a power-law photon index of $2.56 \pm 0.23_{\rm stat} \pm 0.2_{\rm syst}$ and $2.85 \pm 0.23_{\rm stat} \pm 0.2_{\rm syst}$ for SRC-1 and SRC-2, respectively. We tested a smoothly broken power-law and exponentially cutoff power- law for SRC-1/2 but found that the spectral fits do not significantly improve.

It has long been known that a complex of giant molecular clouds surrounds SNR W44; the spatial extent is as large as 100 pc and the total mass of the complex amounts to $\sim 1 \times 10^6 M\odot$ (Dame et al., 1986; Seta et al., 1998). We have investigated the possibility that the γ-ray emission in the vicinity of W44 would be caused by imperfection of the maps of gas column densities used in the model of the Galactic interstellar diffuse emission, or to a local enhancement of CR density. The former implies that the mass in the gamma-ray-emitting region around W44 is underestimated by a large factor (~ 5), or it requires the presence of unknown background clouds with a huge mass of $10^6 M\odot$. Therefore an overabundance of CRs in the vicinity of W44 offers a more sensible explanation. Assuming $1 < D_{27} < 30$ for the diffusion constant at 10 GeV, the model of cosmic-ray escape proposed by Yasunobu and applied to the case of SRC-1 and SRC-2 implies that the total kinetic energy channeled into the escaping CRs is $\sim (0.3 - 3) \times 10^{50}$ erg. As for the case of W28, such energy would be sufficient to place SNRs as the main sources of Galactic CRs.

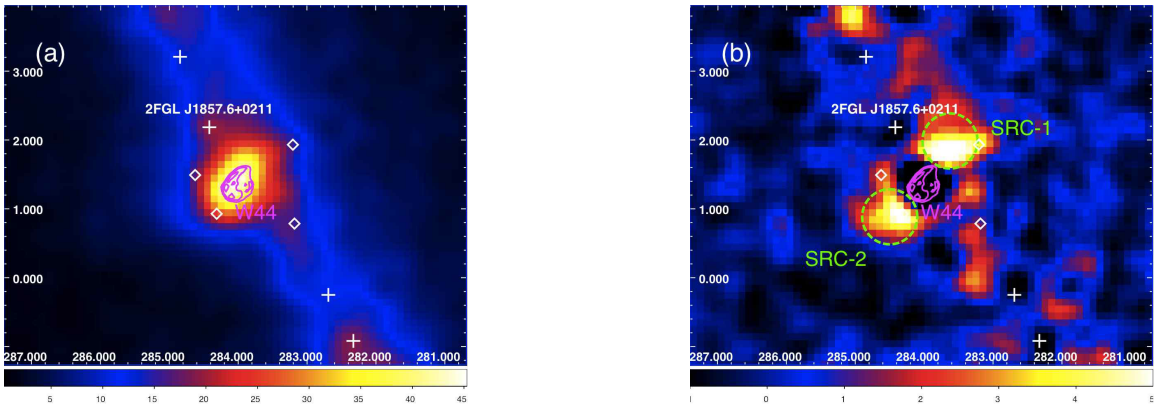

Figure 4.5: *(a)* Fermi *LAT γ-ray count map for 2–100 GeV around SNR W44 in units of counts per pixel ($0.1^\circ \times 0.1^\circ$) in celestial coordinates (J2000). Gaussian smoothing with a kernel $\sigma = 0.3^\circ$ is applied to the count maps. Green contours represent a 10 GHz radio map of SNR W44 (Handa et al., 1987). 2FGL sources included in the maximum likelihood model are shown as crosses, while those removed from the model are indicated by diamonds. (b) The difference between the count map in (a) and the best-fit (maximum likelihood) model consisting of the Galactic diffuse emission, the isotropic model, 2FGL sources (crosses), and SNR W44 represented by the radio map. Excess γ-rays in the vicinity of W44 are referred to as SRC-1 and SRC-2. These Figures are taken from (Uchiyama et al., 2012).*

4.2.3 The unidentified TeV source HESS J1729−345

The supernova remnant HESS J1731−347 was analyzed by my PhD student, Benjamin Condon, who defended his thesis in October 2017. A distinctive feature of the HESS J1731−347 environment is another resolved TeV source, HESS J1729−345, located just outside of the SNR (H.E.S.S. Collaboration et al., 2011a). This source is in apparent spatial coincidence – at least in projection – with molecular clouds seen through sub-mm molecular line emission. Since no other local particle accelerators are known so far, a scenario in which particles that have escaped the SNR HESS J1731−347 and are presently penetrating the molecular clouds coincident with HESS J1729−345, leading to enhanced γ-ray emission, was suggested by Cui et al. (2016). In contrast to W28 and W44, HESS J1731−347 is much younger and is presently still accelerating super-TeV particles. It offers the opportunity to model the evolution of the SNR and its associated particle acceleration and escape history up to the present time with rather good precision. To constrain the parameters of this model, we decided to analyze the region with the eight years of Pass 8 data between 1 GeV and 2 TeV used to study the shell-type remnants SN 1006 and HESS J1731−347 as discussed in Section 3.3.3. In the model of the region corresponding to HESS J1731−347, we added a Gaussian source to represent the potential emission of HESS J1729−345, using the position and extension reported in the H.E.S.S. paper (R.A. = 262.39°, Dec.=-34.54°,σ= 0.14°) and performed a new fit of the region. As it resulted in a non-detection (TS < 3), we derived a 95% C.L. upper limit (1.30×10^{-12} erg cm^{-2}s^{-1} between 1 GeV and 2 TeV) presented in Figure 4.6 (middle). This upper limit is a factor of two above the TeV data and cannot constrain the origin of the γ-ray emission of HESS J1729−345. However, it confirmed a turnover between the *Fermi*-LAT and H.E.S.S. data, and according to Cui et al. (2016)'s model, it is well below the sensitivity of the LAT in the Galactic plane. Therefore, we do not expect any constraints in the near future coming from the LAT on this unidentified source. In addition to the detection of HESS J1729−345, Cui et al. (2016) investigated the possibility that CRs were diffusing from the SNR forward shock to nearby molecular clouds and made predictions regarding

the γ-ray emission of an hypothetical cloud called MC-core located at a position coincident with the HII region G353.43−0.37. This cloud is located very close to a LAT γ-ray source detected in this region called S0 in our *Fermi* paper (see left side of Figure 4.6). For those reasons, we studied the spectrum of S0 in the GeV band and found a spectral index of $\Gamma = 2.50 \pm 0.05_{\rm stat}$ and an energy flux of $(4.90 \pm 1.28_{\rm stat}) \times 10^{-12}$ erg cm^{-2} s^{-1}, as presented in Figure 4.6 (right). If S0 corresponds to MC-core, this result does not support Cui et al. (2016)'s models which predicted a hard index at GeV energies. However, it should be noted that the model depends on several parameters, the most important one might be the distance between the SNR and the cloud which is very poorly known. Since S0 could be another background source and not related to MC-core, we added another point source, at the same position. In this situation, no significant signal was found in addition to S0 and the derived upper limit (9.31×10^{13} erg cm^{-2} s^{-1} between 1 GeV and 2 TeV) could not constrain the predicted models. All results are discussed in the *Fermi* paper (Condon et al., 2017) and in Benjamin Condon's thesis.

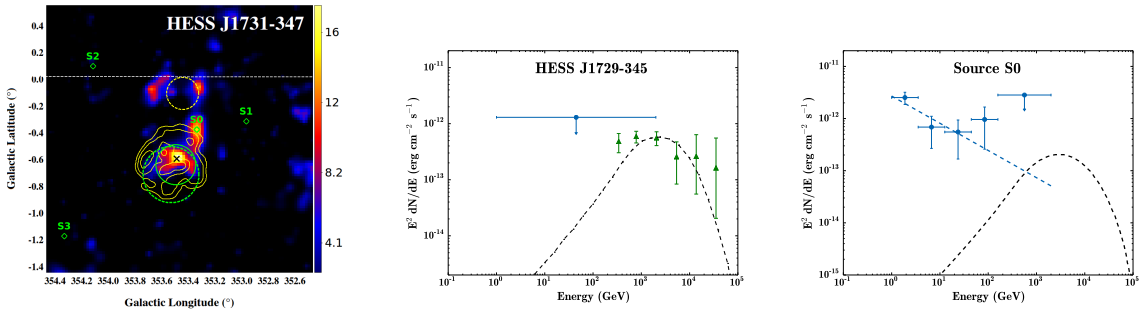

Figure 4.6: *Left: TS map (1 GeV − 2 TeV) in Galactic coordinates showing a $2° \times 2°$ region centered on the position of HESS J1731−347. Green diamonds correspond to additional background sources while the black cross and green circle correspond to the best-fit position (for $E > 1$ GeV) of HESS J1731−347 as a point source and a uniform disk respectively. The best uniform disk above 10 GeV is represented by the green dashed circle. The TeV morphology of the shell is represented by the yellow contours and the yellow dashed circle shows the position of HESS J1729−345. Middle:* Fermi-*LAT γ-ray spectrum of HESS J1729−345 using eight years of Pass 8 data between 1 GeV and 2 TeV in blue (Condon et al., 2017) together with the H.E.S.S. spectrum of HESS J1729−345 (H.E.S.S. Collaboration et al., 2011a) in green. Right:* Fermi-*LAT γ-ray spectrum of S0 with the same dataset. In both figures, the black dashed line corresponds to the prediction from Cui et al. (2016).*

Since it became clear that very few constraints on HESS J1729−345 can be obtained with the LAT, we decided to analyze archival data unpublished by the H.E.S.S. collaboration to see if new results could be obtained on this region. For the last publication of the H.E.S.S. collaboration (H.E.S.S. Collaboration et al., 2011a), a total of 59 hours was used. However, since then, 32 hours were taken on this region with the four small telescopes but were not used for any publication yet. After quality selection cuts, a total of 91 hours was used for this re-analysis. The data set was analyzed using the Model analysis (de Naurois and Rolland, 2009) which exploits the full pixel information by comparing the recorded shower images with a pre-calculated shower model using log-likelihood minimization. Spectral and spatial analyses were carried out using a minimum image intensity of 60 photoelectrons (p.e.) resulting in an energy threshold of ∼240 GeV. For the background estimation in the image and in the morphology studies, the ring background method presented in Berge et al. (2007) was used. Regions of $0.4°$, $0.2°$ and $0.2°$ around HESS J1731−347, HESS J1729−345 and MC-core respectively were excluded as seen in Figure 4.7 a).

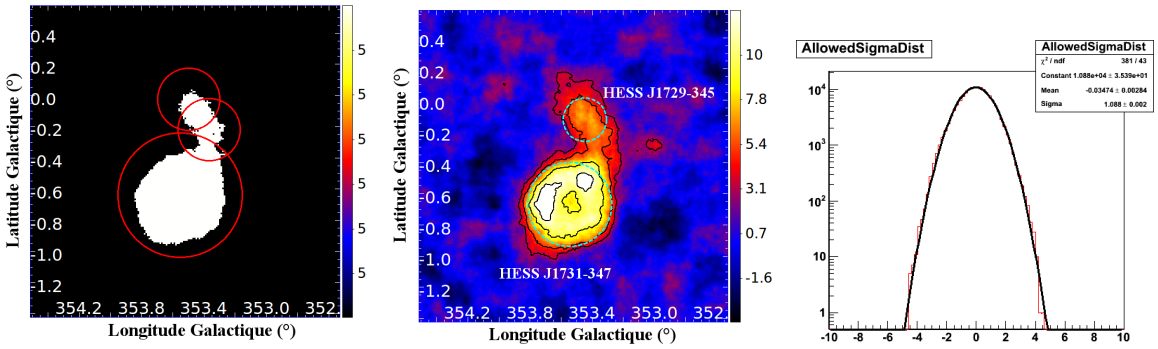

Figure 4.7: *Left: Exclusion regions (red) superimposed to the significance map highlighting pixels above 5σ. Middle: Significance map obtained using the ring background method. Dotted circles indicate the positions and sizes of HESS J1731−347 and HESS J1729−345 according to (H.E.S.S. Collaboration et al., 2011a). Right: Significance distribution in the OFF regions (red). The black line corresponds to the fit with a Gaussian.*

The significance map obtained in Figure 4.7 (middle) reveals a morphology different from the one published by H.E.S.S. Collaboration et al. (2011a): instead of a point-like source, the emission coming from HESS J1729−345 seems to be diffuse, elongated and connected to HESS J1731−347. To characterize this gamma-ray emission and quantify a potential difference with respect to the previous H.E.S.S. publication, we used Chandra's modeling and fitting package released by NASA called Sherpa[2]. Several morphological fits have been performed to characterize HESS J1729−345 assuming a disk spatial model, a 2D-Gaussian or an asymmetric 2D-Gaussian and fitting at the same time the parameters of the 2D-shell representing HESS J1731−347. The results are reported in Table 4.1 showing that the best fit is obtained for an extended source. An improvement at 3.8σ level is obtained using the asymmetrical 2D-Gaussian with respect to the simple 2D-Gaussian. This confirms the visual impression that we had looking at Figure 4.7 (middle): the emission is significantly extended and elongated. Interestingly, this emission seems to coincide with the distribution of molecular gas at $\sim$3.2 kpc as evidenced by CS(1-0) emission with the Mopra radio telescope (Maxted et al., 2018). This is another evidence in favor of a runaway CR scenario. Observations at lower energies especially with HESS-II or with CTA-South will be of prime importance to provide a confirmation that protons are indeed being accelerated by HESS J1731−347 and escaped in the surrounding medium to create the γ-ray signal seen by H.E.S.S. in the North of the shell.

HESS J1731−347	HESS J1729−345	$\log(\mathcal{L})$	Test Statistic	$N_{\rm dof}$
2D-shell	–	−90473	–	6
2D-shell	Disk	−90396	154	10
2D-shell	2D-Gauss	−90392	162	10
2D-shell	Asym 2D-Gauss	−90383	180	12

Table 4.1: *Morphological fits of HESS J1729−345. $N_{\rm dof}$ is the number of degrees of freedom for each model.*

[2]This analysis package is available at: http://cxc.harvard.edu/sherpa/

4.3 Middle-aged SNRs in the ISM

Fermi-LAT also reported the detection of evolved SNRs with gamma-ray luminosity of $\sim 10^{33}$ erg/s between 1 and 100 GeV, much lower than those of GeV-emitting SNRs interacting with MCs. This is the case of Cygnus loop and S147. The Cygnus Loop (G74.0−8.5) is one of the most famous and well-studied middle-aged SNRs. The shell-like X-ray emission from thermal plasma is prominent in the northern region of the remnant, with a blowout in the southern rim (Ku et al., 1984). The distance from Earth is estimated to be 540 pc based on the proper motion of optical filaments in conjunction with models of non-radiative shocks (Blair et al., 2005). The age has been estimated to be $\sim 2 \times 10^4$ yr based on plasma parameters derived from X-ray data (Miyata et al., 1994) and $\sim 1.4 \times 10^4$ yr based on the shock model and X-ray measurements (Levenson et al., 1998). SNR S147 (G180.0−1.7), located toward the Galactic anticenter, is one of the most evolved SNRs in our Galaxy. S147 has a nearly circular shape with an angular diameter of ≈ 200 arcminute. No indication of interactions with molecular clouds has been reported for these 2 SNRs. In both cases, the best fit to the LAT data is obtained using multi-wavelength spatial templates (Hα emission or X-ray) rather than simple geometrical shapes. Since I contributed to the publication on S147 only, I will concentrate on this remnant and briefly summarize the results obtained since they are of interest in the context of the Crushed Cloud model proposed by Uchiyama et al. (2010) to explain the gamma-ray emission from SNRs interacting with MCs.

For this analysis, we used ∼31 months of LAT data collected from 2008 August 4 to 2011 March 1. The morphological analysis was performed above 1 GeV. First, we generated a Test Statistic (TS) map of the region. It is clear from Figure 4.8 that the excess gamma rays above backgrounds are distributed inside the SNR boundary and the spatial extent of the source is consistent with the remnant size. Using the different spatial templates (disk, sphere, shell and Hα template[3]), we perform maximum likelihood fits and compare the best-fit parameters in the energy range of 1–200 GeV. S147 source is significantly detected in each case, and the obtained fluxes and spectral shapes are almost the same. The Hα image has the largest TS among all templates, despite the fact that the other templates have three more free parameters (position and diameter) than those of the Hα image. Comparisons between gamma-ray and Hα fluxes on five distinct regions of S147 indicate a possible correlation between them but more statistics is needed to confirm this result. The results of the correlation diagram and the fits of the different spatial templates suggest that the gamma-ray emission exhibits a possible correlation with Hα filaments and therefore also with synchrotron radio filaments given a tight correlation between the Hα and radio maps (Xiao et al., 2008). This means that the high-energy particles responsible for the gamma-ray emission are in the vicinity of the shock regions since the Balmer-dominated filaments define the current location of the blast wave and mark the presence of neutral material. Junichiro Katsuta modeled the multi-wavelength spectra assuming that the gamma-ray emission comes from two distinct regions: 1) the intercloud medium in which the blast wave is propagating, 2) the filaments formed through radiative shocks driven in atomic clouds. Obviously, due to the large PSF of the LAT, these components are only separated spectrally in the gamma-ray band. His model well reproduces the multi-wavelength data and shows that the gamma-ray flux is dominated by the pion-decay emission from the dense filaments due to the high densities of gas and CRs. The model also indicates that the re-acceleration of pre-existing CRs and subsequent adiabatic compression is sufficient to supply the required CR density in filaments. SNR S147 thus offers a first example of realization of the Crushed Cloud model in an atomic cloud version (i.e without any MC interaction), and supports the importance of dense filaments in SNRs as gamma-ray production sites.

[3] 3-2 transition in neutral atomic H, used as a tracer of ionized gas

All results on S147 are published in Katsuta et al. (2012). The GeV gamma-ray emission from the Cygnus Loop (Katagiri et al., 2011) may be explained by the Crushed Cloud model as well.

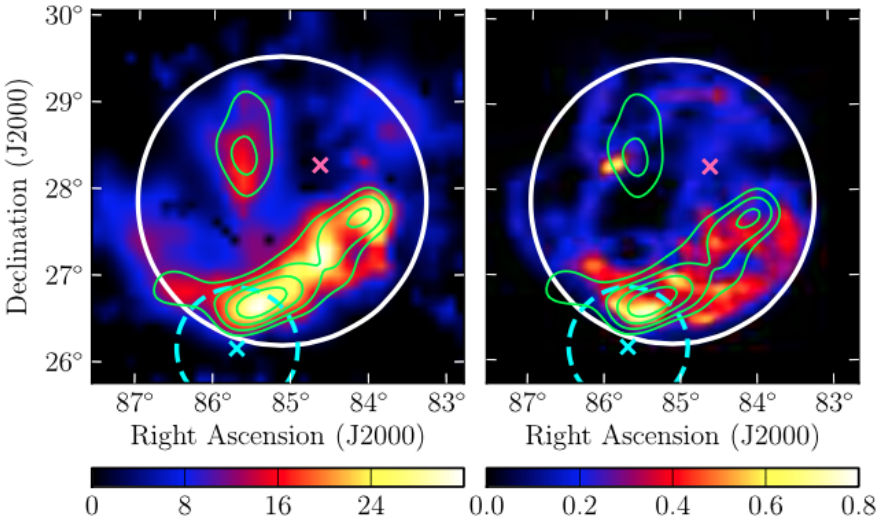

Figure 4.8: *Left: TS map obtained with maximum likelihood analysis of the* Fermi*-LAT data in the vicinity of SNR S147 above 1 GeV. Overlaid are linear contours of the background-subtracted count map above 1 GeV. A white circle represents the outer boundary of SNR S147. A cyan cross and circle represent a position and positional error (95% confidence level) of the EGRET source 3EG J0542+2610, respectively (Hartman et al., 1999). A magenta cross indicates the position of PSR J0538+2817. Right: Hα flux intensity map of SNR S147 in units of rayleighs ($10^6/4\pi$) photons cm^{-2}s^{-1}sr^{-1}(Finkbeiner, 2003), with the contours of the background-subtracted count map overlaid.*

4.4 Puppis A: a transition case

Puppis A is a SNR adiabatically expanding into the interstellar medium in the vicinity of a large molecular cloud. At an age of only $\sim$4500 years (Becker et al., 2012) implying that the SNR is currently in the Sedov-Taylor evolutionnary phase, it is amongst the youngest Galactic SNRs known to be interacting at several locations throughout the shell with dense gas seen as a complex of small HI and CO clouds. This makes Puppis A an interesting transitional case between young SNRs still evolving into a circumstellar medium (e.g. Cas A), and older SNRs which are interacting with large, dense molecular clouds (e.g. IC 443). Located at a distance of 2.2 $\pm$ 0.3 kpc (Reynoso et al., 2003), it is one of the three oxygen-rich SNRs known in the Galaxy. This, together with the presence of a compact object strongly supports the idea that Puppis A originates from a core-collapse SN explosion. Recent high-resolution X-ray observations of the whole SNR (Dubner et al., 2013) have confirmed the presence of a decreasing gradient in the emission from NE to SW and also revealed a highly structured and filamentary morphology with unprecedented detail, indicating that Puppis A is evolving in an inhomogeneous, knotty ISM. Observations with Spitzer have shown a clear correlation between infrared (IR) and X-rays at all spatial scales, demonstrating that the thermal IR emission arises from dust collisionally heated by the hot, shocked plasma (Arendt et al., 2010).
We used 36 months of *Fermi*-LAT observations to analyze the source and report the detection of the SNR Puppis A (Hewitt et al., 2012). As a first step, we performed a morphological analysis of the source and found that Puppis A is clearly spatially extended at energies above 800 MeV, with a GeV

morphology well correlated with X-ray and IR emissions. Then, using the X-ray template, we performed a maximum likelihood fit using gtlike and compared the best-fit parameters in the wide energy range 0.2–100 GeV. To avoid any bias due to the brightness of the Vela pulsar in this energy interval, the spectral fit was performed in the off-pulse phase interval. No evidence for cutoff or break is visible and, in all cases, the *Fermi*-LAT data are well described by a power-law of index $2.09 \pm 0.07 \pm 0.09$ in the LAT energy range. We also searched for spectral variations across the γ-ray emission associated with Puppis A by dividing the X-ray template into two halves. We allowed an independent normalization and spectral index for the two X-ray parts. Interestingly, the spectrum of the Western half-disk is found to be steeper by an index of 0.3 (2σ) above 200 MeV, with respect to the Eastern half-disk as can be seen in Figure 4.10. However, more statistics are needed to confirm spectral differences between the Eastern and Western regions. For this paper, we worked together with Jack Hewitt from the NASA Goddard Space Center who analyzed WMAP data at 20 to 93 GHz allowing a detection of Puppis A in this energy band as well. Extending the radio spectrum to high energies reveals a putative spectral break or cutoff at a frequency above 40 GHz. Very few SNRs have been convincingly shown to have breaks at high frequencies. One such SNR is S147, which has a break at $\sim$1.5 GHz. However, there are significant differences between S147 and Puppis A. S147 is an order of magnitude older and has entered the radiative phase (indicated by dense Hα filaments), while Puppis A is still non-radiative, except for a few bright X-ray knots. The radio break in S147 occurs at $\sim$1.5 GHz, and may be explained by synchrotron cooling over the long lifetime of the remnant while the break frequency in Puppis A is more difficult to explain. A synchrotron break at $\sim$40 GHz would require a magnetic field in excess of 1 mG to have existed for the entire lifetime of Puppis A, in order to cool the electron spectrum. However, no corresponding break is observed in the LAT spectrum with the current statistics, so two electron populations would be required to fit the radio and γ-ray data.
If we do not take into account this indication of spectral break, the radio to γ-ray SEDs was fit using IC, Bremsstrahlung and hadronic dominated models presented in Figure 4.9. All emission mechanisms are able to fit the data, though with different magnetic field strengths and energetics of relativistic particles. In the leptonic models, the electron-to-proton ratio needs to be larger than 0.1, and thus in excess of the ratio found for local cosmic-ray abundances, to inject a reasonable energy content in radiating electrons. For the hadronic model a total energy in CR protons of $\mathrm{Wp} \sim 4{\times}10^{49}$ erg is needed: this is comparable to the total energy in non-thermal protons estimated in Cas A in the hadronic model (see section 3.2). In contrast, SNR W49B has a luminosity one order of magnitude greater than Puppis A, with a total energy content in protons of only $\sim$few times 10^{49} erg (in hadronic models), similar to Puppis A and a similar age. The difference in luminosity can be easily explained by the much higher average density in W49B, as it is interacting with large molecular clouds. Cas A is thought to have a target density comparable to that of Puppis A, and so a comparable luminosity is to be expected. It can also easily be concluded that gamma-ray emission from Puppis A cannot be due to interactions of background CRs with interstellar gas. In the region of Puppis A the spectral index of CRs inferred from the Galactic diffuse gamma-ray emission is about 2.7, which is close to the locally observed one but much softer than that inferred for Puppis A. Furthermore, the mean energy density of CRs responsible for the gamma-ray emission of Puppis A, ≈ 37 eV cm^{-3}, derived with $\mathrm{n} \times \mathrm{Wp}/\mathrm{M_{gas}}$, is higher than that of the background CRs. Therefore, the gamma-ray emission is most likely produced by particles accelerated at the shock of SNR Puppis A. All results were later confirmed by a separate analysis by Xin et al. (2017) using Pass 8 data which also found a break in the full gamma-ray spectrum at 7.92 ± 1.91 GeV. This would need to be cross-checked since this new analysis started at only 1 GeV and did not perform the spectral analysis in the off-pulse window of the Vela pulsar which could contaminate slightly the spectrum between 1 and 10 GeV.

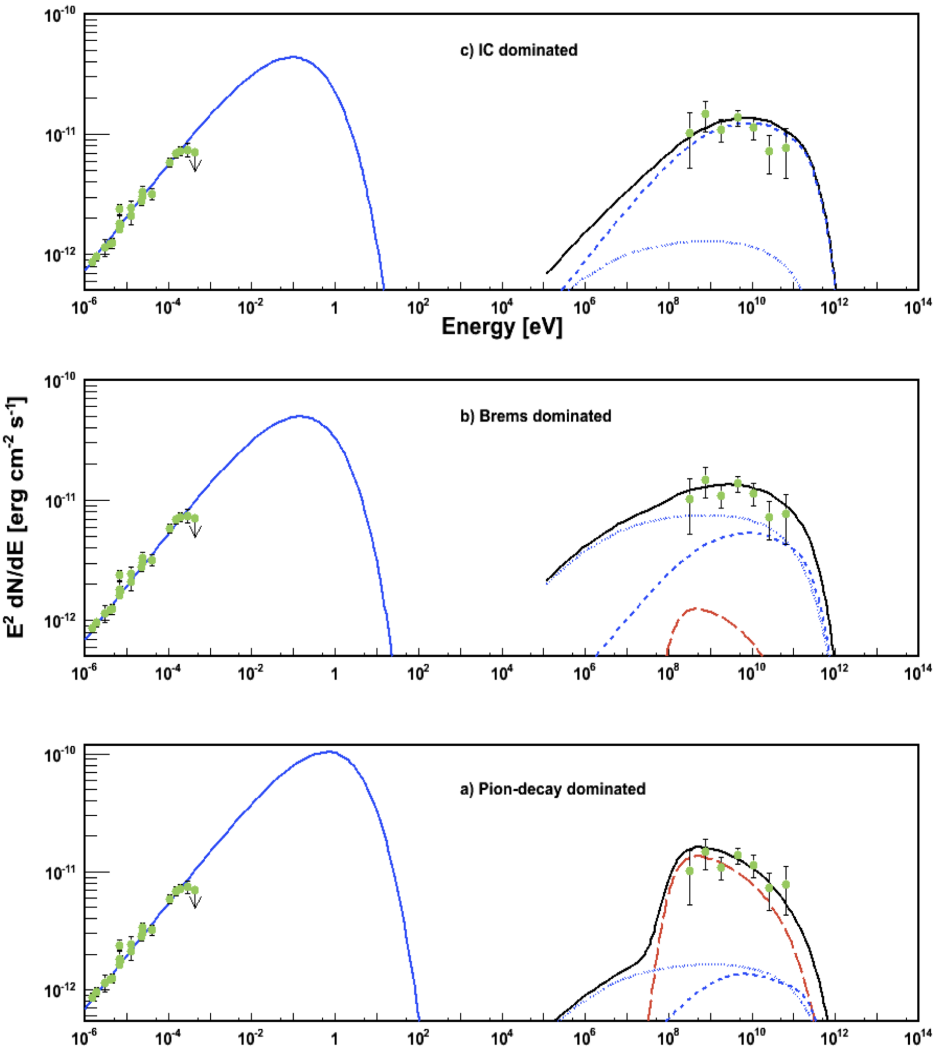

Figure 4.9: *SED models for Puppis A, for which IC (top), Bremsstrahlung (middle) and π^0-decay (bottom) are the dominant emission mechanism taken from Hewitt et al. (2012). In each model the radio data are fit with a synchrotron component. All models show the contributions of π^0-decay (long dashed, red), Bremsstrahlung (dotted, blue), and IC emission (dashed, blue) from CMB, IR dust photon field, and stellar optical photons. The sum of the three γ-ray components is shown as a solid black curve.*

Following up with this result, I worked together with Diane Fernandez and Matthieu Renaud (LUPM, Montpellier) on the H.E.S.S. observations of this source using data taken from 2005 to 2013 with the four-telescope array alone. The statistical significance of a potential VHE gamma-ray emission from Puppis A was determined after background subtraction with the reflected background method (Berge et al., 2007). No significant signal was found within the ON-region. In total, eight excess counts were measured, corresponding to a significance of 0.1σ. Similar analyses have been performed for the two half-disk regions where no signal was found as well. Presuming that the accelerated particle spectra are power-laws (PL) with exponential cutoffs as predicted by the diffusive shock acceleration mechanism (see Section 2.3), the gamma-ray spectrum resulting from the different emission processes should also follow a PL with exponential cutoff. To evaluate the existence of such a cutoff energy in the spectrum of the whole SNR, a likelihood estimator L was defined as the com-

bination of the likelihoods from the *Fermi*-LAT data points and H.E.S.S. measurements. The profile of the log-likelihood ratio test statistic -2lnΛ has an approximate χ^2 distribution with one degree of freedom (Rolke et al., 2005). The minimum is reached at around ~ 150 GeV. Below these energies, -2lnΛ increases rapidly because of the constraints imposed by the *Fermi*-LAT detection. Above that, the H.E.S.S. data become more constraining and lead to an increase in the -2lnΛ value. The 99% CL ULs on the cutoff energy correspond to 450 GeV which corresponds to ULs on $E_{\rm max}$ of ~ 2 TeV, ~ 3 TeV, or ~ 5 TeV depending on whether the gamma-ray emission results from Bremsstrahlung, IC or proton-proton interactions radiation mechanisms. Throughout the SNR evolution, particles are accelerated at the forward shock up to a maximum energy $E_{\rm max}$, typically determined by the SNR's finite age, finite size, or radiative losses. These effects become relevant when the characteristic timescales are close to the acceleration timescale, leading to cutoffs in the spectra of accelerated particles residing in the SNR. Using the equations for the acceleration, synchrotron loss and proton-proton interaction loss timescales, we could conclude that none of the standard limitations (age, size, radiative losses) on the particle acceleration mechanism, assumed to be continuing at present, can explain the lack of VHE signal. However, as said above, multi-wavelength data suggest that Puppis A has already interacted with MCs in some localised regions along the shell and that the NE region coincident with the bulk of GeV emission is possibly interacting with a far-IR MC. If this is true, the acceleration of particles could have ceased some time ago, and either a radiative cutoff or a break of a non-radiative origin could be expected. In the latter case, the break is expected at somewhat higher energies than those measured in several SNRs known to be interacting with MCs, which lie in the 1–20 GeV energy range. All results have been published in H. E. S. S. Collaboration et al. (2015b).

This source could well be an example of transition from fresh acceleration of cosmic-rays in some part of the remnant to re-acceleration of the cosmic-ray sea in the interaction region. Clearly, further observations to characterize the radio and γ-ray spectra are needed. High-frequency radio observations are needed to spatially resolve the radio spectral break or cutoff. Increased sensitivity with the continued observations by $Fermi$-LAT will allow any differences between the Eastern and Western regions to be firmly established. Observations at TeV energies of Puppis A with CTA will be interesting in several respects: (1) to determine the energy of the spectral cutoff or break and discriminate between emission mechanisms, (2) to measure differences between Eastern and Western hemispheres and the effects of shock-cloud interactions, and (3) to search for escaping CRs which may have encountered the nearby Eastern cloud.

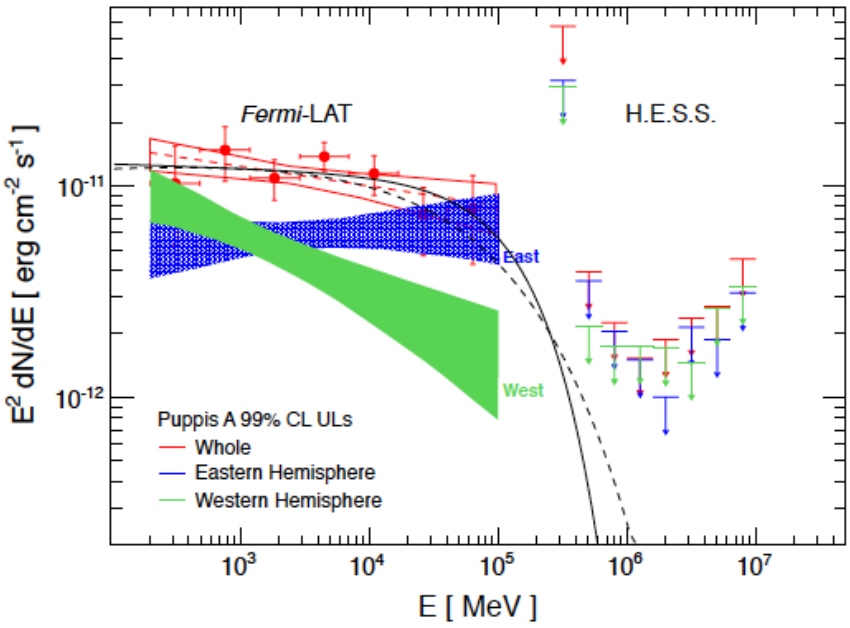

Figure 4.10: *H.E.S.S. 99% CL upper limits on the differential flux (arrows), together with the* Fermi*-LAT spectra from Puppis A, as reported in H. E. S. S. Collaboration et al. (2015b). Red, blue and green symbols correspond to* Fermi*-LAT and H.E.S.S. measurements for the whole SNR, the E and W hemisphere, respectively. The data points show the LAT fluxes and 1σ statistical and systematic errors, whilst the bowtie areas define the 68% CL bands. The solid and dashed lines indicate the preferred γ-ray spectra for the exponential and sub-exponential cutoff models, respectively.*

Summary

- Middle-aged SNRs are the dominant class of SNRs detected by the LAT
- Four middle-aged SNRs show the characteristic pion bump feature, naturally attributed to proton-proton interaction. This is the evidence that protons are accelerated (or simply re-accelerated and adiabatically compressed) in SNRs.
- Intensive work on W49B for a joint publication between *Fermi*-LAT and H.E.S.S.: the characteristic pion-bump feature as well as two energy breaks have been identified. The gamma-ray emission can be reproduced by proton-proton interaction in the framework of the direct interaction model.
- Two middle-aged SNRs show cosmic-ray escape and interaction in nearby molecular clouds: W44 and W28. With my PhD student, Benjamin Condon, we have focused on HESS J1729−345 that could be explained by the emission from runaway cosmic rays accelerated by the young SNR HESS J1731−347 and that are now interacting with molecular clouds coincident with the unidentified TeV source.
- Middle-aged SNRs without MC interaction also show γ-ray emission from the filaments formed through radiative shocks driven in atomic clouds. S147 is an excellent example of this category.
- A transition between fresh acceleration of cosmic-rays in young SNRs to re-acceleration of the cosmic-ray sea must occur during the SNR lifetime. Puppis A was analyzed with *Fermi*-LAT and H.E.S.S. data and might be an excellent example of this class of sources.
- The environment in which the SNR is evolving is a key characteristic controlling the γ-ray spectrum: we have studied the case of G349.7+0.2 which has roughly the same age as W49B and shows an energy break which is ~ 5 times higher.

The results presented in this chapter have been published in (bold faces indicate those for which I am corresponding author; I am co-author of all others):

- **Abdalla H. et al., 2016, to be published in Astronomy & Astrophysics, arXiv:1609.00600: "The supernova remnant W49B as seen with H.E.S.S. and Fermi-LAT"**
- Abramowski A. et al. 2015, Astronomy & Astrophysics, 575, A81: "H.E.S.S. reveals a lack of TeV emission from the supernova remnant Puppis A"
- Abramowski A. et al. 2015, Astronomy & Astrophysics, 574, A100, "H.E.S.S. detection of TeV emission from the interaction region between the supernova remnant G349.7+0.2 and a molecular cloud"
- Hanabata Y. et al. 2014, The Astrophysical Journal, 786, 145: "Detailed Investigation of the Gamma-Ray Emission in the Vicinity of SNR W28 with Fermi-LAT"
- Ackermann M. et al. 2013, Science, 339, 807: "Detection of the Characteristic Pion-Decay Signature in Supernova Remnants"

- **Hewitt J. W. et al. 2012, The Astrophysical Journal, 759, 89: "Fermi-LAT and WMAP Observations of the Puppis A Supernova Remnant"**
- Katsuta J. et al. 2012, The Astrophysical Journal, 752, 135: "Fermi Large Area Telescope Observation of Supernova Remnant S147"
- Uchiyama Y. et al. 2012, The Astrophysical Journal Letters, 749, L35: "Fermi Large Area Telescope Discovery of GeV Gamma-Ray Emission from the Vicinity of SNR W44"
- Abdo A. A. et al. 2010, The Astrophysical Journal, 712, 459: "Observation of Supernova Remnant IC 443 with the Fermi Large Area Telescope"
- Abdo A. A. et al. 2010, Science, 327, 1103: "Gamma-Ray Emission from the Shell of Supernova Remnant W44 Revealed by the Fermi LAT"

CHAPTER

5

Catalogs and the path to other cosmic-ray accelerators

Contents

SN 1006

5.1 First GeV catalog of Galactic extended sources

The past several years have seen unprecedented growth in the field of gamma-ray astronomy with the publication of several catalogs, both at TeV and GeV energies. These catalogs revealed different classes of astrophysical sources such as supernova remnants (SNRs), pulsar wind nebulae (PWNe), and molecular clouds (MCs) for what concerns our Galaxy. Many are observed as spatially extended with respect to the angular resolution of the instruments. This morphological aspect is important for several reasons. First, finding a coherent source extension across different energy bands can help to

associate a gamma-ray source with a potential counterpart. Then, such multi-wavelength studies can also help to determine the emission mechanisms producing these high energy photons. Finally, due to the energy dependence of the point spread function (PSF), the spatial and spectral characterization of a source cannot be decoupled. An incorrect spatial model will bias the spectral model of the source and vice versa, and can also skew the spectra of point sources in the vicinity of the extended source.

5.1.1 A pipeline adapted to extended sources study with *Fermi*

$Pointlike$ analysis of individual sources

In the early days of *Fermi*, I started to work with my PhD student Marie-Helene Grondin in coordination with *Fermi*-LAT colleagues from Stanford University (namely Stefan Funk and his PhD student Joshua Lande) to modify an already existing analysis method developed by Toby Burnett[1] to search for signs of spatially extended emission beyond the PSF. I received a France-Stanford grant to invite Joshua in Bordeaux and to spend a month at SLAC. The extension fitting method works by convolving the intrinsic LAT PSF with a spatial model of the candidate source to create a "pseudo-PSF" of the expected source appearance. The parameters of the spatial extension model are then varied to find the shape that most closely matches the spatial distribution of observed photons. The foremost challenge of measuring angular extents with the LAT is to properly account for a PSF that ranges a full 2 orders of magnitude in size over the energy range of the instrument and has a long non-Gaussian tail. In order to address these complications, $pointlike$ groups photons into separate energy bands. Photons in an energy band are grouped into spatial bins that scale in size with the changing PSF as a function of energy. The angular size of the bins used for analysis narrows at high energies to mimic the improved spatial resolution of the LAT. The model is fit to the data using a binned likelihood analysis. The significance of the detection of a source's extension is then calculated using a standard likelihood ratio test. This analysis method has been applied for several sources detected with *Fermi*-LAT, especially a first search of extension of several bright point sources detected by *Fermi* (Lande et al., 2012).

Blind search for extended sources in the Galactic plane

The above-mentioned publication started from already LAT detected sources. The next step was to work blindly in the Galactic plane. In this context, I developed an analysis pipeline based on $pointlike$ to perform a complete search for extended sources located within 7° from the Galactic plane. This pipeline was launched over 216 regions of radius 10°, centered on b = 0° and $\pm$ 5° with overlapping neighboring regions separated by 5.0° in Galactic longitude (Figure 5.1). To homogenize the analysis, extended sources were all fit assuming a uniform disk shape. The pipeline included extended sources from the 3FGL catalog, which were initialized at their best-fit disk extension. If the source was previously modeled with a Gaussian shape in the 3FGL catalog, we initialized the disk radius at $1.85\ \sigma_{Gaussian}$ as suggested by Lande et al. (2012). If the source was previously modeled with a multi-wavelength template, we used the average between the semi-major and semi-minor axes, reported in the 3FGL catalog, to initialize the disk radius. In each region, the pipeline is used to find all point and extended sources and evaluate the best-fit position and extension, as well as preliminary spectral values. Then, using those morphologies, the pipeline subsequently employed gtlike to obtain the best-fit spectral parameters (initializing spectra at the $pointlike$-determined values) and statistical

[1] This method was originally called $Sourcelike$ and was adapted only to the search of point-like sources. The different upgrades led to the analysis method called $pointlike$ that we are currently using.

significances. Sources detected as extended with this pipeline as well as with the alternative pipeline developed by Jamie Cohen during his PhD thesis at NASA Goddard Space Flight Center were kept and reported in our two studies at high energy:

- the first one above 50 GeV included in the 2FHL catalog (Ackermann et al., 2016) allowed the detection of 5 new extended sources (in addition to 25 already published ones),

- the second one above 10 GeV published as a stand-alone paper (Ackermann et al., 2017) revealed 16 new extended sources as well as 30 already published ones. This constitutes the first catalog of hard *Fermi*-LAT extended sources, named the *Fermi* Galactic Extended Source Catalog, which allows a thorough study of the properties of the Galactic plane in the sub-TeV domain.

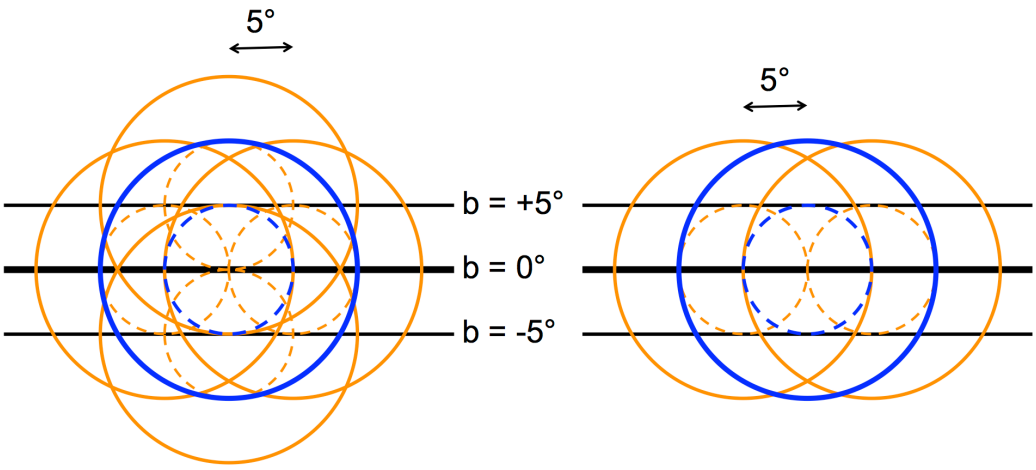

Figure 5.1: *Schematic representations of the arrangement of the analysis regions for the two pipelines used for localization and extension. Left: description of my pipeline, as defined in Section 5.1.1; each region (solid blue circle) of radius 10° is centered on $b = 0°$ and $\pm$ 5° and separated from its neighboring regions (orange circles) by 5° in Galactic longitude; all sources within 5° of the center (dashed circle with the same color) were set free for the primary pipeline. Right: details of the secondary pipeline developed by Jamie Cohen: each region (marked by a solid blue circle) of radius 10° is centered on $b = 0°$ and separated from its neighbors (orange circles) by 5° in Galactic longitude.*

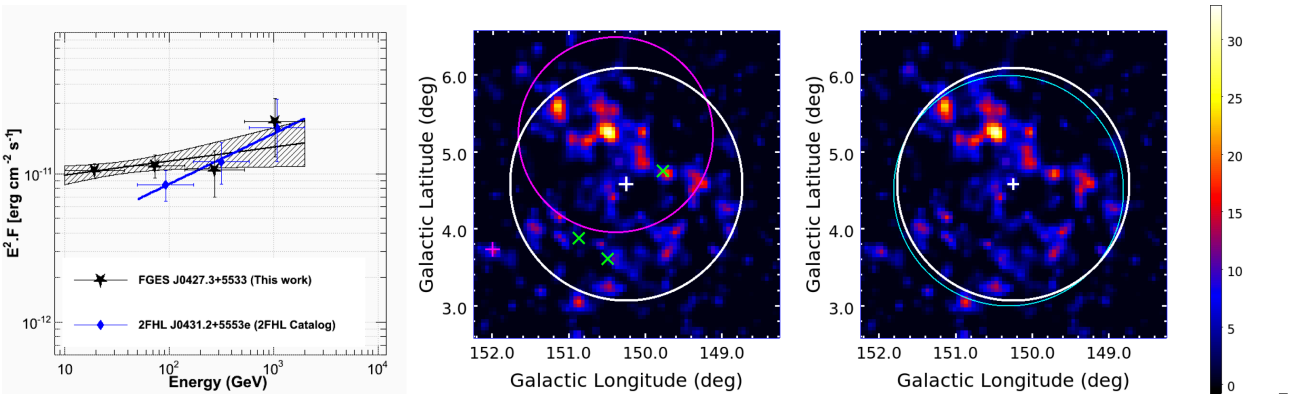

Figure 5.2: *Left: Spectral energy distributions of the SNR G150.3+4.5 with data points from this analysis (black stars and dashed butterfly) and 2FHL catalog (blue diamonds and line). Middle and right: Background-subtracted TS maps of SNR G150.3+4.5. The white circle and central cross indicate the disk extension and centroid as fit in the* Fermi *Galactic Extended Source Catalog. Right : the radio extent of the SNR is shown in cyan (Gao and Han, 2014). Figures taken from Ackermann et al. (2017).*

5.1.2 New extended SNRs

Among the sources reported in these 2 analyses, the case of the SNR G150.3+4.5 is extremely interesting. The search for extended sources performed for the 2FHL catalog allowed the detection of an extended source coincident with the northern side of the faint radio SNR G150.3+4.5 (Gao and Han, 2014). Then, the analysis above 10 GeV confirmed the detection of this extended source, and thanks to the increased statistics, the *Fermi*-LAT source perfectly matches the size and location of the radio SNR, as can be seen in Figure 5.2. The hard spectrum of this SNR derived from 10 GeV up to 2 TeV, with $\Gamma = 1.91 \pm 0.09 \pm 0.02$, is more similar to that of young shell-type remnants while its large radius of $1.52^\circ \pm 0.03^\circ \pm 0.08^\circ$ and faintness would suggest an old age. A deeper analysis especially using *Fermi*-LAT data down to 100 MeV and Cherenkov data above 2 TeV would help to constrain the characteristics of this SNR. However, its large size is an issue with the small field of view of current imaging Cherenkov telescopes. CTA-North could prove very useful for such study, as well as the High Altitude Water Cherenkov (HAWC) Gamma-Ray Observatory since this source is visible from the Northern hemisphere (see Section 2.5.1 for more information on these experiments). The diffuse source FGES J0619.6+2229 is another intriguing source detected in the catalog above 10 GeV. This source overlaps with IC 443 (see Figure 5.3) and extends to the North towards the bright arc and H II region S249 seen at 1420 MHz (Leahy, 2004). This source of almost 1° radius presents a harder spectrum than IC 443 and may be produced by cosmic rays accelerated by the shell of IC 443 and diffusing in the surrounding medium. It could also have a different origin with a connection to the SNR G189.6+3.3 which presents non-thermal emission in radio and X-rays (Asaoka and Aschenbach, 1994; Leahy, 2004). Future observations at TeV energies by CTA-North or HAWC would be again extremely useful to determine the nature of this SNR candidate or even constrain diffusion parameters in this region of interaction with molecular clouds.

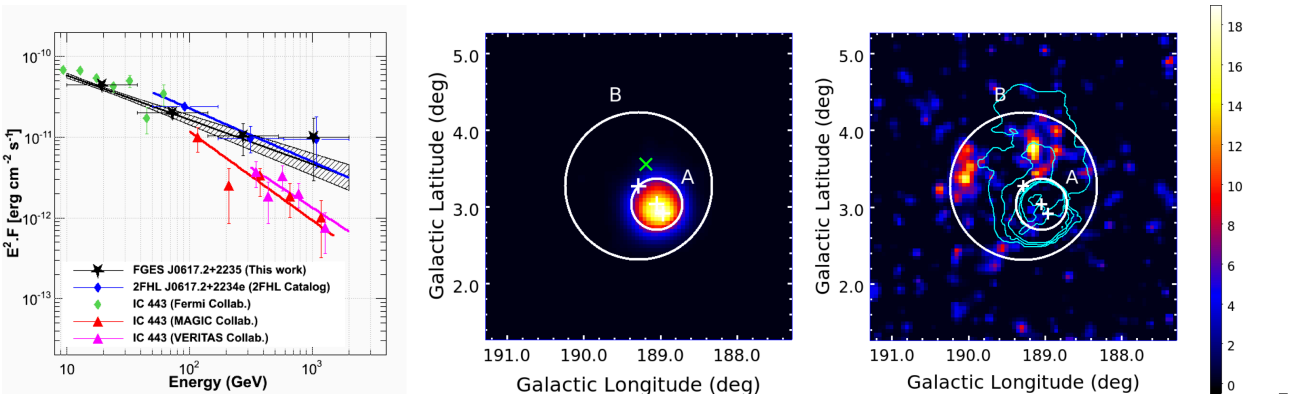

Figure 5.3: *Left: Spectral energy distributions of the SNR IC 443 (FGES J0617.2+2235) with data points from this analysis (black stars and dashed butterfly), from the 2FHL catalog (blue diamonds and line), a previous* Fermi*-LAT publication (green diamonds, Ackermann et al., 2013a) and IACT data (red and pink triangles are taken from Albert et al. (2007b) and Acciari et al. (2009) respectively). Middle and right: Background-subtracted TS maps of IC 443. The 3FGL and 2FHL source for the SNR IC 443 are exactly coincident with our FES source J0617.2+2235. White circles and crosses indicate the disk extensions and centroids fit in the* Fermi *Galactic Extended Source Catalog for FGES J0617.2+2235 (A) and FGES J0619.6+2229 (B). Right : the bright emission from FGES J0617.2+2235 is included in the model to highlights the emission coming from the largest source FGES J0619.6+2229. Cyan contours represent the radio emission at 1420 MHz (Leahy, 2004). Figures taken from Ackermann et al. (2017).*

5.2 Unidentified sources: missing piece in the Galactic puzzle ?

A key mystery emerging from these catalogs has been the fact that a large fraction of the Galactic sources detected are unidentified (UNID). These UNID gamma-ray sources have no obvious counterpart(s) at other wavelengths and hence there is considerable speculation surrounding the acceleration region and types of particles accelerated. Galactic γ-ray sources can be placed into the following categories: shell-type supernova remnants (Shell SNR), SNRs interacting with adjacent molecular clouds (Shell/MC), SNRs with radio shell and filled X-ray components (SNR/Composite), pulsar wind nebulae (PWNe), pulsars, binary systems with a compact remnant (neutron star or black hole), massive stellar clusters, superbubbles, and globular clusters. These gamma-ray sources could play a role in the acceleration of cosmic-rays and are therefore of great interest in this context.

5.2.1 The large offset TeV source HESS J1507−622

The case of the gamma-ray source HESS J1507−622 is quite puzzling. Most γ-ray sources in the inner Galaxy H.E.S.S. survey tend to cluster within 1° in latitude around the Galactic plane. HESS J1507−622 instead is unique, since it is located at a latitude of $\sim 3.5^\circ$ and does not have any obvious counterpart in other multi-wavelength data. Up to now, this slightly extended source (with a Gaussian width of $0.15^\circ \pm 0.02^\circ$) is still unidentified. HESS J1507−622 was first detected in the *Fermi*-LAT energy range as a point source (Domainko and Ohm, 2012) with a rather flat spectrum from the GeV to the TeV regime. The analysis that we have conducted above 10 GeV in the *Fermi* Galactic Extended Source Catalog (see Section 5.1) confirms the former spectrum and shows for the

first time a significant extension in the GeV regime, in agreement with the TeV size (see Figure 5.4). The gamma-ray results challenge an extragalactic origin due to the large energetics needed to power the source and the very extended nature of the emission in such a scenario. Indeed, 3×10^{53}(d/1 Mpc)^2 erg in electrons would be needed in a leptonic scenario and the source would spread over 2.6 (d/1 Mpc) kpc. A few extragalactic sources have been detected with kiloparsec extension at GeV energies, such as the radio galaxies Centaurus A and Fornax A, but no object with such a large spatial dimension has been found in the TeV regime so far. One, typically unknown, key quantity of unidentified gamma-ray sources is their distance. For Galactic sources, observations of their X-ray counterpart may help to constrain their location in the Milky Way. Following up on its original detection by H.E.S.S., the region around HESS J1507−622 has been observed once with Chandra (H.E.S.S. Collaboration et al., 2011c), twice with XMM-Newton (Tibolla et al., 2014) and with Suzaku (Eger et al., 2015). From these X-ray observations, it comes out that the best X-ray counterpart would be the faint and extended X-ray source (CXOU J150706.0−621443) first detected with a statistical significance of $\sim 7\sigma$ by Chandra and spatially consistent with the VHE gamma-ray emission region. One possibility explaining this very faint X-ray counterpart would then be that HESS J1507−622 is a relic PWN with a very low magnetic field ($\sim 1\mu$G). Such a low magnetic field leads to a very faint X-ray nebula along with a large accumulation of highly energetic electrons radiating predominantly TeV gamma-rays via the IC mechanism. However, if the extension of HESS J1507−622 is driven by diffusion of energetic electrons for a time-scale of $\sim 2 \times 10^4$ years, the distance to the object needs to be very large (10 kpc) to be compatible with the apparent compactness of the TeV source. In turn, this implies a very large distance from the Galactic plane, larger than the scale height of the distribution of VHE gamma-ray emitting pulsars. In addition, no pulsar has been detected so far and the very soft *Fermi* spectrum does not look like any other GeV PWN. Another possibility, taking into account the soft spectrum detected by *Fermi*, would be that the particles radiating at gamma-ray energies are protons (through proton-proton interaction). Since HESS J1507-622 is located off the Galactic disk, the density of target material is lower than in the Galactic plane and can be obtained as a function of distance, following the density profile of the interstellar medium perpendicular to the Galactic plane. Using the best-fitting model (Lockman 1984) for the density profile off the Galactic plane, Domainko and Ohm (2012) found that about 10^{50} ($\sim 10^{51}$) erg of cosmic rays at a distance of 2 (4) kpc are needed to explain the VHE emission observed in HESS J1507−622. In turn, a supernova remnant at a distance of 2 kpc with the apparent angular size of HESS J1507-622 would be in the pressure-driven Sedov phase with an age of less than 1000 years. Such SNR should feature similar observable properties as the remnant of SN 1006 which is also off-plane. However, SN 1006 is a prominent emitter of non-thermal X-ray emission, and the absence of such X-ray emission in HESS J1507−622 disfavors any SNR origin for this VHE source. HESS J1507−622 thus remains a puzzling object, challenging established models for Galactic gamma-ray source populations.

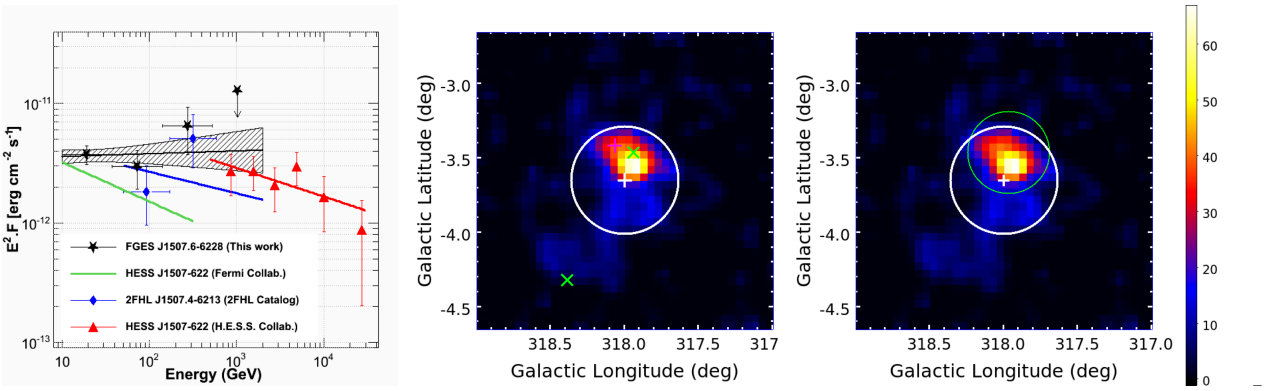

Figure 5.4: *Left: Spectral energy distributions of the TeV source HESS J1507−622 with data points from this analysis (black stars and dashed butterfly), from the 2FHL catalog (blue diamonds and line), a previous* Fermi*-LAT publication (green line, Acero et al., 2013a) and IACT data (red triangles and line, H.E.S.S. Collaboration et al., 2011c). Middle and right: Background-subtracted TS maps of HESS J1507−622 using the above-quoted references for the TeV extent shown in green. A white circle and cross indicate the disk extension and centroid fit in the* Fermi *Galactic Extended Source Catalog. Figures taken from Ackermann et al. (2017).*

5.2.2 Extended emission from the G25.0+0.0 region: association with a star forming region ?

Within 2°, the confused G25.0+0.0 region contains five point sources in the 3FGL catalog in addition to the extended source associated to the PWN HESS J1837−069 represented by a disk of 0.33° radius as derived by Lande et al. (2012). However, the H.E.S.S. source HESS J1837−069 is almost two times smaller than the LAT extended source and its peak emission is located on the edge of the LAT source. This highlights well the complexity of this region. In the catalog of extended sources that I conducted above 10 GeV, the region is divided into three extended sources as can be seen in Figure 5.5: FGES J1836.5−0652 and FGES J1839.0−0704 covering HESS J1837−069 and FGES J1834.1−0706 in the North whose size and spectrum agrees with those derived by Acero et al. (2016). It is coincident with the composite SNR G24.7+0.6 and matches the radio size, supporting the association. However, the PWN HESS J1837−069 can only partly explain the two other extended sources FGES J1836.5−0652 and FGES J1839.0−0704 since they are much brighter and larger than the TeV signal. Katsuta et al. (2017) performed a separate morphological and spectral analysis of this region using *Fermi*-LAT and *XMM-Newton* X-ray data and proposed a scenario in which the diffuse gamma-ray emission would be produced by a star-forming region (SFR) driven by a candidate young massive OB association/cluster G25.18+0.26 observed in X-rays, in addition to the PWN HESS J1837−069. This would be the second case detected by the LAT with the Cygnus Cocoon and, indeed, they share similar properties: the γ-ray sources in both regions are spatially extended, their energy spectra are described as power-law indices of 2.1–2.2 without any significant spectral curvature at least up to a few hundred GeV and the LAT finds no significant spectral variation in either region. Katsuta et al. (2017) detected a bubble-like structure of the molecular and the HI gas (G25 bubble) at 7.7 kpc, which may be created by a putative powering source and found that G25.18+0.26 resides in the G25 bubble. The unabsorbed X-ray luminosity of the object at the assumed distance (7.7 kpc) is comparable to that of Cygnus OB2, one of the most massive OB associations in the Galaxy. This suggests that G25.18+0.26 is also a massive OB association ($\sim 2 \times 10^4$ $M_\odot$). In addition, with near-IR data, a candidate massive OB association has been claimed in this direction (Rahman et al., 2013).

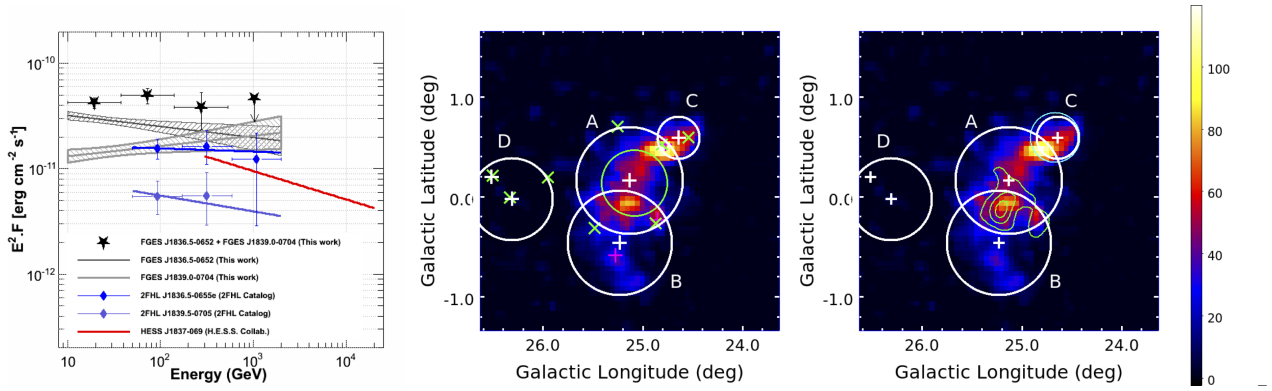

Figure 5.5: *Left: Spectral energy distributions of the pulsar wind nebula HESS J1837−069 with data points from this analysis (black and grey dashed butterflies for FGES J1836.5−0652 and FGES J1839.0−0704 respectively), 2FHL catalog (blue and purple diamonds and lines for 2FHL J1836.5−0655e and 2FHL J1839.5−0705 respectively) and TeV data (red line, Aharonian et al., 2006a). Middle and right: Background-subtracted TS maps of HESS J1837−069 and above-quoted references for the TeV contours shown in green. White circles and crosses indicate the disk extensions and centroids fit for FGES J1836.5−0652 (A) and FGES J1839.0−0704 (B) as well as nearby extended sources FGES J1834.1−0706 (C) and FGES J1839.4−0554 (D). Figures taken from Ackermann et al. (2017).*

This scenario would indicate that the particle acceleration in the Cygnus cocoon is not a special case and that other young massive SFRs have capabilities to accelerate particles via the same mechanism. Spectral and spatial information in the TeV band would enable us to study this interesting source in more detail, confirm or refute the association with the star forming region and especially constrain the maximum energy at which particles are being accelerated in SFRs. In the VHE energy range, so far, no detection of star forming region was announced in our Galaxy [2]. One of the main issue is the identification of the source which is not easy in the Galactic plane. The best candidate for a TeV detection remains W49A, which is one of the brightest giant radio H II regions in the Galaxy. This star forming region is located in the densest $\sim$15 pc of a 10 $M_\odot$ giant molecular cloud of $\sim$100 pc in size. Evidence for the TeV detection of the star forming region W49A by H.E.S.S. was announced by our joint *Fermi*-H.E.S.S. paper on W49B, located next to W49A. Indeed, using the Model analysis, significant signal was detected towards W49A but it could not be confirmed (above 5σ) with the cross-check analysis. Therefore, only the VHE emission coincident with W49B was discussed in the paper. But, one important point was raised in the concluding section: assuming that the distances to W49B and W49A are comparable, the observed difference between the γ-ray luminosities of the two objects would imply that in the absence of recognizable supernova remnants – as in W49A – the other possible energetic particle sources like the shocks expected from interacting or collective stellar winds appear not very effective for HE and VHE γ-ray emission in the case of W49A. Future observations with CTA will be very useful.

[2]Note that the H.E.S.S. collaboration recently announced the detection of the superbubble 30 Dor C in the Large Magellanic Cloud.

5.2.3 Unidentified sources as potential pulsar wind nebulae candidates

Non-thermal emission from pulsar wind nebulae

Since the TeV detection of the Crab PWN in 1989 with the Whipple telescope, tens of Galactic sources have meanwhile been associated with TeV pulsar wind nebulae, setting this class of sources as the most populous TeV gamma-ray emitters. Most of these objects are situated in the inner Galaxy; many were therefore discovered and extensively investigated from the southern hemisphere using the H.E.S.S. array (H. E. S. S. Collaboration et al., 2017a). The latest results show that they are one of the best candidates for the sites of cosmic-ray acceleration even if it is widely argued that the radiation in PWN is produced by electrons, which represent a very small fraction of the cosmic rays. As can be seen from the individual case of HESS J1507−622, a scenario involving a PWN is often proposed to explain the nature of the source. The reason is easy to understand. Electrons emitting VHE gamma-rays are usually less energetic than X-ray-emitting ones, they do not suffer from severe radiative losses due to the relatively low magnetic field and the majority of them may survive from (and hence probe) early epochs of the PWN evolution. These electrons can produce TeV emission via IC scattering off the ambient low-energy background photons (such as CMB, diffuse Galactic infrared background, or starlight), leading to the formation of a relic PWN emitting in the VHE domain. This relic PWN is very faint or absent in X-rays because the pulsar wind electrons become too cold (due to radiative losses) and their characteristic synchrotron frequencies move outside the X-ray band. One of the biggest advantages of this scenario is that it provides a natural explanation for almost one third of the Galactic TeV sources that are still lacking a lower energy (radio and X-ray) counterpart: they form the important class of unidentified sources (UNIDs). See de Jager and Djannati-Ataï (2009) for more details. HESS J1303−631 was the first H.E.S.S. source classified as a UNID due to the lack of detected counterparts in radio and X-rays with Chandra (Mukherjee and Halpern, 2005). H.E.S.S. Collaboration et al. (2012) found only one plausible counterpart in the vicinity of HESS J1303−631: PSR J1301−6305 with a spin-down power of 1.70×10^{36} erg s^{-1}. The authors also presented the detection of a very weak X-ray PWN using XMM-Newton observations. This, together with the energy-dependent morphology observed by H.E.S.S., led to the conclusion that HESS J1303−631 is an old PWN offset from its powering pulsar. Multiwavelength observations of VHE UNIDs and dedicated pulsar searches within the extent of VHE are therefore crucial to identify PWNe systems and reveal the energetics and composition of pulsar winds. This was the main objective of the ERC Starting Grant that I obtained in 2010. One of the main input from the work conducted during the three years of the ERC P-WIND project, besides individual sources analysis such as HESS J1641−463 discussed in Section 5.3.3, is a population study of PWNe with the LAT.

Population study of PWNe at GeV energies with the LAT

To better understand the emission mechanisms taking place in TeV PWNe and find new ones at GeV energies among the unidentified TeV sources, I performed a *Fermi*-LAT analysis using 45 months of data near the position of 58 TeV PWNe and UNIDs within 5° of the Galactic Plane with my PhD student Romain Rousseau (Acero et al., 2013a). Of the 58 sources, 30 were detected, and our work provides their gamma-ray fluxes for energies above 10 GeV as well as upper limits for non detected sources. Among the 30 sources: nine may be contaminated by pulsar emission for energies above 10 GeV, seven sources cannot be clearly associated with a PWN, eleven are PWN candidates (such as HESS J1420−607 and HESS J1119−614) and three are clearly identified as PWNe: HESS J1825−137, HESS J1514−591 (aka MSH 15−52) already detected and published during Marie-Helene Grondin's PhD thesis that I supervised with David Smith (Grondin et al., 2011; Abdo et al.,

2010d) and HESS J1356−645 detected for the first time in this analysis. Adding the Crab Nebula and Vela X (whose detections were also first reported during Marie-Helene Grondin's thesis) to the three clearly identified PWNe and eleven candidates, this made 16 PWNe candidates detected with the LAT at this time. All of them are associated with young (with an age between 1 and 30 kyr) and powerful pulsars with a spin-down power between 10^{36} and 10^{39} erg s^{-1} and typically have an efficiency in converting rotational energy into gamma rays below 10%. Indeed, VHE sources older than 30 kyr are not detected by our analysis, while Mayer et al. (2012) predict a higher flux in the LAT energy range than in the VHE experiments' energy range. However it should be noted that among these VHE sources, at least 7 suffer one or several biases:

- Source misidentification: for example, HESS J1912+101 has recently been proposed to be a shell-type SNR (Gottschall et al., 2017), but some of the emission could originate in the pulsar wind. Similarly, HESS J1702−420 and HESS J1646−458B cannot be clearly associated as PWNe and deeper multi-wavelength observations are needed to classify the emission.
- Potential characteristic age overestimation (see for example HESS J1809−193 by Sheidaei, 2011).
- HESS J1026−582, HESS J1809−193, HESS J1831−098 and HESS J1849−000 are located in regions of strong diffuse emission where the LAT is less sensitive to any potential emission.

Therefore, the lack of a population of old γ-ray-loud PWNe cannot be proven given the current statistics and systematics associated with this analysis. Since then, several others PWNe have been detected by the LAT (see for instance the case of 3C58 which is the weakest VHE PWN detected to date and the only one first detected at GeV energies) but none of them are associated to pulsars older than 30 kyrs.

5.3 Looking for the sources of highest energy emission

As stated in Section 2.1, the chemical composition of CRs is dominated by protons for particle energies below that of the knee, while heavier nuclei become important above it. This fact, together with the evidence that the transition between galactic and extragalactic CRs takes place at particle energies exceeding the PeV, implies that the sources of galactic CRs must be proton PeVatrons. This explains the never-ending search for the highest energy gamma-ray in our Galaxy as a way to find the origin of the Galactic CRs.

5.3.1 The Crab nebula: a famous electron PeVatron

The Crab Nebula and its pulsar are among the most famous and best-studied objects in astronomy. It is the remnant of an historical SN, recorded in 1054 A.D., located at a distance of 2 kpc. The SN explosion left a pulsar behind, which continuously emits a wind of magnetized plasma of electron/positron pairs. These particles lose energy by synchrotron radiation, visible from radio up to hundreds of MeV, and IC scattering of the generated synchrotron and ambient radiation fields, detected at gamma-ray energies. The observed rate of spin down implies that kinetic energy is being dissipated at a rate of $\sim 5 \times 10^{38}$ erg.s^{-1} which means that the pulsar has steadily released a third of its reservoir of $\sim 5 \times 10^{49}$ ergs of rotational energy into its surrounding nebula over the last 960 years.

This is in sharp contrast with shell-like supernova remnants in which the dominant energy source is the 10^{51} ergs of kinetic energy released at the moment of the original supernova explosion. However, the observation of the $\sim$30 TeV gamma-rays from the Crab Nebula and the softening seen in the spectrum at high energies (Aharonian et al., 2006b) indicate the existence of particles with energies up to $\sim 10^{15}$ eV at least inside this PWN.

The large-scale integrated emission from the Crab Nebula is expected to be steady within a few percent and is thus often used to calibrate X-ray and Tcherenkov telescopes and to check their stability over time. Recently, variability in the X-ray flux from the nebula by $\sim$3.5% per year has been detected (1999 – 2008), setting limits on the accuracy of this practice (Wilson-Hodge et al., 2011). In addition, instabilities in the flux of high-energy gamma rays have been reported in recent years by AGILE and the *Fermi*-LAT (see the review written by Bühler and Blandford, 2014). These flares have all shown increased emission (up to a factor 20) from the synchrotron component of the Crab Nebula while emission from the IC component of the nebula as well as the Crab pulsar remained consistent with the average level. An approximate flux doubling timescale of 6 hr was reported for the two brightest ones. The detection of synchrotron photons up to energies of > 1 GeV confirms that electrons are fastly accelerated to energies above 1 PeV in the Crab Nebula, with a magnetic field value as high as 1 mG. These brief time scales and the requirement that the emission volume be causally connected imply that the flaring region must be compact ($< 10^{-2}$ pc) and the acceleration be extremely efficient (which poses serious challenges on scenarios invoking Diffusive Shock Acceleration as in SNRs). Structures this small are found only in the inner part of the nebula, close to the termination shock. Several new ideas have been proposed to explain these recurring flares ($\sim$1 per year), one of them being magnetic reconnection (Cerutti et al., 2014), but they still remain mysterious and, to date, despite extensive efforts a detection of the flares outside of the HE gamma-ray band remains elusive. This absence of plausible counterparts at other wavelengths is certainly one of the most surprising aspects of the flare phenomenon and reinforce very well the needs of future gamma-ray observations with higher sensitivity and improved angular resolution.

Recently, first maps of the gamma-ray sky above 50 TeV as seen by HAWC were presented by Malone and HAWC Collaboration (2017) at the TeVPA conference showing three regions detected at 5σ: MGRO J1908+06, MGRO J2019+37 and HESS J1825$-$13/HESS J1826$-$130. Interestingly, even though these regions are confused and still unidentified, they all have a pulsar and a PWN in the vicinity. This further highlight the importance of pulsars and PWNe in our Galaxy and their efficient acceleration of particles. However, as said above, it is mostly believed that the radiation in PWNe is produced by electrons, which represent a very small fraction of the cosmic rays.

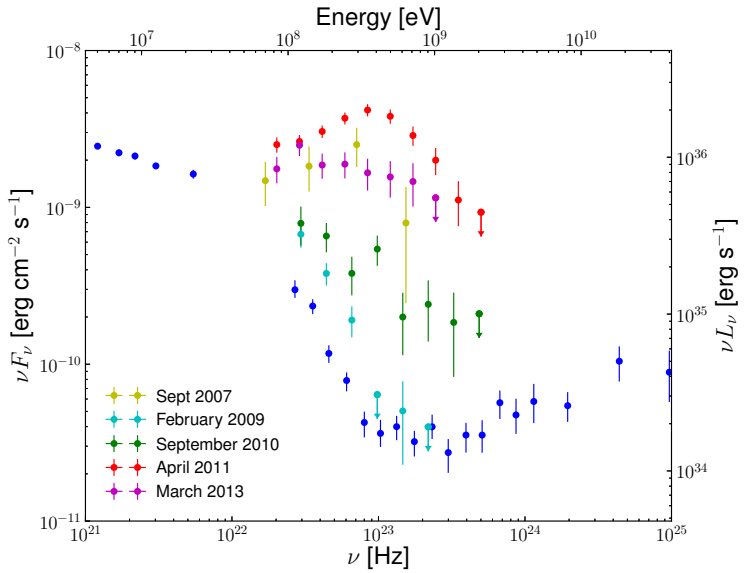

Figure 5.6: *Spectral energy distribution at the maximum flux level for the five Crab nebula flares. The blue points represent the average Crab nebula flux values. The spectral points from September 2007 were obtained by AGILE, while the other points were obtained with the* Fermi*-LAT. Figure taken from Bühler and Blandford (2014).*

5.3.2 The Galactic center: first Galactic proton PeVatron ?

Now focusing on protons at very high energy, two extremely important results have been obtained using *Fermi* and H.E.S.S. observations. The first one, detected by Su et al. (2010) in a search for a gamma-ray counterpart to the Wilkinson Microwave Anisotropy Probe (WMAP) haze, is called the *Fermi* bubbles. These are two large structures in the gamma-ray sky extending to 55° above and below the Galactic center (clearly visible at high energy in Figure 5.7) with an approximately E^{-2} gamma-ray spectrum between 1 GeV and 100 GeV and well defined edges (Ackermann et al., 2014). Soon after the discovery of the *Fermi* bubbles, several models of their formation as well as the acceleration of particles and gamma-ray production were proposed. All of them assume that the bubbles were created by a phenomenon in or around the Galactic center by the emission of a jet from the black hole (Guo and Mathews, 2012), a spherical outflow from the black hole (Zubovas et al., 2011), a wind from supernova explosions (Crocker and Aharonian, 2011), or a sequence of shocks from several accretion events onto the black hole (Cheng et al., 2011). The second result was provided by deep gamma-ray observations with arcminute angular resolution of the region surrounding the Galactic Centre by the H.E.S.S. telescopes, leading to the detection of a diffuse emission in the central 300 pc of the Galactic centre extended along the Galactic plane (HESS Collaboration et al., 2016). The spatial correlation of the TeV emission with the giant molecular clouds of the Central Molecular Zone (CMZ), as seen in Figure 5.8, hints for acceleration of hadronic CRs in this region, where the gamma rays result from decays of neutral pions produced by the interactions of relativistic protons with the ambient gas. The density of these protons has an almost spherically symmetric distribution but drops with the distance R to the Galactic Center following closely a 1/R law. This distribution is characteristic of a central source injecting accelerated protons continuously (on a 1000 to 10000 year timescales) into the ambient medium. After injection, these protons propagate diffusively interacting with the CMZ gas, producing neutral pions, which then decay producing gamma-rays and other sub-products. The best fit to the data is found for a spectrum following a power law extending with a photon index of

2.3 to energies up to tens of TeV without any evidence of energy cut-off or break. Assuming a cut-off in the parent proton spectrum, the corresponding secondary gamma-ray spectrum deviates from the H.E.S.S. data at 68%, 90% and 95% confidence levels for cut-offs at 2.9 PeV, 0.6 PeV and 0.4 PeV, respectively. This establishes the first robust detection of a VHE cosmic hadronic accelerator which operates as a source of PeV particles, i.e. a PeVatron. The authors suggest that the supermassive black hole Sagittarius A* is linked to this PeVatron. Combined with the recent *Fermi*-LAT observations showing a harder spectrum in the Galactic centre region (Gaggero et al., 2017) and the evidence of the *Fermi* bubbles, it is hard to escape the conclusion that there is a lot of high-energy particle acceleration associated with the centre of our Galaxy. It was even suggested that in the "knee" region of the CR spectrum, we see a significant contribution from past Galactic centre activity. At lower energies (< 1 PeV), SNRs would still be the best candidates for the acceleration of cosmic-rays but this would alleviate the issues currently encountered to accelerate protons in these sources at energies higher than 1 PeV.

5.3.3 The PeVatron candidate HESS J1641−463

Beside the Galactic centre, H.E.S.S. observations recently revealed three other PeVatron candidates: HESS J1641−463, HESS J1741−302 and HESS J1826−130 (Angüner et al., 2017). These three galactic sources present a hard spectrum extending beyond 10–20 TeV, without any evidence for a cut-off. The case of HESS J1641−463 is particularly interesting since it is detected both at GeV and TeV energies which is extremely useful to constrain the nature and mechanism taking place. Located only 0.25° away from the SNR HESS J1640−465, HESS J1641−463 remained unnoticed using the standard detection technique used by the H.E.S.S. Collaboration. Its detection became possible only by using an energy threshold of 4 TeV (Abramowski et al., 2014). This new TeV source presents one of the hardest spectrum ever detected in TeV astronomy ($\Gamma \sim 2$), extending up to 30 TeV without evidence of a cut-off, which explains why the distinction between the two TeV sources became more evident above a few TeV. It is one the prime PeVatron candidate in our Galaxy detected by H.E.S.S.. Because of the remarkably hard TeV spectrum, although a leptonic scenario for the emission measured at TeV cannot be conclusively excluded, the favored scenario by Abramowski et al. (2014) is that the radiation from HESS J1641−463 is produced by cosmic-ray protons colliding with the ambient gas. In this scenario, the gamma-ray spectral shape predicted by interactions of protons is too hard to fit the gamma-ray spectrum observed from SNR RX J1713.7−3946 at energies above few TeV and the required proton spectrum must extend close to 1 PeV (see Figure 5.9). HESS J1641-463 may represent a source population contributing significantly to the Galactic cosmic ray flux around the knee.

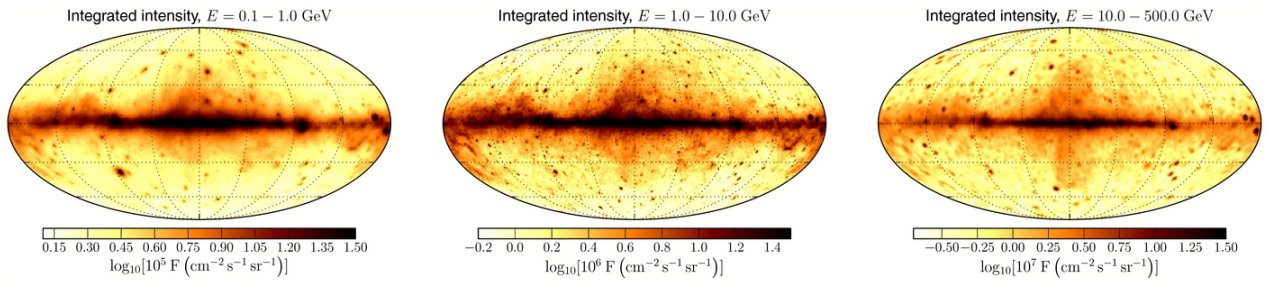

Figure 5.7: *Gamma-ray intensity maps integrated in three large energy bins (Ackermann et al., 2014). The pixel size is* 0.9°. *The map on the right is smoothed with a Gaussian kernel of* 1°.

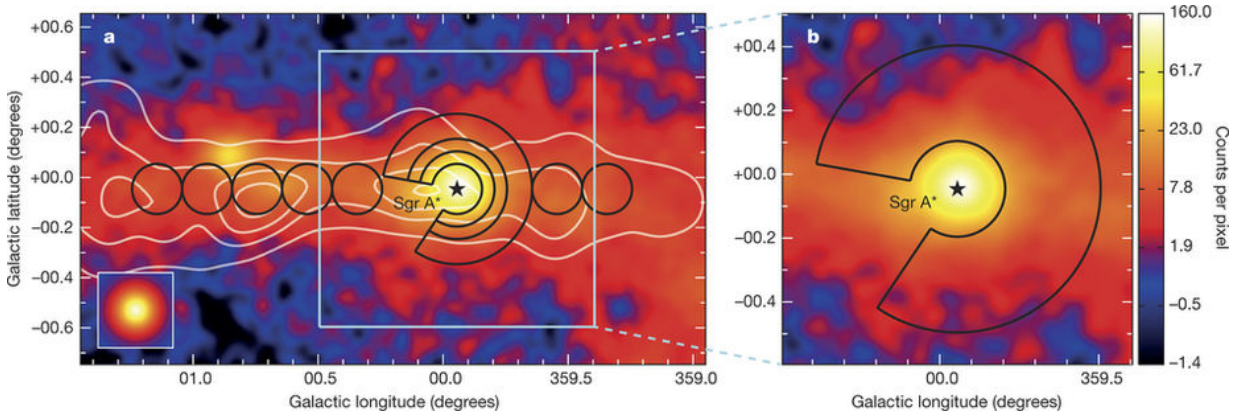

Figure 5.8: *VHE gamma-ray image of the Galactic Centre region as seen by H.E.S.S. (HESS Collaboration et al., 2016). The color scale indicates counts per* $0.02^\circ \times 0.02^\circ$ *pixel. a) The black lines outline the regions used to calculate the cosmic-ray energy density throughout the central molecular zone. White contour lines indicate the density distribution of molecular gas, as traced by its CS line emission. The black star indicates the location of Sgr A*. b) Zoomed view of the inner* ~ 70 *pc and the contour of the region used to extract the spectrum of the diffuse emission.*

Using *Fermi*-LAT data, we carried out the analysis of the region surrounding both TeV sources and published the detection of HESS J1640−465 and HESS J1641−463 above 100 MeV (Lemoine-Goumard et al., 2014). The softest emission in this region comes from the TeV source HESS J1641−463 which is well fitted with a power law of index $\Gamma = 2.47 \pm 0.05 \pm 0.06$ and presents no significant γ-ray signal above 10 GeV, which contrasts with its hard spectrum at TeV energies (see Figure 5.10). This could imply that two different mechanisms or sources produce the γ-ray photons detected in each energy band. This recalls the case of HESS J1356−645, within which *Fermi*-LAT detects the pulsed emission of PSR J1357−6429 while, at TeV energies, H.E.S.S. observes its associated PWN (H.E.S.S. Collaboration et al., 2011b). In such a PSR/PWN scenario, the flux density of the X-ray source nearest to HESS J1641−463 is a factor 15 less energetic when compared with the energy flux density of the TeV source (Abramowski et al., 2014), which would resemble the numerous associations of "dark" TeV sources and weak X-ray synchrotron PWN that have been established so far. Another possibility in such a "two source" scenario, emphasized by the good positional coincidence between HESS J1641−643 with SNR G338.5+0.1, would be that the γ-ray photons detected at TeV energies are produced by fresh accelerated protons from this SNR interacting with the ambient gas, as suggested by Abramowski et al. (2014), while *Fermi* would be seeing a contaminating pulsar. Finally, another scenario would be that HESS J1641−463 is a binary system similar to LS 5039 and LSI +61°303, both showing a pulsar-like spectrum at GeV energies that does not connect to the TeV spectrum (Hadasch et al., 2012). The fact that no variability could be observed from these sources can not be taken as evidence for disfavoring a binary origin because of the low statistics, while the lack of an optical counterpart can be related to high optical extinction or the location of sources close to the Galactic plane.
Future observations with CTA (thus overlapping with the energy domain covered currently by *Fermi* and the one covered by HESS) of this PeVatron candidate are therefore of prime interest to constrain the nature of this source as well as the type of particles accelerated (namely protons or electrons).

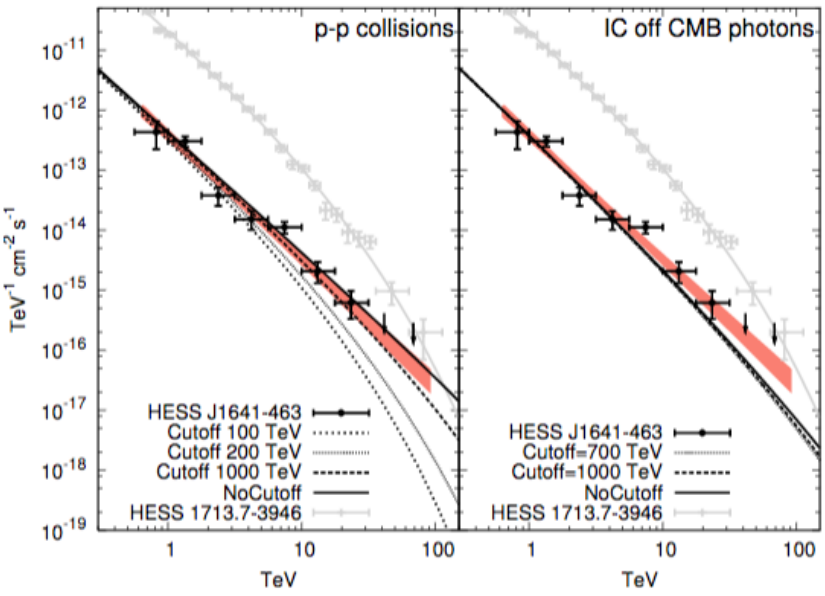

Figure 5.9: *Differential VHE gamma-ray spectrum of HESS J1641−463 for energies between 0.64 TeV and 100 TeV, together with the expected emission from proton-proton interaction (left) and IC off CMB photons (right) taken from Abramowski et al. (2014). The red butterfly represents the 1σ confidence region for the fit to a power law model, the black data points the H.E.S.S. measured photon flux (1σ uncertainties), the arrows the 95% CL upper limits on the flux level, and the black curves the expected emission from the models, assuming different particle energy cut-off values. For comparison, the gray data points and curve represent the archival spectrum and the corresponding best fit model, respectively, of the young SNR RX J1713.7−3946.*

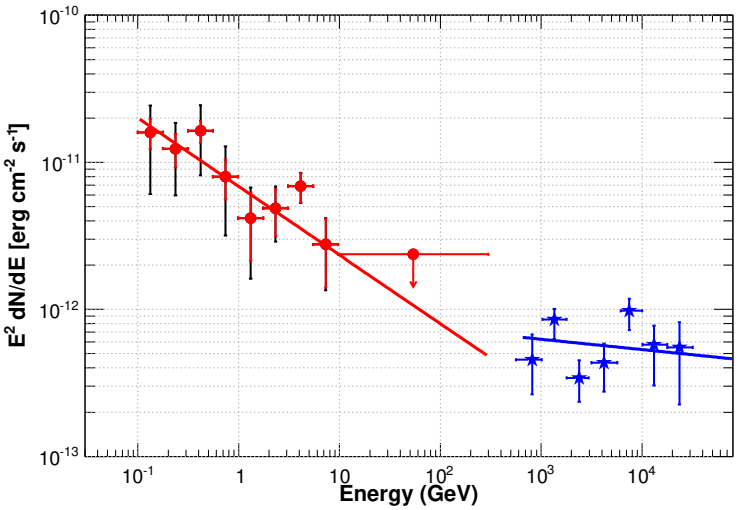

Figure 5.10: *Gamma-ray spectra of HESS J1641−463, using the best point source position from Abramowski et al. (2014). The red data points (crosses) indicate the fluxes measured in each of the 14 energy bins indicated by the extent of their horizontal lines. The statistical errors are shown in red, while the black lines take into account both the statistical and systematic errors. A 95% C.L. upper limit is computed when the statistical significance is lower than 2σ. The blue data points and the best spectral fit (represented as a blue line) are extracted from Abramowski et al. (2014). Figure taken from Lemoine-Goumard et al. (2014).*

The results presented in this chapter have been published in (bold faces indicate those for which I am corresponding author; I am co-author of all others):

- **Ackermann M. et al., 2017, The Astrophysical Journal, 843, 139: "Search for Extended Sources in the Galactic Plane Using Six Years of *Fermi*-Large Area Telescope Pass 8 Data above 10 GeV"**
- Ackermann M. et al., 2016, The Astrophysical Journal Supplement, 222, 5: "2FHL: The Second Catalog of Hard *Fermi*-LAT Sources"
- **Lemoine-Goumard M. et al., 2014, The Astrophysical Journal, 794, L16:"HESS J1640−465 and HESS J1641−463: Two Intriguing TeV Sources in Light of New *Fermi*-LAT Observations"**
- **Acero F. et al., 2013, The Astrophysical Journal, 773, 77, "Constraints on the Galactic Population of TeV Pulsar Wind Nebulae Using *Fermi* Large Area Telescope Observations"**
- Lande J. et al., 2012, The Astrophysical Journal, 765, 5: "Search for Spatially Extended *Fermi* Large Area Telescope Sources Using Two Years of Data"

Summary

- We have entered an era of catalogs, revealing different classes of astrophysical sources such as supernova remnants (SNRs), pulsar wind nebulae (PWNe), and molecular clouds (MCs).
- Intensive work on three population studies published by the *Fermi*-LAT collaboration: a catalog of PWNe at GeV energies, a catalog of extended sources above 50 GeV published in the 2FHL catalog and a stand-alone catalog called the *Fermi* Galactic plane Extended Sources Catalog (FGES). The first one was done together with the validation of the extension method in the framework of an ERC Starting Grant obtained in 2010.
- New SNRs have been detected such as the SNR G150.3+4.5. With its hard spectrum and large size, it is a puzzling source of high priority for CTA-North or HAWC.
- Young massive star forming regions have capabilities to accelerate particles to (at least) TeV energies. In addition to the Cygnus Cocoon detected by the LAT, another candidate was discovered in the confused G25.0+0.0 region. A firm detection of the star forming region W49A at TeV energies is awaited.
- Pulsar wind nebulae is the dominant class of sources at TeV energies. Several unidentified sources could well be old (relic) PWNe. HESS J1507−622, first detected as an extended GeV source in the FGES catalog could fall in this category. They are also excellent accelerators, the most famous electron PeVatron being the Crab nebula.
- A first proton PeVatron in the Galaxy has been detected recently: the Galactic center. Past Galactic centre activity could contribute significantly in the "knee" region of the CR spectrum.
- Other proton PeVatron candidates are being studied currently. We have focused on the case of HESS J1641−463 which shows one of the hardest spectrum at TeV energies and is located close to the SNR HESS J1640−465.

CHAPTER

6

Conclusions and future perspectives

Contents

It is clear today that supernova remnants are able to accelerate particles (electrons and protons) to very high energies through diffusive shock acceleration. We have seen evidences in favor of proton acceleration in several cases: the historical SNRs Cassiopeia A and Tycho (Section 3.2) as well as the transition case Puppis A and the middle-aged SNRs W44, IC443, W51C and W49B (Section 4). Morphologically-resolved spectral analysis of shell-type SNRs, such as RX J1713.7$-$3946 and SN 1006 (Section 3.3), suggest that protons are accelerated at the shock but the γ-ray emission is high enough to be detected only in dense regions. This means that, even if the dominant mechanism in play for several remnants is leptonic, there could be some smaller subregions (e.g. dense clumps) where

the hadronic mechanism significantly contribute to the local γ-ray emission and thus that protons are accelerated at the shock. We have also seen that Tycho and Cassiopeia A seem to fulfill three important criteria to be CR accelerators: 1) they accelerate protons, 2) the cosmic-ray efficiency ξ_{CR} is high enough and close to the standard value of $\sim 10\%$, 3) the injected CR spectrum follows a power-law which translates into an index of 2.7 after diffusion in the Galaxy, well reproducing the CR spectrum (assuming a diffusion coefficient proportional to $E^{1/3}$).

One might think that the mystery of the origin of Galactic cosmic-ray is solved. This is absolutely not true. Indeed, if one tries to get a closer look at the problem, it appears more complex and several issues need to be solved. First, the maximum energy at which SNRs are able to accelerate CRs is not well constrained and, even worse, observations do not seem to show any evidence of acceleration above 100 TeV. Models suggest that type Ia SNe are not able to reach 1 PeV in agreement with the current observations of SN 1006 and Tycho (Section 3.4). However, core collapse SNe should be able to act as PeVatron which seems to be invalidated by the TeV detection of a cut-off in the spectrum of Cassiopeia A (Section 3.2). If confirmed and extrapolated to other cases taking into account the evolution of the maximum energy with time, such result could be a threat against SNRs as the prime CR accelerators in the Galaxy. In my view, this is the most important issue to solve in the coming years. The evolution of the CR efficiency with time is also not very well constrained up to now. Indeed, it highly depends on the mixture of hadronic versus leptonic for most shell-type SNRs and even more on the density of the surrounding medium which can vary by one order of magnitude from one side to the other of the remnant (Section 3.4). This CR efficiency is also expected to vary with time, which means that population studies will be needed to really be able to provide strong constraints at different ages of the SNR evolution. Another requirement if SNRs are the prime accelerators in the Galaxy, is that they need to reproduce the CR spectral index of 2.7. However, the spectrum observed at Earth results from an integration in time of the escape flux during the expansion of the SN shell, the release of the particles trapped in the downstream after the SN shell has come to a stop, and the diffusion in the Galaxy. All these contributions are rather uncertain and so is the spectrum of CRs injected by an individual SNR. Observations of CR escape and diffusion surrounding SNRs would be very valuable to better understand these mechanisms. Finally, we have seen that other types of cosmic-ray accelerators might contribute significantly to the CR spectrum: star forming region and superbubble from one side and the Galactic centre from the other side, are the best examples of this class (Section 5). Observations and modelings of these regions are crucial to constrain their potential contribution to the Galactic CR spectrum.

We live in exciting times. The new precision data from the current generation of experiments is revealing fine detail and surprises that require even more sensitive instruments and/or observations for instance detailed morphologically-resolved spectral analysis on smaller regions for shell-type SNRs. I will detail below the main perspectives for this domain in my view, meaning that these are the topics on which I am mostly interested. Some might be feasible very soon while some others might take a very long exposure time or will need instruments not yet operational. Moreover, the list of sources to observe to fulfill our objectives is not complete: they are only cited as examples. All in all, ten years might be needed to complete all these different steps. Obviously, one cannot anticipate important discoveries, as it always happen with new instruments, which might delay even more some of these perspectives.

6.1 Observations of historical SNRs

6.1.1 Cassiopeia A, Tycho, Kepler and SN 1006: the most obvious targets

Few historical SNRs are known in our Galaxy and they are obviously prime candidates to constrain the maximum energy. The case of Cassiopeia A is extremely intriguing and needs to be confirmed with more statistics either with CTA or with longer exposure time using the current Northern experiments VERITAS and MAGIC. Until now, no energy cutoff has been reported by TeV instruments for Tycho but the steep spectral index of 2.92 ± 0.42 suggests that there should be a cutoff in the TeV domain and that more statistics will allow its detection. Indeed, recent models published on this SNR uses a cutoff energy for the primary particles of ~ 40 TeV (see Table 3.4). The observations of the two other historical SNRs known in our Galaxy would be extremely valuable. First, SN 1006 has been detected at TeV energies by H.E.S.S. and then, more recently, by *Fermi*-LAT. This SNR does not have a cut-off energy measured at TeV energies and the indication of spectral variation seen with the LAT indicates that different mechanisms are occurring in the south-western part of the remnant which is interacting with an atomic cloud. Deep observations with CTA would enable us to see if the same occurs at TeV energies and to constrain the maximum energy reached by particles in the two sides of the remnant, as well as the cosmic-ray efficiency if a hadronic component can be confirmed.
The second SNR of interest is called Kepler. In October 1604 several astronomers, among them Johannes Kepler, observed a "new star" which today is believed to have been a bright supernova. Since then, the remnant of this supernova has been a target of observations along the entire electromagnetic spectrum. A detection at gamma-ray energies is still awaited and upper limits with H.E.S.S. imply a distance of at least 6.4 kpc for the source (Aharonian et al., 2008a). As Tycho and SN 1006, Kepler originates from a Type Ia SN and is not expected to act as a PeVatron but observational estimates on the maximum energy for different ages of SNRs are extremely useful to better model the temporal evolution of particle acceleration at shock wave.

6.1.2 The youngest SNR G1.9+0.3: looking at the earliest stage of the SNR evolution

In 1984, a radio survey using the Very Large Array (VLA) at 4.9 GHz led to the discovery of G1.9+0.3 (also G1.87+0.33), identified as a SNR based on its shell-like morphology and non-thermal radio emission (Green and Gull, 1984). G1.9+0.3 had the smallest angular extent ever measured for a Galactic SNR ($\sim$1.2') suggesting a young age of 10^3 years and/or a large distance. *Chandra* X-ray Observatory data confirmed that this young remnant is in the freely expanding phase as a X-ray-synchrotron-dominated shell supernova remnant (Reynolds et al., 2008) and subsequent radio and X-ray observations confirmed its expansion and brightening for an age younger than 150 years (Green et al., 2008). Spectral variations in X-rays, interpreted in terms of magnetic field obliquity dependence of cosmic ray acceleration, have been used to argue for a Type Ia event (Reynolds et al., 2009). The most recent X-ray measurements by Carlton et al. (2011) result in an age of 110 years and a density of 0.022 cm^{-3}, meaning that this is the youngest SNR in our Galaxy but it is also the only Galactic SNR increasing in flux, with important implications for the physics of electron acceleration in shock waves. G1.9+0.3 is located $\sim 2^\circ$ from the supermassive black hole at the Galactic center and therefore benefit from the deep observation of this region by the H.E.S.S. telescopes. After data quality cuts, keeping only observations with an offset smaller than 1.5°, 67 hours of data could be used. Despite this long observation time, no significant VHE γ-ray signal was detected from G1.9+0.3 and upper

limits on the integral fluxes above the 0.26 TeV energy threshold were calculated for three assumed spectral indices, $\Gamma = 2.0$, 2.5 and 3.0 (H.E.S.S. Collaboration et al., 2014a). The upper limits on the TeV γ-ray flux provide an opportunity to estimate a lower limit on the magnetic field of 12μG in the context of a leptonic particle acceleration scenario. This low value can be satisfied without requiring magnetic field amplification beyond simple compression by the shock wave. In a hadronic scenario, the upper limits are two orders of magnitude greater than the flux prediction for a density of 0.022 cm^{-3}. This low ambient density together with the remoteness of the source in comparison to other young remnants detected might explain the non-detection by H.E.S.S.. Another reason could be that, during the free expansion stage of the SNR's evolution the CR efficiency is expected to be very low, and Ksenofontov et al. (2010) estimated that it should be about 3×10^{-3} for G1.9+0.3. A future detection with CTA would be extremely useful to constrain the population of high-energy particles injected at the shock for such young remnant in addition to the maximum energy that they reach.

6.1.3 Gamma-ray monitoring of SN 1987A

As already said above, models favor core-collapse SNe for the acceleration of CRs above 100 TeV and up to 1 PeV. Unfortunately, the only young object of this type in our Galaxy is Cassiopeia A which seems to show a cut-off in the TeV domain. Since Cassiopeia A is not anymore in the free-expansion phase, we expect that the maximum energy is already below 1 PeV. In addition, Cassiopeia A may also be located in a very diffusive region of the Galaxy, resulting in a very fast escape of high-energy protons. Therefore, we need other sources of this type at different ages to study the production and temporal evolution of the gamma-ray emission from CR acceleration during the earliest SNR stages. One excellent candidate is the very young SN 1987A in the Large Magellanic Cloud (LMC), the remnant of the nearest naked-eye supernova since Kepler in 1604. Due to its proximity, it has been extensively observed at all wavelengths from the radio to the soft γ-ray band. Observations of the initial burst of neutrinos were consistent with the notion that the core of the progenitor collapsed and formed a compact object, most likely a neutron star. SN 1987A results from a Type II SN and more precisely from a blue supergiant progenitor. The non-thermal radio and X-ray emission from the remnant is evidence of particle acceleration in the supernova blast wave, which is impacting at the current epoch on the dense shell produced by the progenitor star (Chevalier and Dwarkadas, 1995). Long-term monitoring of the target will then provide a unique opportunity for studying the interaction between the SN shock wave and the circumstellar medium (CSM). It has been suggested by Berezhko et al. (2011) that TeV gamma rays should be produced by the interaction of the cosmic rays at the shock with the protons in the CSM. Depending on the assumptions about the CSM properties, the expected flux was predicted to be rising in time and to have reached a level of $\sim 2.5 \times 10^{-13}$ photons cm^{-2} s^{-1} in 2010. With deep observations of the LMC, H.E.S.S. has detected three luminous examples of CR sources in an external galaxy and among them the first superbubble at TeV energies (see Section 6.5), but no significant signal was reported on SN 1987A (H.E.S.S. Collaboration et al., 2015). The H.E.S.S. upper limit above 1 TeV of 5×10^{-14} photons cm^{-2} s^{-1} at a 99% confidence level, obtained from observations made between 2003 and 2012, is below the aforementioned predictions. This shows that these observations in combination with the radio and hard X-ray observations can put interesting constraints on the efficiency of cosmic-ray acceleration. For SN 1987A, H.E.S.S. Collaboration et al. (2015) estimate that less than 1% of the explosion energy is injected in cosmic rays. This fraction is rather small compared to typical values of $\sim$10% for young SNRs (of ages $\sim$1000 – 2000 years), but is not unreasonable for a very young object like SN 1987A. Recently, Berezhko et al. (2015) have revised their model to better comply with the observed structure and parameters of the CSM. In particular, the mass of the equatorial ring was decreased by an order of magnitude.

With this change, the predicted gamma-ray flux decreased to close to the upper limit from H.E.S.S. (Figure 6.1 left). According to their calculation, the most promising time for the detection of SN 1987A at TeV energies is the 10 year period from 2008 to 2018 (Figure 6.1 right). At later epochs, SN 1987A should be detectable in the VHE range only by an instrument with a higher sensitivity than that of H.E.S.S., such as CTA. A detection by CTA would allow to both constrain the efficiency of cosmic-ray acceleration and the maximum energy at which particles are accelerated. If SN 1987A is detected, a long-term monitoring of the target will then provide a unique opportunity for studying the evolution of cosmic-ray acceleration and the interaction between the SN shock wave and the CSM.

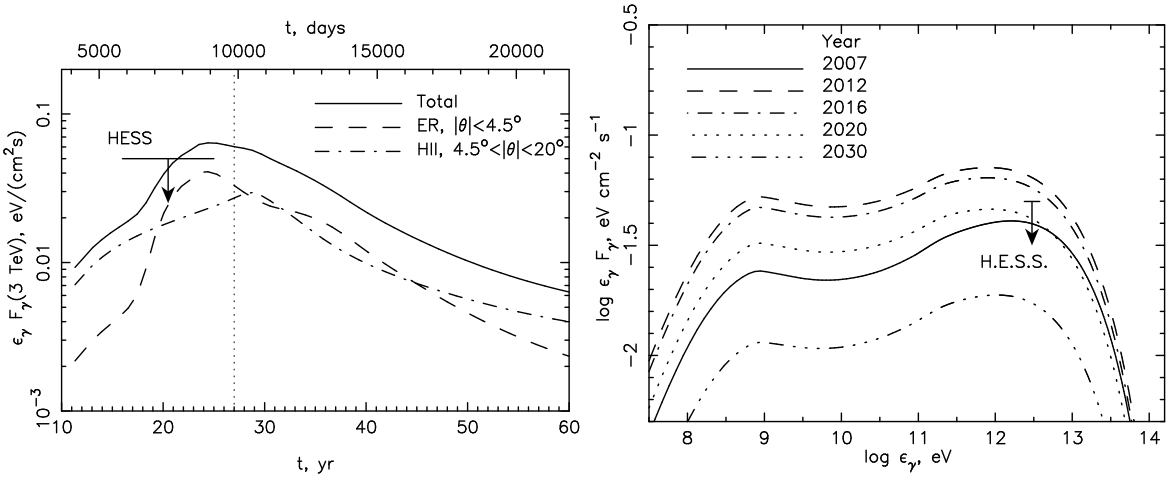

Figure 6.1: *Left: Integral γ-ray energy flux density above 3 TeV from SN 1987A as a function of time. Right: Spatially integrated γ-ray spectral energy flux density, calculated for five epochs. The H.E.S.S. upper limit (H.E.S.S. Collaboration et al., 2015), corresponding to the observational period 2005–2012 year, is shown in both cases. Figures taken from Berezhko et al. (2015).*

6.2 Search for PeVatron SNRs in the Galaxy

The above description focused on the observation of known and identified SNRs to constrain the acceleration mechanisms taking place at the shock. One way to constrain the maximum energy at which Galactic sources can accelerate cosmic rays is obviously to look directly for PeVatron candidates whatever their nature (identified or not). This implies a large survey of the Galactic plane and adapted analysis methods to search for sources showing hard spectra. For instance, the detection of the source HESS J1641−463 became possible only by using an energy threshold of 4 TeV (Abramowski et al., 2014), highlighting the need to look directly at these very high energies. One of the best future instruments at gamma-ray energies devoted to this Galactic Plane Survey and PeVatron search is CTA. And this is not a surprise that CTA has indeed two Key Science Programs (KSP) on the Galactic Plane Survey (GPS) and on PeVatron search. The GPS KSP will carry out a survey of the full Galactic plane using both the southern and northern CTA observatories; the survey will be graded so that more promising regions (especially the inner Galactic region of $-60^\circ < l < 60^\circ$) will receive significantly more observation time than other regions. The 10-year GPS program of the Galactic plane achieves a sensitivity better than 4.2 mCrab over the entire Galactic plane and 1.8 mCrab in the inner Galactic region. In the Northern hemisphere, with its increased spectroscopic capability, CTA will complement and extend observations made by the water Cherenkov telescope HAWC with a better sensitivity up

to ∼20 TeV (e.g. factor of 5 better at 1 TeV as seen in Figure 2.5). In the Southern hemisphere, CTA will have access to the highest energies thanks to the Small Sized Telescopes (SSTs) with an increased sensitivity in comparison to HAWC up to ∼ 70 TeV (for sources visible in both hemispheres). This unique capability of CTA will enable the detection of the most energetic photons ever observed and the sampling of the highest energy particles in the Galaxy up to the PeV scale. The possibility of CTA to probe possible spectral features at very high energies was investigated for several sources and, more specifically, for the case of HESS J1641−463 (Trichard, 2017). The results are shown in Figure 6.2 indicating that a cutoff lower limit of 100 TeV is expected to be reached in ∼7h to ∼38h depending on the source cutoff energy. The probability of detecting an exponential cutoff after 15h of observation is ∼19% with a median of the cutoff energy distribution of 45 TeV. Such measurements are extremely useful, not only to constrain the maximum energy. It can also constrain the type of particles that are radiating. Indeed, at energies above 50 TeV, the problematic ambiguity between leptonic and hadronic origin is nearly completely resolved, since 100 TeV photons are produced preferentially by hadronic processes. This is a result of the Klein-Nishina effect, where the cross-section for inverse-Compton electron-photon interactions decreases very quickly above a few tens of TeV. Therefore unlike other energy intervals, the interpretation of gamma-ray observations at these energies is free of confusion and reduces to the only possible mechanism: proton-proton interaction.

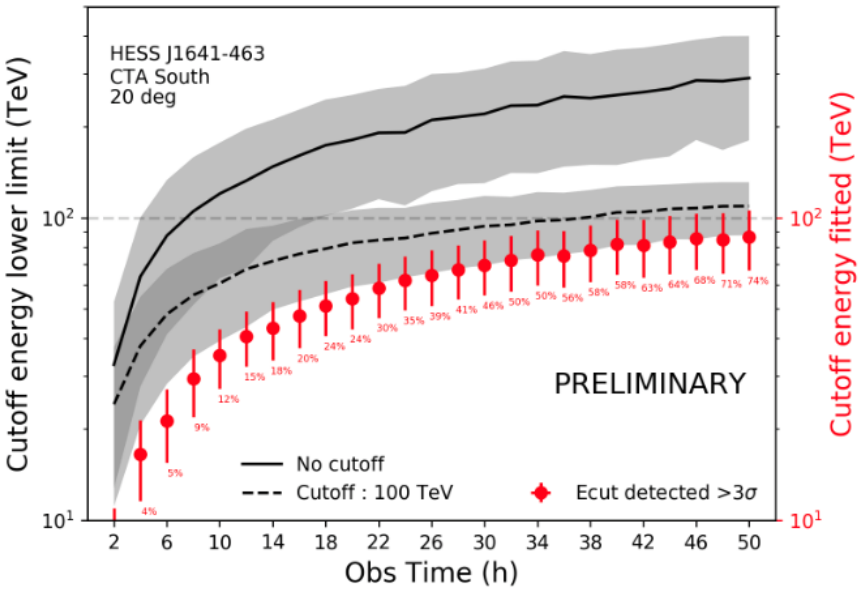

Figure 6.2: *Median of the cutoff energy lower limit (at 95% confidence level) distribution as a function of observation time (lines). The continuous and dashed lines represent a source without cutoff energy and with a cutoff energy at 100 TeV (when the fit with an exponential cut-off power-law is less than 3σ significant) respectively. The grey bands show 68% width of the distribution. The red dots are the median of the fitted cutoff energy when the fit with an an exponential cut-off power-law is more than 3σ significant. The red error bars represent the 68% width of the distribution. The values indicate the probability that the fit with an an exponential cut-off power-law is significant. Plot taken from Trichard (2017).*

Thanks to its very large array of scintillators called KM2A, LHAASO will have access to the highest energies (see Section 2.5.1). At 10 TeV, the effective area of KM2A can reach about 0.3 km^2, the angular resolution is about $0.86°$, and the energy resolution for γ-rays is about 42%. The corresponding values are 0.8 km^2, $0.5°$, 33% at 30 TeV, and 0.9 km^2, $0.3°$, 20% at 100 TeV respectively.

With the large area of muon detectors, KM2A will reject the hadronic shower background at a level of 10^{-4} at 50 TeV and even 10^{-5} at higher energies, so that γ-ray samples are almost background free above 100 TeV. This will make LHAASO the most sensitive experiment above 30 TeV after one single year of observation. Liu et al. (2016) have investigated the cases of the young SNR Tycho and Cassiopeia A showing that, after 5 years of observations with LHAASO, a strong constraint could be provided on the type of particles and on their maximum energy. LHAASO, as an all-sky monitor, will have a real advantage in comparison to CTA since it does not need to define a priori the target for the observation. This offers a unique opportunity to discover new type of sources at the highest energies.

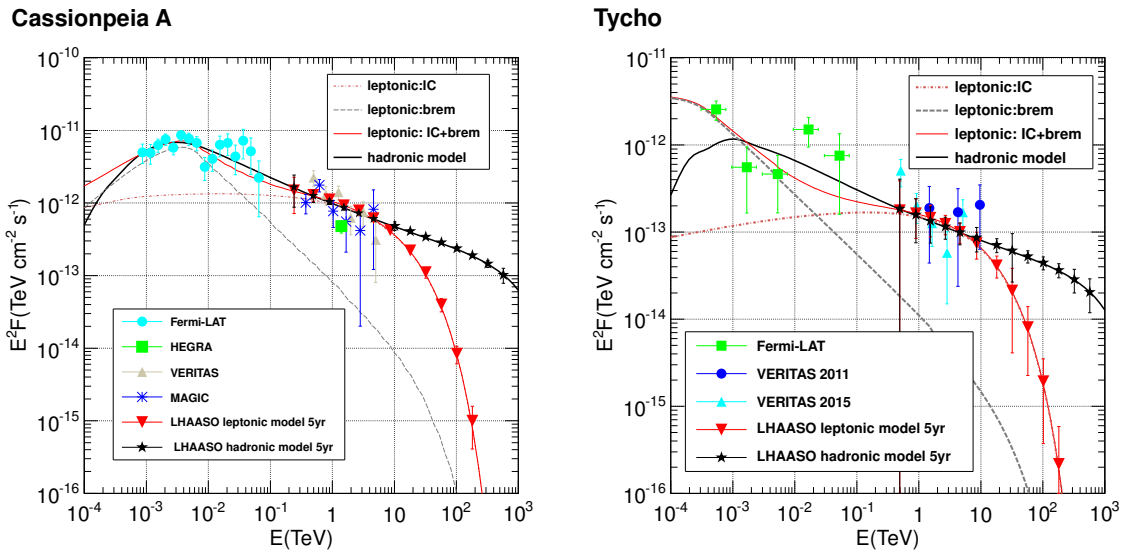

Figure 6.3: *Expectation of the LHAASO project on the spectrum of the historical SNRs Tycho and Cassiopeia in two different scenarii investigated. Plot taken from Liu et al. (2016).*

6.3 Observations of γ-ray emission close to SNRs

It should be noted that the number of SNRs that are currently bright above 50 TeV is expected to be very limited. Indeed, as discussed in Section 3.4.4, PeV protons are expected to be accelerated by core-collapse SNRs during a relatively short period of the SNR evolution. This ideal time is the free-expansion phase when the shock velocity is high enough to allow sufficiently high acceleration rate. When the SNR enters the Sedov phase, the shock gradually slows down and, in turn, the maximum energy of the particles that can be confined within the SNR decreases. This determines the escape of the most energetic particles from the SNR (Ptuskin and Zirakashvili, 2005). Type II SN enter their adiabatic phase only a few tens of years after the explosion and even the young SNR Cassiopeia A is not anymore in the free-expansion phase. This directly means that catching a PeVatron SNR in the Galaxy will be very challenging. This is why Gabici and Aharonian (2007) suggested to search for multi-TeV gamma-rays generated by the CRs that escape the SNR and diffused up to a nearby cloud.

6.3.1 A few words on the original theory

Here is a brief description of the original idea proposed by Gabici and Aharonian (2007). The highest energy particles escape the shell first. Moreover, generally they diffuse in the interstellar medium

faster than low energy particles. Therefore they arrive first to the cloud, producing there gamma-rays. As time passes, these high energy CRs finally reach the cloud and produce there gamma rays with very hard energy spectra when interacting with the dense cloud environment via proton-proton interaction. This makes the cloud an effective multi-TeV gamma-ray emitter. As lower and lower energy particles reach the cloud, the peak of the gamma-ray emission accordingly shifts toward the lower, TeV and GeV, energies. As can be seen in Figure 6.4, the gamma-ray emission at the cloud, produced by PeV protons that escaped the shock, peaks at 100 TeV. This hadronic gamma-ray emission at the cloud is significantly weaker than the one from the SNR, but its detection might be easier because of its longer duration (10^4 years vs a few hundred years). Indeed, the duration of gamma-ray emission in this case is determined by the time of propagation of CRs from the SNR to the cloud which is poorly known. However, it is often believed that the CR diffusion coefficient in the vicinity of CR sources might be suppressed with respect to the average galactic one. Therefore the gamma-ray emission of the cloud lasts much longer than the emission of the SNR itself. Moreover, the leptonic contribution to the cloud emission is likely negligible. Electrons accelerated at the SNR cannot reach the cloud because they remain confined at the shock due to severe synchrotron losses. Secondary electrons can be produced in the cloud, but they cool mainly via synchrotron emission in the cloud magnetic field. The idea would then be to search for hard spectral sources coincident with molecular clouds. Such detection would imply that a nearby accelerator was able to produce very high energy protons that are now interacting within the cloud. This is the theory. What about observations at gamma-ray energies ?

6.3.2 Escaping cosmic-rays from young remnants

In Section 4.2.3, I have dicussed the case of the unidentified TeV source HESS J1729−345 for which such a scenario was suggested: particles that have escaped the young shell-type SNR HESS J1731−347 are presently penetrating the molecular clouds coincident with HESS J1729−345 and are producing gamma-rays. We have also seen that the upper limit on this source with *Fermi*-LAT is a factor of two above the TeV data and cannot constrain the origin of the γ-ray emission. Deep observations have been carried out at all wavelengths. Using the Mopra Galactic Plane CO Survey, Maxted et al. (2018) have shown, at the assumed distance of 3.2 kpc for the SNR, dense gas traced by CS(1-0) emission coincident with the north of HESS J1731−347, the nearby HII region G353.43−0.37 and the nearby unidentified gamma-ray source HESS J1729−345. This dense gas supports the idea that HESS J1729−345 and HESS J1731−347 are connected. New constraints on the origin of the gamma-ray emission will have to wait deep observations with Cherenkov instruments. And, since HESS J1729−345 is visible from the Southern hemisphere, the ideal instrument for this observation will be CTA-South. A confirmation of this scenario by CTA would not only constrain the diffusion coefficient in the vicinity of a CR accelerator (the shell-type SNR HESS J1731−347) but it would also provide a clear evidence that protons are accelerated at the shock of the SNR as well as an estimate of the CR efficiency of this shell. In my view, it should be one of the top priority for CTA-South.
Still in the context of escaping CRs, Gallant et al. (2013) used the original idea from Gabici and Aharonian (2007) for the case of Cassiopeia A. They concluded that, for an average density of the interstellar medium (ISM) surrounding the SNR of 1 cm^{-3}, if Cassiopeia A was a PeVatron during the free expansion phase, a halo of gamma-ray emission should be visible surrounding the source due to the interaction of escaped PeV CRs with the ISM. This produces a hard spectrum peaking above 20 TeV. Their estimated flux should be visible only by LHAASO using the KM2A array since Cassiopeia A is in the Northern hemisphere and the sensitivity of CTA-North and HAWC will not allow its detection. A detection by LHAASO would be a clear evidence that, even if Cassiopeia A is no

more acting as a PeVatron, it was in the early days of its evolution as suggested by models. In my view, such detection is extremely challenging (especially due to the very low flux and relatively poor angular resolution of LHAASO) but would represent a major breakthrough.
Recently, the presence of gamma-ray emission extending beyond the SNR shell of RX J1713.7−3946 has been reported by the H.E.S.S. Collaboration (H. E. S. S. Collaboration et al., 2016a). In the context of the Key Science Program of CTA on PeVatrons, simulations show that CTA will provide clear measurements of: i) the extension of the gamma-ray bright shell, constraining the emission of the high-energy runaway particles interacting with the dense medium, ii) the radial profile, which is expected to differ if the gamma rays are produced mainly by electrons or hadrons, and iii) the spectral distribution in different regions of the shell, sampling differences in magnetic fields and/or in dense, clumpy regions. CTA will also be able to probe the maximum energy reached in the source in different regions of the SNR. Such observations would confirm if, as recent results provided by *Fermi* and H.E.S.S. seem to suggest, protons are being accelerated at the SNR shock and are only radiating in dense enough regions. Moreover, if a hadronic component is confirmed, CTA will be able to probe the maximum energy reached by these protons. A complete study of the capabilities offered by CTA for this famous SNR is reported by Acero et al. (2017b).

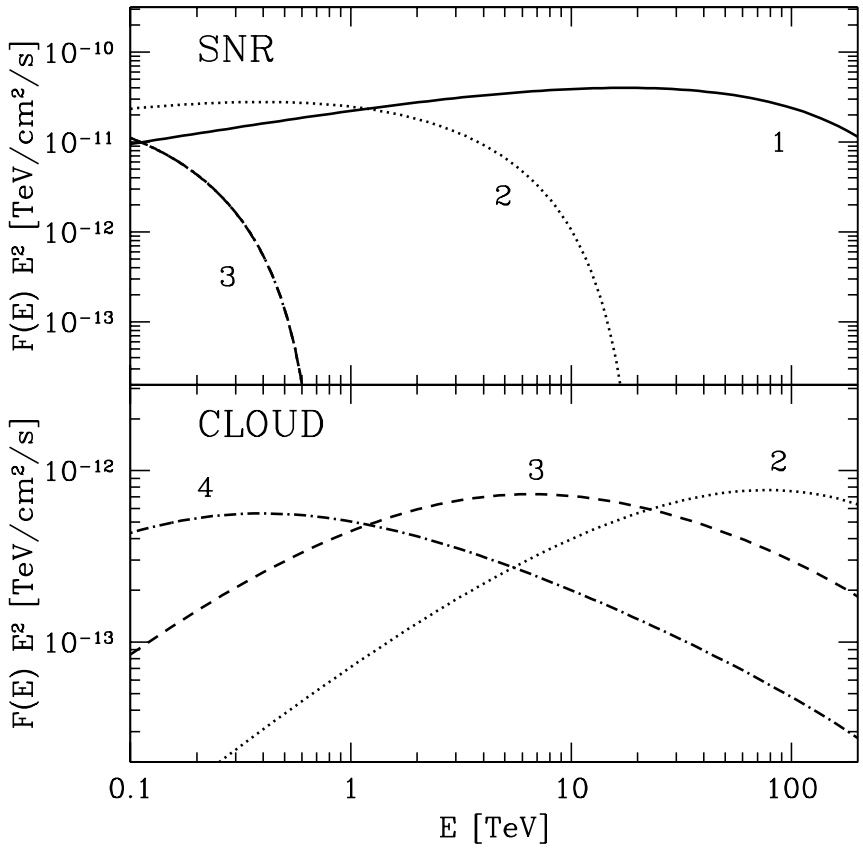

Figure 6.4: *Gamma ray spectra from a SNR (top) and from a cloud of* $10^4 M_\odot$ *located 100 pc away from the SNR (bottom). The distance is 1 kpc. Curves refer to different times after the explosion: 400 (curve 1), 2000 (2), 8000 (3),* $3.2\,10^4$ *(4) yr. Plot taken from Gabici and Aharonian (2007).*

6.4 The population of Galactic SNRs

Thanks to the new generation of instruments, the past several years have seen unprecedented growth in the field of gamma-ray astronomy with the publication of several catalogs, both at TeV and GeV energies. These catalogs are extremely useful since they can be used to constrain general physical parameters of a class of gamma-ray source. For instance, this was the objective of the study that we carried on pulsar wind nebulae with my PhD student Romain Rousseau (Acero et al., 2013a). The upcoming gamma-ray instruments, HAWC, CTA and LHAASO, will allow to generalize this work, operating a transition from individual source study to population studies.

6.4.1 Constraints on CR acceleration

For what concern supernova remnants, the growing number of detections allowed the LAT and H.E.S.S. collaborations to publish a first catalog (Acero et al., 2016; H. E. S. S. Collaboration et al., 2018). The LAT catalog lists 30 classified and 14 marginal SNR candidates with a false identification limit of $<22\%$. Within the limits of existing multi-wavelength data, the LAT observations generally support previous findings of changes in spectral slope at or near TeV energies and a softening and brightening in the GeV range with age. This could be due to the decreasing shock speed and maximum energy causing a softening in the GeV index but we have also seen in this manuscript that the environment that the SNR encounters is one of the most important quantity. The H.E.S.S. publication is based on the results of the Galactic Plane Survey: 50 SNRs are coincident with a H.E.S.S source and in 8 cases the very-high-energy emission is firmly identified as an SNR (H. E. S. S. Collaboration et al., 2018). Assuming that 10% of the kinetic energy of a supernova (10^{51} erg) is injected into cosmic-rays and using H.E.S.S. upper limits from all undetected SNRs, the authors have been able to constrain typical ambient density values around shell-type SNRs to $\leq$ 7 cm^{-3} and the electron-to-proton ratio above 10 TeV to $\leq 5 \times 10^{-3}$. With the increased sensitivity offered by CTA and its Galactic Plane Survey, one can expect that the number of detected SNRs will increase dramatically. Renaud and CTA Consortium (2011b) considered the three shell-type SNRs RX J1713.7$-$3946, Vela Junior and RCW 86 to be representative of the SNR Galactic population in the VHE domain. Their morphological and spectral characteristics, as measured with H.E.S.S., together with their respective distance estimates, have been used to simulate sources throughout the inner Galaxy. They concluded that 20 – 70 TeV shell-type SNRs should be detected, among which $\sim$ 7 – 15 would be resolved with CTA.
This work was done in 2011 and the knowledge on TeV SNRs has greatly improved. A recent study by Cristofari et al. (2017) takes into account the evolution of SNRs in the Galaxy and estimates the SNR population that CTA is expected to detect in the TeV domain. To do so, the authors have used a Monte Carlo approach to simulate the time and position of explosion of supernovae within the Galaxy. This procedure is then coupled with a model which describes the acceleration of particles at SNR shocks and the associated gamma-ray emission, assuming that SNRs are the main source of Galactic CRs. They varied two important parameters (the spectral index of the injected particles and the electron-to-proton ratio) and concluded that the number of detected SNRs greatly depends on the assumed values. For an observation of the entire Galaxy with a sensitivity of $\sim$1mCrab, 200 $\pm$ 20, 21 $\pm$ 5 or 8 $\pm$ 3 SNRs are detected depending on the values of these two parameters (2.05, 10^{-2}; 2.2, 10^{-2}; 2.2, 10^{-5}, respectively). This clearly shows that CTA will be able to give powerful insight on the values of the parameters governing particle acceleration. Moreover, in the first case (2.05, 10^{-2}), the number of detected SNRs is comparable to the one of already detected SNRs in the Galaxy, showing that CTA could well be a very efficient observatory to detect SNRs.

Here, I focused on our Galaxy, but the Large Magellanic Cloud (LMC) is an excellent place to perform a population study and comparison of SNRs. The current population of known SNRs in the LMC amounts to 60 objects, plus 20 plausible candidates. Not all of them are expected to be detected by CTA, but, the radiation field energy densities and gas densities being higher in the LMC, a higher gamma-ray flux should be produced on average, implying more sources to be detectable than in our Milky Way. Both young and interacting remnants are detected in the LMC which is an excellent advantage for a complete population study.

6.4.2 From young SNRs to interacting SNRs

Population study of SNRs can provide constraints on particle acceleration at SNR shocks. It also provides estimates on the influence of the environment surrounding the source if SNRs in different environments are detected. I have compiled in Figure 6.5, the LAT gamma-ray surface brightness (provided by the LAT energy flux above 1 GeV divided by the solid angle of the SNR) as a function of cosmic-ray energy swept up by the SNR (directly provided by the energy density of cosmic-rays in the Galaxy multiplied by the volume of the SNR) for all LAT detected remnants using parameters published in Acero et al. (2016) and updating the LAT flux if a new publication occurred since then. SNRs with clear evidence of interaction are in red, while young non-thermal X-ray SNRs are in blue. All others are in black. We have seen that middle-aged remnants interacting with MCs are very bright in the GeV domain in Section 4: this trend is clearly visible here as well. The gamma-ray luminosity of shell-type remnants, best explained by leptonic scenarios, is relatively low at GeV energies and comparable with the one of the old SNRs Cygnus Loop or S147 that are best explained by re-acceleration of pre-existing CRs and subsequent adiabatic compression in dense filaments. This clearly shows that the gamma-ray luminosity of a SNR in the GeV domain cannot be used to disentangle between leptonic and hadronic processes, at least for sources of relatively low luminosity. When the gamma-ray surface brightness is very high, there is a high probability that the mechanism producing the detected gamma-rays is proton-proton interaction. Indeed, as seen in Section 4, leptonic scenarios require very high electron-to-proton ratio to produce such a high flux. This is not a surprise that the four remnants clearly interacting with MCs and showing the famous "pion bump" W49B, IC443, W44 and W51C present high luminosity values in this Figure. A population study with the LAT looking for spectral breaks at low energy for all SNRs in this group of sources, characteristic of proton-proton interaction, would be extremely valuable. This is one of my top priorities for the next years, as soon as a model of the Galactic diffuse background will be available within the LAT collaboration. This should be the case by summer 2018. A support from the CNES covering half of the expenses for a PhD thesis has been obtained, showing that this topic was considered as important by the committee as well.

We have seen in Section 4 that we expect to see a transition from fresh acceleration of cosmic-rays to re-acceleration of the cosmic-ray sea when the SNR encounters a molecular cloud. Looking at SNRs, in different environments and at different stages of the interaction, would give important information on how it can affects the maximum energy of the particle spectrum at the shock. This maximum energy and its evolution with time can be probed by TeV instruments. We have already seen that G349.7+0.2, which has roughly the same age as W49B, shows an energy break which is ~ 5 times higher. This difference is not completely understood yet but may come from the environment in which the SNR is evolving. A larger sample of TeV detected remnants in interaction with MCs would be extremely valuable in this context. Moreover, current models involving re-acceleration of pre-existing CRs mainly focus on the re-accelerated ambient CRs, while the relic particles from thermal injection

are usually ignored for simplification. Several open questions need deep TeV observations of middle-aged remnants: how much relic particles are still left in middle-aged remnants ? How would they affect the primary CR spectrum and the corresponding gamma-ray emission ?
More specifically, if I would have to choose one or two important individual targets to observe for this topic, I would choose the SNRs W44 and Puppis A (Section 4.4) which are both undetected at TeV energies. Puppis A is already interacting with MCs in some localised regions along the shell, especially in the Eastern side. A detection by CTA together with a measure of spectral differences between the Eastern and Western hemispheres would directly probe the effects of shock-cloud interactions. For what concern W44, its non detection at TeV energies is a puzzle since it is extremely bright at GeV energies and other interacting SNRs with similar LAT brightness have now been detected by H.E.S.S. (such as W51C). Tang (2017) suggested that in W44 thermal injected particle still dominates the seed particles, while in the other middle-aged SNRs ambient CRs already become the dominant component in seed particles. In this case, according to him, we would expect that the TeV spectrum in SNR/MC gradually changes from an exponential cut-off like shape to a power-law profile as the remnant age increases and interacts with the cloud. Such scenario could be tested with TeV observations by CTA.

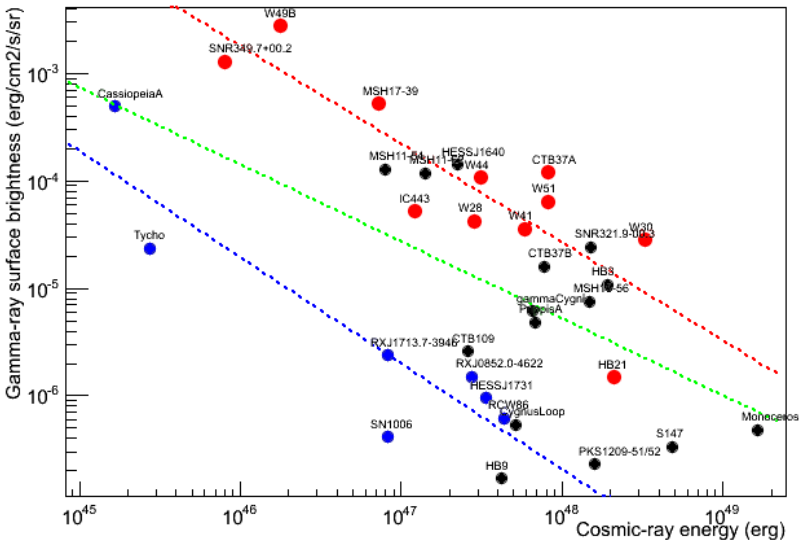

Figure 6.5: *LAT gamma-ray surface brightness as a function of cosmic-ray energy swept up by the SNR. SNRs with clear evidence of interaction with MCs are in red, while young non-thermal X-ray SNRs are in blue. All others are in black. Values are taken from Acero et al. (2016) and updated if a new publication occurred since then. The red dotted line represents the fit of all SNRs with clear evidence of interaction with MCs; the blue dotted line indicates the fit of all SNRs with non-thermal X-ray, while the green dotted line is the fit of all SNRs.*

6.5 Contribution from other types of accelerators

6.5.1 Acceleration of cosmic rays in star forming regions and superbubbles

We have seen that diffusive shock acceleration in isolated SNRs can accelerate cosmic-rays up to $\sim$100 TeV. This seems to be the case for Type Ia SNe with the detection of Tycho for which hadronic

models are preferred and indicate that the current value of the maximum energy reached by protons is $\sim$ 40 TeV. For core-collapse supernovae, the low cutoff energy detected for Cassiopeia A is extremely intriguing since it is even lower than the maximum energy estimated for the 1.6 kyr remnant RX J1713.7−3946. However, most core-collapse SNe occur in star forming regions and superbubbles, these hot and tenuous large structures that are formed around OB associations by the powerful winds and the explosions of massive stars. In such complex environment, the collective effect of multiple SNRs and strong winds from young massive stars may be able to re-energize CR particles and even extend the spectrum of accelerated particles beyond the knee (Parizot et al., 2004). Indeed, the larger size of superbubbles (hundreds of parsecs rather than the several parsecs that characterize SNRs), allows an effective confinement inside the acceleration region of very energetic particles (this way of reasoning is known in the literature as Hillas criterium). Though this scenario might explain PeV particles, until very recently it was considered virtually untestable due to the lack of observations able to reveal the presence of cosmic rays. The recent detection in gamma rays of two of such objects, the Cygnus region with the LAT (Ackermann et al., 2011) and 30 Doradus C with H.E.S.S. (H.E.S.S. Collaboration et al., 2015), together with three other candidates (Westerlund 1, W49A and the G25.0+0+0 region discussed in Section 5.2.2) opens new possibilities. Moreover, recently, elemental abundances of galactic CRs from $_{26}$Fe to $_{40}$Zr were measured by the SuperTIGER (Trans-Iron Galactic Element Recorder) instrument during 55 days of exposure on a long-duration balloon flight over Antarctica (Murphy et al., 2016). These results support a model of cosmic-ray origin in which the source material consists of a mixture of 19^{+11}_{-6}% material from massive stars and $\sim$81% normal interstellar medium material with solar system abundances. This fact brings support to a scenario in which CRs are not only accelerated by individual SNRs, but also at OB stellar associations or inside superbubbles. The recent detection of ^{60}Fe in cosmic-rays by the Cosmic Ray Isotope Spectrometer (CRIS) aboard NASA's Advanced Composition Explorer (ACE) strengthens this conclusion (Binns et al., 2016). Indeed, ^{60}Fe is believed to be produced primarily in core-collapse supernovae of massive stars, which occur mostly in associations of massive stars (OB associations). Following these results, the review by Tatischeff and Gabici (2018) also concludes that the superbubble model provides the most satisfactory explanation for the measured evolution of the light elements in the Milky Way.
Several models tried to predict the shape of the CR spectrum accelerated inside superbubbles showing that it highly depends on the magnetic field turbulence (Ferrand and Marcowith, 2010). If superbubbles are highly magnetized and turbulent (which is a debated issue), very hard spectra can be obtained. The authors also concluded that spectra inside superbubbles are highly variable: at a given time they depend on the particular history of a given cluster. This seems to be in contradiction with the featureless Galactic CR spectrum observed at Earth. Up to now, the lack of detections of star forming regions and superbubbles were a clear obstacle (and even a puzzle if they really are the site of CR acceleration). But now, with the increased sensitivity offered by CTA, several candidates will be observed deeply. The Key Science Program lists three main targets in addition to the Large Magellanic Cloud:

- the Carina nebula, one of the largest, most active and best studied HII regions in our Galaxy,
- the Cygnus region, and more specifically the Cygnus OB2 association, which contains the first ever unidentified source discovered at VHE energies TeV J2032+4130. It is also the place of the cocoon of freshly-accelerated cosmic rays detected by the LAT which stretches between Cygnus OB2, the NGC 6910 open cluster and the SNR Gamma Cygni;
- Westerlund 1, the most massive stellar cluster in our Galaxy, contains a very rich population of massive stars, including a magnetar. An unidentified H.E.S.S. source is coincident with the

cluster but with a size twenty times larger which would imply that particles accelerated in the cluster, escape and interact with the surrounding material and a nearby HII region.

Here are some of the questions that CTA will have to tackle thanks to these observations and detections: What happens to cosmic rays freshly escaping from their sources ? Are they confined for some time, and potentially reaccelerated in the highly turbulent medium of bubbles and superbubbles (such as hinted at by the detection of the Cygnus cocoon) ? Are they advected into the Galactic halo after bubble breakout, thus contributing to the Galactic wind ? What is the contribution of different source classes to the cosmic-ray population in star forming systems ? Where and when are particles accelerated, how do they leave and what is their impact on the surrounding ISM ? What is the maximum energy that can be reached in superbubbles ? What are the parameters that constrain this maximum energy and does it vary from one system to another ? Answering these questions is a first step towards a complete understanding of CR acceleration and propagation in our Galaxy.

6.5.2 Acceleration of cosmic-rays by the Galactic centre

Recently, HESS Collaboration et al. (2016) reported the first discovery of a galactic PeVatron with H.E.S.S., suggesting that it is associated with the supermassive black hole located at the Galactic centre (see Section 5.3.2). Thus, we now know that proton PeVatrons other than SNRs do exist in the galaxy. This makes the picture of the acceleration of CRs in our Galaxy even more intriguing. But the scenario might be much more complex than what has been envisaged. Indeed, the environment in the Galactic centre is often compared with the one of a starburst system. Around 2% of the Galaxy's massive star formation occur in this region and many SNRs are visible through their radio and X-ray thermal emission. Knowing that the kinetic energy released by a supernova is 10^{51} erg, Crocker et al. (2011) estimated that the injection power from these sources is around 10^{40} erg s^{-1}, assuming a high SN rate of 4×10^{-4} yr^{-1} at the Galactic centre (this value is in the range of 0.02 to 0.08 SN per century determined from stellar composition). This estimate is several orders of magnitude higher than the luminosity observed by H.E.S.S.. This implies that CRs injected and accelerated by SNRs in this region cannot be neglected at first order. This led Jouvin et al. (2017) to develop a 3D-model of CR injection and diffusion by SNRs spread throughout the Galactic centre with a realistic 3D gas distribution. They concluded that, to be able to reproduce the total gamma-ray flux observed with H.E.S.S., they need to assume a very low acceleration efficiency of 2% for SNRs located in this region. This further highlights that one needs to take into account the recurrent CR injections from the numerous SNe observed through the Central Molecular Zone. However, it might be that Diffusive Shock Acceleration is less efficient in this region due to the very hot and dense medium in which it takes place. And, to render the picture even more complex, a complete understanding of this region would also need to explain and reproduce the emission detected from the famous Fermi Bubbles. Finally, one should remember that the nature of the central gamma-ray source detected by H.E.S.S. is still a source of debate: the emission may originate from close to the supermassive black hole, from winds driven out from it, from a background pulsar wind nebula, or from a variety of other possibilities. This is largely due to source confusion in this complex region and limited sensitivity to variability and small-scale morphology of the current instruments. For all these reasons, deep observation of this region is a top priority for the future generation of gamma-ray instruments.
Observations of the Galactic centre should be taken primarily with a southern instrument due to the declination of the region of interest $\sim 30°$. This means that the best suited instrument for this science is again CTA-South. For what concern the Fermi Bubbles, a side will be visible from the northern hemisphere, but due to its cutoff energy of $\sim$110 GeV, a rather low energy threshold will

be needed. This makes CTA-North better suited than HAWC for this task although the large field of view of HAWC is a real advantage in comparison to CTA. The science prospect is enormous. The Key Science Program of CTA (Cherenkov Telescope Array Consortium et al., 2017) lists them all and I do not aim to be exhaustive here. The excellent angular resolution of CTA might allow the determination of the nature of the central source, the increase in sensitivity will provide the ability to study the energy-dependent morphology of the diffuse region and will enable the extraction of detailed spectra at various points, possibly showing spectral variations expected if the diffuse emission was caused by a past, point-like outburst. The excellent sensitivity of CTA will also allow the discovery of new sources that are presently not resolvable, including young massive stellar clusters such as the Arches and Quintuplet clusters. Such observation of the richest known environment in our Galaxy is also a sine qua non for the understanding of CR acceleration and propagation in our Galaxy.

6.6 Contribution from multi-wavelength instruments

6.6.1 Multi-wavelength synergy

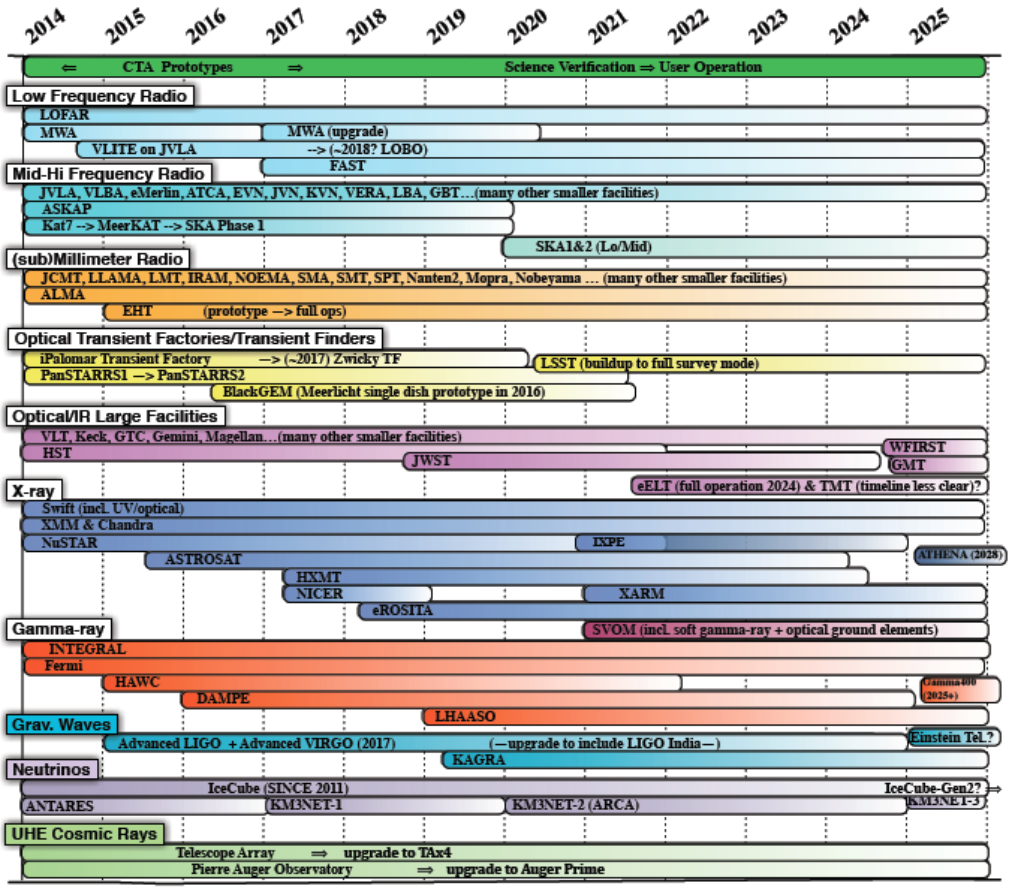

Figure 6.6: *Timeline of the major multi-wavelength facilities in the next decade. Figure taken from Cherenkov Telescope Array Consortium et al. (2017).*

The need for multi-wavelength observations is crucial at gamma-ray energies. First, due to the poor angular resolution of current instruments in this energy range, the identification of a gamma-ray

source heavily depends on radio and X-ray data. Indeed, the gain in sensitivity offered by CTA will allow the detection of 20–70 SNRs among which 7–15 only would be resolved with CTA (Renaud and CTA Consortium, 2011a). Since the morphology is an important criterium to identify a source, we expect that 7–15 sources at maximum can be clearly identified as SNRs with the gamma-ray data only.

Hopefully, *XMM-Newton* and *Chandra* will continue to operate in the next few years. In 2012, NuSTAR (Nuclear Spectroscopic Telescope Array) was launched: it is the first focusing telescope at hard X-rays (2 – 80 keV). In addition to these three satellites, the mission eRosita will be launched from Baikonur in 2018 (Merloni et al., 2012). It will perform the first imaging all-sky survey in the 2 – 10 keV energy range and will certainly become a reference for source identification (see below). At more longer term, *Athena+* will be a major facility at X-ray energies (Nandra et al., 2013). Spatially-resolved high-resolution spectroscopy will allow the measurement of ion post-shock temperature, a key information notably for determining the efficiency of particle acceleration. These data are also extremely powerful to constrain the magnetic field in the source, the electron-to-proton ratio and the particle energy distribution when they are combined to gamma-ray data in models of supernova remnants as we have seen in Sections 3 and 4. *Athena+* X-ray Integral Field Unit will make possible the detection of weak thermal emission in non-thermal rims and allow to constrain the density in these regions, which is a key parameter to discriminate between hadronic and leptonic scenarios.

For such modelings, one also need to know the distance of the source and the density of the surrounding medium in which a supernova remnant is evolving. Sub-millimeter facilities are extremely useful in this respect. One can cite the degree-scale survey of Mopra in Australia (Burton et al., 2013), APEX (Güsten et al., 2006) and Nanten2 (Mizuno and Fukui, 2004) in Chile and Nobeyama 45m in Japan (Umemoto et al., 2017). For supernova remnants, the overlap between infra-red astronomy and gamma-ray astronomy is smaller, but it can be extremely useful in particular cases. For instance, in the case of RCW 86, the infra-red observations by *WISE* and *SPITZER* allowed the detection of the entire shell at 24 and 22 μm, providing constraints on the post-shock gas densities in small regions of the remnants (Williams et al., 2011).

Finally, two MeV missions are currently proposed, the european e-ASTROGAM (De Angelis et al., 2017) and the american All-Sky Medium Energy Gamma-ray Observatory (AMEGO, McEnery (2017)). If one of them is accepted, it could have a major impact on the search for interacting SNRs, with excellent sensitivity in the energy domain where the characteristic pion-bump is located, and nucleosynthesis studies thanks to excellent capabilities for MeV spectroscopy.

This is a short summary of the most important instruments used for supernova remnant's studies. An exhaustive description of all facilities in the next decade is provided in Cherenkov Telescope Array Consortium et al. (2017) and listed in Figure 6.6. I also describe below in Section 6.6.2 what could be one of the most important contribution coming from this multi-wavelength synergy (on supernova remnants) in the next few years. Neutrino astronomy could also become very useful within the next ten years. Indeed, the recent detection of a flux of high energy (> 10 TeV) astrophysical neutrinos by the IceCube collaboration has opened a new window on the Universe (IceCube Collaboration, 2013). In a combined fit to all available IceCube data, the flux was characterized from 25 TeV to 2.8 PeV as a power law with spectral index 2.50 ± 0.09 (Aartsen et al., 2015). A recent analysis of only muon neutrinos in the northern sky, with a higher energy threshold of 191 TeV and sensitive up to 8.3 PeV, yields a harder spectral index of 2.13 ± 0.13 (Aartsen et al., 2016). This difference could indicate either a spectral break or a spatial anisotropy. It could also well be that a relatively soft Galactic contribution dominates in the southern sky in addition to a harder, isotropic extragalactic component. Aartsen et al. (2017) have shown that most Galactic scenarios can only have a limited contribution to the astrophysical signal: diffuse Galactic emission ($\leq$50%), supernova remnants ($\leq$65%), extended dif-

fuse emission from the Fermi bubbles ($\leq$25%) or unidentified TeV sources ($\leq$25%). But the present data cannot exclude a subdominant flux of Galactic origin in the IceCube data. More specifically, the possibility that the hot spot close to the Galactic center is produced by a single point source with a flux normalization of 6×10^{-8} GeV cm^{-2}s^{-1} has been excluded by the observations made with the ANTARES neutrino telescope, showing that neutrino upper limits are already constraining some astrophysical scenarios (Adrián-Martínez et al., 2014). On an individual source basis, an independent and straightforward proof of the hadronic origin of the gamma-ray emission from a supernova remnant would be the detection of multi-TeV neutrinos spatially correlated with the γ-ray source. One of the brightest SNR detected at gamma-ray energies is RX J1713.7$-$3946. This explains why it is often used as a best candidate for neutrino telescopes, even if this source is likely leptonic dominated (hadronic being dominant only in dense clumps, see Section 3.3.1). Adrián-Martínez et al. (2016) have evaluated the significance of the signal observed on this source with the KM3NeT/ARCA and concluded that a 3σ signal can be reached in about 4 years of observation time if the γ-ray signal is entirely hadronic (see Figure 6.7). This means that KM3NeT should be able to constrain the fraction of protons in this source within the lifetime of the experiment. The diffuse emission from the Galactic centre is another good candidate for the observation with neutrino telescope since it has the advantage to be produced by protons with no sign of cutoff at gamma-ray energies. HESS Collaboration et al. (2016) estimated the neutrino flux that should accompany the observed gamma-ray flux and concluded that it can be marginally detected by a km^3-scale detector after several years of exposure. These results suggest that, over the lifetime of the CTA Observatory, neutrino telescopes might have opened a new window on our Galaxy even on a single source basis.

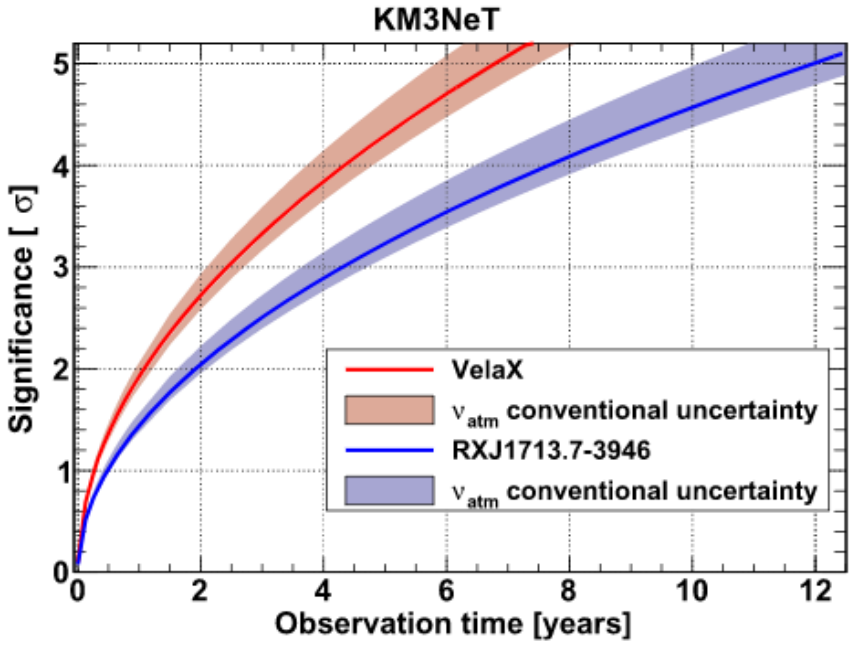

Figure 6.7: *Significance as a function of KM3NeT/ARCA observation time for the detection of the Galactic sources RX J1713.7−3946 and Vela-X. The bands represent the effect of the uncertainties on the conventional component of the atmospheric neutrino flux. Figure taken from Adrián-Martínez et al. (2016).*

6.6.2 Search for missing SNRs in the Galaxy

Of the 295 remnants listed in the most recent version of the Green catalogue (Green, 2017), most have been first identified at radio wavelengths, or – if identified at other wavebands – have subsequently been detected at radio wavelengths. At optical and X-ray wavelengths only about 40% and 30%, respectively, of the catalogued SNRs have been detected (which is not surprising, due to Galactic absorption that affects these wavelengths). At gamma-ray energies even fewer remnants have been detected, with a total of $\sim$30 sources as likely GeV SNRs seen by *Fermi*. Approximately the same number is detected by Cherenkov telescopes. Radio observations and survey of the Galactic plane is therefore crucial to discover new SNRs.
The case of the SNR G150.3+4.5 discussed in Section 5.1.2 is a good example of a faint remnant with a low surface brightness recently detected in our Galaxy. Using the Urumqi 6 cm Galactic plane survey data, Gao and Han (2014) concluded that G150.3+4.5 is a shell-type SNR looking at the shell-like structures and their non-thermal nature at radio frequencies. It was then detected at gamma-ray energies with our catalogs of extended sources (Ackermann et al., 2016, 2017). The hard spectrum of this SNR derived from 10 GeV up to 2 TeV, with $\Gamma \sim 1.9$, is more similar to that of young shell-type remnants since most middle-aged remnants have a steeper spectrum above 10 GeV due to a spectral break between 1 and 10 GeV. This source is therefore an excellent candidate for future observations by Cherenkov instruments such as HAWC (with its large field of view well adapted for such a large source) or CTA-North. This would allow the coverage of the high energy spectrum of the source, providing constraints on the maximum energy of the particles accelerated as well as on the type of particles (electrons or protons).
In my view, two upcoming facilities will provide extremely valuable information for CTA as well as detection of several new remnants: SKA and eROSITA.

The radio band and SKA

The Square Kilometre Array (SKA) is a large international radio telescope project characterized, as suggested by its name, by a total collecting area of approximately one square kilometre, and consisting of several interferometric arrays to observe at metric and centimetric wavelengths (Acero et al., 2017a). The deployment of the SKA will take place in two sites, in South Africa and Australia, and in two successive phases. The start of construction of Phase 1 is planned for 2020 with a commissioning by 2024. It consists of installing approximately 10% of the final arrays. Phase 2 is envisaged for 2030. The frequency range that the SKA is expected to cover is unprecedented, going from approximately 50 MHz to 15 GHz using low frequency aperture array in Australia (SKA1-LOW) and mid-frequency aperture array in South Africa (SKA1-MID) presented in Figure 6.8. The SKA1-LOW, with frequency range between 50 MHz and 350 MHz and a field of view of 30 deg^2, hosts great potential to discover a large number of SNRs and will be of crucial importance to identify gamma-ray sources or to constrain their non-thermal morphology. With a field of view of only 0.5 deg^2 but an excellent angular resolution of 0.22" (with respect to 11" for SKA1-LOW), the SKA1-MID will be ideal to detect and resolve young SNRs ($<$ 1000 years) which are the best candidates for the acceleration of PeV protons. In addition to discovery potential, it will help to identify sources detected at TeV energies by CTA or HAWC. Observations by SKA as well as other multi-wavelength instruments (such as *XMM-Newton* and *Chandra* cited above) will become crucial. Moreover, we have seen that several middle-aged remnants interacting with molecular clouds present a low energy break called "pion bump". This directly implies that the spectrum of secondary electrons begins to diverge from a pure power-law below $\sim$1 GeV finally cutting off below $\sim$100 MeV. The primary electron distribution, on

the other hand, would display no such features. This implies that this spectral feature can be detected at frequencies below 100 MHz (B/10 μG). SKA will therefore be able to track directly the presence of protons accelerated at SNR shock and even constrain the cosmic-ray efficiency in case of detections of such spectral feature (Aharonian et al., 2013).

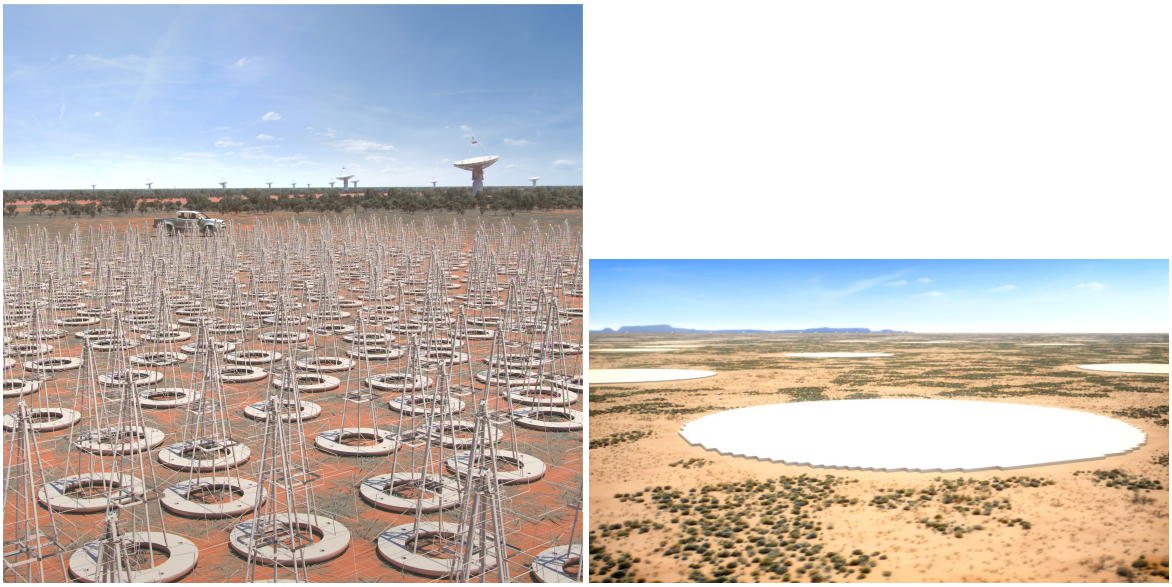

Figure 6.8: *Left: Artist impression of the low frequency aperture array in Australia (SKA1-LOW). Right: Artist impression of the mid-frequency aperture array in South Africa (SKA1-MID). Credit: SKA Organisation*

At X-ray energies: *eROSITA*

The radio band is an excellent domain to look for supernova remnants, but two important selection effects exist in this energy range: 1) intrinsically faint remnants (i.e. low surface brightness) are difficult to identify, and 2) physically small but distant remnants are difficult to recognize as SNRs, due to their small angular sizes. For example, the Effelsberg 2.7-GHz survey has a resolution of 4.3 arcmin, and SNRs would have to be several times this angular size for their structure to be recognized. Most of the missing small angular size remnants are young but distant SNRs that lie on the far side of the Galaxy, and hence concentrated towards l = 0°, b = 0°, where confusion due to other Galactic sources along the line of sight makes their identification difficult. In the opposite, if a remnant is too old and its radio emission has faded already, it will be hard to identify the source by the limited surface-brightness sensitivity of previous sky-surveys. It is thus crucial to use other facilities to complete the catalog of Galactic SNRs. One of the best way to do so is to use X-ray data. The ROSAT All-Sky survey has demonstrated the potential power for finding new SNR. The examples of RX J1713.7−3946 and Vela Junior (also known as RX J0852.0−4622) highlight very well that low surface brightness SNR are missed by radio surveys but can be identified at X-ray energies (Pfeffermann and Aschenbach, 1996a; Aschenbach, 1998). This has motivated Schaudel et al. (2002) to investigate the all-sky survey data more systematically in order to search for unidentified supernova remnants. From their candidate list several sources have been confirmed meanwhile as SNR (e.g. Jackson et al., 2008; Robbins et al., 2012). These identifications suggest that many of their SNR candidates are indeed radio under-luminous, explaining why past radio surveys could not identify them before. The correlation of *eROSITA* data with radio surveys will allow us further identification studies on more than 140 faint

and diffuse X-ray sources, which have been by now classified as SNR candidates in the ROSAT all-sky survey (Prinz and Becker, 2012). In addition to this complete sample of Galactic X-ray SNRs, *eROSITA* will be able to survey the Large Magellanic Cloud and provide a catalog of sources in this region, including supernova remnants.

Summary

- Upcoming gamma-ray facilities such as CTA or LHAASO, will have increased sensitivity and angular resolution to provide a new light on our Galaxy and discover new SNRs.
- Gamma-ray observations of historical SNRs is crucial to constrain the maximum energy reached by protons as well as the early stage of evolution of a supernova remnant. The SNR SN 1987A in the LMC is an excellent target in addition to traditional Galactic SNRs.
- Up to now, one single PeVatron in the Galaxy was discovered, likely related to the central black hole. Search for PeVatron in the Galaxy, thanks to Galactic plane survey or deep γ-ray observation of sources with hard spectra, is thus crucial to test the SNR paradigm.
- The escape of CRs from the SNR shock and their propagation in the surrounding medium is still poorly known. Gamma-ray observations of remnants starting to interact with molecular clouds (such as Puppis A) or remnants located in dense medium (such as RX J1713.7$-$3946) can provide new clues on these mechanisms.
- The increased sensitivity of the new generation of gamma-ray instruments will increase the number of detected SNRs allowing to perform population studies. This will help to understand the evolution of CR acceleration as well as the influence of the environment surrounding the shock.
- Other type of Galactic accelerators might contribute significantly to the CR spectrum and needs to be observed deeply. Star forming regions, superbubbles and the Galactic centre are the best candidates.
- A complete multi-wavelength synergy is being set between gamma-ray instruments and other facilities, in particular radio and X-ray instruments for supernova remnants. Neutrino telescopes might play a role within the lifetime of CTA. New discoveries by eROSITA and SKA are likely to provide a large number of new discoveries.
- Major breakthroughs are expected on this field in the coming years !

The results presented in this chapter have been published in (bold faces indicate those for which I am corresponding author):

- **Ackermann M. et al., 2017, The Astrophysical Journal, 843, 139: "Search for Extended Sources in the Galactic Plane Using Six Years of Fermi-Large Area Telescope Pass 8 Data above 10 GeV"**
- F. Acero et al., 2017, arXiv:1712.06950: "French SKA White Book - The French Community towards the Square Kilometre Array"

- F. Acero et al., 2017, arXiv:1709.03483: "Cherenkov Telescope Array Contributions to the 35th International Cosmic Ray Conference (ICRC2017)"
- **Lemoine-Goumard M., 2015, Rapporteur talk of the 34th International Cosmic Ray Conference (ICRC2015), The Hague, The Netherlands: "Ground-based gamma-ray astronomy"**
- A. Abramowski et al. (H.E.S.S. collaboration), 2014, MNRAS, 441, 790: "TeV γ-ray observations of the young synchrotron-dominated SNRs G1.9+0.3 and G330.2+1.0 with H.E.S.S."
- K. Nandra et al., 2013, arXiv:1306.2307: "The Hot and Energetic Universe: A White Paper presenting the science theme motivating the Athena+ mission"

APPENDIX

A

Curriculum Vitae

Informations personnelles:
Grade: Chargée de Recherches 1^{ere} classe au CNRS
Statut actuel: Membre des collaborations internationales Fermi, H.E.S.S. et CTA
Établissement: Centre d'Études Nucléaires de Bordeaux Gradignan (UMR 5797)
Adresse: 19 Chemin du Solarium, CS 10120, F-33175 GRADIGNAN Cedex
Courrier électronique: lemoine@cenbg.in2p3.fr

Formation:

Habilitation: Habilitation à Diriger des Recherches soutenue le 18 Juin 2018 "Unveiling Galactic cosmic-ray accelerators with gamma-ray observations: their relation to supernova remnants"; autorisation de soutenance de l'Université de Bordeaux obtenue en Juin 2017
Doctorat: Thèse de doctorat soutenue le 11 Mai 2006 "Stéréoscopie des gerbes de γ avec les télescopes H.E.S.S.: premières images de vestiges de supernovae au TeV" - Mention Très honorable avec les félicitations du jury - Laboratoire Leprince-Ringuet, École Polytechnique (Palaiseau) - Directeur de thèse: Bernard Degrange

Responsabilités institutionnelles:

2018: Membre du jury de sélection du poste de maître de conférences de l'Université Paris 7
Depuis 2016: Membre élue du conseil de laboratoire du CENBG
2016: Membre du comité stratégique de décision de la station de radioastronomie de Nançay
2012 – 2016: Membre du conseil scientifique du "Programme National Hautes Energies"
2012: Membre du jury de sélection du poste de maître de conférences de l'Université Paris 7
2008 – 2012: Membre du conseil scientifique "Particules et Univers" du CNRS
Depuis 2008: Membre du comité d'organisation de l'atelier annuel "Pulsars et leurs environnements"
Jury de thèse: Anna Zajczyk (NCAC, Poland, 2012), Lola Falletti (LUPM, France, 2013), R. Lopez-Coto (UAB, Espagne, 2015), C. Trichard (LAPP, France, 2015), F. Gate (Subatech, France, 2016), C. Mariaud (LLR, France, 2018)

Comité de thèse: Lola Falletti (2010 – 2013), D. Fernandez (2012 – 2015), J. Devin (2015 – 2018), Michelle Tsirou (2016 –), L. Brahimi (2017 –)

Bourses et distinctions:

Depuis 2018: Co-porteur de l'ANR PECORA (2018 – 2022, 161 keuros alloués au CENBG)
Janvier 2016: Thomson Reuters's Highly cited scientist
2011: Médaille de Bronze du CNRS (IN2P3)
Août 2010: Bourse Starting Grant "European Research Council" pour le projet "New light on the gamma-ray sky: unveiling cosmic-ray accelerators in the Milky Way and their relation to pulsar wind nebulae"
Mai 2008: Bourse de 15 k$ France-Stanford avec R. Romani
Mai 2007: Prix de Thèse de l'Ecole Polytechnique
Février 2007: Prix Daniel Guinier de la Société Française de Physique

Responsabilités scientifiques et techniques:

Depuis 2012: Responsable du projet H.E.S.S. au CENBG
Depuis 2012: Responsable de l'écriture des données H.E.S.S. sur site et copie au CC-IN2P3
2012 – 2014: Responsable du groupe "Sources galactiques" de la collaboration Fermi
2008 – 2012: Responsable du sous-groupe "Vestiges de Supernovae et Nébuleuse de pulsars" de la collaboration Fermi
Depuis 2007: Rapporteur pour The Astrophysical Journal, Astronomy and Astrophysics et Astroparticle Physics

Encadrement scientifique:

Doctorant: M-H Grondin (2007 – 2010, Université), R. Rousseau (2010 – 2013, Bourse ERC), B. Condon (2014 – 2017, Financement CNES–CNRS)
Post-doctorants: J. Méhault (2010 – 2013, Bourse ERC), M. Dalton (2010 – 2013, Bourse ERC), H. Laffon (2012 – 2015, Financement CNRS), F. Brun (2016 – 2018, Overheads ERC)

Organisation de conférences et ateliers:

- Conférence "Very High Energy Phenomena in the Universe", Vietnam (Août 2018)
- Conférence "Cosmic Rays and the InterStellar Medium", Grenoble (Juin 2018)
- Fermi Symposium, Garmisch-Partenkirchen (Octobre 2017)
- Symposium IAU "SN 1987A 30 years after", île de la Réunion (Fevrier 2017)
- Conférence TeV Particle Astrophysics, Genève (Septembre 2016)
- Atelier analyse H.E.S.S., Bordeaux (Septembre 2016)
- Conférence TeVPA-IDM, Amsterdam (Juin 2014)
- Conférence "Cosmic-ray Origin: Beyond the standard models", San Vito di Cadore (Septembre 2014)
- Conférence "Very High Energy Phenomena in the Universe", Vietnam (Août 2014)
- Réunion de collaboration H.E.S.S., Bordeaux (Octobre 2013)
- Ecole d'été "Cosmic Accelerators", Cargese (Mai 2013)
- Symposium IAU "Supernova environmental impacts", Calcutta (Janvier, 2013)
- Atelier "Pulsars and their environment", Bordeaux (Novembre 2010)
- Réunion du groupe "Galactic science" de la collaboration Fermi, Bordeaux (Juin 2009)

Production scientifique:

Publications:
- 209 dans des revues avec comité de lecture dont 17 en auteur correspondant
- Un chapitre publié en 2015 dans les Comptes Rendus Annuels de l'Académie des Sciences sur les vestiges de supernovae
- Rapport de session "Astronomie gamma au sol" à l'International Cosmic Ray Conference 2015

Conférences internationales:
- 23 présentations orales dont 12 revues invitées

Vulgarisation scientifique:

2018: Conférence grand public à l'Institut d'Astrophysique de Paris; la conférence à été filmée et mise en ligne sur Canal-U.
2016: Participation à la réalisation d'un film visant à promouvoir la recherche à l'Université de Bordeaux: https://www.youtube.com/watch?v=kAEkdap8l6o
2014: "L'univers des pulsars se décrypte à Gradignan", Journal Sud Ouest
2013: "Rayons cosmiques: on a percé le secret de leur origine", Journal Science et Vie
2012: "Elle fait la chasse aux pulsars", Journal Sud Ouest
2011: Ecole d'été européenne de l'Université de Strasbourg
2010: Les chercheurs de l'Université de Bordeaux ont la cote, Journal Sud Ouest
2009: Intervention lors de la semaine de l'Astroparticules organisée au sommet de la Tour Montparnasse (Opera Cosmique: http://www.opera-cosmique.fr/)
2008: Participation à la réalisation d'un film de vulgarisation sur le groupe Fermi du CENBG. Ce film a été produit en anglais et en français: https://www.youtube.com/watch?v=54IBWt-O8Co
Depuis 2007: Intervention régulière à la Société Astronomique de Bordeaux

ACRONYMS

CMB cosmic microwave background.

CR cosmic ray.

CSM circumstellar medium.

CTA Cherenkov Telescope Array.

DSA diffusive shock acceleration.

HE high energy.

IACT imaging atmospheric Cherenkov telescope.

IC inverse Compton.

IRF instrument response function.

ISM interstellar medium.

LAT Large Area Telescope.

MC molecular cloud.

PSF point spread function.

PWN pulsar wind nebula.

SN supernova.

SNR supernova remnant.

VHE very high energy.

BIBLIOGRAPHY

A. Aab, P. Abreu, M. Aglietta, E. J. Ahn, I. Al Samarai, I. F. M. Albuquerque, I. Allekotte, J. Allen, P. Allison, A. Almela, and et al. Depth of maximum of air-shower profiles at the Pierre Auger Observatory. I. Measurements at energies above 1 $0^{17.8}$ eV. Phys. Rev. D, 90(12):122005, December 2014. doi: 10.1103/PhysRevD.90.122005.

M. G. Aartsen, K. Abraham, M. Ackermann, J. Adams, J. A. Aguilar, M. Ahlers, M. Ahrens, D. Altmann, T. Anderson, M. Archinger, and et al. A Combined Maximum-likelihood Analysis of the High-energy Astrophysical Neutrino Flux Measured with IceCube. ApJ, 809:98, August 2015. doi: 10.1088/0004-637X/809/1/98.

M. G. Aartsen, K. Abraham, M. Ackermann, J. Adams, J. A. Aguilar, M. Ahlers, M. Ahrens, D. Altmann, K. Andeen, T. Anderson, and et al. Observation and Characterization of a Cosmic Muon Neutrino Flux from the Northern Hemisphere Using Six Years of IceCube Data. ApJ, 833:3, December 2016. doi: 10.3847/0004-637X/833/1/3.

M. G. Aartsen, M. Ackermann, J. Adams, J. A. Aguilar, M. Ahlers, M. Ahrens, I. A. Samarai, D. Altmann, K. Andeen, T. Anderson, and et al. Constraints on Galactic Neutrino Emission with Seven Years of IceCube Data. ApJ, 849:67, November 2017. doi: 10.3847/1538-4357/aa8dfb.

R. U. Abbasi, M. Abe, T. Abu-Zayyad, M. G. Allen, et al. The hybrid energy spectrum of Telescope Array's Middle Drum Detector and surface array. *Astroparticle Physics*, 68:27–44, August 2015. doi: 10.1016/j.astropartphys.2015.02.008.

A. A. Abdo, M. Ackermann, M. Ajello, A. Allafort, et al. Fermi-Lat Discovery of GeV Gamma-Ray Emission from the Young Supernova Remnant Cassiopeia A. ApJ, 710:L92–L97, February 2010a. doi: 10.1088/2041-8205/710/1/L92.

A. A. Abdo, M. Ackermann, M. Ajello, A. Allafort, et al. Fermi Large Area Telescope Observations of the Supernova Remnant W28 (G6.4-0.1). ApJ, 718:348–356, July 2010b. doi: 10.1088/0004-637X/718/1/348.

A. A. Abdo, M. Ackermann, M. Ajello, L. Baldini, et al. Gamma-Ray Emission from the Shell of Supernova Remnant W44 Revealed by the Fermi LAT. *Science*, 327:1103, February 2010c. doi: 10.1126/science.1182787.

A. A. Abdo, M. Ackermann, M. Ajello, et al. Detection of the Energetic Pulsar PSR B1509-58 and its Pulsar Wind Nebula in MSH 15-52 Using the Fermi-Large Area Telescope. ApJ, 714:927–936, May 2010d. doi: 10.1088/0004-637X/714/1/927.

A. A. Abdo, M. Ackermann, M. Ajello, A. Allafort, et al. Observations of the Young Supernova Remnant RX J1713.7-3946 with the Fermi Large Area Telescope. ApJ, 734:28, June 2011. doi: 10.1088/0004-637X/734/1/28.

A. U. Abeysekara, A. Albert, R. Alfaro, C. Alvarez, et al. The 2HWC HAWC Observatory Gamma-Ray Catalog. ApJ, 843:40, July 2017. doi: 10.3847/1538-4357/aa7556.

A. Abramowski, F. Aharonian, F. Ait Benkhali, A. G. Akhperjanian, E. O. Angüner, M. Backes, S. Balenderan, A. Balzer, A. Barnacka, Y. Becherini, and et al. Discovery of the Hard Spectrum VHE γ-Ray Source HESS J1641-463. ApJ, 794:L1, October 2014. doi: 10.1088/2041-8205/794/1/L1.

V. A. Acciari, E. Aliu, T. Arlen, T. Aune, et al. Observation of Extended Very High Energy Emission from the Supernova Remnant IC 443 with VERITAS. ApJ, 698:L133–L137, June 2009. doi: 10.1088/0004-637X/698/2/L133.

V. A. Acciari, E. Aliu, T. Arlen, T. Aune, et al. Discovery of TeV Gamma-ray Emission from Tycho's Supernova Remnant. ApJ, 730:L20, April 2011. doi: 10.1088/2041-8205/730/2/L20.

F. Acero, J. Ballet, and A. Decourchelle. The gas density around SN 1006. A&A, 475:883–890, December 2007. doi: 10.1051/0004-6361:20077742.

F. Acero, F. Aharonian, A. G. Akhperjanian, and H.E.S.S. Collaboration. First detection of VHE γ-rays from SN 1006 by HESS. A&A, 516:A62, June 2010. doi: 10.1051/0004-6361/200913916.

F. Acero, M. Ackermann, M. Ajello, A. Allafort, et al. Constraints on the Galactic Population of TeV Pulsar Wind Nebulae Using Fermi Large Area Telescope Observations. ApJ, 773:77, August 2013a. doi: 10.1088/0004-637X/773/1/77.

F. Acero, Y. Gallant, J. Ballet, M. Renaud, and R. Terrier. A new nearby pulsar wind nebula overlapping the RX J0852.0-4622 supernova remnant. A&A, 551:A7, March 2013b. doi: 10.1051/0004-6361/201220799.

F. Acero, M. Lemoine-Goumard, M. Renaud, J. Ballet, J. W. Hewitt, R. Rousseau, and T. Tanaka. Study of TeV shell supernova remnants at gamma-ray energies. *A&A*, 580:A74, August 2015. doi: 10.1051/0004-6361/201525932.

F. Acero, M. Ackermann, M. Ajello, L. Baldini, et al. The First Fermi LAT Supernova Remnant Catalog. ApJS, 224:8, May 2016. doi: 10.3847/0067-0049/224/1/8.

F. Acero, J.-T. Acquaviva, R. Adam, N. Aghanim, et al. French SKA White Book - The French Community towards the Square Kilometre Array. *ArXiv e-prints*, December 2017a.

F. Acero, R. Aloisio, J. Amans, E. Amato, L. A. Antonelli, C. Aramo, T. Armstrong, F. Arqueros, K. Asano, M. Ashley, and et al. Prospects for Cherenkov Telescope Array Observations of the Young Supernova Remnant RX J1713.7-3946. ApJ, 840:74, May 2017b. doi: 10.3847/1538-4357/aa6d67.

M. Ackermann, M. Ajello, A. Allafort, L. Baldini, et al. A Cocoon of Freshly Accelerated Cosmic Rays Detected by Fermi in the Cygnus Superbubble. *Science*, 334:1103, November 2011. doi: 10.1126/science.1210311.

M. Ackermann, M. Ajello, A. Allafort, L. Baldini, et al. Detection of the Characteristic Pion-Decay Signature in Supernova Remnants. *Science*, 339:807–811, February 2013a. doi: 10.1126/science.1231160.

M. Ackermann, M. Ajello, A. Allafort, L. Baldini, et al. Detection of the Characteristic Pion-Decay Signature in Supernova Remnants. *Science*, 339:807–811, February 2013b. doi: 10.1126/science.1231160.

M. Ackermann, A. Albert, W. B. Atwood, et al. The Spectrum and Morphology of the Fermi Bubbles. ApJ, 793:64, September 2014. doi: 10.1088/0004-637X/793/1/64.

M. Ackermann, M. Ajello, W. B. Atwood, L. Baldini, et al. 2FHL: The Second Catalog of Hard Fermi-LAT Sources. ApJS, 222:5, January 2016. doi: 10.3847/0067-0049/222/1/5.

M. Ackermann, M. Ajello, L. Baldini, J. Ballet, et al. Search for Extended Sources in the Galactic Plane Using Six Years of Fermi-Large Area Telescope Pass 8 Data above 10 GeV. ApJ, 843:139, July 2017. doi: 10.3847/1538-4357/aa775a.

S. Adrián-Martínez, A. Albert, M. André, M. Anghinolfi, et al. Searches for Point-like and Extended Neutrino Sources Close to the Galactic Center Using the ANTARES Neutrino Telescope. ApJ, 786:L5, May 2014. doi: 10.1088/2041-8205/786/1/L5.

S. Adrián-Martínez, M. Ageron, F. Aharonian, S. Aiello, A. Albert, F. Ameli, E. Anassontzis, M. Andre, G. Androulakis, M. Anghinolfi, and et al. Letter of intent for KM3NeT 2.0. *Journal of Physics G Nuclear Physics*, 43(8):084001, August 2016. doi: 10.1088/0954-3899/43/8/084001.

M. Aglietta, B. Alessandro, P. Antonioli, F. Arneodo, and EAS-TOP Collaboration. The cosmic ray proton, helium and CNO fluxes in the 100 TeV energy region from TeV muons and EAS atmospheric Cherenkov light observations of MACRO and EAS-TOP. *Astroparticle Physics*, 21: 223–240, June 2004. doi: 10.1016/j.astropartphys.2004.01.005.

F. Aharonian, A. G. Akhperjanian, A. R. Bazer-Bachi, M. Beilicke, et al. The H.E.S.S. Survey of the Inner Galaxy in Very High Energy Gamma Rays. ApJ, 636:777–797, January 2006a. doi: 10.1086/498013.

F. Aharonian, A. G. Akhperjanian, A. R. Bazer-Bachi, et al. Observations of the Crab nebula with HESS. A&A, 457:899–915, October 2006b. doi: 10.1051/0004-6361:20065351.

F. Aharonian, A. G. Akhperjanian, A. R. Bazer-Bachi, et al. H.E.S.S. Observations of the Supernova Remnant RX J0852.0-4622: Shell-Type Morphology and Spectrum of a Widely Extended Very High Energy Gamma-Ray Source. ApJ, 661:236–249, May 2007. doi: 10.1086/512603.

F. Aharonian, A. G. Akhperjanian, U. Barres de Almeida, et al. HESS upper limits for Kepler's supernova remnant. *A&A*, 488:219–223, September 2008a. doi: 10.1051/0004-6361:200809401.

F. Aharonian, A. G. Akhperjanian, A. R. Bazer-Bachi, et al. Discovery of very high energy gamma-ray emission coincident with molecular clouds in the W 28 (G6.4-0.1) field. A&A, 481:401–410, April 2008b. doi: 10.1051/0004-6361:20077765.

F. Aharonian, A. G. Akhperjanian, U. B. de Almeida, et al. Discovery of Gamma-Ray Emission From the Shell-Type Supernova Remnant RCW 86 With H.E.S.S. ApJ, 692:1500–1505, February 2009. doi: 10.1088/0004-637X/692/2/1500.

F. Aharonian, T. G. Arshakian, B. Allen, R. Banerjee, et al. Pathway to the Square Kilometre Array - The German White Paper -. *ArXiv e-prints*, January 2013.

F. A. Aharonian and A. M. Atoyan. On the emissivity of πˆ0ˆ-decay gamma radiation in the vicinity of accelerators of galactic cosmic rays. A&A, 309:917–928, May 1996.

F. A. Aharonian, A. G. Akhperjanian, K.-M. Aye, et al. High-energy particle acceleration in the shell of a supernova remnant. Nature, 432:75–77, November 2004. doi: 10.1038/nature02960.

M. L. Ahnen, S. Ansoldi, L. A. Antonelli, et al. A cut-off in the TeV gamma-ray spectrum of the SNR Cassiopeia A. MNRAS, 472:2956–2962, December 2017. doi: 10.1093/mnras/stx2079.

M. Ajello, L. Baldini, G. Barbiellini, D. Bastieri, et al. Deep Morphological and Spectral Study of the SNR RCW 86 with Fermi-LAT. *ApJ*, 819:98, March 2016. doi: 10.3847/0004-637X/819/2/98.

J. Albert, E. Aliu, H. Anderhub, P. Antoranz, et al. Observation of VHE γ-rays from Cassiopeia A with the MAGIC telescope. A&A, 474:937–940, November 2007a. doi: 10.1051/0004-6361:20078168.

J. Albert, E. Aliu, H. Anderhub, P. Antoranz, et al. Discovery of Very High Energy Gamma Radiation from IC 443 with the MAGIC Telescope. ApJ, 664:L87–L90, August 2007b. doi: 10.1086/520957.

G. E. Allen, K. Chow, T. DeLaney, M. D. Filipović, J. C. Houck, T. G. Pannuti, and M. D. Stage. On the Expansion Rate, Age, and Distance of the Supernova Remnant G266.2-1.2 (Vela Jr.). ApJ, 798: 82, January 2015. doi: 10.1088/0004-637X/798/2/82.

R. Aloisio, P. Blasi, I. De Mitri, and S. Petrera. Selected Topics in Cosmic Ray Physics. *ArXiv e-prints*, July 2017.

E. O. Angüner, S. Casanova, I. Oya, F. Aharonian, P. Bordas, and A. Ziegler for the H. E. S. S. Collaboration. Very high energy emission from the hard spectrum sources HESS J1641-463, HESS J1741-302 and HESS J1826-130. *ArXiv e-prints*, August 2017.

W. D. Apel, J. C. Arteaga-Velázquez, K. Bekk, M. Bertaina, et al. KASCADE-Grande measurements of energy spectra for elemental groups of cosmic rays. *Astroparticle Physics*, 47:54–66, July 2013. doi: 10.1016/j.astropartphys.2013.06.004.

W. D. Apel, J. C. Arteaga-Velázquez, K. Bekk, M. Bertaina, et al. The KASCADE-Grande energy spectrum of cosmic rays and the role of hadronic interaction models. *Advances in Space Research*, 53:1456–1469, May 2014. doi: 10.1016/j.asr.2013.05.008.

S. Archambault, A. Archer, W. Benbow, R. Bird, et al. Gamma-Ray Observations of Tycho's Supernova Remnant with VERITAS and Fermi. ApJ, 836:23, February 2017. doi: 10.3847/1538-4357/836/1/23.

R. G. Arendt, E. Dwek, W. P. Blair, P. Ghavamian, U. Hwang, K. S. Long, R. Petre, J. Rho, and P. F. Winkler. Spitzer Observations of Dust Destruction in the Puppis A Supernova Remnant. ApJ, 725: 585–597, December 2010. doi: 10.1088/0004-637X/725/1/585.

I. Asaoka and B. Aschenbach. An X-ray study of IC443 and the discovery of a new supernova remnant by ROSAT. A&A, 284:573–582, April 1994.

B. Aschenbach. Discovery of a young nearby supernova remnant. Nature, 396:141–142, November 1998. doi: 10.1038/24103.

W. Atwood, A. Albert, L. Baldini, M. Tinivella, J. Bregeon, M. Pesce-Rollins, C. Sgrò, P. Bruel, E. Charles, A. Drlica-Wagner, A. Franckowiak, T. Jogler, L. Rochester, T. Usher, M. Wood, J. Cohen-Tanugi, and S. Zimmer for the Fermi-LAT Collaboration. Pass 8: Toward the Full Realization of the Fermi-LAT Scientific Potential. *ArXiv e-prints*, March 2013.

W. B. Atwood, A. A. Abdo, M. Ackermann, W. Althouse, B. Anderson, M. Axelsson, L. Baldini, J. Ballet, D. L. Band, G. Barbiellini, and et al. The Large Area Telescope on the Fermi Gamma-Ray Space Telescope Mission. ApJ, 697:1071–1102, June 2009. doi: 10.1088/0004-637X/697/2/1071.

W. Baade and F. Zwicky. Cosmic Rays from Super-novae. *Proceedings of the National Academy of Science*, 20:259–263, May 1934. doi: 10.1073/pnas.20.5.259.

C. Badenes, J. P. Hughes, E. Bravo, and N. Langer. Are the Models for Type Ia Supernova Progenitors Consistent with the Properties of Supernova Remnants? ApJ, 662:472–486, June 2007. doi: 10.1086/518022.

X. Barcons, D. Barret, A. Decourchelle, J. W. den Herder, A. C. Fabian, H. Matsumoto, D. Lumb, K. Nandra, L. Piro, R. K. Smith, and R. Willingale. Athena: ESA's X-ray observatory for the late 2020s. *Astronomische Nachrichten*, 338:153–158, March 2017. doi: 10.1002/asna.201713323.

B. Bartoli, P. Bernardini, X. J. Bi, Z. Cao, , and ARGO-YBJ Collaboration. Knee of the cosmic hydrogen and helium spectrum below 1 PeV measured by ARGO-YBJ and a Cherenkov telescope of LHAASO. Phys. Rev. D, 92(9):092005, November 2015. doi: 10.1103/PhysRevD.92.092005.

W. Becker, T. Prinz, P. F. Winkler, and R. Petre. The Proper Motion of the Central Compact Object RX J0822-4300 in the Supernova Remnant Puppis A. ApJ, 755:141, August 2012. doi: 10.1088/0004-637X/755/2/141.

A. R. Bell. The acceleration of cosmic rays in shock fronts. I. MNRAS, 182:147–156, January 1978. doi: 10.1093/mnras/182.2.147.

A. R. Bell, K. M. Schure, B. Reville, and G. Giacinti. Cosmic-ray acceleration and escape from supernova remnants. MNRAS, 431:415–429, May 2013. doi: 10.1093/mnras/stt179.

E. G. Berezhko, L. T. Ksenofontov, and H. J. Völk. Cosmic ray acceleration parameters from multi-wavelength observations. The case of SN 1006. A&A, 505:169–176, October 2009. doi: 10.1051/0004-6361/200911948.

E. G. Berezhko, L. T. Ksenofontov, and H. J. Völk. Expected Gamma-Ray Emission of Supernova Remnant SN 1987A. ApJ, 732:58, May 2011. doi: 10.1088/0004-637X/732/1/58.

E. G. Berezhko, L. T. Ksenofontov, and H. J. Völk. Re-examination of the Expected Gamma-Ray Emission of Supernova Remnant SN 1987A. ApJ, 810:63, September 2015. doi: 10.1088/0004-637X/810/1/63.

D. Berge, S. Funk, and J. Hinton. Background modelling in very-high-energy γ-ray astronomy. A&A, 466:1219–1229, May 2007. doi: 10.1051/0004-6361:20066674.

W. R. Binns, M. H. Israel, E. R. Christian, A. C. Cummings, G. A. de Nolfo, K. A. Lave, R. A. Leske, R. A. Mewaldt, E. C. Stone, T. T. von Rosenvinge, and M. E. Wiedenbeck. Observation of the ^{60}Fe nucleosynthesis-clock isotope in galactic cosmic rays. *Science*, 352:677–680, May 2016. doi: 10.1126/science.aad6004.

R. Bird and for the VERITAS Collaboration. VERITAS observations of the Cygnus Region. *ArXiv e-prints*, August 2017.

W. P. Blair, R. Sankrit, and J. C. Raymond. Hubble Space Telescope Imaging of the Primary Shock Front in the Cygnus Loop Supernova Remnant. AJ, 129:2268–2280, May 2005. doi: 10.1086/429381.

P. Blasi and E. Amato. Diffusive propagation of cosmic rays from supernova remnants in the Galaxy. II: anisotropy. *JCAP*, 1:011, January 2012. doi: 10.1088/1475-7516/2012/01/011.

J. Blümer, R. Engel, and J. R. Hörandel. Cosmic rays from the knee to the highest energies. *Progress in Particle and Nuclear Physics*, 63:293–338, October 2009. doi: 10.1016/j.ppnp.2009.05.002.

F. Bocchino, J. Vink, F. Favata, A. Maggio, and S. Sciortino. A BeppoSAX and ROSAT view of the RCW86 supernova remnant. A&A, 360:671–682, August 2000.

S. Broersen, A. Chiotellis, J. Vink, and A. Bamba. The many sides of RCW 86: a Type Ia supernova remnant evolving in its progenitor's wind bubble. MNRAS, 441:3040–3054, July 2014. doi: 10.1093/mnras/stu667.

C. L. Brogan, J. D. Gelfand, B. M. Gaensler, N. E. Kassim, and T. J. W. Lazio. Discovery of 35 New Supernova Remnants in the Inner Galaxy. ApJ, 639:L25–L29, March 2006. doi: 10.1086/501500.

R. Bühler and R. Blandford. The surprising Crab pulsar and its nebula: a review. *Reports on Progress in Physics*, 77(6):066901, June 2014. doi: 10.1088/0034-4885/77/6/066901.

M. G. Burton, C. Braiding, C. Glueck, P. Goldsmith, J. Hawkes, D. J. Hollenbach, C. Kulesa, C. L. Martin, J. L. Pineda, G. Rowell, R. Simon, A. A. Stark, J. Stutzki, N. J. H. Tothill, J. S. Urquhart, C. Walker, A. J. Walsh, and M. Wolfire. The Mopra Southern Galactic Plane CO Survey. *Publications of the Astronomical Society of Australia*, 30:e044, August 2013. doi: 10.1017/pasa.2013.22.

A. M. Bykov, D. C. Ellison, S. M. Osipov, G. G. Pavlov, and Y. A. Uvarov. X-ray Stripes in Tycho's Supernova Remnant: Synchrotron Footprints of a Nonlinear Cosmic-ray-driven Instability. ApJ, 735:L40, July 2011. doi: 10.1088/2041-8205/735/2/L40.

M. Cardillo, E. Amato, and P. Blasi. On the cosmic ray spectrum from type II supernovae expanding in their red giant presupernova wind. *Astroparticle Physics*, 69:1–10, September 2015. doi: 10.1016/j.astropartphys.2015.03.002.

A. K. Carlton, K. J. Borkowski, S. P. Reynolds, U. Hwang, R. Petre, D. A. Green, K. Krishnamurthy, and R. Willett. Expansion of the Youngest Galactic Supernova Remnant G1.9+0.3. ApJ, 737:L22, August 2011. doi: 10.1088/2041-8205/737/1/L22.

G. Cassam-Chenaï, A. Decourchelle, J. Ballet, J.-L. Sauvageot, G. Dubner, and E. Giacani. XMM-Newton observations of the supernova remnant RX J1713.7-3946 and its central source. A&A, 427:199–216, November 2004. doi: 10.1051/0004-6361:20041154.

G. Cassam-Chenaï, J. P. Hughes, J. Ballet, and A. Decourchelle. The Blast Wave of Tycho's Supernova Remnant. ApJ, 665:315–340, August 2007. doi: 10.1086/518782.

D. Castro and P. Slane. Fermi Large Area Telescope Observations of Supernova Remnants Interacting with Molecular Clouds. ApJ, 717:372–378, July 2010. doi: 10.1088/0004-637X/717/1/372.

B. Cerutti, G. R. Werner, D. A. Uzdensky, and M. C. Begelman. Gamma-ray flares in the Crab Nebula: A case of relativistic reconnection ?). *Physics of Plasmas*, 21(5):056501, May 2014. doi: 10.1063/1.4872024.

K.-S. Cheng, D. O. Chernyshov, V. A. Dogiel, C.-M. Ko, and W.-H. Ip. Origin of the Fermi Bubble. ApJ, 731:L17, April 2011. doi: 10.1088/2041-8205/731/1/L17.

T. Cherenkov Telescope Array Consortium, :, B. S. Acharya, I. Agudo, I. A. Samarai, R. Alfaro, J. Alfaro, C. Alispach, R. Alves Batista, J.-P. Amans, and et al. Science with the Cherenkov Telescope Array. *ArXiv e-prints*, September 2017.

R. A. Chevalier and V. V. Dwarkadas. The Presupernova H II Region around SN 1987A. ApJ, 452: L45, October 1995. doi: 10.1086/309714.

A. Chiotellis, K. M. Schure, and J. Vink. The imprint of a symbiotic binary progenitor on the properties of Kepler's supernova remnant. *A&A*, 537:A139, January 2012. doi: 10.1051/0004-6361/201014754.

D. F. Cioffi, C. F. McKee, and E. Bertschinger. Dynamics of radiative supernova remnants. *ApJ*, 334: 252–265, November 1988. doi: 10.1086/166834.

D. H. Clark and J. L. Caswell. A study of galactic supernova remnants, based on Molonglo-Parkes observational data. MNRAS, 174:267–305, February 1976. doi: 10.1093/mnras/174.2.267.

M. J. Claussen, D. A. Frail, W. M. Goss, and R. A. Gaume. Polarization Observations of 1720 MHz OH Masers toward the Three Supernova Remnants W28, W44, and IC 443. ApJ, 489:143–159, November 1997. doi: 10.1086/304784.

B. Condon, M. Lemoine-Goumard, F. Acero, and H. Katagiri. Detection of Two TeV Shell-type Remnants at GeV Energies with FERMI-LAT: HESS J1731-347 and SN 1006. ApJ, 851:100, December 2017. doi: 10.3847/1538-4357/aa9be8.

Benjamin Condon. *Observations de vestiges de supernovae en coquille avec le Fermi Large Area Telescope*. PhD thesis, University of Bordeaux, 2017.

P. Cristofari, S. Gabici, T. B. Humensky, M. Santander, R. Terrier, E. Parizot, and S. Casanova. Supernova remnants in the very-high-energy gamma-ray domain: the role of the Cherenkov telescope array. MNRAS, 471:201–209, October 2017. doi: 10.1093/mnras/stx1574.

R. M. Crocker and F. Aharonian. Fermi Bubbles: Giant, Multibillion-Year-Old Reservoirs of Galactic Center Cosmic Rays. *Physical Review Letters*, 106(10):101102, March 2011. doi: 10.1103/PhysRevLett.106.101102.

R. M. Crocker, D. I. Jones, F. Aharonian, C. J. Law, F. Melia, and J. Ott. γ-rays and the far-infrared-radio continuum correlation reveal a powerful Galactic Centre wind. MNRAS, 411:L11–L15, February 2011. doi: 10.1111/j.1745-3933.2010.00983.x.

Y. Cui, G. Pühlhofer, and A. Santangelo. A young supernova remnant illuminating nearby molecular clouds with cosmic rays. A&A, 591:A68, June 2016. doi: 10.1051/0004-6361/201628505.

T. M. Dame, B. G. Elmegreen, R. S. Cohen, and P. Thaddeus. The largest molecular cloud complexes in the first galactic quadrant. ApJ, 305:892–908, June 1986. doi: 10.1086/164304.

A. De Angelis, V. Tatischeff, I. A. Grenier, J. McEnery, M. Mallamaci, M. Tavani, U. Oberlack, L. Hanlon, R. Walter, A. Argan, and et al. Science with e-ASTROGAM (A space mission for MeV-GeV gamma-ray astrophysics). *ArXiv e-prints*, November 2017.

A. Y. De Horta, M. D. Filipovic, E. J. Crawford, F. H. Stootman, T. G. Pannuti, L. M. Bozzetto, J. D. Collier, E. R. Sommer, and A. R. Kosakowski. Radio-Continuum Emission from the Young Galactic Supernova Remnant G1.9+0.3. *Serbian Astronomical Journal*, 189:41–51, December 2014. doi: 10.2298/SAJ140605001H.

O. C. de Jager and A. Djannati-Ataï. Implications of HESS Observations of Pulsar Wind Nebulae. In W. Becker, editor, *Astrophysics and Space Science Library*, volume 357 of *Astrophysics and Space Science Library*, page 451, 2009. doi: 10.1007/978-3-540-76965-1_17.

M. de Naurois and L. Rolland. A high performance likelihood reconstruction of γ-rays for imaging atmospheric Cherenkov telescopes. *Astroparticle Physics*, 32:231–252, December 2009. doi: 10.1016/j.astropartphys.2009.09.001.

G. Di Sciascio and LHAASO Collaboration. The LHAASO experiment: From Gamma-Ray Astronomy to Cosmic Rays. *Nuclear and Particle Physics Proceedings*, 279:166–173, October 2016. doi: 10.1016/j.nuclphysbps.2016.10.024.

W. Domainko and S. Ohm. Exploring the nature of the unidentified very-high-energy gamma-ray source HESS J1507-622. A&A, 545:A94, September 2012. doi: 10.1051/0004-6361/201118472.

V. Doroshenko, G. Pühlhofer, A. Bamba, F. Acero, W. W. Tian, D. Klochkov, and A. Santangelo. XMM-Newton observations of the non-thermal supernova remnant HESS J1731-347 (G353.6-0.7). A&A, 608:A23, December 2017. doi: 10.1051/0004-6361/201730983.

G. Dubner, E. Giacani, E. Reynoso, and S. Parón. The molecular clouds in the environs of the supernova remnants G349.7+0.2 and G18.8+0.3. A&A, 426:201–212, October 2004. doi: 10.1051/0004-6361:20041327.

G. Dubner, N. Loiseau, P. Rodríguez-Pascual, M. J. S. Smith, E. Giacani, and G. Castelletti. The most complete and detailed X-ray view of the SNR Puppis A. A&A, 555:A9, July 2013. doi: 10.1051/0004-6361/201321401.

G. M. Dubner, E. B. Giacani, W. M. Goss, A. J. Green, and L.-Å. Nyman. The neutral gas environment of the young supernova remnant SN 1006 (G327.6+14.6). A&A, 387:1047–1056, June 2002. doi: 10.1051/0004-6361:20020365.

V. V. Dwarkadas and R. A. Chevalier. Interaction of Type IA Supernovae with Their Surroundings. *ApJ*, 497:807–823, April 1998. doi: 10.1086/305478.

P. Eger, W. F. Domainko, and J. Hahn. Exploring the potential X-ray counterpart of the puzzling TeV gamma-ray source HESS J1507-622 with new Suzaku observations. MNRAS, 447:3564–3575, March 2015. doi: 10.1093/mnras/stu2746.

D. C. Ellison, E. G. Berezhko, and M. G. Baring. Nonlinear Shock Acceleration and Photon Emission in Supernova Remnants. ApJ, 540:292–307, September 2000. doi: 10.1086/309324.

K. A. Eriksen, J. P. Hughes, C. Badenes, R. Fesen, P. Ghavamian, D. Moffett, P. P. Plucinksy, C. E. Rakowski, E. M. Reynoso, and P. Slane. Evidence for Particle Acceleration to the Knee of the Cosmic Ray Spectrum in Tycho's Supernova Remnant. ApJ, 728:L28, February 2011. doi: 10.1088/2041-8205/728/2/L28.

S. Federici, M. Pohl, I. Telezhinsky, A. Wilhelm, and V. V. Dwarkadas. Analysis of GeV-band γ-ray emission from supernova remnant RX J1713.7-3946. *A&A*, 577:A12, May 2015. doi: 10.1051/0004-6361/201424947.

E. Fermi. On the Origin of the Cosmic Radiation. *Physical Review*, 75:1169–1174, April 1949. doi: 10.1103/PhysRev.75.1169.

G. Ferrand and A. Marcowith. On the shape of the spectrum of cosmic rays accelerated inside superbubbles. A&A, 510:A101, February 2010. doi: 10.1051/0004-6361/200913520.

R. A. Fesen, R. Kremer, D. Patnaude, and D. Milisavljevic. The SN 393-SNR RX J1713.7-3946 (G347.3-0.5) Connection. AJ, 143:27, February 2012. doi: 10.1088/0004-6256/143/2/27.

D. P. Finkbeiner. A Full-Sky Hα Template for Microwave Foreground Prediction. ApJS, 146:407–415, June 2003. doi: 10.1086/374411.

D. A. Frail, W. M. Goss, and V. I. Slysh. Shock-excited maser emission from the supernova remnant W28. ApJ, 424:L111–L113, April 1994. doi: 10.1086/187287.

Y. Fujita, F. Takahara, Y. Ohira, and K. Iwasaki. Alfvén wave amplification and self-containment of cosmic rays escaping from a supernova remnant. MNRAS, 415:3434–3438, August 2011. doi: 10.1111/j.1365-2966.2011.18980.x.

T. Fukuda, S. Yoshiike, H. Sano, K. Torii, H. Yamamoto, F. Acero, and Y. Fukui. Interstellar Protons in the TeV γ-Ray SNR HESS J1731-347: Possible Evidence for the Coexistence of Hadronic and Leptonic γ-Rays. ApJ, 788:94, June 2014. doi: 10.1088/0004-637X/788/1/94.

S. Gabici. Cosmic ray escape from supernova remnants . Mem. Soc. Astron. Italiana, 82:760, 2011.

S. Gabici and F. A. Aharonian. Searching for Galactic Cosmic-Ray Pevatrons with Multi-TeV Gamma Rays and Neutrinos. ApJ, 665:L131–L134, August 2007. doi: 10.1086/521047.

S. Gabici and F. A. Aharonian. Hadronic gamma-rays from RX J1713.7-3946? MNRAS, 445: L70–L73, November 2014. doi: 10.1093/mnrasl/slu132.

S. Gabici, F. A. Aharonian, and P. Blasi. Gamma rays from molecular clouds. Ap&SS, 309:365–371, June 2007. doi: 10.1007/s10509-007-9427-6.

S. Gabici, S. Casanova, F. A. Aharonian, and G. Rowell. Constraints on the cosmic ray diffusion coefficient in the W28 region from gamma-ray observations. In S. Boissier, M. Heydari-Malayeri, R. Samadi, and D. Valls-Gabaud, editors, *SF2A-2010: Proceedings of the Annual meeting of the French Society of Astronomy and Astrophysics*, page 313, December 2010.

B. M. Gaensler and P. O. Slane. The Evolution and Structure of Pulsar Wind Nebulae. ARA&A, 44: 17–47, September 2006. doi: 10.1146/annurev.astro.44.051905.092528.

D. Gaggero, D. Grasso, A. Marinelli, M. Taoso, and A. Urbano. Diffuse Cosmic Rays Shining in the Galactic Center: A Novel Interpretation of H.E.S.S. and Fermi-LAT γ -Ray Data. *Physical Review Letters*, 119(3):031101, July 2017. doi: 10.1103/PhysRevLett.119.031101.

T. K. Gaisser, T. Stanev, and S. Tilav. Cosmic ray energy spectrum from measurements of air showers. *Frontiers of Physics*, 8:748–758, December 2013. doi: 10.1007/s11467-013-0319-7.

Y. Gallant, E. Amato, and J. Lavalle. Ultra-High-Energy gamma-ray Halos around Short-Lived Galactic PeVatrons. Presented at the Texas Symposium, Dallas, United States, 2013.

X. Y. Gao and J. L. Han. Discovery of a new supernova remnant G150.3+4.5. A&A, 567:A59, July 2014. doi: 10.1051/0004-6361/201424128.

J. D. Gelfand, P. O. Slane, and W. Zhang. A Dynamical Model for the Evolution of a Pulsar Wind Nebula Inside a Nonradiative Supernova Remnant. ApJ, 703:2051–2067, October 2009. doi: 10.1088/0004-637X/703/2/2051.

F. Giordano, M. Naumann-Godo, J. Ballet, K. Bechtol, S. Funk, J. Lande, M. N. Mazziotta, S. Rainò, T. Tanaka, O. Tibolla, and Y. Uchiyama. Fermi Large Area Telescope Detection of the Young Supernova Remnant Tycho. ApJ, 744:L2, January 2012. doi: 10.1088/2041-8205/744/1/L2.

A. Giuliani, M. Cardillo, M. Tavani, Y. Fukui, S. Yoshiike, K. Torii, G. Dubner, G. Castelletti, G. Barbiellini, A. Bulgarelli, P. Caraveo, E. Costa, P. W. Cattaneo, A. Chen, T. Contessi, E. Del Monte, I. Donnarumma, Y. Evangelista, M. Feroci, F. Gianotti, F. Lazzarotto, F. Lucarelli, F. Longo, M. Marisaldi, S. Mereghetti, L. Pacciani, A. Pellizzoni, G. Piano, P. Picozza, C. Pittori, G. Pucella, M. Rapisarda, A. Rappoldi, S. Sabatini, P. Soffitta, E. Striani, M. Trifoglio, A. Trois, S. Vercellone, F. Verrecchia, V. Vittorini, S. Colafrancesco, P. Giommi, and G. Bignami. Neutral Pion Emission from Accelerated Protons in the Supernova Remnant W44. ApJ, 742:L30, December 2011. doi: 10.1088/2041-8205/742/2/L30.

M. A. K. Glasmacher, M. A. Catanese, M. C. Chantell, C. E. Covault, J. W. Cronin, B. E. Fick, L. F. Fortson, J. W. Fowler, K. D. Green, D. B. Kieda, J. Matthews, B. J. Newport, D. F. Nitz, R. A. Ong, S. Oser, D. Sinclair, and J. C. van der Velde. The cosmic ray composition between 10^{14} and 10^{16} eV. *Astroparticle Physics*, 12:1–17, 1999. doi: 10.1016/S0927-6505(99)00076-6.

D. Gottschall, M. Capasso, C. Deil, A. Djannati-Atai, A. Donath, P. Eger, V. Marandon, N. Maxted, G. Pühlhofer, M. Renaud, M. Sasaki, R. Terrier, J. Vink, and H.E.S.S. Collaboration. Discovery of new TeV supernova remnant shells in the Galactic plane with H.E.S.S. In *6th International Symposium on High Energy Gamma-Ray Astronomy*, volume 1792 of *American Institute of Physics Conference Series*, page 040030, January 2017. doi: 10.1063/1.4968934.

D. A. Green. VizieR Online Data Catalog: A Catalogue of Galactic Supernova Remnants (Green 2017). *VizieR Online Data Catalog*, 7278, June 2017.

D. A. Green and S. F. Gull. Two new young galactic supernova remnants. Nature, 312:527–529, December 1984. doi: 10.1038/312527a0.

D. A. Green, S. P. Reynolds, K. J. Borkowski, U. Hwang, I. Harrus, and R. Petre. The radio expansion and brightening of the very young supernova remnant G1.9+0.3. MNRAS, 387:L54–L58, June 2008. doi: 10.1111/j.1745-3933.2008.00484.x.

I. A. Grenier and A. K. Harding. Gamma-ray pulsars: A gold mine. *Comptes Rendus Physique*, 16: 641–660, August 2015. doi: 10.1016/j.crhy.2015.08.013.

M.-H. Grondin, S. Funk, M. Lemoine-Goumard, A. Van Etten, J. A. Hinton, F. Camilo, I. Cognard, C. M. Espinoza, P. C. C. Freire, J. E. Grove, L. Guillemot, S. Johnston, M. Kramer, J. Lande, P. Michelson, A. Possenti, R. W. Romani, J. L. Skilton, G. Theureau, and P. Weltevrede. Detection of the Pulsar Wind Nebula HESS J1825-137 with the Fermi Large Area Telescope. ApJ, 738:42, September 2011. doi: 10.1088/0004-637X/738/1/42.

F. Guo and W. G. Mathews. The Fermi Bubbles. I. Possible Evidence for Recent AGN Jet Activity in the Galaxy. ApJ, 756:181, September 2012. doi: 10.1088/0004-637X/756/2/181.

X.-L. Guo, Y.-L. Xin, N.-H. Liao, Q. Yuan, W.-H. Gao, and Y.-Z. Fan. Detection of GeV Gamma-Ray Emission in the Direction of HESS J1731-347 with Fermi-LAT. ApJ, 853:2, January 2018. doi: 10.3847/1538-4357/aaa3f8.

R. Güsten, L. Å. Nyman, P. Schilke, K. Menten, C. Cesarsky, and R. Booth. The Atacama Pathfinder EXperiment (APEX) - a new submillimeter facility for southern skies -. A&A, 454:L13–L16, August 2006. doi: 10.1051/0004-6361:20065420.

H. E. S. S. Collaboration, A. Abramowski, F. Aharonian, F. Ait Benkhali, A. G. Akhperjanian, E. O. Angüner, M. Backes, S. Balenderan, A. Balzer, A. Barnacka, and et al. H.E.S.S. detection of TeV emission from the interaction region between the supernova remnant G349.7+0.2 and a molecular cloud. A&A, 574:A100, January 2015a. doi: 10.1051/0004-6361/201425070.

H. E. S. S. Collaboration, A. Abramowski, F. Aharonian, F. Ait Benkhali, A. G. Akhperjanian, E. O. Angüner, M. Backes, S. Balenderan, A. Balzer, A. Barnacka, and et al. H.E.S.S. reveals a lack of TeV emission from the supernova remnant Puppis A. *A&A*, 575:A81, March 2015b. doi: 10.1051/0004-6361/201424805.

H. E. S. S. Collaboration, :, H. Abdalla, H. Abdalla, A. Abramowski, F. Aharonian, F. Ait Benkhali, A. G. Akhperjanian, T. Andersson, E. O. Angüner, and et al. H.E.S.S. observations of RX J1713.7-3946 with improved angular and spectral resolution; evidence for gamma-ray emission extending beyond the X-ray emitting shell. *ArXiv e-prints*, September 2016a.

H. E. S. S. Collaboration, H. Abdalla, A. Abramowski, F. Aharonian, F. Ait Benkhali, A. G. Akhperjanian, T. Andersson, E. O. Angüner, M. Arakawa, M. Arrieta, and et al. Deeper H.E.S.S. Observations of Vela Junior (RX J0852.0-4622): Morphology Studies and Resolved Spectroscopy. *ArXiv e-prints*, November 2016b.

H. E. S. S. Collaboration, H. Abdalla, A. Abramowski, F. Aharonian, F. Ait Benkhali, A. G. Akhperjanian, T. Andersson, E. O. Angüner, M. Arrieta, P. Aubert, and et al. The supernova remnant W49B as seen with H.E.S.S. and Fermi-LAT. *ArXiv e-prints*, September 2016c.

H. E. S. S. Collaboration, A. Abramowski, F. Aharonian, F. Ait Benkhali, A. G. Akhperjanian, E. O. Angüner, M. Backes, A. Balzer, Y. Becherini, J. Becker Tjus, and et al. Detailed spectral and morphological analysis of the shell type SNR RCW 86. *ArXiv e-prints*, January 2016d.

H. E. S. S. Collaboration, :, H. Abdalla, A. Abramowski, F. Aharonian, F. Ait Benkhali, A. G. Akhperjanian, T. Andersson, E. O. Angüner, M. Arrieta, and et al. The population of TeV pulsar wind nebulae in the H.E.S.S. Galactic Plane Survey. *ArXiv e-prints*, February 2017a.

H. E. S. S. Collaboration, :, H. Abdalla, A. Abramowski, F. Aharonian, F. Ait Benkhali, A. G. Akhperjaniany, T. Andersson, E. O. Angüner, M. Arakawa, and et al. Contributions of the High Energy Stereoscopic System (H.E.S.S.) to the 35th International Cosmic Ray Conference (ICRC), Busan, Korea. *ArXiv e-prints*, September 2017b.

H. E. S. S. Collaboration, :, H. Abdalla, A. Abramowski, F. Aharonian, F. Ait Benkhali, A. G. Akhperjanian, T. Andersson, E. O. Angüner, M. Arakawa, and et al. A search for new supernova remnant shells in the Galactic plane with H.E.S.S. *ArXiv e-prints*, January 2018.

D. Hadasch, D. F. Torres, T. Tanaka, R. H. D. Corbet, A. B. Hill, R. Dubois, G. Dubus, T. Glanzman, S. Corbel, J. Li, Y. P. Chen, S. Zhang, G. A. Caliandro, M. Kerr, J. L. Richards, W. Max-Moerbeck, A. Readhead, and G. Pooley. Long-term Monitoring of the High-energy γ-Ray Emission from LS I +61°303 and LS 5039. ApJ, 749:54, April 2012. doi: 10.1088/0004-637X/749/1/54.

Y. Hanabata, H. Katagiri, J. W. Hewitt, J. Ballet, Y. Fukazawa, Y. Fukui, T. Hayakawa, M. Lemoine-Goumard, G. Pedaletti, A. W. Strong, D. F. Torres, and R. Yamazaki. Detailed Investigation of the Gamma-Ray Emission in the Vicinity of SNR W28 with FERMI-LAT. ApJ, 786:145, May 2014. doi: 10.1088/0004-637X/786/2/145.

T. Handa, Y. Sofue, N. Nakai, H. Hirabayashi, and M. Inoue. A radio continuum survey of the Galactic plane at 10 GHz. PASJ, 39:709–753, 1987.

R. C. Hartman, D. L. Bertsch, S. D. Bloom, A. W. Chen, P. Deines-Jones, J. A. Esposito, C. E. Fichtel, D. P. Friedlander, S. D. Hunter, L. M. McDonald, P. Sreekumar, D. J. Thompson, B. B. Jones, Y. C. Lin, P. F. Michelson, P. L. Nolan, W. F. Tompkins, G. Kanbach, H. A. Mayer-Hasselwander, A. Mücke, M. Pohl, O. Reimer, D. A. Kniffen, E. J. Schneid, C. von Montigny, R. Mukherjee, and B. L. Dingus. The Third EGRET Catalog of High-Energy Gamma-Ray Sources. ApJS, 123: 79–202, July 1999. doi: 10.1086/313231.

E. A. Helder, J. Vink, C. G. Bassa, A. Bamba, J. A. M. Bleeker, S. Funk, P. Ghavamian, K. J. van der Heyden, F. Verbunt, and R. Yamazaki. Measuring the Cosmic-Ray Acceleration Efficiency of a Supernova Remnant. *Science*, 325:719, August 2009. doi: 10.1126/science.1173383.

H.E.S.S. Collaboration, A. Abramowski, F. Acero, F. Aharonian, A. G. Akhperjanian, et al. A new SNR with TeV shell-type morphology: HESS J1731-347. A&A, 531:A81, July 2011a. doi: 10.1051/0004-6361/201016425.

H.E.S.S. Collaboration, A. Abramowski, F. Acero, F. Aharonian, et al. Discovery of the source HESS J1356-645 associated with the young and energetic PSR J1357-6429. A&A, 533:A103, September 2011b. doi: 10.1051/0004-6361/201117445.

H.E.S.S. Collaboration, F. Acero, F. Aharonian, A. G. Akhperjanian, et al. Discovery and follow-up studies of the extended, off-plane, VHE gamma-ray source HESS J1507-622. A&A, 525:A45, January 2011c. doi: 10.1051/0004-6361/201015187.

H.E.S.S. Collaboration, A. Abramowski, F. Acero, et al. Identification of HESS J1303-631 as a pulsar wind nebula through γ-ray, X-ray, and radio observations. A&A, 548:A46, December 2012. doi: 10.1051/0004-6361/201219814.

H.E.S.S. Collaboration, A. Abramowski, F. Aharonian, F. A. Benkhali, A. G. Akhperjanian, E. Angüner, G. Anton, S. Balenderan, A. Balzer, A. Barnacka, and et al. TeV γ-ray observations of the young synchrotron-dominated SNRs G1.9+0.3 and G330.2+1.0 with H.E.S.S. MNRAS, 441: 790–799, June 2014a. doi: 10.1093/mnras/stu459.

H.E.S.S. Collaboration, A. Abramowski, F. Aharonian, F. A. Benkhali, A. G. Akhperjanian, E. Angüner, G. Anton, S. Balenderan, A. Balzer, A. Barnacka, and et al. TeV γ-ray observations of the young synchrotron-dominated SNRs G1.9+0.3 and G330.2+1.0 with H.E.S.S. *MNRAS*, 441: 790–799, June 2014b. doi: 10.1093/mnras/stu459.

H.E.S.S. Collaboration, A. Abramowski, F. Aharonian, F. Ait Benkhali, et al. The exceptionally powerful TeV γ-ray emitters in the Large Magellanic Cloud. *Science*, 347:406–412, January 2015. doi: 10.1126/science.1261313.

HESS Collaboration, A. Abramowski, F. Aharonian, F. A. Benkhali, A. G. Akhperjanian, E. O. Angüner, M. Backes, A. Balzer, Y. Becherini, J. B. Tjus, and et al. Acceleration of petaelectronvolt protons in the Galactic Centre. Nature, 531:476–479, March 2016. doi: 10.1038/nature17147.

J. W. Hewitt, J. Rho, M. Andersen, and W. T. Reach. Spitzer Observations of Molecular Hydrogen in Interacting Supernova Remnants. ApJ, 694:1266–1280, April 2009. doi: 10.1088/0004-637X/694/2/1266.

J. W. Hewitt, M.-H. Grondin, M. Lemoine-Goumard, T. Reposeur, J. Ballet, and T. Tanaka. Fermi-LAT and WMAP Observations of the Puppis A Supernova Remnant. *ApJ*, 759:89, November 2012. doi: 10.1088/0004-637X/759/2/89.

J. Hinton. Gamma-ray Astronomy. *ArXiv e-prints*, December 2007.

J. P. Hughes, C. E. Rakowski, and A. Decourchelle. Electron Heating and Cosmic Rays at a Supernova Shock from Chandra X-Ray Observations of 1E 0102.2-7219. ApJ, 543:L61–L65, November 2000. doi: 10.1086/312945.

U. Hwang and J. M. Laming. A Chandra X-Ray Survey of Ejecta in the Cassiopeia A Supernova Remnant. ApJ, 746:130, February 2012. doi: 10.1088/0004-637X/746/2/130.

IceCube Collaboration. Evidence for High-Energy Extraterrestrial Neutrinos at the IceCube Detector. *Science*, 342:1242856, November 2013. doi: 10.1126/science.1242856.

R. Indebetouw, M. Matsuura, E. Dwek, et al. Dust Production and Particle Acceleration in Supernova 1987A Revealed with ALMA. *ApJL*, 782:L2, February 2014. doi: 10.1088/2041-8205/782/1/L2.

M. S. Jackson, S. Safi-Harb, R. Kothes, and T. Foster. XMM-Newton, Chandra, and CGPS observations of the Supernova Remnants G85.4+0.7 and G85.9-0.6. ApJ, 674:936-953, February 2008. doi: 10.1086/524098.

T. Jogler and S. Funk. Revealing W51C as a Cosmic Ray Source Using Fermi-LAT Data. ApJ, 816: 100, January 2016. doi: 10.3847/0004-637X/816/2/100.

L. Jouvin, A. Lemière, and R. Terrier. Does the SN rate explain the very high energy cosmic rays in the central 200 pc of our Galaxy? MNRAS, 467:4622–4630, June 2017. doi: 10.1093/mnras/stx361.

H. Katagiri, L. Tibaldo, J. Ballet, F. Giordano, I. A. Grenier, T. A. Porter, M. Roth, O. Tibolla, Y. Uchiyama, and R. Yamazaki. Fermi Large Area Telescope Observations of the Cygnus Loop Supernova Remnant. ApJ, 741:44, November 2011. doi: 10.1088/0004-637X/741/1/44.

S. Katsuda, H. Tsunemi, and K. Mori. The Slow X-Ray Expansion of the Northwestern Rim of the Supernova Remnant RX J0852.0-4622. ApJ, 678:L35, May 2008. doi: 10.1086/588499.

S. Katsuda, R. Petre, K. S. Long, S. P. Reynolds, P. F. Winkler, K. Mori, and H. Tsunemi. The First X-Ray Proper-Motion Measurements of the Forward Shock in the Northeastern Limb of SN 1006. ApJ, 692:L105–L108, February 2009. doi: 10.1088/0004-637X/692/2/L105.

J. Katsuta, Y. Uchiyama, T. Tanaka, H. Tajima, K. Bechtol, S. Funk, J. Lande, J. Ballet, Y. Hanabata, M. Lemoine-Goumard, and T. Takahashi. Fermi Large Area Telescope Observation of Supernova Remnant S147. ApJ, 752:135, June 2012. doi: 10.1088/0004-637X/752/2/135.

J. Katsuta, Y. Uchiyama, and S. Funk. Extended Gamma-Ray Emission from the G25.0+0.0 Region: A Star-forming Region Powered by the Newly Found OB Association? ApJ, 839:129, April 2017. doi: 10.3847/1538-4357/aa6aa3.

J. W. Keohane, W. T. Reach, J. Rho, and T. H. Jarrett. A Near-Infrared and X-Ray Study of W49 B: A Wind Cavity Explosion. ApJ, 654:938–944, January 2007. doi: 10.1086/509311.

O. Krause, M. Tanaka, T. Usuda, T. Hattori, M. Goto, S. Birkmann, and K. Nomoto. Tycho Brahe's 1572 supernova as a standard typeIa as revealed by its light-echo spectrum. Nature, 456:617–619, December 2008. doi: 10.1038/nature07608.

L. T. Ksenofontov, H. J. Völk, and E. G. Berezhko. Nonthermal Properties of Supernova Remnant G1.9+0.3. ApJ, 714:1187–1193, May 2010. doi: 10.1088/0004-637X/714/2/1187.

W. H.-M. Ku, S. M. Kahn, R. Pisarski, and K. S. Long. Einstein Observations of the Cygnus Loop. ApJ, 278:615–618, March 1984. doi: 10.1086/161829.

J. Lande, M. Ackermann, A. Allafort, J. Ballet, K. Bechtol, T. H. Burnett, J. Cohen-Tanugi, A. Drlica-Wagner, S. Funk, F. Giordano, M.-H. Grondin, M. Kerr, and M. Lemoine-Goumard. Search for Spatially Extended Fermi Large Area Telescope Sources Using Two Years of Data. ApJ, 756:5, September 2012. doi: 10.1088/0004-637X/756/1/5.

J. S. Lazendic, P. O. Slane, J. P. Hughes, Y. Chen, and T. M. Dame. Chandra Detection of Ejecta in the Small-Diameter Supernova Remnant G349.7+0.2. ApJ, 618:733–743, January 2005. doi: 10.1086/426114.

J. S. Lazendic, M. Wardle, J. B. Whiteoak, M. G. Burton, and A. J. Green. Multiwavelength observations of the supernova remnant G349.7+0.2 interacting with a molecular cloud. MNRAS, 409: 371–388, November 2010. doi: 10.1111/j.1365-2966.2010.17315.x.

D. A. Leahy. 1420 and 408 MHz Continuum Observations of the IC 443/G189.6+3.3 Region. AJ, 127:2277–2283, April 2004. doi: 10.1086/382241.

M. Lemoine-Goumard, M. Renaud, J. Vink, G. E. Allen, A. Bamba, F. Giordano, and Y. Uchiyama. Constraints on cosmic-ray efficiency in the supernova remnant RCW 86 using multi-wavelength observations. A&A, 545:A28, September 2012. doi: 10.1051/0004-6361/201219896.

M. Lemoine-Goumard, M.-H. Grondin, F. Acero, J. Ballet, H. Laffon, and T. Reposeur. HESS J1640-465 and HESS J1641-463: Two Intriguing TeV Sources in Light of New Fermi-LAT Observations. ApJ, 794:L16, October 2014. doi: 10.1088/2041-8205/794/1/L16.

N. A. Levenson, J. R. Graham, L. D. Keller, and M. J. Richter. Panoramic Views of the Cygnus Loop. ApJS, 118:541–561, October 1998. doi: 10.1086/313136.

Y. Liu, Z. Cao, S. Chen, Y. Chen, S. Cui, H. He, X. Huang, X. Ma, Q. Yuan, X. Zhang, and LHAASO Collaboration. Expectation on Observation of Supernova Remnants with the LHAASO Project. ApJ, 826:63, July 2016. doi: 10.3847/0004-637X/826/1/63.

K. S. Long and W. P. Blair. The identification of Balmer-dominated filaments in RCW 86. ApJ, 358: L13–L16, July 1990. doi: 10.1086/185768.

T. A. Lozinskaya. Interferometry of the supernova remnant W28. Soviet Ast., 17:603, April 1974.

M. A. Malkov, P. H. Diamond, and R. Z. Sagdeev. On the mechanism for breaks in the cosmic ray spectruma). *Physics of Plasmas*, 19(8):082901, August 2012. doi: 10.1063/1.4737584.

K. Malone and HAWC Collaboration. The gamma-ray sky above 50 TeV with the HAWC Observatory. In *APS April Meeting Abstracts*, page X4.008, January 2017.

S. Mattila, P. Lundqvist, P. Gröningsson, P. Meikle, R. Stathakis, C. Fransson, and R. Cannon. Abundances and Density Structure of the Inner Circumstellar Ring Around SN 1987A. *ApJ*, 717:1140–1156, July 2010. doi: 10.1088/0004-637X/717/2/1140.

N. Maxted, M. Burton, C. Braiding, G. Rowell, H. Sano, F. Voisin, M. Capasso, G. Pühlhofer, and Y. Fukui. Probing the local environment of the supernova remnant HESS J1731-347 with CO and CS observations. MNRAS, 474:662–676, February 2018. doi: 10.1093/mnras/stx2727.

M. Mayer, J. Brucker, M. Holler, I. Jung, K. Valerius, and C. Stegmann. Unidentified VHE γ-ray sources and evolved pulsar wind nebulae - A possible connection? In F. A. Aharonian, W. Hofmann, and F. M. Rieger, editors, *American Institute of Physics Conference Series*, volume 1505 of *American Institute of Physics Conference Series*, pages 341–344, December 2012. doi: 10.1063/1.4772267.

J. E. McEnery. All-Sky Medium Energy Gamma-ray Observatory (AMEGO) - A discovery mission for the MeV gamma-ray band. In *AAS/High Energy Astrophysics Division #16*, volume 16 of *AAS/High Energy Astrophysics Division*, page 103.13, August 2017.

A. Merloni, P. Predehl, W. Becker, H. Böhringer, et al. eROSITA Science Book: Mapping the Structure of the Energetic Universe. *ArXiv e-prints*, September 2012.

M. Miceli, F. Bocchino, A. Decourchelle, G. Maurin, J. Vink, S. Orlando, F. Reale, and S. Broersen. XMM-Newton evidence of shocked ISM in SN 1006: indications of hadronic acceleration. A&A, 546:A66, October 2012. doi: 10.1051/0004-6361/201219766.

M. Miceli, F. Acero, G. Dubner, A. Decourchelle, S. Orlando, and F. Bocchino. Shock-Cloud Interaction and Particle Acceleration in the Southwestern Limb of SN 1006. ApJ, 782:L33, February 2014. doi: 10.1088/2041-8205/782/2/L33.

M. Miceli, S. Orlando, V. Pereira, F. Acero, S. Katsuda, A. Decourchelle, F. P. Winkler, R. Bonito, F. Reale, G. Peres, J. Li, and G. Dubner. Modeling the shock-cloud interaction in SN 1006: Unveiling the origin of nonthermal X-ray and γ-ray emission. A&A, 593:A26, August 2016. doi: 10.1051/0004-6361/201628725.

E. Miyata, H. Tsunemi, R. Pisarski, and S. E. Kissel. The plasma structure of the north-east rim of the Cygnus Loop as observed with ASCA. PASJ, 46:L101–L104, June 1994.

A. Mizuno and Y. Fukui. Physical properties of molecular clouds as revealed by NANTEN CO survey: from the galactic center to the galactic warp. In D. Clemens, R. Shah, and T. Brainerd, editors, *Milky Way Surveys: The Structure and Evolution of our Galaxy*, volume 317 of *Astronomical Society of the Pacific Conference Series*, page 59, December 2004.

Y. Moriguchi, K. Tamura, Y. Tawara, H. Sasago, K. Yamaoka, T. Onishi, and Y. Fukui. A Detailed Study of Molecular Clouds toward the TeV Gamma-Ray Supernova Remnant G347.3-0.5. ApJ, 631:947–963, October 2005. doi: 10.1086/432653.

G. Morlino and P. Blasi. Spectra of accelerated particles at supernova shocks in the presence of neutral hydrogen: the case of Tycho. A&A, 589:A7, May 2016. doi: 10.1051/0004-6361/201527761.

G. Morlino and D. Caprioli. Strong evidence for hadron acceleration in Tycho's supernova remnant. A&A, 538:A81, February 2012. doi: 10.1051/0004-6361/201117855.

R. Mukherjee and J. P. Halpern. Chandra Observation of the Unidentified TeV Gamma-Ray Source HESS J1303-631 in the Galactic Plane. ApJ, 629:1017–1020, August 2005. doi: 10.1086/431581.

R. P. Murphy, M. Sasaki, W. R. Binns, T. J. Brandt, T. Hams, M. H. Israel, A. W. Labrador, J. T. Link, R. A. Mewaldt, J. W. Mitchell, B. F. Rauch, K. Sakai, E. C. Stone, C. J. Waddington, N. E. Walsh, J. E. Ward, and M. E. Wiedenbeck. Galactic Cosmic Ray Origins and OB Associations: Evidence from SuperTIGER Observations of Elements $_{26}$Fe through $_{40}$Zr. ApJ, 831:148, November 2016. doi: 10.3847/0004-637X/831/2/148.

T. Murphy, T. Mauch, A. Green, R. W. Hunstead, B. Piestrzynska, A. P. Kels, and P. Sztajer. The second epoch Molonglo Galactic Plane Survey: compact source catalogue. MNRAS, 382:382–392, November 2007. doi: 10.1111/j.1365-2966.2007.12379.x.

K. Nandra, D. Barret, X. Barcons, A. Fabian, J.-W. den Herder, L. Piro, M. Watson, C. Adami, J. Aird, J. M. Afonso, and et al. The Hot and Energetic Universe: A White Paper presenting the science theme motivating the Athena+ mission. *ArXiv e-prints*, June 2013.

A. J. Nayana, P. Chandra, S. Roy, D. A. Green, F. Acero, M. Lemoine-Goumard, A. Marcowith, A. K. Ray, and M. Renaud. 325 and 610 MHz radio counterparts of SNR G353.6-0.7 also known as HESS J1731-347. MNRAS, 467:155–163, May 2017. doi: 10.1093/mnras/stx044.

P. L. Nolan, A. A. Abdo, M. Ackermann, M. Ajello, A. Allafort, E. Antolini, W. B. Atwood, M. Axelsson, L. Baldini, J. Ballet, and et al. Fermi Large Area Telescope Second Source Catalog. ApJS, 199:31, April 2012. doi: 10.1088/0067-0049/199/2/31.

Y. Ohira, K. Murase, and R. Yamazaki. Gamma-rays from molecular clouds illuminated by cosmic rays escaping from interacting supernova remnants. MNRAS, 410:1577–1582, January 2011. doi: 10.1111/j.1365-2966.2010.17539.x.

J. F. Ormes, M. E. Ozel, and D. J. Morris. On the high-energy gamma-ray signature of cosmic-ray sources. ApJ, 334:722–733, November 1988. doi: 10.1086/166873.

E. Parizot, A. Marcowith, E. van der Swaluw, A. M. Bykov, and V. Tatischeff. Superbubbles and energetic particles in the Galaxy. I. Collective effects of particle acceleration. A&A, 424:747–760, September 2004. doi: 10.1051/0004-6361:20041269.

E. Parizot, A. Marcowith, J. Ballet, and Y. A. Gallant. Observational constraints on energetic particle diffusion in young supernovae remnants: amplified magnetic field and maximum energy. A&A, 453:387–395, July 2006. doi: 10.1051/0004-6361:20064985.

N. Park. Status of ground based gamma-ray observations, 2017. URL `https://pos.sissa.it/301/1116/pdf`.

D. J. Patnaude, C. Badenes, S. Park, and J. M. Laming. The Origin of Kepler's Supernova Remnant. *ApJ*, 756:6, September 2012. doi: 10.1088/0004-637X/756/1/6.

M. Paz Arribas, U. Schwanke, I. Sushch, N. Komin, F. Acero, S. Ohm, and for the H. E. S. S. Collaboration. H.E.S.S. deeper observations on SNR RX J0852.0-4622. *ArXiv e-prints*, March 2012.

O. Petruk, V. Beshley, F. Bocchino, and S. Orlando. Some properties of synchrotron radio and inverse-Compton gamma-ray images of supernova remnants. MNRAS, 395:1467–1475, May 2009. doi: 10.1111/j.1365-2966.2009.14563.x.

E. Pfeffermann and B. Aschenbach. ROSAT observation of a new supernova remnant in the constellation Scorpius. In H. U. Zimmermann, J. Trümper, and H. Yorke, editors, *Roentgenstrahlung from the Universe*, pages 267–268, February 1996a.

E. Pfeffermann and B. Aschenbach. ROSAT observation of a new supernova remnant in the constellation Scorpius. In H. U. Zimmermann, J. Trümper, and H. Yorke, editors, *Roentgenstrahlung from the Universe*, pages 267–268, February 1996b.

T. Prinz and W. Becker. Radio Follow-Up Observations of X-ray Selected Supernova Remnant Candidates. ATNF Proposal, April 2012.

V. S. Ptuskin and V. N. Zirakashvili. On the spectrum of high-energy cosmic rays produced by supernova remnants in the presence of strong cosmic-ray streaming instability and wave dissipation. A&A, 429:755–765, January 2005. doi: 10.1051/0004-6361:20041517.

V. S. Ptuskin, I. V. Moskalenko, F. C. Jones, A. W. Strong, and V. N. Zirakashvili. Dissipation of Magnetohydrodynamic Waves on Energetic Particles: Impact on Interstellar Turbulence and Cosmic-Ray Transport. ApJ, 642:902–916, May 2006. doi: 10.1086/501117.

M. Rahman, C. D. Matzner, and D.-S. Moon. OB Associations at the Upper End of the Milky Way Luminosity Function. ApJ, 766:135, April 2013. doi: 10.1088/0004-637X/766/2/135.

W. T. Reach, J. Rho, and T. H. Jarrett. Shocked Molecular Gas in the Supernova Remnants W28 and W44: Near-Infrared and Millimeter-Wave Observations. ApJ, 618:297–320, January 2005. doi: 10.1086/425855.

J. E. Reed, J. J. Hester, A. C. Fabian, and P. F. Winkler. The Three-dimensional Structure of the Cassiopeia A Supernova Remnant. I. The Spherical Shell. ApJ, 440:706, February 1995. doi: 10.1086/175308.

M. Renaud and CTA Consortium. Supernova remnants and pulsar wind nebulae in the Cherenkov Telescope Array era. Mem. Soc. Astron. Italiana, 82:726, 2011a.

M. Renaud and CTA Consortium. Supernova remnants and pulsar wind nebulae in the Cherenkov Telescope Array era. *MmSAI*, 82:726, 2011b.

B. Reville and A. R. Bell. Universal behaviour of shock precursors in the presence of efficient cosmic ray acceleration. MNRAS, 430:2873–2884, April 2013. doi: 10.1093/mnras/stt100.

S. P. Reynolds. Supernova Remnants at High Energy. ARA&A, 46:89–126, September 2008. doi: 10.1146/annurev.astro.46.060407.145237.

S. P. Reynolds, K. J. Borkowski, D. A. Green, U. Hwang, I. Harrus, and R. Petre. The Youngest Galactic Supernova Remnant: G1.9+0.3. ApJ, 680:L41, June 2008. doi: 10.1086/589570.

S. P. Reynolds, K. J. Borkowski, D. A. Green, U. Hwang, I. Harrus, and R. Petre. X-Ray Spectral Variations in the Youngest Galactic Supernova Remnant G1.9+0.3. ApJ, 695:L149–L153, April 2009. doi: 10.1088/0004-637X/695/2/L149.

E. M. Reynoso and J. G. Mangum. CO Observations toward Supernova Remnants with Associated OH 1720 MHZ Masers. ApJ, 545:874–884, December 2000. doi: 10.1086/317854.

E. M. Reynoso, A. J. Green, S. Johnston, G. M. Dubner, E. B. Giacani, and W. M. Goss. Observations of the neutral hydrogen surrounding the radio-quiet neutron star RX J0822-4300 in Puppis A. MNRAS, 345:671–677, October 2003. doi: 10.1046/j.1365-8711.2003.06978.x.

J. Rho, R. Petre, E. M. Schlegel, and J. J. Hester. An X-ray and optical study of the supernova remnant W44. ApJ, 430:757–773, August 1994. doi: 10.1086/174446.

J. Rho, K. K. Dyer, K. J. Borkowski, and S. P. Reynolds. X-Ray Synchrotron-emitting Fe-rich Ejecta in Supernova Remnant RCW 86. ApJ, 581:1116–1131, December 2002. doi: 10.1086/344248.

W. J. Robbins, B. M. Gaensler, T. Murphy, S. Reeves, and A. J. Green. A multiwavelength study of the radio source G296.7-0.9: confirmation as a Galactic supernova remnant. MNRAS, 419: 2623–2632, January 2012. doi: 10.1111/j.1365-2966.2011.19912.x.

W. A. Rolke, A. M. López, and J. Conrad. Limits and confidence intervals in the presence of nuisance parameters. *Nuclear Instruments and Methods in Physics Research A*, 551:493–503, October 2005. doi: 10.1016/j.nima.2005.05.068.

M. Rosado, P. Ambrocio-Cruz, E. Le Coarer, and M. Marcelin. Kinematics of the galactic supernova remnants RCW 86, MSH 15-56 and MSH 11-61A. A&A, 315:243–252, November 1996.

T. Sato and J. P. Hughes. Direct Ejecta Velocity Measurements of Tycho's Supernova Remnant. ApJ, 840:112, May 2017. doi: 10.3847/1538-4357/aa6f60.

D. Schaudel, W. Becker, W. Voges, B. Aschenbach, W. Reich, and M. Weisskopf. Galactic SNR Candidates in the ROSAT All-Sky Survey. In P. O. Slane and B. M. Gaensler, editors, *Neutron Stars in Supernova Remnants*, volume 271 of *Astronomical Society of the Pacific Conference Series*, page 391, 2002.

K. M. Schure and A. R. Bell. Cosmic ray acceleration in young supernova remnants. MNRAS, 435: 1174–1185, October 2013. doi: 10.1093/mnras/stt1371.

M. Seta, T. Hasegawa, T. M. Dame, S. Sakamoto, T. Oka, T. Handa, M. Hayashi, J.-I. Morino, K. Sorai, and K. S. Usuda. Enhanced CO J = 2-1/J = 1-0 Ratio as a Marker of Supernova Remnant-Molecular Cloud Interactions: The Cases of W44 and IC 443. ApJ, 505:286–298, September 1998. doi: 10.1086/306141.

F. Sheidaei. Discovery of very-high-energy gamma-ray emission from the vicinity of PSR J1831-952 with H.E.S.S. In *International Cosmic Ray Conference*, volume 7 of *International Cosmic Ray Conference*, page 243, 2011.

P. Slane. Pulsar Wind Nebulae. *ArXiv e-prints*, March 2017.

P. Slane, S.-H. Lee, D. C. Ellison, D. J. Patnaude, J. P. Hughes, K. A. Eriksen, D. Castro, and S. Nagataki. A CR-hydro-NEI Model of the Structure and Broadband Emission from Tycho's Supernova Remnant. ApJ, 783:33, March 2014. doi: 10.1088/0004-637X/783/1/33.

P. Slane, A. Bykov, D. C. Ellison, G. Dubner, and D. Castro. Supernova Remnants Interacting with Molecular Clouds: X-Ray and Gamma-Ray Signatures. *SSRv*, 188:187–210, May 2015. doi: 10.1007/s11214-014-0062-6.

J. Sollerman, P. Ghavamian, P. Lundqvist, and R. C. Smith. High resolution spectroscopy of Balmer-dominated shocks in the RCW 86, Kepler and SN 1006 supernova remnants. A&A, 407:249–257, August 2003. doi: 10.1051/0004-6361:20030839.

P. Sreekumar, D. L. Bertsch, B. L. Dingus, C. E. Fichtel, R. C. Hartman, S. D. Hunter, G. Kanbach, D. A. Kniffen, Y. C. Lin, and J. R. Mattox. Constraints on the cosmic rays in the Small Magellanic Cloud. *Physical Review Letters*, 70:127–129, January 1993. doi: 10.1103/PhysRevLett.70.127.

A. W. Strong, I. V. Moskalenko, and V. S. Ptuskin. Cosmic-Ray Propagation and Interactions in the Galaxy. *Annual Review of Nuclear and Particle Science*, 57:285–327, November 2007. doi: 10.1146/annurev.nucl.57.090506.123011.

M. Su, T. R. Slatyer, and D. P. Finkbeiner. Giant Gamma-ray Bubbles from Fermi-LAT: Active Galactic Nucleus Activity or Bipolar Galactic Wind? ApJ, 724:1044–1082, December 2010. doi: 10.1088/0004-637X/724/2/1044.

T. Tanaka, A. Allafort, J. Ballet, S. Funk, F. Giordano, J. Hewitt, M. Lemoine-Goumard, H. Tajima, O. Tibolla, and Y. Uchiyama. Gamma-Ray Observations of the Supernova Remnant RX J0852.0-4622 with the Fermi Large Area Telescope. ApJ, 740:L51, October 2011. doi: 10.1088/2041-8205/740/2/L51.

X. Tang. Similarity of γ-ray spectrum in middle aged supernova remnants interacting with molecular clouds: challenge for current models. *ArXiv e-prints*, July 2017.

V. Tatischeff and S. Gabici. Particle acceleration by supernova shocks and spallogenic nucleosynthesis of light elements. *ArXiv e-prints*, March 2018.

The Pierre Auger Collaboration, A. Aab, P. Abreu, M. Aglietta, I. A. Samarai, I. F. M. Albuquerque, I. Allekotte, A. Almela, J. Alvarez Castillo, J. Alvarez-Muñiz, and et al. Observation of a Large-scale Anisotropy in the Arrival Directions of Cosmic Rays above 8×10^{18} eV. *ArXiv e-prints*, September 2017.

W. W. Tian and D. A. Leahy. SNR G349.7+0.2: A γ-Ray Source in the Far 3 kpc Arm of the Galactic Center. ApJ, 783:L2, March 2014. doi: 10.1088/2041-8205/783/1/L2.

W. W. Tian, D. A. Leahy, M. Haverkorn, and B. Jiang. Discovery of the Radio and X-Ray Counterpart of TeV γ-Ray Source HESS J1731-347. ApJ, 679:L85, June 2008. doi: 10.1086/589506.

O. Tibolla, S. Kaufmann, and K. Kosack. XMM-Newton and Chandra X-ray follow-up observations of the VHE gamma-ray source HESS J1507-622. A&A, 567:A74, July 2014. doi: 10.1051/0004-6361/201321778.

C. Trichard. Searching for PeVatrons in the CTA Galactic Plane Survey. *ArXiv e-prints*, September 2017.

J. K. Truelove and C. F. McKee. Evolution of Nonradiative Supernova Remnants. ApJS, 120:299–326, February 1999. doi: 10.1086/313176.

Y. Uchiyama, F. A. Aharonian, T. Tanaka, T. Takahashi, and Y. Maeda. Extremely fast acceleration of cosmic rays in a supernova remnant. Nature, 449:576–578, October 2007. doi: 10.1038/nature06210.

Y. Uchiyama, R. D. Blandford, S. Funk, H. Tajima, and T. Tanaka. Gamma-ray Emission from Crushed Clouds in Supernova Remnants. ApJ, 723:L122–L126, November 2010. doi: 10.1088/2041-8205/723/1/L122.

Y. Uchiyama, S. Funk, H. Katagiri, J. Katsuta, M. Lemoine-Goumard, H. Tajima, T. Tanaka, and D. F. Torres. Fermi Large Area Telescope Discovery of GeV Gamma-Ray Emission from the Vicinity of SNR W44. ApJ, 749:L35, April 2012. doi: 10.1088/2041-8205/749/2/L35.

T. Umemoto, T. Minamidani, N. Kuno, S. Fujita, et al. FOREST unbiased Galactic plane imaging survey with the Nobeyama 45 m telescope (FUGIN). I. Project overview and initial results. PASJ, 69:78, October 2017. doi: 10.1093/pasj/psx061.

B. van Veelen, N. Langer, J. Vink, G. García-Segura, and A. J. van Marle. The hydrodynamics of the supernova remnant Cassiopeia A. The influence of the progenitor evolution on the velocity structure and clumping. A&A, 503:495–503, August 2009. doi: 10.1051/0004-6361/200912393.

S. Vaupré, P. Hily-Blant, C. Ceccarelli, G. Dubus, S. Gabici, and T. Montmerle. Cosmic ray induced ionisation of a molecular cloud shocked by the W28 supernova remnant. A&A, 568:A50, August 2014. doi: 10.1051/0004-6361/201424036.

P. F. Velázquez, G. M. Dubner, W. M. Goss, and A. J. Green. Investigation of the Large-scale Neutral Hydrogen near the Supernova Remnant W28. AJ, 124:2145–2151, October 2002. doi: 10.1086/342936.

J. Vink and J. M. Laming. On the Magnetic Fields and Particle Acceleration in Cassiopeia A. ApJ, 584:758–769, February 2003. doi: 10.1086/345832.

J. Vink, J. Bleeker, K. van der Heyden, A. Bykov, A. Bamba, and R. Yamazaki. The X-Ray Synchrotron Emission of RCW 86 and the Implications for Its Age. ApJ, 648:L33–L37, September 2006. doi: 10.1086/507628.

A. E. Vladimirov, G. Jóhannesson, I. V. Moskalenko, and T. A. Porter. Testing the Origin of High-energy Cosmic Rays. ApJ, 752:68, June 2012. doi: 10.1088/0004-637X/752/1/68.

Z. R. Wang, Q.-Y. Qu, and Y. Chen. Is RX J1713.7-3946 the remnant of the AD393 guest star? *A&A*, 318:L59–L61, February 1997.

T. C. Weekes, M. F. Cawley, D. J. Fegan, K. G. Gibbs, A. M. Hillas, P. W. Kowk, R. C. Lamb, D. A. Lewis, D. Macomb, N. A. Porter, P. T. Reynolds, and G. Vacanti. Observation of TeV gamma rays from the Crab nebula using the atmospheric Cherenkov imaging technique. ApJ, 342:379–395, July 1989. doi: 10.1086/167599.

G. Westerhout. A survey of the continuous radiation from the Galactic System at a frequency of 1390 Mc/s. Bull. Astron. Inst. Netherlands, 14:215, December 1958.

B. J. Williams, W. P. Blair, J. M. Blondin, K. J. Borkowski, P. Ghavamian, K. S. Long, J. C. Raymond, S. P. Reynolds, J. Rho, and P. F. Winkler. RCW 86: A Type Ia Supernova in a Wind-blown Bubble. ApJ, 741:96, November 2011. doi: 10.1088/0004-637X/741/2/96.

C. A. Wilson-Hodge, M. L. Cherry, G. L. Case, W. H. Baumgartner, E. Beklen, P. Narayana Bhat, M. S. Briggs, A. Camero-Arranz, V. Chaplin, V. Connaughton, M. H. Finger, N. Gehrels, J. Greiner, K. Jahoda, P. Jenke, R. M. Kippen, C. Kouveliotou, H. A. Krimm, E. Kuulkers, N. Lund, C. A. Meegan, L. Natalucci, W. S. Paciesas, R. Preece, J. C. Rodi, N. Shaposhnikov, G. K. Skinner, D. Swartz, A. von Kienlin, R. Diehl, and X.-L. Zhang. When a Standard Candle Flickers. ApJ, 727:L40, February 2011. doi: 10.1088/2041-8205/727/2/L40.

P. F. Winkler, B. J. Williams, S. P. Reynolds, R. Petre, K. S. Long, S. Katsuda, and U. Hwang. A High-resolution X-Ray and Optical Study of SN 1006: Asymmetric Expansion and Small-scale Structure in a Type Ia Supernova Remnant. ApJ, 781:65, February 2014. doi: 10.1088/0004-637X/781/2/65.

L. Woltjer. Supernovae and the Interstellar Medium. In H. J. Habing, editor, *Interstellar Gas Dynamics*, volume 39 of *IAU Symposium*, page 229, 1970.

H. A. Wootten. The molecular cloud associated with the supernova remnant W44. ApJ, 216:440–445, September 1977. doi: 10.1086/155485.

L. Xiao, E. Fürst, W. Reich, and J. L. Han. Radio spectral properties and the magnetic field of the SNR S147. A&A, 482:783–792, May 2008. doi: 10.1051/0004-6361:20078461.

Y.-L. Xin, X.-L. Guo, N.-H. Liao, Q. Yuan, S.-M. Liu, and D.-M. Wei. Revisiting SNR Puppis A with Seven Years of Fermi Large Area Telescope Observations. ApJ, 843:90, July 2017. doi: 10.3847/1538-4357/aa74bb.

Y. Xing, Z. Wang, X. Zhang, and Y. Chen. The Likely Fermi Detection of the Supernova Remnant SN 1006. ApJ, 823:44, May 2016. doi: 10.3847/0004-637X/823/1/44.

H. Yamaguchi, K. Koyama, H. Nakajima, A. Bamba, R. Yamazaki, J. Vink, and A. Kawachi. Suzaku Observation of the RCW86 Northeastern Shell. PASJ, 60:S123–S130, January 2008. doi: 10.1093/pasj/60.sp1.S123.

Q. Yuan, X. Huang, S. Liu, and B. Zhang. Fermi Large Area Telescope Detection of Supernova Remnant RCW 86. ApJ, 785:L22, April 2014. doi: 10.1088/2041-8205/785/2/L22.

Y. Yuan, S. Funk, G. Jóhannesson, J. Lande, L. Tibaldo, and Y. Uchiyama. Fermi Large Area Telescope Detection of a Break in the Gamma-Ray Spectrum of the Supernova Remnant Cassiopeia A. ApJ, 779:117, December 2013. doi: 10.1088/0004-637X/779/2/117.

G. Zanardo, L. Staveley-Smith, R. Indebetouw, R. A. Chevalier, M. Matsuura, B. M. Gaensler, M. J. Barlow, C. Fransson, R. N. Manchester, M. Baes, J. R. Kamenetzky, M. Lakićević, P. Lundqvist, J. M. Marcaide, I. Martí-Vidal, M. Meixner, C.-Y. Ng, S. Park, G. Sonneborn, J. Spyromilio, and J. T. van Loon. Spectral and Morphological Analysis of the Remnant of Supernova 1987A with ALMA and ATCA. ApJ, 796:82, December 2014. doi: 10.1088/0004-637X/796/2/82.

X. Zhang, Y. Chen, H. Li, and X. Zhou. On the hadronic γ-ray emission from Tycho's supernova remnant. MNRAS, 429:L25–L29, February 2013. doi: 10.1093/mnrasl/sls016.

X. Zhou, M. Miceli, F. Bocchino, S. Orlando, and Y. Chen. Unveiling the spatial structure of the overionized plasma in the supernova remnant W49B. MNRAS, 415:244–250, July 2011. doi: 10.1111/j.1365-2966.2011.18695.x.

V. N. Zirakashvili, F. A. Aharonian, R. Yang, E. Oña-Wilhelmi, and R. J. Tuffs. Nonthermal Radiation of Young Supernova Remnants: The Case of CAS A. *ApJ*, 785:130, April 2014. doi: 10.1088/0004-637X/785/2/130.

A. Zoglauer, S. P. Reynolds, H. An, S. E. Boggs, F. E. Christensen, W. W. Craig, C. L. Fryer, B. W. Grefenstette, F. A. Harrison, C. J. Hailey, R. A. Krivonos, K. K. Madsen, H. Miyasaka, D. Stern, and W. W. Zhang. The Hard X-Ray View of the Young Supernova Remnant G1.9+0.3. *ApJ*, 798:98, January 2015. doi: 10.1088/0004-637X/798/2/98.

K. Zubovas, A. R. King, and S. Nayakshin. The Milky Way's Fermi bubbles: echoes of the last quasar outburst? MNRAS, 415:L21–L25, July 2011. doi: 10.1111/j.1745-3933.2011.01070.x.

Remerciements

Cette habilitation à diriger des recherches résume en quelque sorte plus de onze années de vie passées au CENBG. Il y a eu de très nombreux moments heureux, des succès, mais aussi des désillusions, et dans tous ces moments, l'appui des proches et des collègues fut essentiel. Il est donc temps de les remercier même si ces quelques lignes sont bien peu par rapport aux joies qu'ils m'ont procurées.

Tout d'abord, je souhaiterais remercier les membres de mon jury: Mathieu de Naurois, Jürgen Knödlseder, Giovanni Lamanna, Eric Nuss et Vincent Tatischeff. Vous avez accepté ce rôle avec enthousiasme malgré des emplois du temps extrêmement chargés. Travailler, discuter avec vous fut toujours un grand plaisir, j'espère que d'autres occasions s'offriront à nous dans le futur. Mathieu, Jürgen, Vincent: un grand merci pour vos rapports et vos commentaires dont la teneur m'a sincèrement touchée.

Je souhaite également vivement remercier les personnes qui m'ont orientée lors de mes premiers contacts avec le domaine scientifique: Michel Tagger, Rosine Lallement et bien sûr Bernard Degrange. Bernard, notre rencontre fut un moment magique suivi par ce stage de DEA (c'est en utilisant ces termes qui n'existent plus qu'on se sent un peu vieux !) qui vit les premières heures du Modèle 3D. Les trois années de thèse à tes côtés furent très intenses mais je n'ai jamais autant appris que pendant cette période. Ton enthousiasme, ta rigueur et ton sens physique vont de pair avec une grande humanité. Merci d'avoir su aussi bien m'épauler et me permettre de mener ma carrière actuelle.

Je me rappelle très bien de mon arrivée au CENBG en Décembre 2006, en particulier grâce à l'appui de Bernard Haas, directeur du laboratoire à l'époque, que je remercie vivement. Malgré des allers et retours encore fréquents sur Paris, le groupe Astro m'a aidé à trouver ma place au sein de la collaboration GLAST et à me lancer sur différents sujets astrophysiques et techniques. Un grand merci tout d'abord à David Smith. Membre de mon jury de thèse, tu as joué un très grand rôle dans les premiers instants de mon insertion dans le groupe Astro. Merci à toi, merci pour ton soutien lors de ma candidature à l'ERC et pour les nombreuses relectures de dossiers variés. Je sais que ma carrière aujourd'hui ne serait pas la même sans les conseils que tu m'as donnés. Merci aussi à tous

les autres membres du groupe, les discussions avec vous, scientifiques ou plus personnelles, me font énormément de bien (en particulier après une journée à débugguer pointlike !). Merci à toi, Thierry, pour ta bonne humeur légendaire (même si tes coups de gueule sont tout autant impressionnants !) et ton soutien inaltéré malgré mes propres coups de gueule. Merci aux doctorants et post-doctorants avec qui j'ai eu la chance de travailler: je vous dois la grande majorité des succès de ces dernières années. Vous avez également été la source de ma motivation quotidienne, en commençant évidemment par la thèse de Marie-Hélène dès 2007. Merci à toi, ça n'a pas toujours été facile mais que de chemin parcouru depuis cette époque. Merci également à toi et François pour avoir relu ce manuscrit et m'avoir aidé à l'améliorer. François, je te souhaite le meilleur au CEA...même si j'aurais préféré te garder à Bordeaux, tu le sais bien.

Un grand merci à tous les membres du CENBG; merci pour vos sourires, pour les discussions lors des cafés labo et séminaires, pour les rigolades dans les couloirs. Malgré l'éloignement du solarium, vous avez tous eu des attentions très sympathiques en particulier ces dernières semaines de préparation à la soutenance. Merci d'y être venu nombreux pour m'écouter sur un sujet qui est très loin de vos préoccupations scientifiques. Vos messages et vos mots de félicitations m'ont touchés. Merci à Aziz et Catherine du service Informatique pour m'avoir aidé à gérer la visioconférence et à déstresser un peu. Enfin, un très grand merci à tout le service Administration. Vous êtes une bouffée de fraîcheur dans ce monde scientifique. Votre bonne humeur fait chaud au cœur. Je voudrais tout particulièrement remercier Nathalie et Sylvie, avec qui j'ai la chance d'interagir régulièrement. Merci, Nathalie, d'avoir préparé le pot et géré les missions, m'enlevant un poids pendant cette période bien chargée pour moi. Merci à toi, Sylvie, témoin des joies, des peines et du 7 !

Durant ces dernières années, j'ai principalement travaillé avec les groupes "Sources Galactiques" des collaborations Fermi et HESS où règne une ambiance stimulante. Je ne peux pas citer tous les membres avec qui j'ai eu la chance d'interagir mais je pense à vous tous, de Bari à Paris en passant par Montpellier, Washington, Palo Alto ou Heidelberg. Vous m'avez beaucoup apporté. Merci. J'espère que de nombreuses autres occasions s'offriront à nous en particulier avec CTA. Un merci tout particulier à Fabio Acero, Stefano Gabici et Matthieu Renaud. Vous avez le don de déclencher des discussions longues et passionantes...qui finissent souvent en belles publications ou en financement. Matthieu, merci pour ta bonne humeur malgré les moments difficiles que tu as traversés. Travailler avec toi fut certainement l'une des plus belles chances que j'ai eu. Je te souhaite plein de bonnes choses à la Réunion ou ici, en espérant en partager encore de nombreuses à tes côtés.

Sur un plan plus personnel, je remercie le groupe de marche nordique de Canéjan. Les discussions en soirée, à la lueur des frontales, m'ont fait un bien fou. La parenthèse bébés et habilitation s'achevant, j'espère de tout cœur rejoindre le groupe dès la rentrée. Merci en particulier à Marie-Christine pour ton soutien et ton écoute. Tu es toujours là, même lorsqu'on te prévient à la dernière minute (par exemple le 7 Janvier 2017 !). Merci à mes parents pour leur amour et leur compréhension. Mes choix vous ont parfois déroutés mais vous avez su me soutenir et m'épauler. J'ai évidemment une pensée pour mon frère, toute ma famille et belle famille pour leur tendresse. Merci en particulier à Denise pour son aide au quotidien, l'année 2017-2018 eut été bien difficile sans vous. J'ai enfin une pensée émue pour ma mamie, qui n'aurait rien compris à ce manuscrit mais aurait su me féliciter comme elle savait si bien le faire. Mes derniers remerciements sont évidemment ceux qui me tiennent le plus à cœur. Ils s'adressent à mon ange qui sait m'entourer et m'épauler jour après jour et à nos loulous qui font pétiller nos vies depuis quinze mois.

Résumé

Depuis leur découverte, un débat sans fin s'anime autour de l'origine des rayons cosmiques, les vestiges de supernovae étant souvent cités comme étant les meilleurs candidats pour leur accélération dans la Galaxie. Après un chapitre résumant mon parcours puis une introduction au domaine, les deux chapitres suivants de ce mémoire résument les observations en rayons gamma du Large Area Telescope (LAT) à bord du satellite Fermi et du High Energy Stereoscopic System (H.E.S.S.) pour deux types de vestiges de supernovae: les vestiges de supernovae jeunes supposés être des accélérateurs efficaces, et les vestiges évolués pour lesquels des signes clairs d'accélération de protons ont été obtenus. Ces chapitres démontrent que les vestiges de supernovae sont capables d'accélérer des particules (électrons et protons) à très haute énergie par accélération diffusive par onde de choc. Des preuves de l'accélération de protons sont visibles dans plusieurs cas: les vestiges de supernovae historiques Cassiopeia A et Tycho, de même que Puppis A et les vestiges évolués W44, IC 443, W51C et W49B. Dans tous les cas étudiés, l'environnement dans lequel le vestige évolue est l'élément clé gouvernant le spectre gamma observé ainsi que la fraction de particules accélérées.
En parallèle, la sensibilité accrue des détecteurs actuels nous a permis d'entrer dans une ère de catalogues, révélant ainsi différentes classes de sources astrophysiques contribuant potentiellement au spectre du rayonnement cosmique, telles que les nébuleuses de pulsar, les nuages moléculaires, les régions de formation d'étoiles et même un premier PeVatron au centre Galactique. C'est l'objet du cinquième chapitre qui décrit également les recherches récentes de nébuleuses de pulsars et de sources étendues dans la Galaxie avec le LAT. Quelques perspectives instrumentales et observationnelles sont enfin proposées dans le dernier chapitre. Ce manuscrit n'est ni une liste exhaustive de tous les résultats du domaine, ni une liste complète des travaux et publications que j'ai menés mais plutôt un mélange entre les deux.

Mots clés: astronomie gamma, Fermi, Large Area Telescope, imagerie Tcherenkov atmosphérique, H.E.S.S., CTA, vestiges de supernovae, rayons cosmiques, nébuleuses de pulsars.

Abstract

Since their discovery, there has been a long standing debate concerning the origin of cosmic rays, supernova remnants (SNR) being often cited as the best candidate for their acceleration in the Galaxy. After a chapter relating my career path and an introduction to the subject, the following two chapters of this manuscript summarize the gamma-ray observations acquired by the Large Area Telescope (LAT) aboard Fermi and by the High Energy Stereoscopic System (H.E.S.S.) on two different types of supernova remnants: young supernova remnants thought to be the most efficient accelerators and middle-aged remnants that show clear signs of proton acceleration. These chapters demonstrate that SNRs are able to accelerate particles (electrons and protons) to very high energies through diffusive shock acceleration. Evidences in favor of proton acceleration are visible in several cases: the historical SNRs Cassiopeia A and Tycho as well as the transition case Puppis A and the middle-aged SNRs W44, IC 443, W51C and W49B. In all cases, the environment in which the SNR is evolving is a key characteristic controlling the gamma-ray spectrum as well as fraction of accelerated particules.
In the meantime, the increased sensitivity of the current detectors allowed us to enter an era of catalogs, revealing different classes of astrophysical sources potentially contributing to the cosmic-ray spectrum, such as pulsar wind nebulae, molecular clouds, star forming regions and even a first PeVatron at the Galactic center. This is described in the fifth chapter that also summarizes the recent searches for pulsar wind nebulae and extended sources in the Galaxy with the LAT. Finally, instrumental and observational perspectives are proposed in the last chapter. This manuscript is neither an exhaustive list of all results in the field, nor a complete list of the works and publications that I carried but rather a mix between the two.

Keywords: gamma-ray astronomy, Fermi, Large Area Telescope, imaging atmospheric Cherenkov, H.E.S.S., CTA, supernova remnants, cosmic rays, pulsar wind nebulae.